Computational and characterization studies of homogeneous and heterogeneous tris(beta-diketonato) complexes with catalytic applications.

Roxanne Gostynski

Computational and characterization studies of homogeneous and heterogeneous tris(beta-diketonato) complexes with catalytic applications.

A dissertation submitted in accordance with the requirements for the degree

Philosophiae Doctor

in the

Department of Chemistry
Faculty of Natural and Agricultural Sciences

at the

University of the Free State

By

Roxanne Gostynski

Supervisor

Prof. J. Conradie

Co-spervisor

Dr. E. Erasmus

June 2017

Table of contents.

Chapter 3
Results and discussion   53

ii

Chapter 4
Experimental   173

Chapter 5
Summary and future perspectives — 191

Appendix (found on attached CD) — A-1

List of abbreviations.

β-diketones

Hacac	2,4-pentanedione (acetylacetone)
Hba	1-phenyl-1,3-butanedione (benzoylacetone)
Hdbm	1,3-diphenyl-1,3-propanedione (dibenzoylmethane)
Hdpm	2,2,6,6-tetramethyl-3,5-heptanedione (dipivaloylmethane)
Htfaa	1,1,1-trifluoro-2,4-pentanedione (trifluoroacetylacetone)
Htfth	4,4,4-trifluoro-1-(2-thenoyl)-1,3-butanedione (trifluorothenoylacetone)
Htffu	4,4,4-trifluoro-1-(2-furoyl)-1,3-butanedione (trifluorofuroylacetone)
Htfba	4,4,4-trifluoro-1-(phenyl)-1,3-butanedione (trifluorobenzoylacetone)
Hhfaa	1,1,1,5,5,5-hexafluoro-2,4-pentanedione (hexafluoroacetylacetone)

*The removal of H in the above abbreviations represents the anion (enolate) of the β-diketone.

Solvents / Chemicals

THF	tetrahydrofuran
CH_3CN	acetonitrile
DCM	dichloromethane
EtOH	ethanol
HDI	hexamethylenediisocyanate
HDU	hexamethylenediurethane

Cyclic Voltammetry

CV	cyclic voltammetry
$E^{0'}$	formal reduction potential
E_{pa}	anodic peak potential
E_{pc}	cathodic peak potential
ΔE_p	separation of anodic and cathodic peak potentials
i_{pa}	anodic peak current
i_{pc}	cathodic peak current
$TBAPF_6$	tetrabutylammonium hexafluorophosphate $[NBu_4][PF_6]$

| TEABF$_4$ | tetraethylammonium tetrafluoroborate |
| SCE | saturated calomel electrode |

Techniques

XPS	X-ray photoelectron spectroscopy
TGA	thermal gravimetric analysis
ATR FTIR	attenuated total reflectance Fourier transform infrared

General

| TOF | turnover frequency |
| ca. | about or approximately |

Acknowledgements

I would like to thank all my friends, family and colleagues for their support, friendship and guidance throughout the, sometimes, very trying period of my studies. Special appreciation must be made to the following people:

List of published work from this study

Some of the work that is presented has been published in the following publications:

1. R. Freitag, J. Conradie, *Electrochimica Acta* **2015** (158) 418-426, "Electrochemical and Computational Chemistry Study of Mn(β-diketonato)$_3$ complexes". DOI: 10.1016/j.electacta.2015.01.147

2. R. Gostynski, P.H. van Rooyen, J. Conradie, *Journal of Moleculaar Structure* **2016** (1119) 48-53, "Jahn-Teller distortion in tris[4,4,4-trifluoro-1-(2-thienyl)-1,3-butanedionato]manganese(III) isomers: An X-ray and computational study". DOI: 10.1016/j.molstruc.2016.04.048

3. R. Gostynski, J. Conradie, E. Erasmus, *RCS Advances* **2017** (7) 27718-27728, "Significance of the electron-density of molecular fragments on the properties of manganese(III) β-diketonato complexes: an XPS and DFT study". DOI: 10.1039/c7ra04921h

4. R. Gostynski, M. Landman, J. Conradie, *Journal of Nano Research* **2016** (44) 1-9, "Electrochemical Behaviour of Cr and W Fischer Ethoxy Carbene Complexes: A Comparative Study". DOI: 10.4028/www.scientific.net/JNanoR.44.1

5. R. Gostynski, R. Fraser, M. Landman, E. Erasmus, J. Conradie, *Polyhedron* **2017** (127) 323-330, "Electrochemical study of chromium(0) Fischer carbene complexes: Trends in redox potential". DOI: 10.1016/j.poly.2017.02.018

6. R. Gostynski, R. Fraser, M. Landman, E. Erasmus, J. Conradie, *Journal of Organometallic Chemistry* **2017** (836-837) 62-67, "Synthesis and XPS characterization of Si-supported chromium(0) Fischer aminocarbene complexes". DOI: 10.1016/j.jorganchem.2017.03.001

Abstract

Nine [Mn(β-diketonato)$_3$] [β-diketonato = dipivaloymethanato (dpm), **1**; acetylacetonato (acac), **2**; benzoylacetonato (ba), **3**; dibenzoylmethanato (dbm), **4**; trifluoroacetylacetonato (tfaa), **5**; thenoyltrifluoroacetonato (tfth), **6**; trifluorofuroylacetonato (tffu), **7**; trifluorobenzoylacetonato (tfba), **8** and hexaflouroacetylacetonato, **9**] complexes were synthesized by adapted methods from literature. An attempt was made to graft [Mn(β-diketonato)$_3$] complexes **2-9** onto two dimensional (2-D) Si-wafer supports (**S5-S12**) via a silane linker. The X-ray photoelectron spectroscopy (XPS) Mn:F atomic ratio results of fluorine containing [Mn(β-diketonato)$_3$] complexes grafted onto amino-functionalized Si-wafer (**S9-S12**) gave an indicaton that the [Mn(β-diketonato)$_3$] complexes decomposed during the grafting process. Studying Mn$_2$O$_3$ on the hydroxylated Si-wafer surface by the use of XPS, it was confirmed that the Mn 2p photoelectron lines observed for **S5**-**S12** consist mostly of Mn$_2$O$_3$ that has no interaction with the silane linker. Eight [Mn(β-diketonato)$_3$] complexes **1**-**8** was wet impregnated onto various three dimensional (3-D) solid supports (**S12**-**S28**) to form [Mn(β-diketonato)$_3$] model catalysts. Additionally a selection of [M(acac)$_3$] complexes ([Co(acac)$_3$], **12**; [Rh(acac)$_3$], **13**, and [Ir(acac)$_3$], **14**) were grafted onto two dimensional (2-D) Si-wafer supports (**S29**-**S31**). While [M(acac)$_3$] complexes ([Cr(acac)$_3$], **10**; [Fe(acac)$_3$], **11**; [Co(acac)$_3$], **12**; [Rh(acac)$_3$], **13**, and [Ir(acac)$_3$], **14**) were wet impregnated onto various three dimensional (3-D) solid supports (forming **S32**-**S36**). The model 2-D and 3-D catalysts were studied and characterized by the means of XPS, TGA and computational chemistry calculations. Selected model 2-D (**S5**, **S7**, **S8**, **S12** and **S29**-**S31**) and Mn(acac)$_3$ immobilized onto SiO$_2$ (3-D catalysts, **S14** as is and heat treated at 100, 130, 250 and 350 °C) were tested for the catalytic self-solvating reaction between ethanol and hexamethylenediisocyanate (HDI) to form hexamethylenediurethane (HDU) to mimic the industrial production of polyurethane. The model 2-D [Mn(β-diketonato)$_3$] (**S5**, **S7**, **S8** and **S12**) catalysts showed that as the total group electronegativity, $3(\chi_R + \chi_{R'})$, increase a general decrease in turnover frequency (TOF) was observed. The model 2-D [M(acac)$_3$] catalysts (**S29**-**S31**) showed that with an increase in the metal centre's Pauling electronegativity a general increase in TOF was observed. The catalytic test on the Mn(acac)$_3$ immobilized onto SiO$_2$ showed that the sample heat treated at 100°C before hand has the highest TOF, which is most probably due to the loss of only one β-diketonato ligand making it more active.

The chromium(0) Fischer carbene complexes (Cr-FCCs) ([Cr(CO)$_4$(PPh$_3$)=C(OEt)(Fu)], **C1**; [Cr(CO)$_5$=C(NHCy)(Fu)], **C2**; [Cr(CO)$_5$=C(NHCy)(Th)], **C3** and [Cr(CO)$_5$=C(OEt)(ThTh)], **C4**) study was in collaboration with the research group of Dr. M Landman at the University of Pretoria. The four Cr(0) FCCs, were obtained and characterized by electrochemistry, XPS and computational chemistry calculations in this study. Penta-carbonyl Cr-FCCs [Cr(CO)$_5$=C(OEt)(Fu)], **C5**, and [Cr(CO)$_5$=C(OEt)(Th)], **C6**, were also supplied and anchored onto an amino-functionalized Si-wafer to create an immobilized Cr-FCCs **C7** and **C8**. XPS results showed that the Cr(CO)$_5$=C(OEt)(Fu)], **C5**, and [Cr(CO)$_5$=C(OEt)(Th)], **C6**, was successfully anchored onto an amino-functionalized Si-wafer (**C7** and **C8**).

The electrochemical study of **C1-4** showed that the oxidation potential (E$_{pa}$) is influenced by the varied substituents on different sites of the Cr-FCCs. The oxidation order of the Cr-FCCs is: [Cr(CO)$_5$=C(OEt)(ThTh)], **C4** > [Cr(CO)$_5$=C(NHCy)(Th)], **C3** > [Cr(CO)$_5$=C(NHCy)(Fu)], **C2** > [Cr(CO)$_4$(PPh$_3$)=C(OEt)(Fu)], **C1**. The reduction followed the same trend except for the [Cr(CO)$_4$(PPh$_3$)=C(OEt)(Fu)], **C1**, complex that is reduced at a higher potential than the aminocarbene complexes, [Cr(CO)$_5$=C(OEt)(ThTh)], **C4** > [Cr(CO)$_4$(PPh$_3$)=C(OEt)(Fu)], **C1** > [Cr(CO)$_5$=C(NHCy)(Th)], **C3** > [Cr(CO)$_5$=C(NHCy)(Fu)], **C2**. The electronic energies of the different conformations obtained by the computational study showed that certain conformations are preferred over others. The computational results were in good agreement with experimental characterization method results. Computational study of HOMO and LUMO orbitals of the Cr-FCCs confirmed that the oxidation process is metal based and the reduction is based across the carbene ligand. The correlation of the oxidation potential (E$_{pa}$) of the Cr^0/Cr^{+1} redox couple and reduction potential (E$_{pc}$) of the ligand based reduction with the HOMO energy (E$_{HOMO}$) and LUMO energy (E$_{LUMO}$) respectively, showed that with decreasing molecular orbital energy (HOMO and LUMO) an increase to more positive E$_{pa}$ and E$_{pc}$ potentials are obtained.

Keywords: Manganese, tris(acetylacetonato)metal, β-diketonato, chromium (0) Fischer carbenes, DFT, cyclic voltammetry, XPS TGA.

Opsomming

Nege [Mn(β-diketonato)$_3$] komplekse (β-diketonato = dpm, **1**; asas, **2**; ba, **3**; dbm, **4**; tfaa, **5**; tfth, **6**; tffu, **7**; tfba, **8** en hfaa, **9**) is gesintetiseer deur aangepaste metodes verkry uit literatuur. 'n Poging was aangewend om die [Mn(β-diketonato)$_3$] komplekse **2-9** te bind aan tweedimensionele (2-D) silikonplaatjies (**S5-S12**) via 'n silaankoppeling. Die X-straal fotoelektron spektroskopie (XPS) Mn:F atoomverhouding van die fluoor bevattende [Mn(β-diketonato)$_3$] komplekse wat gebind is aan 'n amino-gefunksionaliseerde silikonplaatjie (**S9-S12**), het aangedui dat die [Mn(β-diketonato)$_3$] komplekse ontbind het tydens die bindingsproses. Die XPS studie van Mn$_2$O$_3$ op 'n gehidroksileerde silikonplaatjie het gewys dat die Mn 2p fotoelektronlyne waargeneem vir **S5-S12** hoofsaaklik van Mn$_2$O$_3$ is, met geen gepaard gaande interaksie met die silaan nie. Agt [Mn(β-diketonato)$_3$] komplekse **1-8** was deur benattingsimpregnasie geïmmobiliseer op verskeie driedimensionele (3-D) ondersteuningsmateriale (**S12-S28**). Benewens is die volgende 2-D katalisatore gemaak deur uitgesoekte [M(asas)$_3$] komplekse ([Co(asas)$_3$], **12**; [Rh(asas)$_3$], **13**, en [Ir(asas)$_3$], **14**) te bind aan amino-gefunksionaliseerde silikonplaatjies (**S29-S31**), sowel as 3-D katalisatore gemaak deur benattingsimpregnasie van [M(asas)$_3$] komplekse ([Cr(asas)$_3$], **10**; [Fe(asas)$_3$], **11**; [Co(asas)$_3$], **12**; [Rh(asas)$_3$], **13**, en [Ir(asas)$_3$], **14**) op SiO$_2$ (**S32-S36**). Die model 2-D en 3-D katalisatore is gekarakteriseer met behulp van XPS, termogravimetriese analise (TGA) en kwantum-berekeningschemie. Gekose 2-D (**S5**, **S7**, **S8**, **S12** en **S29-S31**) en Mn(asas)$_3$ geïmmobiliseerd op SiO$_2$ (3-D katalisator, **S14** netso sowel as **S14** behandeld deur hitte by 100, 130, 250 en 350 °C) se katalitiese aktiwiteit is getoets deur die self-oplossende reaksie tussen etanol en heksametileendiisosianaat (HDI) met heksametileendiuretaan (HDU) (model reaksie vir die industriële produksie van poliuretaan). Die omset frekwensies van die 2-D [Mn(β-diketonato)$_3$] katalisatore (**S5**, **S7**, **S8** en **S12**) het 'n algemene afnemende neiging gewys met die vehoging van die elektronegatiwiteit, $3(\chi_R + \chi_{R'})$, van die β-diketonato ligande. Die omset frekwensie van die 2-D [M(acac)$_3$] katalisatore (**S29-S31**) het toegeneem met verhoging in die metaal se Pauling elektronegatiwiteit. Die katalitiese aktiwitets toetsing op die Mn(asas)$_3$ geïmmobiliseerd of SiO$_2$ het gewys dat die monster wat alvorens by 'n temperatuur van 100 °C behandel is het die hoogste omset frekwensie vertoon. Dit is mees waarskynlik asgevolg van die verlies van een van die β-diketonato ligande.

Die chroom(0) Fischer karbeen kompleks (Cr-FKK) studie is in samewerking met die navorsingsgroep van Dr. M. Landman van die Universiteit van Pretoria gedoen. Vier Cr-FKKs

(Cr-FKK) ([Cr(CO)$_4$(PPh$_3$)=C(OEt)(Fu)], **C1**; [Cr(CO)$_5$=C(NHCy)(Fu)], **C2**; [Cr(CO)$_5$=C(NHCy)(Th)], **C3** en [Cr(CO)$_5$=C(OEt)(ThTh)], **C4**) was ontvang en is gekarakteriseer met behulp van elektrochemie, XPS en kwantum-berekeningschemie. Penta-karboniel Cr-FKKs [Cr(CO)$_5$=C(OEt)(Fu)], **C5**, and [Cr(CO)$_5$=C(OEt)(Th)], **C6**, verkry vanaf die Universiteit van Pretoria is gebind aan amino-gefunksionaliseerde silikonplaatjies om geïmmobiliseerde Cr-FKKs **C7** en **C8** te maak. XPS resultate het bewys dat die Cr(CO)$_5$=C(OEt)(Fu)], **C5**, en [Cr(CO)$_5$=C(OEt)(Th)], **C6**, suksesvol gebind het op amino-aangepaste silikomplaatjies (**C7** and **C8**).

Die elektrochemiese studie van **C1-4** met behulp van sikliese voltammetrie het gewys dat die oksidasie potensiaal (E$_{pa}$) van die Cr^0/Cr^{1+} redokskoppel beïnvloed word deur die varierende substituente op die veskeie bindings omgewings van die Cr-FKKs. Die orde van meer positiewe oksidasie potensiaal van die Cr-FKKs na minder positief is: [Cr(CO)$_5$=C(OEt)(ThTh)], **C4** > [Cr(CO)$_5$=C(NHCy)(Th)], **C3** > [Cr(CO)$_5$=C(NHCy)(Fu)], **C2** > [Cr(CO)$_4$(PPh$_3$)=C(OEt)(Fu)], **C1**. Die reduksie potensiaal volg dieselfde neiging, behalwe dat die [Cr(CO)$_4$(PPh$_3$)=C(OEt)(Fu)], **C1**, kompleks gereduseer word by hoër potensiaal vergeleke met die aminokarbeenkomplekse, [Cr(CO)$_5$=C(OEt)(ThTh)], **C4** > [Cr(CO)$_4$(PPh$_3$)=C(OEt)(Fu)], **C1** > [Cr(CO)$_5$=C(NHCy)(Th)], **C3** > [Cr(CO)$_5$=C(NHCy)(Fu)], **C2**. Die kwantum-berekeningschemie studie het bepaal dat die Cr-FKKs sekere konformasies bo ander konformasies ver kies en die resultate wat verkry is deur die berekeningschemie is in goeie ooreenstemming met die eksperimentele resultate. Die berekende hoogste besette molekuêre orbitale (HBMO) en die laagste onbesette molekulêre orbitale (LOMO) bewys dat die oksidasieproses metaal verband is en die reduksieproses veband is met die reduksie van die ligand tydens die electrochemiese studie van die Cr-FKKs. 'n Verwantskap tussen die oksidasie potensiaal (E$_{pa}$) van die Cr^0/Cr^{1+} redokskoppel en die reduksie potensiaal (E$_{pc}$) van die ligandgebaseerde reduksie, met die HBMO energie (E$_{HBMO}$) en die LOMO energie (E$_{LOMO}$) onderskeidelik, toon 'n verhoging in orbitaal energie 'n meer positiewe potensiaal tot gevolg het.

Sleutelwoorde: Mangaan, tris(asetielasetonato)metaal(III), β-diketonato, chroom (0) Fischer karbeen, kwantum-berekeningschemie, sikliese voltammetrie, X-straal foto-electron spektroskopie (XPS), termogravimetriese analise (TGA).

Declaration

I Roxanne Gostynski declares that the dissertation hereby submitted by me for the degree Philosophiae Doctor at the University of the Free State is my own independent work and has not previously been submitted by me at another university/faculty. I further more cede copyright of the dissertation in favour of the University of the Free State.

Signed:...   Date:...

1 Introduction

Berzelius identified in 1836 a new substance and called it a "catalyst". His view of "catalysis" is when the "catalyst" is added to a reaction, it can speed up the rate of the reaction without being produced or consumed in the process. However, much earlier, fermentation processes could be viewed as an example of biocatalysis. Since the beginning of the twentieth century, catalysis played a major role in chemical industry.[1] A suitable catalyst can improve the thermodynamically viable reaction rate but cannot shift the position of thermodynamic equilibrium. Catalytic reactions are cyclic processes where in simplified terms, a complex between the catalyst and reactant/reactant's are formed which opens an energetically favourable pathway for the reactant/reactant's transformation into the product/products. After the product is formed the catalyst is released and free to start the next cycle. Practically, catalysts can however not take part in the cycle an infinite amount of times due to deactivation, attributed to side products or structural changes. The deactivated catalyst therefore needs to be reactivated or replaced.[2] Catalysts are viewed as the workhorses in the chemical industry as about 85-90% of the products in this industry is currently produced through catalytic processes. The catalytic processes include the production of transportation fuels, bulk and fine chemicals in the chemical industry and the reduction of pollution by end-of-pipe solutions at automotive and industrial exhausts.[3]

Catalysts are divided into three groups namely homogeneous (catalyst in the same phase as reactants), heterogeneous (catalyst in different phase as the reactants) and heterogenized (homogeneous catalyst that is immobilized onto a solid support). Heterogeneous and heterogenized catalysts are normally in the solid phase, which catalyse reactions in the gas or solution phase. Heterogeneous catalysts are mostly favoured in the chemical and petrochemical

---

[1] E. Farnetti, R.D. Monte, J. Kašpar, *INORGANIC AND BIO-INORGANIC CHEMISTRY – Homogeneous and Heterogeneous catalysis*, 2nd Volume, EolSS Publishers Co. Ltd., Oxford, United Kingdom, **2009**, p 50-55. ISBN: 978-1-84826-665-0

[2] O. Deutschmann, H. Knözinger, K. Kochloefl, T. Turek, *Ullmann's Encyclopedia of Industrial Chemistry - Heterogeneous catalysis and solid catalysts*, Wiley-VCH Verlag GmbH & Co. KGaA, Weinheim, **2009**. ISBN: 3527306730

[3] I. Chorkendorff, J.W. Niemantsverdriet, Concepts of Modern Catalysis and Kinetics, 2nd edition, WILEY-VCH Verlag GmbH &Co. KGaA, Weinheim, **2007**, p 1-10. ISBN: 978-3-527-31672-4

industry due to the relative ease and cost efficient way of separation and reutilization of the heterogeneous catalyst compared to the homogeneous catalyst.[4]

As an example of homogeneous catalyst, manganese Schiff base complexes are good in epoxidation reactions showing high activity and selectivity. The manganese Schiff base complexes can easily deactivate in solution as homogeneous catalyst due to the formation of μ-oxo dimers and some polymeric species. Strategies to stabilize the manganese Schiff base catalyst, involve for example heterogenization of the complexes onto solid supports.[5] Solid supports such at MCM-41 and metal organic frameworks (MOFs) are examples that were tested. The high surface area and large pore diameter channel of the MCM-41 support makes it an attractive support. MCM-41 also contains a lot of silanol groups on the surface which makes it suitable to anchor metal complexes onto the surface via amino linkers.[6] A relatively new class of crystalline porous material is metal-organic frameworks (MOFs). MOFs have a large surface area as well as pore volumes.[7] Initially studies on these frameworks were focussing on the gas sorption properties of the MOFs. In recent years the possibility of using the MOFs as a heterogeneous catalyst/support was of great interest.[8] It was found that post-modifications of the MOFs play a key role in the formation of catalytically active sites.[9]

---

[4] E. Farnetti, R.D. Monte, J. Kašpar, *INORGANIC AND BIO-INORGANIC CHEMISTRY – Homogeneous and Heterogeneous catalysis*, 2nd Volume, EolSS Publishers Co. Ltd., Oxford, United Kingdom, **2009**, p 50-55. ISBN: 978-1-84826-665-0

[5] P. Oliveira, A. Machado, A.M. Ramos, I.M. Fonseca, F.M. Braz Fernandes, A.M. Botelho do Rego, J. Vital, *Catalysis Communications* **2007** (8) 1366-137, "Anchoring manganese acetylacetonate complex on MCM-41: Catalytic testing on limonene oxidation". DOI: 10.1016/j.catcom.2006.12.004

[6] D.T. On, D. Desplantier-Giscard, C.D. Danumah, S. Kaliaguine, *Applied Catalysis A: General* **2003** (253) 545-602, "Perspectives in catalytic applications of mesostructured materials". DOI: 10.1016/S0926-860X(03)00195-9

[7] G. Férey, *Chem. Soc. Rev.* **2008** (37) 191-214, "Hybrid porous solids: past, present, future". DOI: 10.1039/b618320b

[8] A. Corma, H. Garcı́a and F. X. Llabrés i Xamena, *Chem. Rev.* **2010** (110) 4606-4655, "Engineering Metal Organic Frameworks for Heterogeneous Catalysis". DOI: 10.1021/cr9003924

[9] M. J. Ingleson, J. P. Barrio, J. B. Guilbaud, Y. Z. Khimyak and M. J. Rosseinsky, *Chem. Commun.* **2008** 2680-2682, "Framework functionalisation triggers metal complex binding". DOI: 10.1039/B718367D

Another class of compounds that was found to have catalytic applications are Fischer carbene complexes (FCCs). The first Fischer carbenes were studied by Fischer and Maasböl.[10] FCCs are known for their double bond between the carbene carbon and the transition metal center. Fischer carbene complexes are known to have characteristics such as an electrophilic carbene carbon and a transition metal center with a relative low oxidation state.[11] Fisher carbene complexes (FCCs) are known to have applications in organic synthesis (*e.g.* the formation of an indolocarbazole ring system through the annulation of Fischer carbene intermediates)[12] and catalysis (*e.g.* using FCC to metathesize dehyro amino acids[13] and in multi-component reactions or in short MCRs[14]). The application of Fischer carbene as a catalyst will be discussed in **Section 1.2**.

The scope of this thesis focuses on the synthesis and characterization of selected tris(β-diketonato)manganese(III) and Cr-carbene complexes as potential catalysts. Below are presented a selection of catalytic applications of these type of complexes.

---

[10] E.O. Fischer, A. Maasböl, *Angew. Chem. Int. Ed.* **1964** (3) 580-581, "On the Existence of a Tungsten Carbonyl Carbene Complex". DOI: 10.1002/anie.196405801

[11] K. Indrajit, *Organometallic Compounds*, Pragati Prakashan, **2007**, p 47-50. ISBN: 9788183984409

[12] C.A. Merlic, Y. You, D.M. McInnes, A.L. Zechman, M.M. Miller, Q. Deng, *Tetrahedron* **2001** (57) 5199-5212, "Benzannulation reactions of Fischer carbene complexes for the synthesis of indolocarbazoles". DOI: 10.1016/S0040-4020(01)00360-X

[13] H. Dialer, K. Polborn, W. Beck, *J. Organomet. Chem* **1999** (589) 21-28, "Metal complexes of biologically important ligands, Part CXVIII. Metathesis of dehydro amino acids with Fischer carbene complexes: synthesis of complexes of amino acid- and peptide-α-carbenes and of isoindoles". DOI: 10.1016/S0022-328X(99)00296-X

[14] M.A. Fernández-Rodríguez, P. García-García, E. Aguilar, *Chem. Commun.* **2010** (46) 7670-7687, "Multi-component reactions involving group 6 Fischer carbene complexes: a source of inspiration for future catalytic transformations". DOI: 10.1039/c0cc02337j

1.1 Tris(β-diketonato)manganese(III), [Mn(β-diketonato)$_3$]

The chemical drying process of alkyd-based paints is taking place in two steps; firstly the unsaturated fatty acid ester side chains are oxidized, and secondly the decay of the newly formed hydroperoxides takes place. The decaying rate of the hydroperoxides (ROOH) are known to be increased by metal catalysis, which improves the overall drying rate of alkyd paints. Cobalt salts were the most widely used catalyst in the oxidative drying process of alkyd-based paints. Since the suspicion of the carcinogenic properties of these cobalt salts were raised, the search for a new drying catalyst was started. Van Gorkum *et al.* looked at the possibility of substituting the cobalt salts with tris(acetylacetonato)manganese(III) [Mn(acac)$_3$]. High catalytic activity was found in the autoxidation of the ethyl linoleate, alkyd resin model compound, when [Mn(acac)$_3$] was used as a catalyst. The catalytic process is summarized in **Scheme 1.1**.[15]
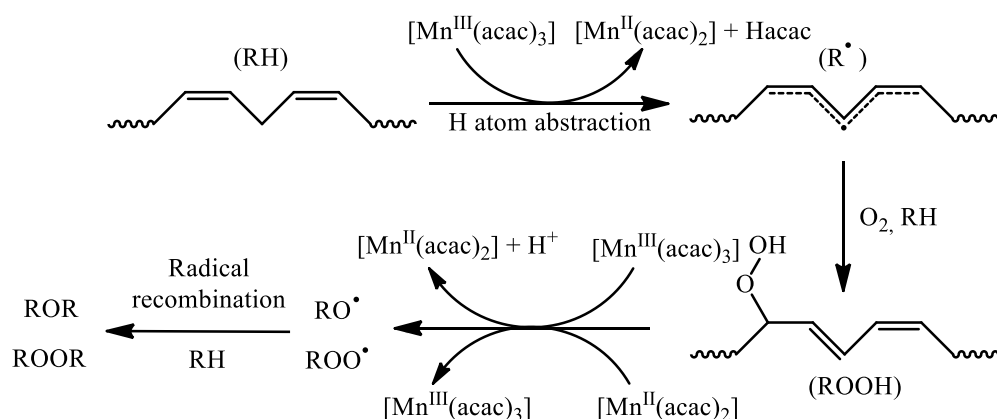
Scheme 1.1: The decay of ethyl linoleate (EL) catalyzed by the [Mn(acac)$_3$] complex. "Reprinted (adapted) with permission from (R. van Gorkum, E. Bouwman, J. Reedijk, *Inorg. Chem.* **2004** (43) 2456-2458, "Fast Autoxidation of Ethyl Linoleate Catalyzed by [Mn(acac)$_3$] and Bipyridine: A Possible Drying Catalyst for Alkyd Paints". DOI: 10.1021/ic0354217). Copyright (2004) American Chemical Society."

Due to the easy deactivation of manganese Schiff base complexes in solution, studies to stabilize the complexes were started. As briefly discussed in the introduction, stabilization of these complexes by the heterogenization of the manganese Schiff base complexes onto solid supports could be a solution. Examples of this heterogenization was done by anchoring acetylacetonate (acac) complexes onto surfaces by the use of an amine functionalized activated carbon linkers by

---

[15] R. van Gorkum, E. Bouwman, J. Reedijk, *Inorg. Chem.* **2004** (43) 2456-2458, "Fast Autoxidation of Ethyl Linoleate Catalyzed by [Mn(acac)$_3$] and Bipyridine: A Possible Drying Catalyst for Alkyd Paints". DOI: 10.1021/ic0354217

Valente *et al.*([Co(acac)$_2$] and [Cu(acac)$_2$]) and Oliveira *et al.*([Co(acac)$_2$]).[16,17] Oliviera *et al.* synthesized the heterogenized catalyst by functionalizing the MCM-41 with a 3-aminopropyltrimethoxysilane linker and then ultimately anchoring the [Mn(acac)$_2$] complex onto the linker ([Mn(acac)$_2$]APTS@MCM-41). This heterogenized catalyst was tested by observing a limonene oxidation with *t*-butyl hydroperoxide (*t*-BHP) and a polymer as a main product. The [Mn(acac)$_2$]APTS@MCM-41 catalyst was determined to be stable as the turn over frequency (TOF) stayed constant.[18]

Rowsell and Yaghi reported that IRMOF-3 contains amino groups in the cubic structure. These amino groups are not taking part in the formation of the 3-D framework and therefore functionalizing the MOF surface. Bhattacharjee *et al.* reported the binding of [Mn(acac)$_2$] onto IRMOF-3 through the functional amino group via a one-step post-synthesis route creating the IRMOF-3[Mn] heterogenized catalyst. They illustrated that the IRMOF-3[Mn] is a highly selective, non-leaching and reusable catalyst in the epoxidation of a number of important alkenes. The formation of the heterogenized catalyst and the epoxidation reactions are illustrated in **Scheme 1.2**.[19]

---

[16] A. Valente, A.M. Botelho do Rego, M.J. Reis, I.F. Silva, A.M. Ramos, J. Vital, *Applied Catalysis A: General* **2001** (207) 221-288, "Oxidation of pinane using transition metal acetylacetonate complexes immobilised on modified activated carbon". DOI: 10.1016/S0926-860X(00)00622-0

[17] P. Oliveira, A.M. Ramos, I. Fonseca, A.M. Botelho do Rego, J. Vital, *Catalyst Today* **2005** (102–103) 67-77, "Oxidation of limonene over carbon anchored transition metal Schiff base complexes: Effect of the linking agent". DOI: 10.1016/j.cattod.2005.02.034

[18] P. Oliveira, A. Machado, A.M. Ramos, I.M. Fonseca, F.M. Braz Fernandes, A.M. Botelho do Rego, J. Vital, *Catalysis Communications* **2007** (8) 1366-137, "Anchoring manganese acetylacetonate complex on MCM-41: Catalytic testing on limonene oxidation". DOI: 10.1016/j.catcom.2006.12.004

[19] S. Bhattacharjee, D.A. Yang, W.S. Ahn, *Chem. Commun.* **2011** (47) 3637-3639, "A new heterogeneous catalyst for epoxidation of alkenesvia one-step post-functionalization of IRMOF-3 with a manganese(II) acetylacetonate complex". DOI: 10.1039/C1CC00069A
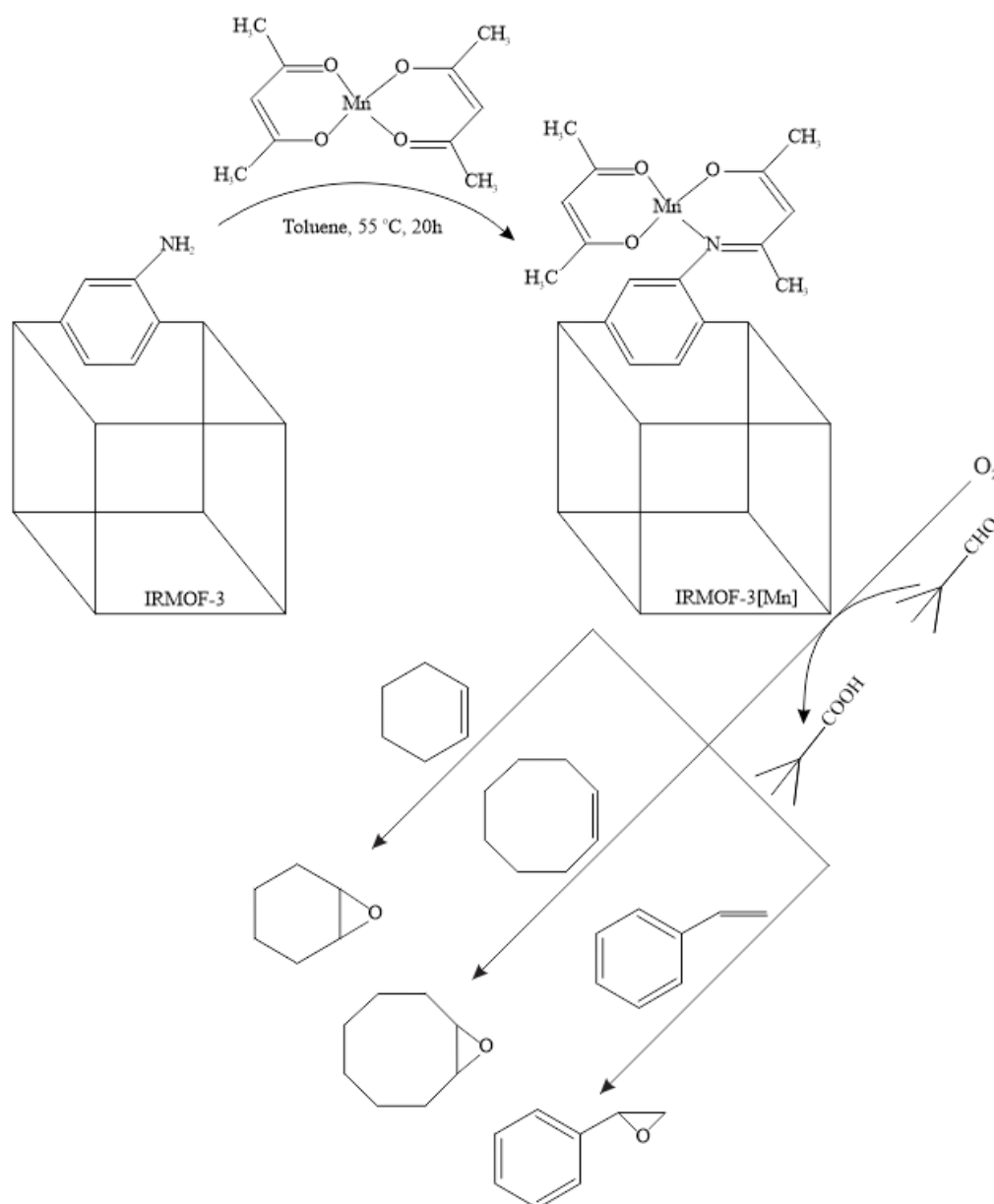
Scheme 1.2: The heterogenization of [Mn(acac)$_2$] onto IRMOF-3 to form IRMOF-3[Mn] and the catalytic synthesis of epoxides from alkenes. Adapted from Ref **19** with permission of The Royal Society of Chemistry**.**

Sodhi and Paul investigated the possibility of [Mn(acac)$_3$] to be anchored onto functionalized silica via an amine linker. A one pot oxidative synthesis of 2-arylbenzimidazole and 2-arylbenzothiazoles as well as the oxidation of benzoins to benzils was studied with the silica functionalized [Mn(acac)$_3$]. Highly active pharmaceuticals are normally derived from 2-benzimidazole and 2-benzothiazole, which makes these products highly favoured. The

functionalization of the silica and the formation of 2-benzimidazole and 2-benzothiazole, is illustrated in **Scheme 1.3**.[20]
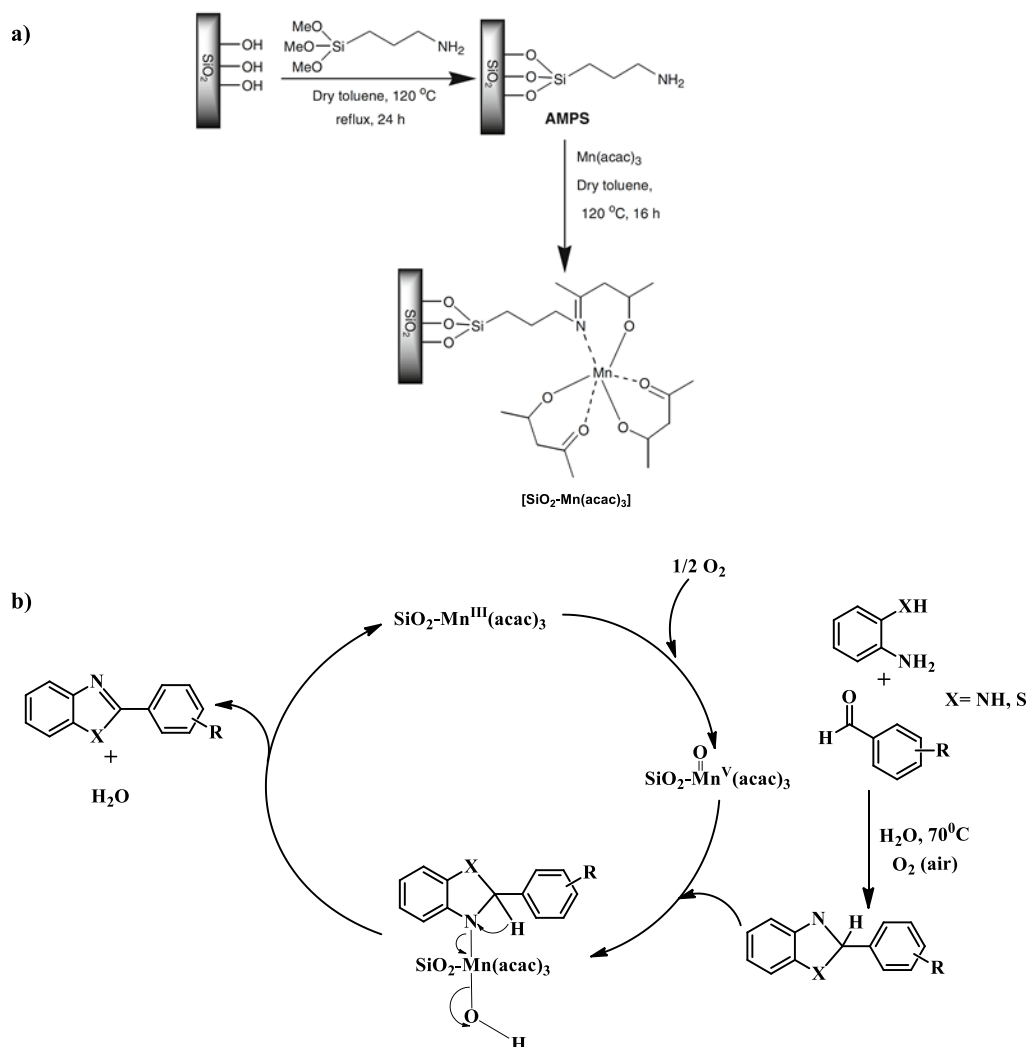
Scheme 1.3: a) Synthesis of silica functionalized [Mn(acac)$_3$] [SiO$_2$-Mn(acac)$_3$]. b) Proposed mechanism for the SiO$_2$-[Mn(acac)$_3$] catalyzed oxidative synthesis of 2-arylbenzimidazoles and 2-arylbenzothiazoles. Springer Catalysis Letters, Nanosized Mn(acac)$_3$ Anchored on Amino Functionalized Silica for the Selective Oxidative Synthesis of 2-arylbenzimidazoles, 2-arylbenzothiazoles and Aerobic Oxidation of Benzoins in Water, 141, 2011, 608-615, R.K. Sodhi, S. Paul, (© Springer Science+Business Media, LLC 2010) "With permission of Springer"

[20] R.K. Sodhi and S. Paul. *Catal. Lett*. **2011** (141) 608-615, "Nanosized Mn(acac)$_3$ Anchored on Amino Functionalized Silica for the Selective Oxidative Synthesis of 2-arylbenzimidazoles, 2-arylbenzothiazoles and Aerobic Oxidation of Benzoins in Water". DOI: 10.1007/s10562-010-0540-8

1.2 Cr-carbene complexes

The use of FCCs as building blocks in multi-component reactions (MCRs) will be discussed in this section. MCRs are defined "as processes in which at least three reagents, added at the same time and under the same conditions, come together in a single reaction vessel to form a new product which contains portions of all of them."[21] The applications in combinatorial chemistry, diverse orientated synthesis, higher atom economy and involvement in cascade reactions of multi-component reactions (MCRs) are most of the reason why it attracted a lot of attention. Here, as an example, two reactions with bulky acetylenes will be discussed. The reaction of FCCs with alkynes can be enhanced when imidazolium ionic liquid is used instead of di-*n*-butyl ether under similar reaction conditions. The imidazolium liquid enhances the activity, selectivity and yield of the reaction. The yield was improved from 27% to 98% when changing the solvent from di-*n*-butyl ether. The reaction in imidazolium liquid is illustrated in **Scheme 1.4**.[21]
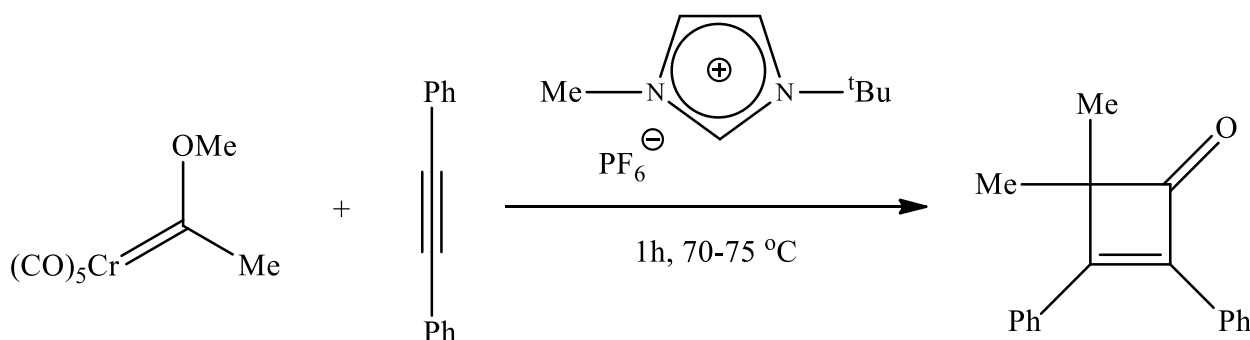
Scheme 1.4: Enhanced reaction of FCCs with alkynes by using imidazolium as solvent[21] with permission of The Royal Society of Chemistry.

Chromium FCCs is thermally reacted to internally silyl-substituted acetylenes, which has highly stable vinylketenes. The vinylketenes that is formed according to the reaction in **Scheme 1.5 a)** are highly stable. The steric congestion formed by the silyl group as well as the stabilization of the ketenes of the silyl groups, have been suggested as a key factor in the final ring closure. The progressions of the reaction are dependent on the nature of the FCCs and alkyne. It was found that the chromium moiety remains linked to the aryl group if the alkynes are aryl-substituted. The

---

[21] M.A. Fernández-Rodríguez, P. García-García, E. Aguilar, *Chem. Commun.* **2010** (46) 7670-7687, "Multi-component reactions involving group 6 Fischer carbene complexes: a source of inspiration for future catalytic transformations". DOI: 10.1039/c0cc02337j

photolytic removal of the chromium moiety as shown in **Scheme 1.5 b)** has (E)-silyl vinylketene as a product which slowly converts into an equilibrium mixture of the (E)-silyl vinylketene and cyclobutanone. [21]

a)

R^1 = n-Bu, Me, Ph, m-MeO-C$_6$H$_4$,

    p-MeO-C$_6$H$_4$, 2-furyl

R = Ph, m-MeO-C$_6$H$_4$, 3,5-di-MeO-C$_6$H$_3$,

    n-Bu,

Si(R^2)$_3$ = TIPS, TBS

30-88%

or

b)

66-73%

R^1 = n-Bu, Ph

R = c-Pr, 2-furyl

TIPS = Si(R^2)$_3$

Scheme 1.5: Cr FCCs thermally reacting to silyl acetylenes. Adapted from Ref 21 with permission of The Royal Society of Chemistry.

The covalent linking of a protein to a surface is crucial in proteome research. Microarray- and biochip-based sensors used in the screening of protein structure and functions with high-throughput is an example of a proteome research study. Sensor devices' performance can be optimized by finding the relevant linkage between a biomolecule and an inorganic solid. Anchoring of proteins covalently to a surface needs to be extremely simplistic and, should form

under ambient conditions in order to preserve the activity and the structure of the protein/enzyme.[22] In recent years great potential of organometallic bioconjugates in radiopharmaceuticals, novel drugs, and even organometallic bioanalysis was released. The conjunctions between metal carboxylic acids and amino acid or peptides through the formation of amides are one of the most popular reactions. Electrophilic alkoxy FCCs [*e.g.* $(CO)_5W=C(OR^1)R^2$] instantly reacts with primary amino or unhindered secondary amino groups, which in turn yields stable Fischer carbene bioconjugates (aminocarbene complexes).[23] Due to the availability, low cost, low intrinsic fluorescence, high mechanical stability and ease of surface modification makes glass surfaces a preferred option. Sawoo *et al.* looked at the use of both glass and Si-wafers as solid supports. The preparation of Si-wafer with the covalently bound FCC onto, is illustrated in **Scheme 1.6**.
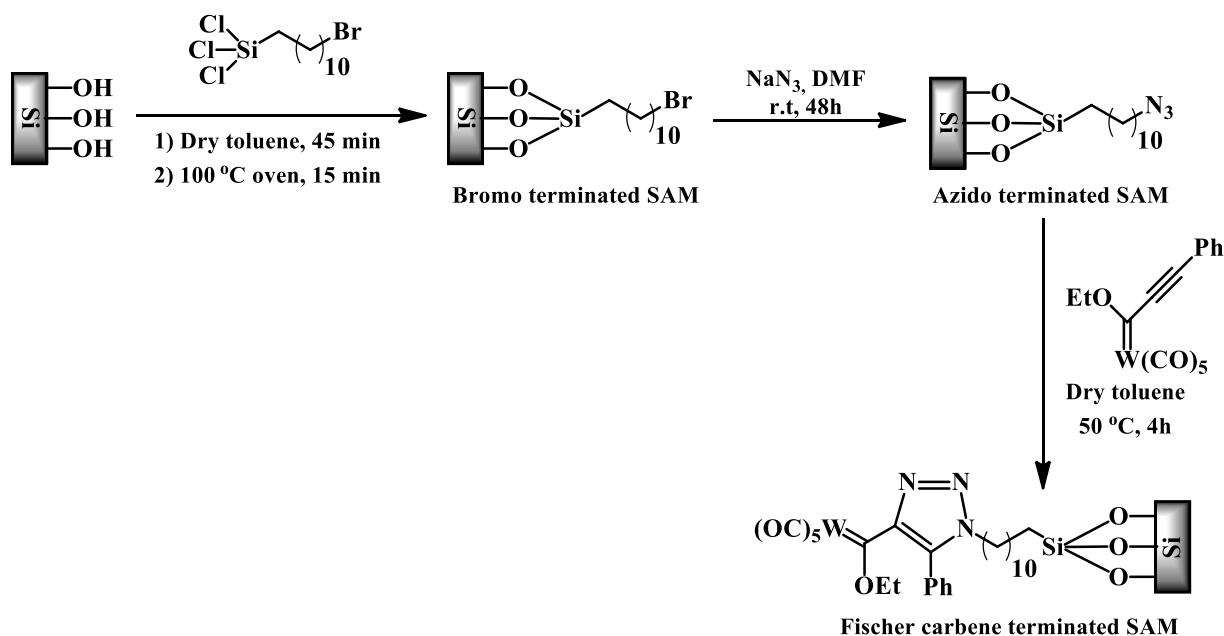
Scheme 1.6: The formation of surface with covalent bound Fischer carbene complex. Adapted from Ref **22** with permission of The Royal Society of Chemistry.

The anchoring of a protein to a Fischer carbene terminated self-assembled monolayer (SAM) is carried out in aqueous borate buffer (pH 9.5) with bovine serum albumin (BSA) at room temperature, as seen in **Scheme 1.7**.

[22] S. Sawoo, P. Dutta, A. Chakraborty, R. Mukhopadhyay, O. Bouloussa, A.Sarkar, *Chem. Commun.* **2008** (45) 5957–5959, "A new bio-active surface for protein immobilization via copper-free 'click' between azido SAM and alkynyl Fischer carbene complex." DOI: 10.1039/B813296H

[23] P. Dutta, S. Sawoo, N. Ray, O. Bouloussa, A.Sarkar, *Bioconjugate Chemistry* **2011** (22) 1202-1209, "Engineering Bioactive Surfaces with Fischer Carbene Complex: Protein A on Self-Assembled Monolayer for Antibody Sensing". DOI: 10.1021/bc200073r
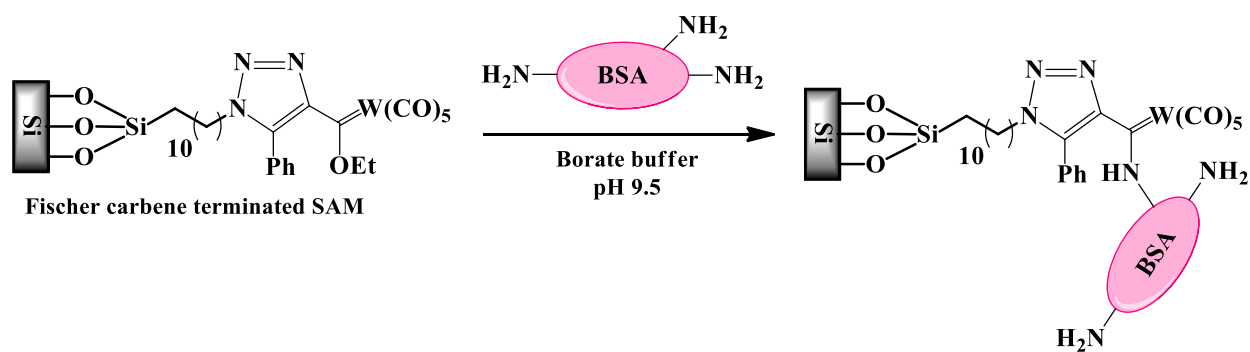
Scheme 1.7: Anchoring of bovine serum albumin (BSA) protein onto the Fischer carbene terminated SAM. Adapted from Ref **22** with permission of The Royal Society of Chemistry.

In 2011 Sawoo *et al.* looked at using a protein A-Fischer carbene terminated SAM on gold surfaces as a biosensor. Protein A binds to the Fischer carbine region of immunoglobulin G (IgG) molecules derived from various mammals in a specific orientation. They found that if the protein A is covalently bound onto the Fischer carbene SAM on gold surface and the inter action of the protein with the IgG is partially reversible when altering the pH, the protein A-Fischer carbene terminated SAM gold surface can be used to sense the IgG and be regenerated after each analysis. The immobilization of rabbit IgG onto a protein A-Fischer carbene terminated SAM gold surface is shown in **Scheme 1.8**.
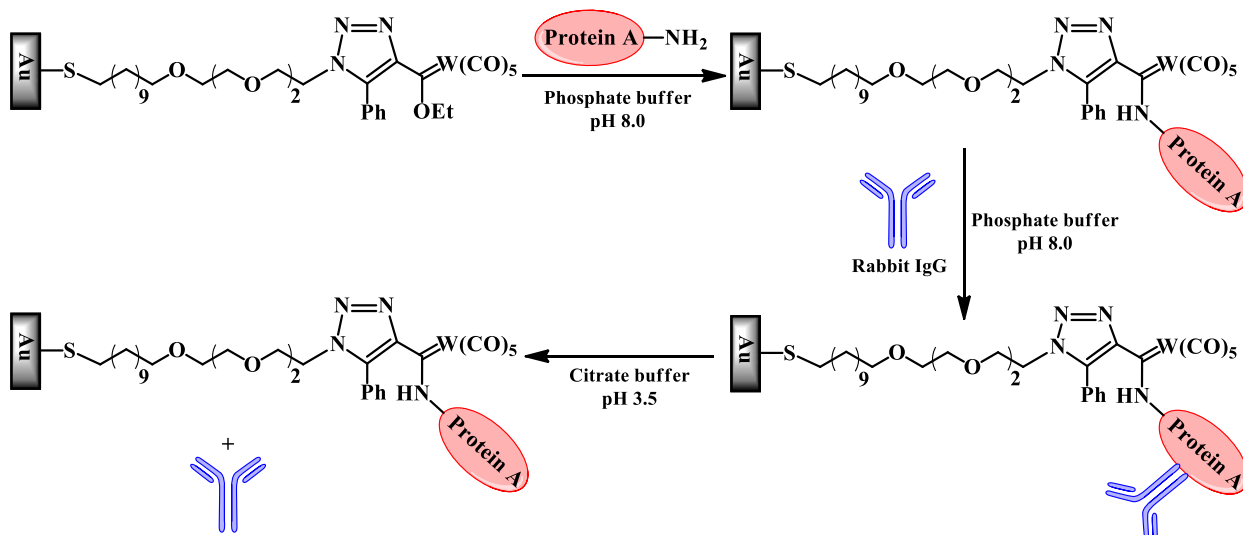
Scheme 1.8: The immobilization of rabbit IgG onto a protein A-Fischer carbene terminated SAM gold surface, as well as the recycling of the protein A-Fischer carbene terminated SAM gold surface. "Reprinted (adapted) with permission from (P. Dutta, S. Sawoo, N. Ray, O. Bouloussa, A.Sarkar, *Bioconjugate Chemistry* **2011** (22) 1202-1209, "Engineering Bioactive Surfaces with Fischer Carbene Complex: Protein A on Self-Assembled Monolayer for Antibody Sensing". DOI: 10.1021/bc200073r). Copyright (2011) American Chemical Society."

1.3 Aims of this study.

The following goals were set for the [Mn(β-diketonato)$_3$] study.

i. The synthesis of [Mn(β-diketonato)$_3$] complexes.

ii. Electrochemical and DFT study of [Mn(dpm)$_3$]. Comparing the results to the related properties of other [Mn(β-diketonato)$_3$] complexes.

iii. Preparation and characterization of 2-D model [Mn(β-diketonato)$_3$] catalyst supported onto amino functionalized Si-wafers. This goal includes the functionalization of the Si-wafer with silane linkers to make the surface suitable for covalent binding of the [Mn(β-diketonato)$_3$] complexes onto it.

iv. Characterization of the amino functionalized 2-D silicon model support as well as the covalent anchored Mn(β-diketonato)$_3$ catalyst onto the amino functionalized Si-wafer by the use of X-ray Photoelectron Spectroscopy (XPS).

v. Testing of the 2-D model [Mn(β-diketonato)$_3$] catalysts. The selected chemical reaction test is the synthesis of urethane from hexamethylenediisocyanate and ethanol.

vi. The preparation of heterogenized [Mn(β-diketonato)$_3$] complexes onto 3-D supports.

vii. Characterization of the immobilization of the [Mn(β-diketonato)$_3$] complexes onto the 3-D supports by XPS and TGA.

viii.   Catalytic testing of a selected [Mn(β-diketonato)$_3$] complex immobilized onto a 3-D support

The following goals were set for the [M(acac)$_3$] study, where M = Cr, Fe, Co, Rh and Ir.

i.   The grafting of [M(acac)$_3$] complexes (with M=Co, Rh and Ir) on Si-wafers and characterizing by XPS. (M=Fe is known)[24]

ii.   The investigation of heterogenization of the [M(acac)$_3$] complexes onto 3-D support system (SiO$_2$). M = Cr, Fe, Co, Rh and Ir.

iii.   Characterization of immobilization of the [M(acac)$_3$] complexes onto the 3-D supports by XPS and TGA.

iv.   Catalytic testing of selected heterogeneous [M(acac)$_3$] complexes on Si-wafers.

The following goals were set for the Cr(0) Fischer carbenes (FCCs) study:

i.   Get an understanding of all the possible isomers/conformations of different Cr(0) FCCs, namely *cis*/*trans* isomerism, *fac*/*mer* isomerism, *E*/*Z* conformations and combinations thereof.

ii.   The investigation of the electrochemical behaviour of Cr(0) FCCs by utilizing cyclic voltammetry and comparing it to other known Cr(0) FCCs.

iii.   Utilizing DFT computational methods to determine the geometric and electronic structure of the Cr(0) FCCs.

iv.   Establishment of relationships between the cyclic voltammetry experimental results and DFT-calculated energies.

v.   Preparation and characterization of 2-D model Cr(0) FCCs covalently bound to amino-functionalized Si-wafers.

vi.   Characterization of the covalent anchoring of Cr(0) FCCs onto the amino-functionalized Si-wafer by the use of X-Ray Photoelectron spectroscopy (XPS).

---

[24] M.M. Conradie, J. Conradie, E. Erasmus, *Polyhedron* **2014** (79) 52-59, "Immobilisation of iron tris(β-diketonates) on a two-dimensional flat amine functionalised silicon wafer: A catalytic study of the formation of urethane, from ethanol and a diisocyanate derivative". DOI: 10.1016/S1381-1169(00)00320-4

2 Literature survey

2.1 Introduction

This chapter consists of a literature survey of [Mn(β-diketonato)$_3$] and chromium(0) Fischer carbene complexes. Basic introduction to methods used to characterize these complexes, published methods that were used to synthesize the [Mn(β-diketonato)$_3$] complexes as well as previous characterizations and studies done on the [Mn(β-diketonato)$_3$] and chromium(0) Fischer carbene complexes, will be reviewed.

2.2 Cyclic Voltammetry (CV)[1,2,3]

The most widely used electrochemical technique to study the oxidation and reduction reactions of a species being investigated (analyte) is cyclic voltammetry (CV). During a CV experiment the potential over an electrode, which is immersed in an unstirred solution containing the analyte, is cycled while the resulting current is measured. The cyclic voltammetry scan starts at a potential where no redox reaction takes place (E$_i$). The potential over the working electrode is then changed linearly over time to a potential just after oxidation/reduction takes place (E$_{\lambda 1}$) as illustrated in **Figure 2.1**. A reverse in the linear potential change over the working electrode is induced at a point where the analyte during the first redox reaction is reduced/oxidized, after which the potential is then taken back to the starting point (E$_{\lambda 2}$). The scan rate (speed of linear potential change) is determined by the gradient of the triangular waveform linear potential *vs* time graph which can be repeated, as can be seen in **Figure 2.1**.

[1] P.T. Kissinger, W.R. Heineman, *J. Chem. Educ.* **1983** (60) 702-706, "Cyclic voltammetry". DOI: 10.1021/ed060p702

[2] D.H. Evans, K.M. O'Connel, R.A. Petersen, M.J. Kelly, *J. Chem. Educ.* **1983** (60) 290-293, "Cyclic voltammetry". DOI: 10.1021/ed060p290

[3] D.A. Skoog, D.M. West, F.J. Holler, S.R. Crouch, *Fundamentals of Analytical Chemistry*, 8th edition, Brooks/Cole, Belmont, **2004**, p694-697. ISBN 10: 0030355230 ISBN 13: 9780030355233.
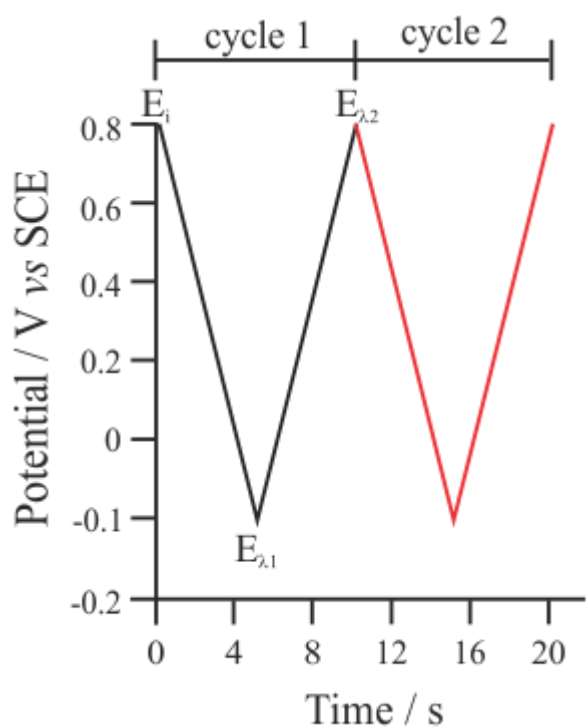
Figure 2.1: Potential changing linearly over time. Reprinted with permission from P.T. Kissinger, W.R. Heineman, J. Chem. Educ. **1983** (60) 702-706. Copyright 1983 American Chemical Society, with stylistic changes.

The resulting voltammogram of cycle 1 in **Figure 2.1** is given in **Figure 2.2**. The graph obtained for the current response to the linear potential change with time (**Figure 2.2**) gives information to better understand the electrochemical reaction, regarding the reversibility (both chemical and electrochemical) as well as the ease of oxidation and/or reduction.
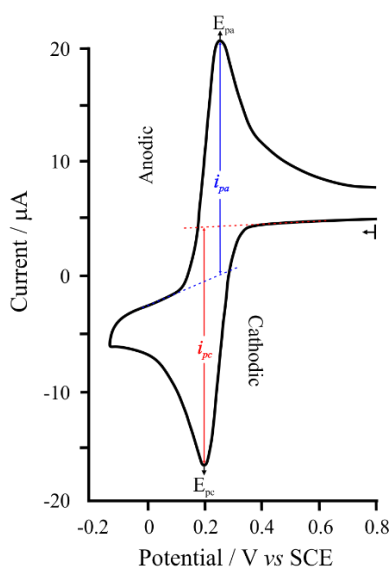
Figure 2.2: Cyclic voltammogram of 6 mM $K_3Fe(CN)_3$ in 1 M KNO_3 at a scan rate of 50 mV.s^{-1}. Reprinted with permission from P.T. Kissinger, W.R. Heineman, J. Chem. Educ. **1983** (60) 702-706. Copyright 1983 American Chemical Society, with stylistic changes.

2.2.1 Important Cyclic Voltammetry Parameters

The four parameters that are of most importance in cyclic voltammetry include: the anodic peak potential (E_{pa}), the cathodic peak potential (E_{pc}) and the magnitudes of the anodic peak current (i_{pa}) and the cathodic peak current (i_{pc}), as illustrated in **Figure 2.2**. The determination of the peak currents is not as direct as obtaining the peak potentials. The peak current is obtained by first drawing in a baseline and then subtracting the current obtained at the baseline and the peak maximum/minimum at the cathodic/anodic peak potential as shown in **Figure 2.2**. The precision with which the baseline is drawn, is crucial in determining correct current values. The ratio (i_{pa}/i_{pc}) between the anodic current (i_{pa}) and the cathodic current (i_{pc}) is used to determine whether the redox couple is chemically reversible. A redox couple that is chemically reversible has a current ratio close to 1 ($i_{pa}/i_{pc} \approx 1$), this indicates that the same amount of the product is obtained after the reduction (or oxidation) of the analyte that was oxidized (or reduced) back to the starting analyte. The peak current, i, is directly proportional to the concentration, C, of the analyte for a reversible system as expressed by the Randles-Sevcik equation, $i_p = (2.69 \text{X} 10^5) n^{1.5} A D^{0.5} C \nu^{0.5}$ (where n is the number of exchanged electrons, A the electrode area (cm^2), D the diffusion coefficient (cm^2 s^{-1}) and C the bulk concentration (mol.cm^{-3}) of the electroactive species.[1]

When there are both an anodic and cathodic redox couple observed during a CV scan, the formal reduction potential ($E^{0'}$) of the couple can be calculated. This formal reduction potential is essentially the potential in the middle of the anodic potential (E_{pa}) and the cathodic potential (E_{pc}) as expressed by **Equation 2.1**.

$$E^{\circ\prime} = \frac{E_{pa} + E_{pc}}{2} \qquad \textbf{Equation 2.1}$$

Electrochemical reversibility is determined by the difference (ΔE_p) between the anodic potential (E_{pa}) and the cathodic potential (E_{pc}). Theoretically a redox couple is electrochemical reversible if ΔE_p is 59 mV at 25 °C for a one electron redox process. Experimental values up to 90 mV is still considered electrochemically reversible,[4] while $90 \leq \Delta E_p \leq 150$ mV is regarded as a quasi-reversible process, and ΔE_p higher than 150 mV is annotated as an irreversible process. Slow

---

[4] H.J. Gericke, N.I. Barnard, E. Erasmus, J.C. Swarts, M.J. Cook, M.A.S. Aquino, *Inorg. Chim. Acta* **2010** (363) 2222-2232, "Solvent and electrolyte effects in enhancing the identification of intramolecular electronic communication in a multi redox-active diruthenium tetraferrocenoate complex, a triple-sandwiched dicadmium phthalocyanine and a ruthenocene-containing β-diketone". DOI: 10.1016/j.ica.2010.03.031

electron transfer at the electrode surface is most likely the cause of peak potential differences (ΔE_P) greater than 90 mV.

$$\Delta E_p = E_{pa} - E_{pc}$$ **Equation 2.2**

2.2.2 Solvent System

The solvent system of a CV experiment consists of two components, the electrolyte and the solvent itself. These components are an integral part of an electrochemical cell, since the potential range that can be studied (solvent window) is determined by the combination of the solvent and the electrolyte. The solvent system must not undergo any redox reaction nor react to the intermediates and/or product formed during the electrochemical reactions of the analyte. Therefore the solvent system must be chemically and electrochemically inert throughout the whole potential range of the solvent window. The solvent should have a low electrical resistance with a supporting electrolyte (*e.g.* tetrabutylammonium hexafluorophosphate) that can lower the electrical resistance even more to promote the undisturbed movement of the charged particles produced during the redox reactions of the analyte.

2.3 Computational Chemistry

2.3.1 Introduction[5,6]

Studying chemical processes by combining mathematical methods and fundamental physics is known as theoretical chemistry. Initially theoretical chemistry was very limited when it came to the size of the molecules that could be studied. Some of the limitations were overcame by using computers as an experimental tool as well as more elaborate mathematic tools, which gave rise to computational chemistry. The calculation of geometric arrangements, relative energies and vibration frequencies should always be treated with some degree of caution due to the amount of approximations that is used in computational chemistry. Computational chemistry can be used to assist in the prediction and understanding of experimental processes that are too dangerous, time consuming, difficult or expensive to do in a laboratory.

---

[5] F. Jensen, *Introduction to Computational Chemistry*, 2nd edition, John Wiley & Sons Ltd, England, **2007**, p1-2.

[6] D.C. Young, *Computational Chemistry: A Practical Guide for Applying Techniques to Real-World Problems*, Wiley-Interscience, New York, **2001**, p3-4.

2.3.2 Basic quantum mechanics[7,8,9,10]

Quantum mechanics mathematically predicts the properties of an individual atom or molecule through describing the behaviour of the electrons by the use of a wave function. Solving (by approximation) the time-independent Schrödinger equation is the main aim of quantum mechanics. The one dimensional equation for a single particle can be presented as:

$$-\frac{\hbar^2}{2m}\frac{d^2\psi(x)}{dx^2} + V(x)\psi(\text{x}) = E\psi(\text{x})$$
Equation 2.3

With Planck's constant $\hbar$, m the mass of the particle, V the potential energy and ψ the wave function is more generally expressed as:

$$H\psi = E\psi$$
Equation 2.4

With the Hamiltonian operator, H, the molecular wave function ψ and the energy E are expressed in the generalized equation of the time-independent Schrödinger equation. The wave function ψ is determined by the electron and nuclear positions of a multiple electron system. An N-particle system's Hamiltonian operator (in atomic units) is generally expressed by the following **Equation 2.5**.

$$H = T + V = -\sum_{i=1}^{N}\frac{\nabla_i^2}{2m_i} + \sum_{i>j}^{N}\frac{q_iq_j}{r_{ij}}$$
Equation 2.5

with

$$\nabla_i^2 = \frac{\partial^2}{\partial x_i^2} + \frac{\partial^2}{\partial y_i^2} + \frac{\partial^2}{\partial z_i^2}$$
Equation 2.6

The Laplacian operator (∇_i^2) acting on particle i (consisting out of electrons and nuclei). The particle's (i) mass and charge is expressed as m_i and q_i respectively, with r_{ij} as the distance between two particles i and j. The particle's potential energy (V) is determined by the Coulomb interactions between the particles and the kinetic energy (T) of the particle is within a wave function. Approximations are needed to determine the Schrödinger equation for an N-particle system where

---

[7] F. Jensen, *Introduction to Computational Chemistry*, 2nd edition, John Wiley & Sons Ltd, England, **2007**, p4-15.

[8] W. Koch, M.C. Holthausen, *A Chemist's Guide to Density Functional Theory*, 2nd edition, Wiley-VCH, Weinhiem, **2001**, p3-6.

[9] D.C. Young, *Computational Chemistry: A Practical Guide for Applying Techniques to Real-World Problems*, Wiley-Interscience, New York, **2001**, p10-11.

[10] W.J. Hehre, *A Guide to Molecular Mechanics and Quantum Chemical Calculations*, Wavefunction, Irvine, **2003**, p21-23.

N > 1. Examples of approximations that were developed are the Born-Oppenheimer and Hartree-Fock approximations.

2.3.3 Basis set[11],[12]

Experimental data is used to compare the performances of the countless amounts of approximations used to solve the Schrödinger equation. The method where no experimental data is fitted when solving the Schrödinger equation is known as the *ab initio* methods. The molecular orbital components can only be defined by the use of a finite basis set, when the orbital components and the chosen basis's coordinate axes corresponds. The accuracy of the description of a system depends on the size of the basis set (smaller basis sets = poorer descriptions) and the type of basis set that is used. The computational effort of the *ab initio* methods scales as M_{basis}^4, therefore, without affecting the accuracy negatively the smallest possible basis set should be used.

The basis functions that are mostly used are Slater Type Orbitals (STOs) and Gaussian Type Orbitals (GTOs). A density functional program that uses the STOs is the Amsterdam density functional theory (ADF) program, the other programs usually make use of the GTOs which comprises out of a number of basis sets available in literature. The pros of the STOs are the appropriate long range decay, the cusp behaviour at the nucleus and the fewer amount of STOs needed to achieve the same level of basis set quality as GTOs.

ADF has a vast amount of basis sets, the one with the fewest number of functions is called the single-zeta (SZ). The exponent of the STOs is commonly denoted as the Greek letter ζ (zeta), hence the origin of the term zeta used for STOs. Double-zeta and triple-zeta consist out of double and triple the amount of basis functions used, respectively. Describing electron distributions in different directions are more effectively done by the use of increasing the amount of basis functions during the calculations. Decreasing the computational time without sacrificing the quality of the result by freezing the deep-core atomic orbitals and reducing the variation size of the basis set, is known as the frozen core approximation. The frozen core approximation is however only

[11] F. Jensen, *Introduction to Computational Chemistry*, 2nd edition, John Wiley & Sons Ltd, England, **2007**, p192-198, 207-208.

[12] G. Te Velde, F.M. Bickelhaupt, E.J. Baerends, C.F. Guerra, S.J.A. Van Gisbergen, J.G. Snijders, T. Ziegler, *J. Comput. Chem* **2001** (22) 931-967, "Chemistry with ADF". DOI: 10.1002/jcc.1056

recommended for an initial geometry optimization and is not a substitution for an all electron calculation.

The same type of basis function, but with a different exponent is needed where one electron is far from the nucleus and the other close, this phenomenon is described by the radial correlation. When two electrons are at opposite sides of the nucleus, basis functions with the same exponent but different angular momentum is needed, this phenomenon is described by the angular correlation. The combination of radial and angular correlations is addressed by the polarization functions. The zeta basis sets can be combined with these polarization functions, *e.g.* triple-zeta plus polarization (TZP).

2.3.4 Density functional theory (DFT) [13,14,15]

In 1964 Hohenberg and Kohn stated that the ground state electronic energy can be determined by just the use of the electron density (ρ), this discovery gave rise to DFT. The Kohn-Sham definition of the DFT energy is:

$$E_{DFT} = T_s[\rho] + E_{ne}[\rho] + J[\rho] + E_{xc}[\rho] \qquad \textbf{Equation 2.7}$$

The Kohn-Sham determined kinetic energy, $T_s[\rho]$, nuclei-electron interaction ($E_{ne}[\rho]$), classical Coulomb electron-electron repulsion ($J[\rho]$) and the non-classical exchange-correlation term ($E_{xc}[\rho]$) is used in **Equation 2.7**

The determination of the kinetic energy $T_s[\rho]$ while using direct density functionals is the main cause of problems, Kohn and Sham created a non-interacting reference system to lessen the problems during the determination of the kinetic energy. By the use of the Kohn-Sham orbitals gave the kinetic energy ($T_s[\rho]$) with good accuracy. Electron-electron repulsion $J[\rho]$ and non-

---

[13] F. Jensen, *Introduction to Computational Chemistry*, 2nd edition, John Wiley & Sons Ltd, England, **2007**, p232-236.

[14] U. von Barth, *Physica Scripta*, **2004** (T109) 9-39, "Basic Density-Functional Theory—an Overview". DOI: 10.1238/Physica.Topical.109a00009/meta

[15] C.J. Cramer, *Essentials of Computational Chemistry – Theories and Models*, 2nd edition, John Wiley & Sons Ltd, Chichester, **2004**, p271, 252-256.

classical contribution $E_{xc}[\rho]$ is combined with $T_s[\rho]$, leaves only a small portion of the energy that is determined by approximation functions.

DFT is known to be the most cost-effective method to achieve a given accuracy.

The DFT methods can differ depending on the functional used to determine the exchange-correlation energy $E_{xc}[\rho]$. This functional is also known as a density functional. Four general functionals are well known: [16],[17]

- **Local density approximation (LDA):** This implies that the density at a certain point is seen as a uniform electron gas. The density at a given position therefore determines the exchange-correlation energy (E_{xc}) at that same position.

- **Generalized gradient approximation (GGA):** Is an addition to the LDA where the first derivative of density is taken into account and the Fermi and Coulomb holes integrating to -1 and 0.

- **Meta-GGA methods:** Meta-GGA (extension of GGA) is dependent on the orbital kinetic density.

- **Hybrid-GGA methods:** Consist out of the combination of GGA and Hartee Fock exchange.

Examples of GGA functionals that consist out of exchange correction, correlation correction and the combined corrections (both exchange correction and correlation corrections) are listed below.

Exchange correction functionals:
- **Becke (B):** In 1988, A.D. Becke proposed a gradient correction in the LDA exchange energy.
- **PW91x:** In 1991, Perdew and Wang proposed the PW91x correction.
- **OPTX:** In 2001, Handy and Cohen proposed the OPTX exchange correction.

Correlation correction functionals:
- **Perdew (P):** In 1986, Perdew proposed the Perdew correlation correction.

---

[16] F. Jensen, *Introduction to Computational Chemistry*, 2nd edition, John Wiley & Sons Ltd, England, **2007**, p242-255.

[17] C.J. Cramer, *Essentials of Computational Chemistry – Theories and Models*, 2nd edition, John Wiley & Sons Ltd, Chichester, **2004**, p257-271.

- **PW91c:** In 1991, Perdew and Wang proposed the PW91c correlation correction.
- **LYP:** In 1988 Lee, Yang and Parr proposed the LYP correlation correction.

Combined corrections:
- **BP86:** The combination of Becke (B) and Perdew (P).
- **PW91:** The combination of PW91x and PW91c.
- **OLYP:** the combination of OPTX and LYP.

Hybrid-GGA functional:
- **B3LYP:** The combination of Becke 3 parameter functional (B3) and LYP.

2.3.5 Amsterdam Density Functional (ADF)[18]

Hartree-Fock-Slater (HFS) is what the computational chemistry program ADF was known as in the seventies when it was created. ADF is constantly being improved and is mainly developed to take full advantage of the density functional theory (DFT). Improvements to the HFS were made by the theoretical chemistry groups of Amsterdam and Calgary, which produced the first class quantum-chemistry package ADF. Gas phase or solution studies of atoms and molecules can be calculated by the use of ADF. Geometry optimization, transition states and spectroscopy characteristics are but only a few properties that can be studied by ADF.

2.3.6 Gaussian 09

Gaussian 09 consist out of a series of electronic structure programs. Gaussian predicts energies, vibrational frequencies, and molecular structures along with molecular properties. Molecules and reactions can be studied at an extensive range of conditions. These conditions include stable species and compounds that are experimentally difficult or impossible to observe, e.g. unstable (short-lived) transition compounds and intermediates.

[18] G. Te Velde, F.M. Bickelhaupt, E.J. Baerends, C.F. Guerra, S.J.A. Van Gisbergen, J.G. Snijders, T. Ziegler, *J. Comput. Chem* **2001** (22) 931-967, "Chemistry with ADF". DOI: 10.1002/jcc.1056

2.4 Theoretical orbital energies *vs.* experimental redox potentials

The Koopman's theorem states that in a closed-shell Hartree-Fock theory the negative orbital energy of the HOMO (highest occupied molecular orbital) is equal to the first ionization energy of a molecular systems.[19] This theory was later used to calculate the electron affinities by the use of the LUMO (lowest unoccupied molecular orbital) energies.[20, 21] The Koopmans' theorem was also extended to the DFT Kohn-Sham orbital energies.[22,23] The calculation of one the energy needed to remove an electron from the HOMO and the energy released when adding an electron to the LUMO of a molecule in the gaseous state, are closely related to the experimentally obtained oxidation potential and reduction potential respectively. From the Marcus quadratic relationship of interfacial electron transfer[24] the following approximate relationship can be derived between the HOMO/LUMO energies and the oxidation/reduction potentials:

$$E_{OX/RED} = a + bE_{HOMO/LUMO} \qquad \textbf{Equation 2.8}$$

$E_{OX/RED}$ represents the oxidation/reduction potential, $E_{HOMO/LUMO}$ the HOMO or LUMO energy and, a and b are constants. Currently more sophisticated pure computational methods are available

[19] T.A. Koopmans, *Physica* **1934** (1) 104-113, "Über die Zuordnung von Wellenfunktionen und Eigenwerten zu den Einzelnen Elektronen Eines Atoms". DOI: 10.1016/S0031-8914(34)90011-2

[20] U.J. Bozkaya, Journal of *Chemical Theory and Computation* **2014** (10) 2041- 2048, "Accurate Electron Affinities from the Extended Koopmans' Theorem Based on Orbital-Optimized Methods". DOI: 10.1021/ct500186j

[21] N. Heinrich, W. Koch, G. Frenking, *Chemical Physics letters* **1986** (124) 20-25, "On the use of koopmans' theorem to estimate negative electron affinities". DOI: 10.1016/0009-2614(86)85005-9

[22] J.P. Perdew, M. Levy, *Physical Review B* **1997** (56) 16021-16028, "Comment on "Significance of the highest occupied Kohn-Sham eigenvalue". DOI: 10.1103/PhysRevB.56.16021; M.E. Casida, *Physical Review B* **1999** (59) 4694-4698, "Correlated optimized effective-potential treatment of the derivative discontinuity and of the highest occupied Kohn-Sham eigenvalue: A Janak-type theorem for the optimized effective-potential model". DOI: 10.1103/PhysRevB.59.4694

[23] S. Hamel, P. Duffy, M.E. Casida, D.R. Salahub, *Journal of Electron Spectroscopy and Related Phenomena* **2002** (123) 345-363, "Kohn–Sham orbitals and orbital energies: fictitious constructs but good approximations all the same". DOI: 10.1016/S0368-2048(02)00032-4

[24] D.D. Méndez-Hernádez, P. Tarakeshwar, D. Gust, T.A. Moore, L.A. Moore, V. Mujica, *Journal of Molecular Modeling* **2013** (19) 2845-, "Simple and accurate correlation of experimental redox potentials and DFT-calculated HOMO/LUMO energies of polycyclic aromatic hydrocarbons". DOI: 10.1007/s00894-012-1694-7

to determine redox potentials.[25,26] However, combining experiment with computed HOMO/LUMO energies in certain cases even give better results than methods based on computational methods alone.[27,28]

2.5 X-ray Photoelectron Spectroscopy (XPS)[29]

X-ray photoelectron spectroscopy is a surface analysis technique where atoms/ions on a surface (top 1-10 nm of surface) absorb photon energy when the sample is irradiated with light of sufficient small wavelength (high photon energy). If the atoms/ions absorbed enough energy, electrons (either core or valence electrons) are emitted from the sample as photoelectrons, see **Figure 2.3**. The kinetic energy (K.E.) that remains on the emitted electron is measured by the XPS and the binding energy (B.E.) of electron in complex is calculated from the equation $KE = h\nu - BE - \emptyset$. Here $h\nu$ is the photon energy from the X-Ray source (from an Al source, $h\nu = 1486.6$ eV) and $\emptyset$ is the spectrometer work function, which is found by calibration. The binding energies are unique in elements and are environment specific, which provide information on the chemical composition and electronic structure of the surface that is being studied. XPS can also give the oxidation state of the atom/ion in the material where normally a shift of *ca.* 1 eV in binding energy is generally equivalent to one oxidation state change. The binding energy of an electron increases as the oxidation state of the atom it is part of, increases. For an atom with a fixed oxidation state, the binding energy of an electron increases as the electronegativity of the ligands attached to the atom increases.[30]

[25] H. Vázquez-Lima, P. Guadarrama, *International Journal of Quantum Chemistry* **2012** (112) 1431-1438, "Analysis of structural factors related to spectroscopic data and redox potentials of CuT1 models through DFT tools". DOI: 10.1002/qua.23130

[26] A. Lewis, J.A. Bumpus, D.G. Truhlar, C.J. Cramer, *Journal of .Chemical Education* **2004** (81) 596-604, "Molecular Modeling of Environmentally Important Processes: Reduction Potentials". DOI: 10.1021/ed081p596

[27] K.G. von Eschwege, J. Conradie, *SA Journal of Chemistry* **2011** (64) 203, "Redox Potentials of Ligands and Complexes – a DFT Approach".

[28] R. Gostynski, R. Fraser, M. Landman, E. Erasmus, J. Conradie, *Polyhedron* **2017** (127) 323-330, "Electrochemical study of Chromium(0) Fischer Carbene complexes: Trends in redox potential". DOI: 10.1016/j.poly.2017.02.018

[29] P. van der Heide, *X-ray Photoelectron Spectroscopy: An introduction to Principles and Practices*, John Wiley & Sons, Inc, Hoboken, New Jersey, **2011**. ISBN: 9781118062531

[30] J. W. Niemantsverdriet, *Spectroscopy in Catalysis*, Edition 3, John Wiley & Sons, Weinheim, p. 44.
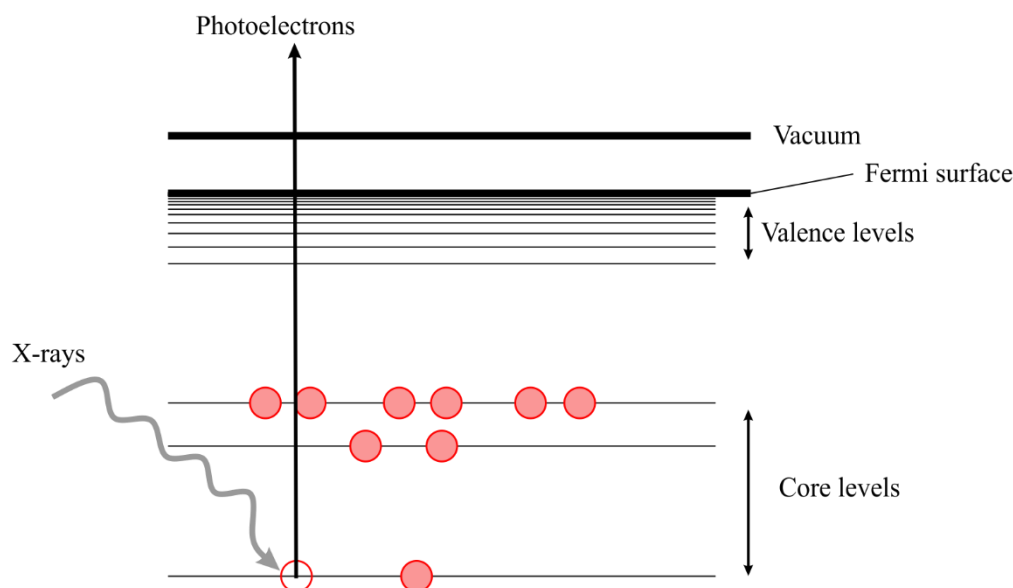
Figure 2.3: Basic principle of XPS

2.6 [Mn(β-diketonato)₃] complexes

2.6.1 Synthesis[31],[32]

Two methods are generally used in the synthesis of [Mn(acac)₃]. **Scheme 2.1** shows the method where acetylacetone is added to $MnCl_2 \cdot 4H_2O$ dissolved in water:ethanol (1:1) and a $KMnO_4$ solution is slowly added. Excess sodium acetate (CH_3COONa) dissolved in ethanol is then added to the mixture.[31] In the presence of acetylacetone the Mn^{2+} is oxidised by $KMnO_4$. The solid product formation drives the reaction to completion. **Scheme 2.2** shows a more direct method of synthesizing [Mn(acac)₃] by adding acetylacetone to an $KMnO_4$ aqueous solution.[32] The precipitation of the product [Mn(acac)₃] drives the reaction to completion. The excess sodium acetate in the first method causes an impure product. Therefore the direct synthesis method was used in the synthesis of [Mn(β-diketonato)₃] complexes in this study presented in Chapter 3 [β-diketonato = benzoylacetonato (ba), trifluoroacetylacetonato (tfaa), phenoyltrifluoroacetonato (tfth), trifluorobenzoylacetonato (tfba), dibenzoylmethanato (dbm), trifluorofuroylacetonato (tffu)].

---

[31] M.M. Ray, J.N. Adhya, N.G. Podder, S.N. Poddar, *Aust. J. Chem.* **1968** (21) 801-802, "A manganese(III) heterochelate: Bis(biguanido)(benzoylacetonato)manganese(III)". DOI: 10.1071/CH9680801

[32] M.N. Bhattacharjee, M.K. Chaudhuri, D.T Khathing, *Dalton Trans*. **1982** (3) 669-670, "Direct Synthesis of Tris(acetylacetonato)manganese(III)". DOI: 10.1039/DT9820000669

a) $MnCl_2 \cdot 4H_2O$ + [β-diketone: H_3C–CO–CH$_2$–CO–CH$_3$] + $KMnO_4$ $\xrightarrow[\text{EtOH}]{CH_3COONa, H_2O}$ [Mn(acac)$_3$ complex structure]

b) $4\ Mn^{2+} + 15$ [β-diketone: H_3C–CO–CH$_2$–CO–CH$_3$] $+ MnO_4^- \longrightarrow 7\ H^+ + 4\ H_2O + 5\ [Mn(acac)_3]$
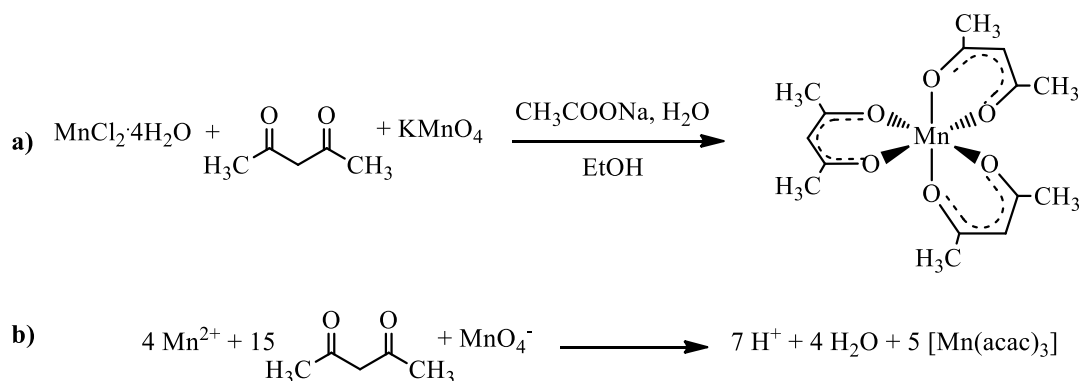
Scheme 2.1: a) Method used in synthesis of [Mn(acac)$_3$] with the balanced redox equation **b)**[31]

a) [β-diketone: H_3C–CO–CH$_2$–CO–CH$_3$] $+ KMnO_4$ $\xrightarrow{H_2O}$ [Mn(acac)$_3$ complex structure]

b) [β-diketone: H_3C–CO–CH$_2$–CO–CH$_3$] $+ KMnO_4 + 4\ H^+ \longrightarrow [Mn(acac)_3] + KOH + 3\ H_2O$
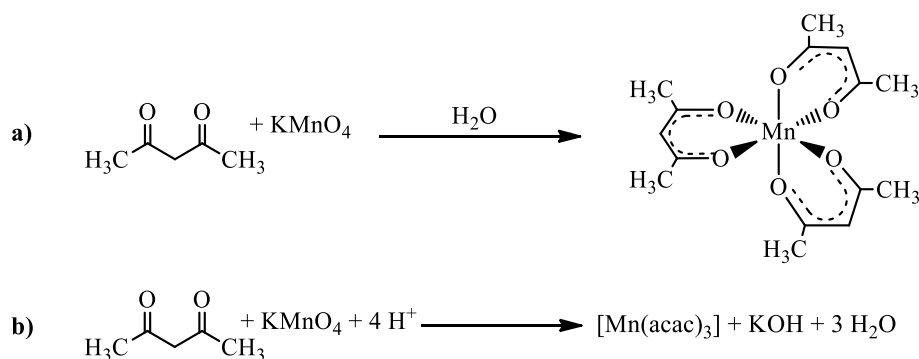
Scheme 2.2: a) The direct synthesis method of [Mn(acac)$_3$] with the balanced equation **b)**.[32]

Due to the hygroscopic nature of the hexafluoroacetylacetone (Hhfac) ligand the [Mn(hfac)$_3$] complex could not be synthesized by using the method in **Scheme 2.2**. A synthesis method to synthesize [Mn(hfac)$_3$] is shown in **Scheme 2.3**. Hexafluoroacetylacetone (Hhfac) and Mn_2O_3 is refluxed in dry n-hexane for 24 h under N_2 atmosphere. Vacuum was used to remove excess solvent and hexafluoroacetylacetone. The product was recrystallized twice in an evacuated ampule at 55-60 $^\circ$C[33] or by sublimation at $65 - 70\ ^\circ$C[34].

---

[33] H. Zhang, B. Li, E.V. Dikarev, *J Clust Sci* **2008** (19) 311-321, "Mn(III) Hexafluoroacetylacetonate as an Oxidative Agent in the Synthesis of Heterobimetallic β-Diketonates". DOI: 10.1007/s10876-007-0174-1

[34] J.R. Bryant, J.E. Taves, J.M. Mayer, *Inorg. Chem.* **2002** (41) 2769-2776, "Oxidations of Hydrocarbons by Manganese(III) Tris(hexafluoroacetylacetonate)". DOI: 10.1021/ic025541z

$$Mn_2O_3 + 6\ (CF_3COCH_2COCF_3) \xrightarrow[\substack{reflux \\ 24\ h}]{dry\ n\text{-hexane}} 2\ [\ldots] + 3\ H_2O$$
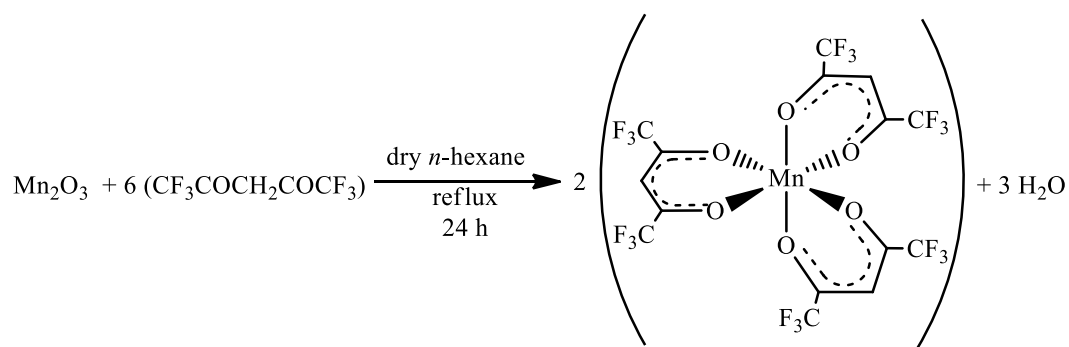
Scheme 2.3: Method used to synthesis [Mn(hfac)$_3$].

2.6.2 Cyclic Voltammetry

The historical cyclic voltammetry studies of [Mn(β-diketonato)$_3$] complexes will be discussed in this section by concentrating on the [Mn(acac)$_3$] complex. The most recent cyclic voltammetry study on [Mn(acac)$_3$] is by S. Carli *et al.* where a 0.1 M LiClO$_4$/CH$_3$CN solvent system was used.[35] The cyclic voltammogram of [Mn(acac)$_3$] in **Figure 2.4** shows two one electron redox reactions namely, the oxidation of the [Mn^{III}(acac)$_3$] species to a Mn^{IV} species (Mn^{III}/Mn^{IV} redox couple) and the reduction of the Mn^{III} species to a Mn^{II} species (Mn^{III}/Mn^{II} redox couple).

Table 2.1: [Mn(acac)$_3$] electrochemical data obtained from **35** in 0.1 M LiClO$_4$/CH$_3$CN, auxiliary electrode Pt, working electrode glassy carbon at 0.1 V.s^{-1} scan rate *vs* SCE.

Mn^{III} / Mn^{II}				Mn^{III} / Mn^{IV}			
E_{pa}/V	E_{pc}/V	ΔE_p/V	Mean of E_{pc} and E_{pa} /V	E_{pa}/V	E_{pc}/V	ΔE_p/V	Mean of E_{pc} and E_{pa} /V
-0.37	0.39	0.760	0.01	0.79	0.97	0.180	0.88

[35] S. Carli, E. Benazzi, L. Casarin, T. Bernardi, V. Bertolasi, R. Argazzi, S. Caramori, C.A. Bignozzi, Physical Chemistry Chemical Physics **2016** (18) 5949-5956 "On the stability of manganese tris(β-diketonate) complexes as redox mediators in DSSCs". DOI: 10.1039/c5cp05524e
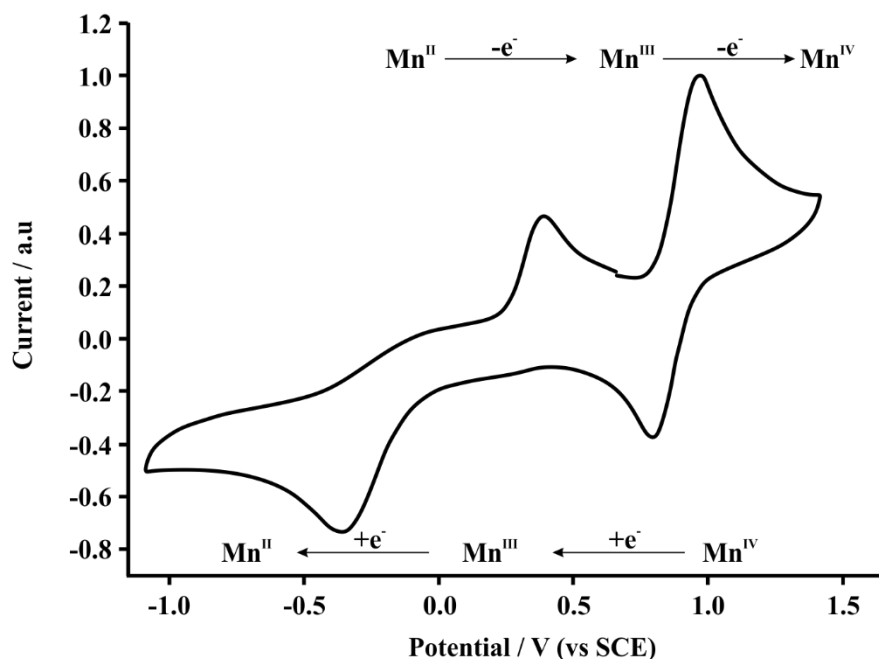
Figure 2.4: Cyclic Voltammogram of [Mn(acac)$_3$]. Adapted from Ref **35** with permission of the PCCP Owner.

Both the Mn^{III}/Mn^{IV} and Mn^{III}/Mn^{II} redox couples are electrochemically irreversible with a ΔE_p value of 0.760 V and 0.180 V respectively (electrochemical reversible if $\Delta E_p < 0.090$ V, quasi-reversible 0.090 V $\leq \Delta E_p \leq 0.150$ V). The chemical irreversibility of the Mn^{III}/Mn^{II} couple might be due to the diffusion of the Mn^{II} to the bulk solution before the reoxidizing to the Mn^{III} could take place or due to slow electron transfer kinetics.

It is known that the solvent can cause the redox potentials *vs* ferrocene to vary. However when converting the redox potentials to values with SCE as reference system[43] the differences are within experimental error and is negligible. This is consistent with the varying solvent polarographic and voltammetric study of [Mn(acac)$_3$] [36], illustrated in **Table 2.2**.

---

[36] G. Gritzner, H. Murauer, V. Gutmann, *Journal of Electroanalytical Chemistry and Interfacial Electrochemistry* **1979** (101) 185-200, "Solvent and salt effects on the redox behaviour of trisacetylacetonato Manganese(III)". DOI: 10.1016/S0022-0728(79)80232-6

Table 2.2: Mean of Epa and Epc of [Mn(acac)₃]found in literature.

Mn^{III}/Mn^{II} E$_{pa}$ and E$_{pc}$ mean			Mn^{III}/Mn^{IV} E$_{pa}$ and E$_{pc}$ mean			Solvent	Ref
As reported in literature		*vs* SCE / V ^{b}	As reported in literature		*vs* SCE / V ^{b}		
V	*vs*		V	*vs*			
0.11	NHE	-0.13	1.21	NHE	0.97	CH₃CN	[37]
-	-	-0.07	-	-	-		[38]
0.64	BBCr ^{a}	-0.09	1.73	BBCr ^{a}	0.98	CH₃CN	[39]
-	-	-0.08	-	-	0.99	CH₃CN	[40]
-	-	-0.14	-	-	0.93	CH₃CN	[41]
-0.52	FcH/FcH$^+$	-0.10	0.571	FcH/FcH$^+$	0.99	CH₃CN	[42]
-	-	0.01	-	-	0.88	CH₃CN	[35]

a Bisbiphenylchromium (BBCr)

b BBCr = 0.73V *vs* NHE, SCE = 0.244 V *vs* NHE, E°' (FcH/FcH$^+$) = 0.66(5) V *vs* NHE in [^{n}(Bu₄)N][PF₆]/CH₃CN and 0.77(5) V

vs NHE in [^{n}(Bu₄)N][PF₆]/DCM [43]

[37] K. Yamaguchi, D.T. Sawyer, *Inorganic Chemistry* **1985** (24) 971–976 "Redox chemistry for the mononuclear tris(picolinato)- tris(acetylacetonata)-, and tris(8-quinolinata) manganese(III) complexes: Reaction mimics for the water-oxidation cofactor in photosystem II". DOI: 10.1021/ic00200a032

[38] O. Sock, P. Lemoine, M. Gross, *Electrochimica Acta.* **1981** (26) 99–109, "Mechanisms of electrochemical reduction of transition metal acetylacetonate complexes". DOI:10.1016/0013-4686(81)80011-4

[39] H. Gritzner, *Journal of Electroanalytical Chemistry* **1979** (101) 177–183, "The polarographic and voltammetric behaviour of acetylacetonato and hexafluoroacetylacetonato complexes in acetonitrile". DOI:10.1016/S0022-0728(79)80231-4

[40] R. van Gorkum, E. Bouwman, J. Reedijk, *Inorganic Chemistry* **2004** (43) 2456–2458, "Fast Autoxidation of Ethyl Linoleate Catalyzed by [Mn(acac)₃] and Bipyridine: A Possible Drying Catalyst for Alkyd Paints". DOI: 10.1021/ic0354217

[41] T. Pacześniak, P. Błoniarz, K. Rydel, A. Sobkowiak, *Electroanalysis* **2007** (19) 945–951, "Electrochemical Catalytic Processes with Hydrogen Peroxide Showing Oxidative and Reductive Properties (Acting as Oxidant or Reductant)". DOI: 10.1002/elan.200603819.

[42] R. Freitag, J. Conradie, *Electrochimica Acta* **2015** (158) 418-426, "Electrochemical and Computational Chemistry Study of Mn(βdiketonato)₃ complexes". DOI: 10.1016/j.electacta.2015.01.147

[43] A.J.L. Pombeiro, *Journal of Organometallic Chemistry* **2005** (690) 6021–6040, "Electron-donor/acceptor properties of carbynes, carbenes, vinylidenes, allenylidenes and alkynyls as measured by electrochemical ligand parameters". DOI: 10.1016/j.jorganchem.2005.07.111

2.7 Heterogeneous catalyst

2.7.1 Introduction

The use of a catalyst to facilitate the formation of products, dates back to the eighteenth century where nitric oxides (NO/NO_2) were used in the oxidation of SO_2 to SO_3.[44] From the start of the twentieth century catalysts played a big role in the chemical industry. Most of the chemicals that are produced go through at least one catalytic step. These industrial processes proceed *via* energetically more favourable mechanisms when using catalysts.[45] This includes running these processes at more reasonable temperature and pressure conditions. Initially catalysts were classified as either homogeneous or heterogeneous. The the term heterogenized catalyst was introduced later. Homogeneous catalysts are known to be in the same phase as where the reaction takes place. Heterogeneous and heterogenized catalysts are in the solid phase and catalyse reactions in the gas or solution phase.[44] Heterogeneous catalysts are mostly favoured in the chemical and petrochemical industry due to the relative ease and cost efficient way of separation and reutilization of the heterogeneous catalyst compared to the homogeneous catalyst.[45] In this section heterogeneous catalysts supported on 3-D supports such as silica (SiO_2 and mesoporous SiO_2 (MCM-41)) will be discussed.

2.7.2 3-D support systems

Heterogeneous catalysts are normally described as inert porous solid materials, which supports the active catalyst, which could be nano-sized particles of expensive materials. This makes the use of heterogeneous catalyst a more economically viable alternative compared to the use of homogenous catalyst.[45] The immobilization of homogeneous catalysts onto solid supports to create heterogeneous catalysts is achieved by anchoring the homogeneous catalyst *via* a silane linker,

[44] E. Farnetti, R.D. Monte, J. Kašpar, *INORGANIC AND BIO-INORGANIC CHEMISTRY – Homogeneous and Heterogeneous catalysis*, 2nd Volume, EolSS Publishers Co. Ltd., Oxford, United Kingdom, **2009**, p 50-55. ISBN: 978-1-84826-665-0

[45] I. Chorkendorff, J.W. Niemantsverdriet, *Concepte of Modern Catalyst and Kinetics*, 2nd edition, WILEY-VCH GmbH & Co. KGaA, Weinheim, **2007**, p1-6. ISBN: 978-3-527-31672-4

exchange reaction with surface OH groups[46] and noncovalent immobilization onto clays or zeolites[47] to name but a view methods. However, these heterogenized catalysts have still not achieved ideal stability and ee (enantiomeric excess) values.[48] Heterogeneous catalysts are easy to separate/recover from the product/reactants as it is in a different phase and in some cases the selectivity to more desired products is increased.

2.7.2.1 [Mn(acac)$_3$] on SiO$_2$

The anchoring of [Mn(acac)$_3$] onto amino functionalized silica was studied by R.K. Sodhi and S. Paul.[49] The [Mn(acac)$_3$] complex was covalently bound to the silica through a 3-aminopropyl(trimethoxy)silane linker. The preparation of the SiO$_2$-[Mn(acac)$_3$] compound is illustrated in **Scheme 2.4**. In this study the activity of this catalyst was tested in the xidative synthesis of 2-arylbenzimidazole and 2-arylbenzothiazoles as well as the oxidation of benzoins to benzils. The [Mn(acac)$_3$] catalyst anchored on SiO$_2$ through the silane linker system that Sodhi and Paul created showed high selectivity, use of molecular oxygen from air as oxidant, mild reaction conditions, high yield of products and recyclability with water as a reaction medium.

[46] Z. Fu, D. Yin, Q. Xie, W. Zhao, A. Lv, D. Yin, Y. Xu, L. Zhang, *Journal of Molecular Catalysis A: Chemical* **2004** (208) 159-166, "Ti complexes assembled HMS as effective catalysts for epoxidation of alkene". DOI: 10.1016/S1381-1169(03)00508-9

[47] P.P. Knops-Gerrits, D.E. De Vos, P.A. Jacobs, *Journal of Molecular Catalysis A: Chemical* **1997** (117) 57-70, "Oxidation catalysis with semi-inorganic zeolite-based Mn catalysts". DOI: 10.1016/S1381-1169(96)00358-5

[48] Q.H. Xia, H.Q. Ge, C.P. Ye, Z.M. Liu, K.X. Su, *Chemical Reviews* **2005** (105) 1603-1662, "Advances in Homogeneous and Heterogeneous Catalytic Asymmetric Epoxidation". DOI: 10.1021/cr0406458

[49] R.K. Sodhi, S. Paul, *Catalysis Letters* **2011** (141) 608-615, "Nanosized Mn(acac)$_3$ Anchored on Amino Functionalized Silica for the Selective Oxidative Synthesis of 2-arylbenzimidazoles, 2-arylbenzothiazoles and Aerobic Oxidation of Benzoins in Water". DOI: 10.1007/BF00772072
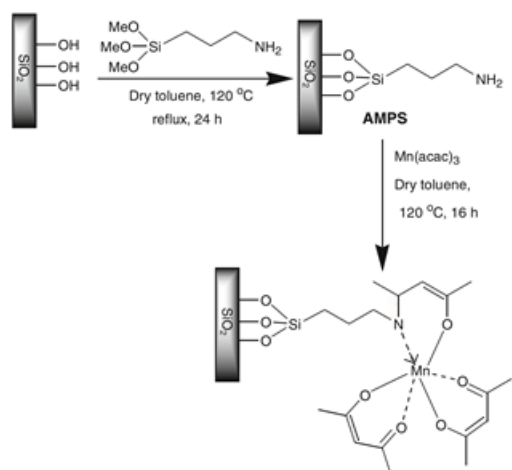
Scheme 2.4: Synthesis of silica functionalized [Mn(acac)$_3$] [SiO$_2$-Mn(acac)$_3$]. "Springer Catalysis Letters, Nanosized Mn(acac)$_3$ Anchored on Amino Functionalized Silica for the Selective Oxidative Synthesis of 2-arylbenzimidazoles, 2-arylbenzothiazoles and Aerobic Oxidation of Benzoins in Water, 141, 2011, 608-615, R.K. Sodhi, S. Paul, (© Springer Science+Business Media, LLC 2010) "With permission of Springer"

2.7.2.2 [Mn(acac)$_2$] grafted on MCM-41[50]

[Mn(acac)$_2$] was successfully anchored onto the MCM-41 (a high surface area with large pore diameter silica) by P. Oliveira *et al.* The silane linker was added onto the MCM-41 surface by first dehydrating the surface overnight and then refluxing a mixture of the MCM-41 support in an anhydrous toluene solution of 3-aminopropyltrimethoxysilane (APTS) under nitrogen atmosphere. The methanol was then distilled off and then the mixture was refluxed for another 6 hours. Afterwards the filtered material was washed with toluene and extracted in a soxhlet apparatus using a DCM (dichloromethane) and diethyl ether (1:1) solution. This modified MCM-41 surface (APTS@MCM-41), was then dried under vacuum at 100 °C overnight. Followed by the anchoring of the [Mn(acac)$_2$] complex onto the APTS@MCM-41 surface by refluxing the modified support in a [Mn(acac)$_2$] solution in dry toluene for 16 hours. The resulting material was then soxhlet extracted with ethanol for 24 hours and dried at 110 °C overnight. The **Scheme 2.5** illustrates the formation of the [Mn(acac)$_2$APTS]@MCM-41.

---

50 P. Oliveira, A. Machado, A.M. Ramos, I.M. Fonseca, F.M. Braz Fernandes, A.M. Botelho do Rego, *Catalysis Communications* **2007** (8) 1366-137, "Anchoring manganese acetylacetonate complex on MCM-41: Catalytic testing on limonene oxidation". DOI: 10.1016/j.catcom.2006.12.004
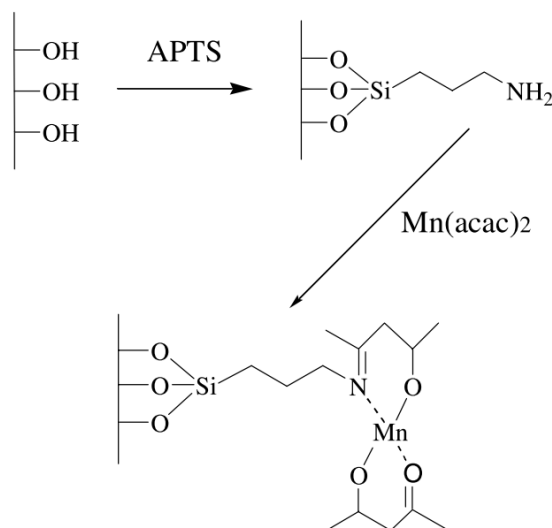
Scheme 2.5: Anchoring of [Mn(acac)$_2$] onto MCM-41 through a silane linker. "Reprinted from Catalysis Communications, 8, P. Oliveira, A. Machado, A.M. Ramos, I.M. Fonseca, F.M. Braz Fernandes, A.M. Botelho do Rego, Anchoring manganese acetylacetonate complex on MCM-41: Catalytic testing on limonene oxidation, 1366-1372, Copyright (2007), with permission from Elsevier."

This catalyst was characterized by techniques such as Inductively Couples Plasma (ICP), X-ray Photoelectron Spectroscopy (XPS), X-Ray Diffraction (XRD), Brunauer-Emmett-Teller (BET), Transmission Electron Microscopy (TEM) and Fourier Transform Infrared Spectroscopy (FTIR). The ICP, XPS and FTIR will be discussed in this section. From the ICP and the XPS results it was concluded that the distribution of the [Mn(acac)$_2$] is favored on the external structure support. The XPS spectra of [Mn(acac)$_2$] and [Mn(acac)$_2$APTS]@MCM-41 is shown in **Figure 2.5**. The Mn $2p_{3/2}$ peak of the [Mn(acac)$_2$] showed a multiplet (two peaks at 641.0 eV and 644.5 eV) that are typical for Mn^{2+} with unpaired electrons. The Mn $2p_{3/2}$ peak of [Mn(acac)$_2$APTS]@MCM-41 has three peaks at 640.7, 642.2 and 644.6 eV. The peaks at 640.7 and 644.6 eV are within experimental error the same as that of [Mn(acac)$_2$], the second peak was assigned to Mn^{4+} with unpaired electrons. The shift of binding energy can however also be a consequence of the Schiff reaction that took place to anchor the [Mn(acac)$_2$] on the amino-functionalized MCM-41 support. The N:Mn ratio obtained by XPS analysis of 0.6:1 shows that there is a possibility of free [Mn(acac)$_2$] on the suface as a ratio of 1:1 is expected if all of the [Mn(acac)$_2$] is bound to the surface through the silane linker.
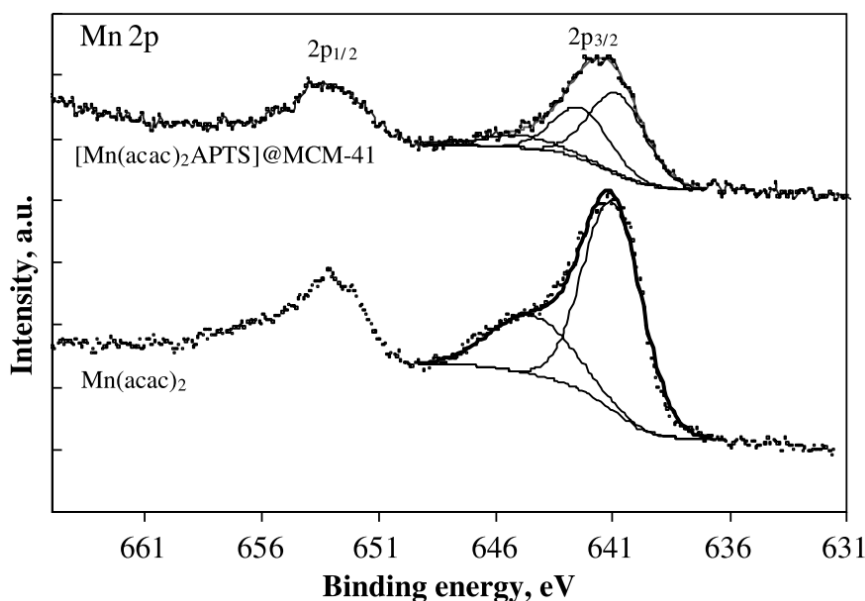
Figure 2.5: The Mn 2p XPS spectra of the catalyst [Mn(acac)2APTS]@MCM-41 and [Mn(acac)$_2$]. "Reprinted from Catalysis Communications, 8, P. Oliveira, A. Machado, A.M. Ramos, I.M. Fonseca, F.M. Braz Fernandes, A.M. Botelho do Rego, Anchoring manganese acetylacetonate complex on MCM-41: Catalytic testing on limonene oxidation, 1366-1372, Copyright (2007), with permission from Elsevier."

The FTIR spectra of MCM-41, APTS@MCM-41, [Mn(acac)$_2$APTS]@MCM-41 and [Mn(acac)$_2$] is seen in **Figure 2.6**. The well-defined bands of [Mn(acac)$_2$] at 1607, 1513 and ~1390 cm^{-1} are allocated to v(C=O), v(C=C) and δ(CH$_3$) respectively.[51, 52] The spectra of the MCM-41 and APTS@MCM-41 predominantly have strong bands with the characteristics of the support matrix, surface hydroxyl groups (3770-3300 cm^{-1}) and lattice vibration 1300-750 cm^{-1}. The strong band at 1085 cm^{-1} and 801 cm^{-1} are attributed to v_{as}(Si-O-Si) and v_s(Si-O-Si) respectively with the band

---

[51] K. Nakamoto, P.J. McCarthy, A.E. Martell, *J. Am. Chem. Soc.* **1961** (83) 1066-1069, "Infrared Spectra of Metal Chelate Compounds. II. Infrared Spectra of Acetylacetonates of Trivalent Metals". DOI: 10.1021/ja01466a014

[52] A. Rautiainen, M. Lindblad, L. Backman, R. Puurunen, *Phys. Chem. Chem. Phys.* **2002** (4) 2466-2472, "Preparation of silica-supported cobalt catalysts through chemisorption of cobalt(II) and cobalt(III) acetylacetonate". DOI: 10.1039/B201168A

at ~970 cm^{-1} assigned to v(Si-OH) vibrations. [53, 54, 55] The fact that there is no significant changes observed between the structure sensitive vibrations between the MCM-41 and APTS@MCM-41 shows that the framework is unchanged. The APTS@MCM-41 spectra has an additional peak at ~2960 cm^{-1} when compared to the unmodified MCM-41. This peak is attributed to the aliphatic (-CH$_2$) stretching of the propyl chain of the silane linker. The spectra of the [Mn(acac)$_2$APTS]@MCM-41 catalyst showed a band at 1670 cm^{-1} (slightly shifted from matrix band) which is assigned to the C=N group[56] and a band that is assignable to the vibration of the acetylacetonate ring at ~1575 cm^{-1}.[57]

[53] M.D. Alba, Z. Luan, J. Klinowski, *J. Phys. Chem.* **1996** (100) 2178, "Titanosilicate Mesoporous Molecular Sieve MCM-41: Synthesis and Characterization". DOI: 10.1021/jp9515895

[54] R. Kureshy, I. Ahmad, N.H. Khan, S. Abdi, S. Singh, P. Pandia, R. Jasra, *J. Catal.* **2005** (235) 28, "New immobilized chiral Mn(III) salen complexes on pyridine N-oxide-modified MCM-41 as effective catalysts for epoxidation of nonfunctionalized alkenes". DOI: 10.1016/j.jcat.2004.11.002

[55] S. Shylesh, A.P. Singh, *J. Catal.* 2004 (228) 333, "Synthesis, characterization, and catalytic activity of vanadium-incorporated, -grafted, and –immobilized mesoporous MCM-41 in the oxidation of aromatics". DOI: 10.1016/j.jcat.2004.08.037

[56] K. Nakanishi, P.H. Solomon, *Infrared Absorption Spectroscopy*, Holden-Day Inc., London, **1977.** ISBN: 9781892803009

[57] H.F. Holtzclaw, Collman Jr., J.P. Collman, *J. Am. Chem. Soc.* **1957** (79) 3318-3322, "Infrared Absorption of Metal Chelate Compounds of 1,3-Diketones". DOI: 10.1021/ja01570a006
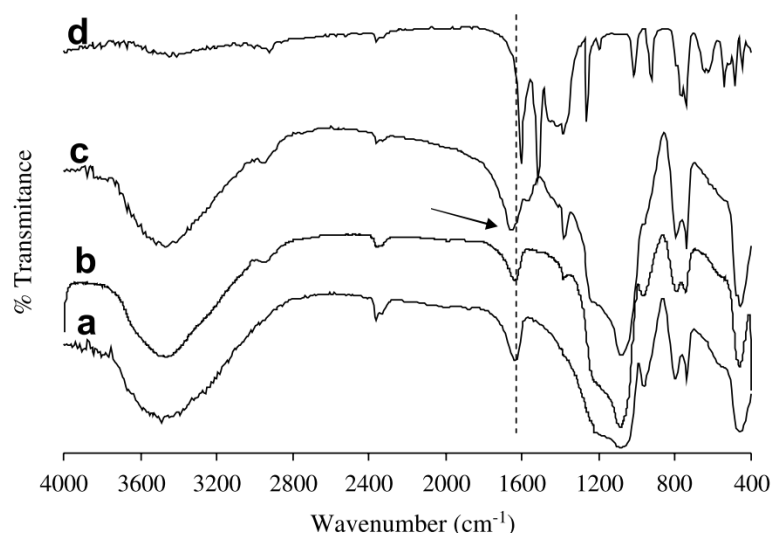
Figure 2.6: The FTIR spectra of a) MCM-41, b) APTS@MCM-41, c) [Mn(acac)2APTS]@MCM-41 and d) [Mn(acac)$_2$]. "Reprinted from Catalysis Communications, 8, P. Oliveira, A. Machado, A.M. Ramos, I.M. Fonseca, F.M. Braz Fernandes, A.M. Botelho do Rego, Anchoring manganese acetylacetonate complex on MCM-41: Catalytic testing on limonene oxidation, 1366-1372, Copyright (2007), with permission from Elsevier."

2.8 Model catalyst supports (2-D)

During a catalytic reaction the catalyst support serves a crucial role in maintaining good separation and dispersion of individual active sites. The study of the metallic particles of catalyst on a molecular level is not effective on 3-D surfaces.[58] The big band-gaps of an industrial catalyst (insulating materials) creates charge problems when spectroscopic techniques are used (e.g. XPS). The dispersion of catalyst into the pores of the 3-D support makes the information that is obtained from surface science techniques such as STM (scanning tunnelling microscopy), AFM (atomic force microscopy), XPS and many more, either impossible to obtain or runs a risk of being misinterpreted.[59,60,61] The photoelectron lines obtained from XPS analysis is normally shifted by

[58] J.W. Niemantsverdriet, *Spectroscopy in Catalysis*, WILEY-VCH GmbH & Co. KGaA, Weinheim, **2007**, p. 19-346. ISBN: 978-3-527-31651-9

[59] X. Lai, D. W. Goodman, *J. Mol. Catal. A. Chem.* **2000** (162) 33-50, "Structure-reactivity correlations for oxide-supported metal catalysts: new perspective from STM". DOI: 10.1016/S1381-1169(00)00320-4

[60] X. Lai, T. P. St Clair, D.W. Goodman, *Faraday Discuss.* **1999** (114) 279-284, "Oxygen-induced morphological changes of Ag nanoclusters supported on TiO$_2$(110)". DOI: 10.1039/A902795E

[61] K.L.E. Eriksson, W.W.Y. Chow, C. Puglia, J.E. Backvall, E. Gothelid, S. Oscarsson, *Langmuir*. **2010** (26) 16349-16354, "Performance of a Biomimetic Oxidation Catalyst Immobilized on Silicon Wafers: Comparison with Its Gold Congener". DOI: 10.1021/la101631m

a few electron volts and distorted due to the charging on the porous 3-D catalysts, which in turn makes the determination of the binding energies and quantification of the peaks problematic. By using 2-D model supports, unfavourable charging can be avoided. Typical model catalyst supports that is used are silicon and aluminium crystals, with an oxidized layer of a few nanometers thick on top. Model catalyst supports create an ideal surface to study the dispersion and chemical states of catalysts.[62,63,64]

2.8.1 Silicon [SiO₂/Si(100)] model support

Despite the fact that zirconium oxide (ZrO_2) has a low surface area, it can be used as both a catalyst and as a catalyst support giving it an amphoteric character.[65] In order to overcome the low surface area of ZrO_2 it can be dispersed and stabilized on silica, SiO_2 (3-D support).[66] Due to the constraints of porous materials discussed in the previous section, the use of $SiO_2/Si(100)$ 2-D model support instead of the 3-D SiO_2 support to study the active sites resulted in the peaks having better resolution and increased the ease of quantification, which is attributed to the flat geometry of the $SiO_2/Si(100)$ model support.[67] This effect is illustrated in **Figure 2.7**.

[62] A. Kolmakov, D.W. Goodman, *Surf. Sci.* **2001** (490) L597-L601, "Scanning tunneling microscopy of gold clusters on TiO₂(110): CO oxidation at elevated pressures". DOI: 10.1016/S0039-6028(01)01318-8

[63] T. Worren, K.H. Hansen, E. Lægsgaard, F. Besenbacher, I. Stensgaard, *Surf. Sci.* **2001** (477) 8-16, "Copper clusters on Al₂O₃/NiAl(1 1 0) studied with STM". DOI: 10.1016/S0039-6028(01)00703-8

[64] L.M. Eshelman, A.M. de Jong, J.W. Niemantsverdriet, *Catal. Lett.* **1991** (10) 201-210, "Preparation of ZrO₂ on flat, conducting SiO₂/Si(100) model supports by wet chemical techniques; X-ray photoelectron spectroscopy and Auger depth profiling". DOI: 10.1007/BF00772072

[65] K. Tanabe, *Mater. Chem. Phys.* **1985** (13) 347-364, "Surface and catalytic properties of ZrO₂". DOI: 10.1016/0254-0584(85)90064-1

[66] T. Yamaguchi, T. Morita, T.M. Salama and K. Tanabe, *Catal. Lett.* **1990** (4) 1-6, "Surface properties of ZrO₂ dispersed on SiO₂". DOI: 10.1007/BF00764864

[67] L.M. Eshelman, A.M. de Jong, J.W. Niemantsverdriet, *Catal. Lett.* **1991** (10) 201-210, "Preparation of ZrO₂ on flat, conducting SiO₂/Si(100) model supports by wet chemical techniques; X-ray photoelectron spectroscopy and Auger depth profiling". DOI: 10.1007/BF00772072
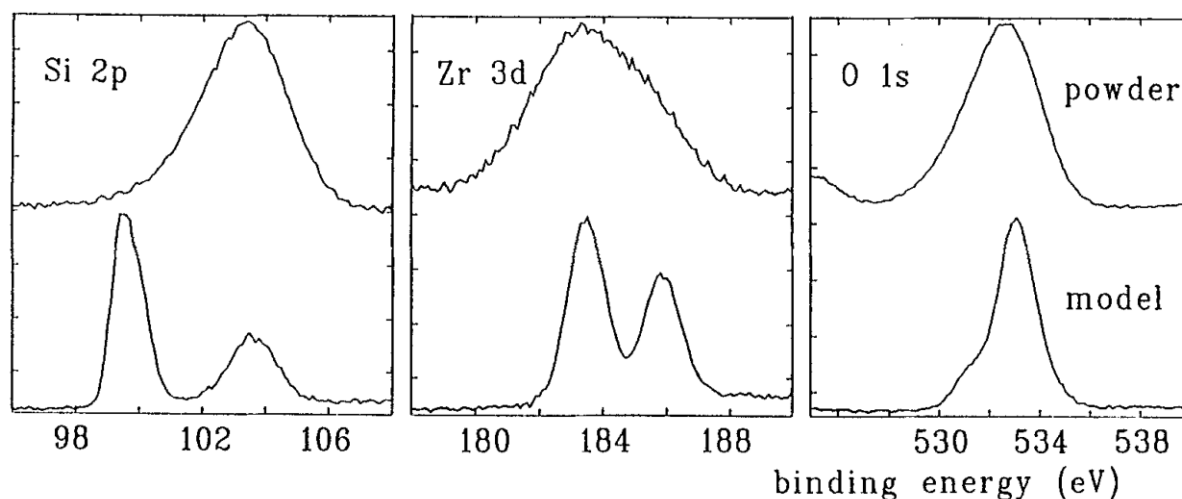
Figure 2.7: XPS spectra of the Si 2p, Zr 3d and O ls peaks of a calcined ZrO_2/SiO_2 powder catalyst (top) and a calcined $ZrO_2/SiO_2/Si(100)$ model catalyst (bottom). The spectra of the powder catalyst have been corrected for charging. "Springer Catalysis Letters, Preparation of ZrO_2 on flat, conducting $SiO_2/Si(100)$ model supports by wet chemical techniques; X-ray photoelectron spectroscopy and Auger depth profiling, 10, 1991, 201-210, L.M. Eshelman, A.M. de Jong, J.W. Niemantsverdriet, (© J.C. Baltzer A.G. Scientific Publishing Company) "With permission of Springer"

The XPS spectra of the ZrO_2 on 3-D SiO_2 (powder) showed broad peaks with a charge shift (7 eV) which was charge corrected shifting the Si 2p peak to 103.4 eV.[68] The Si 2p spectra of the model catalyst showed two peaks, i.e. one asymmetric peak at 103.4 eV (unresolved Si $2p_{3/2}$ and Si $2p_{1/2}$ doublet) of the SiO_2 layer and the silicon of the surface at binding energy of 99.5 eV with full width half maximum (FWHM) value of 1.8 eV and 1.1 eV respectively. The Zr 3d photoelectron lines are not seen as two distinct peaks when the ZrO_2 is dispersed on the SiO_2 powder due to the inhomogeneous charge peak broadening with line widths of 3.4 eV. When the ZrO_2 is dispersed on the 2-D $SiO_2/Si(100)$ the Zr $3d_{5/2}$ and Zr $3d_{3/2}$ peaks are fully resolved with line width of 1.4 eV with Zr $3d_{5/2}$ at a binding energy of 183.3 eV which is ~0.3 eV higher than that of the Zr $3d_{5/2}$ peak (183.0 eV) found for the 3-D catalyst, and is in line with a Zr^{4+} character of ZrO_2. The oxygen O 1s spectra has two contributions, the one O^{2-} from SiO_2 (532.9 eV) and the other O^{2-} from ZrO_2 (531.0 eV). The distinction between the two peaks is only visible on the catalyst where the ZrO_2

[68] C.D. Wagner, W.M. Riggs, L.E. Davis, J.F. Moulder and G.E. Muilenberg, *Handbook of XPS*, Perkin Elmer Corporation, Eden Prairie MN, USA, **1978**. DOI: 10.1002/sia.740030412

is dispersed on the 2-D $SiO_2/Si(100)$ model support. This shows that the finer details of XPS spectra can be observed when using model catalyst supports rather than 3-D supports.[69]

2.9 Homogeneous catalyst dispersion onto solid support systems

There are various ways to disperse homogeneous catalyst onto solid supports such as wet impregnation (fixed on surface with Van der Waals forces),[70] anchoring on the surface through ligand exchange reactions[71] and covalent anchoring of a complex through the use of a linker[72] (functionalized silane). The latter is seen as one of the most popular methods. Wet impregnation and covalent anchoring (silane linkers) of homogeneous catalyst onto solid supports will be discussed in the next sections.

2.9.1 Wet Chemical Impregnation of homogeneous catalysts onto 3-D solid supports[73]

Impregnation of homogeneous catalysts onto solids are normally done where the solid support is introduced to a solution of the catalyst. This method consists out of three steps namely:

[69] L.M. Eshelman, A.M. de Jong, J.W. Niemantsverdriet, *Catal. Lett.* **1991** (10) 201-210, "Preparation of ZrO_2 on flat, conducting $SiO_2/Si(100)$ model supports by wet chemical techniques; X-ray photoelectron spectroscopy and Auger depth profiling". DOI: 10.1007/BF00772072

[70] E. Erasmus, P.C. Thüne, M.W.G.M. (Tiny) Verhoeven, J.W. Niemantsverdriet, J.C. Swarts, *Cat. Commun.* **2012** (27) 193-199, "Anewapproach to silver-catalysed aerobic oxidation of octadecanol: Probing catalysts utilising a flat, two-dimensional silicon-based model support system". DOI: 10.1016/j.catcom.2012.07.013

[71] a) E. Erasmus, J.W. Niemantsverdriet, J.C. Swarts, *Langmuir* **2012** (28) 16477-16484, "Preparation and Characterization of Supported Bimetallic Pd^{IV}-Co^{III} Model Catalyst from Organometallic Single Source Precursor for Aerobic Oxidation of Alcohols". DOI: 10.1021/la3032978

b) E. Erasmus, *S. Afr. J. Chem.* **2013** (66) 216-220, "Hydrogenation of Cinnamaldehyde over an Ionic Cobalt Promoted Alumina-Supported Palladium Catalyst". ISSN: 0379-4350

[72] C. Merckle, J. Blumel, *Topics Catal.* **2005** (34) 5-15, "Improved rhodium hydrogenation catalysts immobilized on silica". DOI: 10.1007/s11244-005-3785-5

[73] C. Perego, P. Villa, *Catal. Today* **1997** (34) 281–305, "Catalyst preparation methods". DOI: 10.1016/S0920-5861(96)00055-7

1. (Contact step) Placing the support in contact with homogeneous catalyst solution for pre-determined time.

2. (Drying step) Removing the liquid from the support *via* drying.

3. (Activation step) Activation of the newly formed heterogeneous catalyst by calcination, reduction or appropriate activation prescribed.

Industrially the contact step can be achieved through two different methods:

1. A solution consisting out of an excess of catalyst is prepared and the support is dipped into the solution for a certain amount of time. The support is then drained and dried. This process can be repeated until one is satisfied with the impregnation of the support. This method is illustrated in **Figure 2.8**.
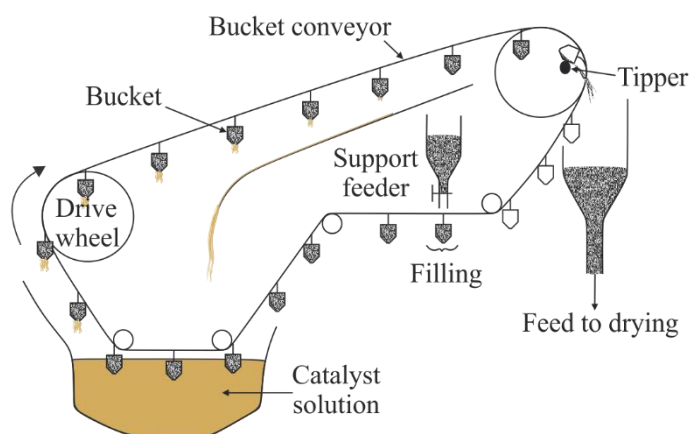
Figure 2.8: Impregnation of support through the excess solution method. Figure is modified from C. Perego and P. Villa publication of Catalyst preparation methods.[73]

2. Repeated application of a solution with known concentration (incipient wetness) of catalyst to support that is in a rotating drum, see **Figure 2.9**. Even though the support is impregnated in a more controlled manner, poorer distribution is observed.
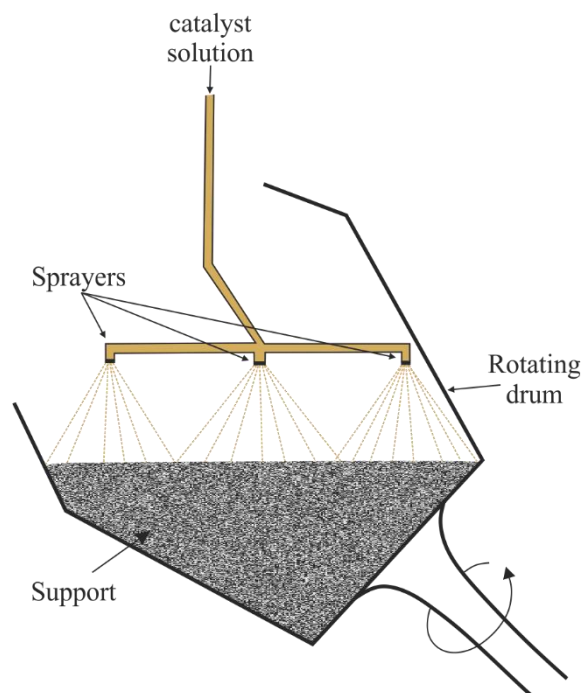
Figure 2.9: Impregnation of support *via* incipient wetness method. Figure is modified from C. Perego and P. Villa publication of Catalyst preparation methods.[73]

2.9.2 Covalent anchoring of homogeneous catalysts onto 2-D catalyst supports[74,75]

The flat 2-D surface of the support has to first go through a few steps of functionalizing before the catalyst can be anchored onto it. When a silicon wafer [Si(100)] is used for example, the following steps are followed to functionalize the surface:

1. Oxidation of Si-wafer. This is achieved by calcining the support in air at 750 $^{\circ}$C for 24 hr to form a thin layer of SiO_2 (-O-Si-O-) over the surface.

2. After etching the surface with a mixture of 1:1 (v/v) H_2O_2 (25% solution) and NH_4OH (35% solution) mixture at room temperature, hydrolyzation of the surface -O-Si-O- layer

[74] M.M. Conradie, J. Conradie, E. Erasmus, *Polyhedron* **2014** (79) 52-59, "Immobilisation of iron tris(β-diketonates) on a two-dimensional flat amine functionalised silicon wafer: A catalytic study of the formation of urethane, from ethanol and a diisocyanate derivative". DOI: 10.1016/S1381-1169(00)00320-4

[75] M. Trzebiatowska-Gusowska, A. Gągor, E. Coetsee, E. Erasmus, H.C. Swart, J.C. Swarts, *Journal of Organometallic Chemistry* **2013** (745-746) 393-403, "Nano islet formation of formyl- and carboxyferrocene, -ruthenocene, -osmocene and cobaltocenium on amine-functionalized siliconwafers highlighted by crystallographic, AFM and XPS studies". DOI: 10.1016/j.jorganchem.2013.08.026

to form silanol groups (Si-OH) is achieved by submerging the oxidized Si-wafer in boiling doubly distilled water for 1 hour. The wafer was then left to dry for 16 hours.

3. Functionalizing the hydrolyzed wafer with a silane is achieved by immersing the hydrolyzed wafer into a solution of 3-aminopropyltrimethoxysilane (500 mg) in dried toluene (20 ml) with gentle stirring for 60 hours. The amino-functionalized wafers was then rinsed three times with isopropanol in a sonicating bath and dried under a nitrogen stream.

The 2-D support surface is now ready for the covalent bonding of the catalyst through appropriate methods determined for the catalyst. To anchor [Fe^{III}(β-diketonato)$_3$] for example, the amino-functionalized wafer was submersed in a 0.5 mol.dm^{-3} solution of [Fe^{III}(β-diketonato)$_3$] in toluene for ~16 hours under gentle reflux. The wafer with covalent bound catalyst was then washed 3 times with isopropanol and dried under a stream of nitrogen. The functionalization of the wafer and the covalent bonding of the catalyst are illustrated in **Scheme 2.6**.
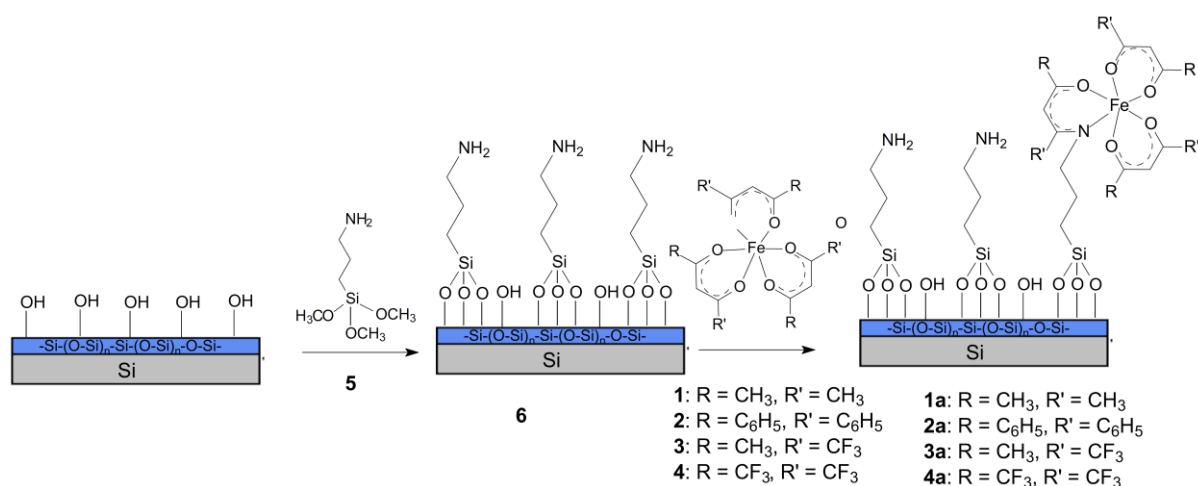
Scheme 2.6: The functionalization of the hydroxylated wafers and covalent bonding of the iron tris(β-diketonates) complexes onto the silane linkers. "Reprinted from Polyhedron, 79, M.M. Conradie, J. Conradie, E. Erasmus, Immobilisation of iron tris(β-diketonates) on a two-dimensional flat amine functionalised silicon wafer: A catalytic study of the formation of urethane, from ethanol and a diisocyanate derivative, 52-59, Copyright (2014), with permission from Elsevier."

2.10 Chromium(0) Fischer Carbene Complexes

2.10.1 Introduction[76],[77],[78]

Fischer carbene complexes were first reported by Fischer and Maasböl,[79] with a characteristic formal double bond between the carbene carbon and a low valent transition metal center (group VI). Since the synthesis of the first carbene complex, [(CO)$_5$WC(OMe)(Ph)] (**Scheme 2.7** (a)) different Fischer type carbenes were reported, see **Scheme 2.7** (b). The electrophilicity of the carbene carbon is stabilized by transferring electron density from the electron-donating (π-donor) substituents, such as heteroatoms or heteroarene rings, to the empty *p*-orbital of the carbene carbon atom. Electron-accepting (π-accepting), carbon monoxide, phosphine or cyclopentadienyl ligands are used to stabilize the low-valent metal center. The phosphine ligands were found to provide the carbene complexes with higher stability in air than the carbonyl equivalents.[80]

[76] K.H. Dötz, P. Tomuschat, *Chem. Soc. Rev* **1999** (28) 187-198, "Annulation reactions of chromium carbene complexes: scope, selectivity and recent developments".

[77] S.C. Nguyen, J.P. Lomont, M.C. Zoerb, P.V. Pham, J.F. Cahoon, C.B. Harris, *Organometallics* **2014** (33) 6149-6153, "Direct Observation of Metal Ketenes Formed by Photoexcitation of a Fischer Carbene using Ultrafast Infrared Spectroscopy".

[78] M. Landman, R. Liu, P.H. van Rooyen, J. Conradie, *Electrochimica Acta* **2013** (114) 205-214, "Electrochemistry of Fischer alkoxycarbene complexes of chromium: The use of density functional theory to predict and understand oxidation and reduction potentials".

[79] E.O. Fischer and A. Maasböl, *Angew. Chem. Int. Ed.* **1964** (3) 580-581, "On the Existence of a Tungsten Carbonyl Carbene Complex".

[80] E.O. Fischer, R. Aumann, *Chemische Berichte* **1969** (102) 1495-1503, "Übergangsmetall-Carben-Komplexe, XI. "Über die Darstellung von *cis*-M(C$_6$H$_5$)$_3$-Methoxy-organylcarben-metall-tetracarbonyl-Komplexen (M = P, As, Sb) des Chroms, Molybdäns und Wolframs aus den M(C$_6$H$_5$)$_3$-Metall-pentacarbonylen durch CH$_3^-$/CH$_3^+$-Addition".

Fischer carbene complexes have application in organic synthesis[81,82] and catalysis.[83] An understanding of the structure and reactivity of these complexes is thus important.
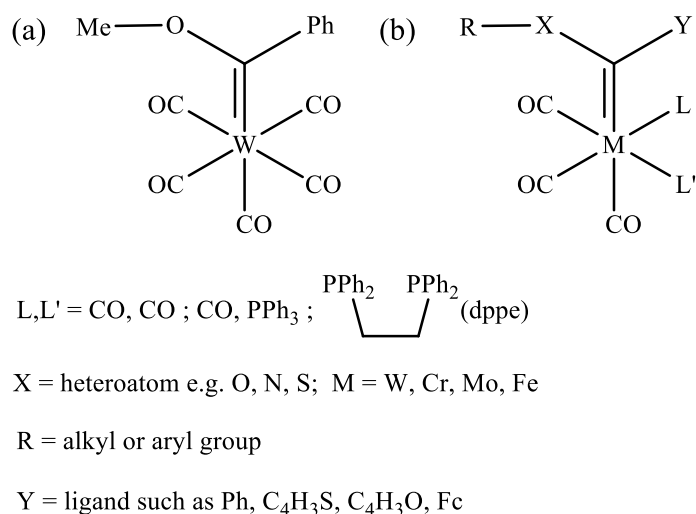
Scheme 2.7: Structure of (a) the first and (b) substituted Fischer carbene complexes.

Fisher carbene complexes can have different conformational preferences due to the different substituents that form part of the complex. When the Y-ligand is a heteroarene ring, *syn* conformation is when the heteroarene ring and the heteroatom are on same side of bond. *Anti* conformation is when the heteroarene ring ligand and heteroatom are on opposite sides of bond, see **Scheme 2.8(a)**. *E* conformation is found when the higher priority moiety on the heteroatom substituent and the metal center lies on the opposite sides of the bond and a *Z* configuration[84] is possible when they are both on the same side of the bond, see **Scheme 2.8(b)**. One or more carbonyl group/s of the Fisher carbene complexes can be substituted with bidentate or monodentate ligands such as diphenylphosphino (dppe) and triphenylphosphine (PPh_3)

[81] J.W. Herndon, *Coordination Chemistry Reviews* **2000** (237) 206–207, "Applications of carbene complexes toward organic synthesis".

[82] C.A. Merlic, Y. You, D.M. McInnes, A.L. Zechman, M.M. Miller, Q. Deng, *Tetrahedron* **2001** (57) 5199, " Benzannulation reactions of Fischer carbene complexes for the synthesis of indolocarbazoles".

[83] H. Dialer, K. Polborn, W. Beck, *Journal of Organometallic Chemistry* **1999** (589) 21, "Metal complexes of biologically important ligands, Part CXVIII. Metathesis of dehydro amino acids with Fischer carbene complexes: synthesis of complexes of amino acid- and peptide-α-carbenes and of isoindoles".

[84] M. Landman, J. Conradie, *Journal of Molecular Structure* **2015** (1094) 36-45, "E versus Z isomers of Fischer aminocarbene complex [Mo(CO)₄(PPh₃){C(NHCy)(2-furyl)}]: N-H⋯O versus C-H⋯O intramolecular hydrogen bonds".

respectively. When a bidentate ligand is present *fac* and *mer* isomers are possible,[85,86] see **Scheme 2.8(c)**. The *fac* isomer is found when the bidentate ligand and the carbene carbon are occupying a face of the octahedron. The *mer* isomer is when the two are occupying the same plane that is passing through the metal center. The monodentate ligand can be positioned either *cis* or *trans* relative to the carbene ligand. The monodentate ligand that is bound $90°$ relative to the carbene carbon is classified as the *cis* isomer. When it is bound $180°$ relative to the carbene carbon it is classified as a *trans* isomer, illustrated in **Scheme 2.8(d)**.

[85] J. Barluenga, K. Muñiz , M. Tomás , A. Ballesteros , S. García-Granda, *Organometallics* **2003** 22 1756-1760," A Simple Approach toward Enantiomerically Pure Fischer Carbene Complexes of Chromium and Molybdenum: Chiral Modification of the Metal Fragment".

[86] M. Landman, R. Liu, R. Fraser, P.H. van Rooyen, J. Conradie, *Journal of Organometallic Chemistry* **2014** (752) 171-182 "Fac and mer dppe-substituted Fischer carbene complexes of chromium: X-ray, DFT and electrochemical study".
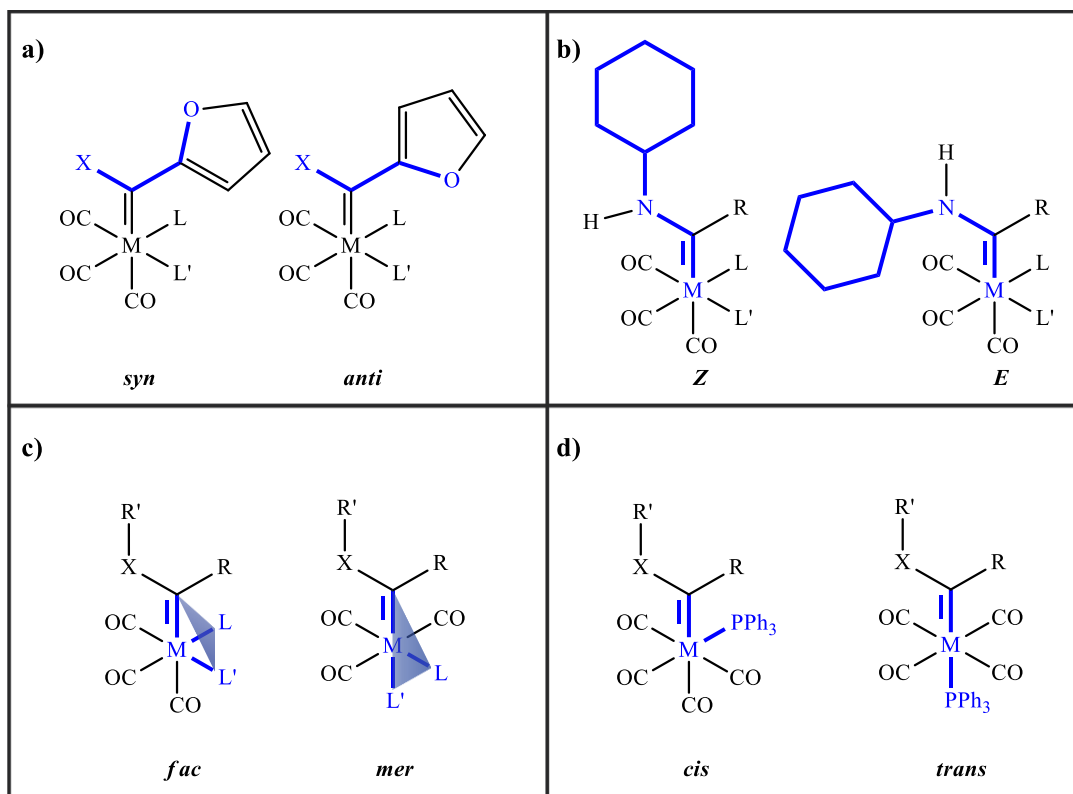
Scheme 2.8: Visualization of the possible conformations of carbenes a) *syn/anti conformations* b) *Z/E conformations* c) fac/mer isomers d) *cis/trans* isomers.

2.10.2　　Electrochemical study [87]

The electrochemical studies done on the group (VI) Fisher carbene complexes have grown in the last couple of years. Studies on chromium Fischer carbene complexes mainly concentrated on the two redox active sites of the complexes, the chromium center and the carbene ligand.[88,89,90]

[87] C. Baldoli, P. Cerea, L. Falciola, C. Giannini, E. Licandro, S. Maiorana, P. Mussini, D. Perdicchia, Journal of Organometallic Chemstry 2005 (690) 5777-5787, "The electrochemical activity of heteroatom-stabilized Fischer-type carbene complexes".

[88] I. Hoskovcová, J. Roháčová, D. Dvořák, T. Tobrman, S. Záliš, R. Zvěřinová, J. Ludvík, *Electrochimica Acta* **2010** (55) 8341-8351 "Synthesis and electrochemical study of iron, chromium and tungsten aminocarbenes Role of ligand structure and central metal nature".

[89] I. Hoskovcová, R. Zvěřinová, J. Roháčová, D. Dvořák, T. Tobrman, S. Záliš, J. Ludvík, *Electrochimica Acta* **2011** (56) 6853-6859" Fischer aminocarbene complexes of chromium and iron: Anomalous electrochemical reduction of p-carbonyl substituted derivatives".

[90] M. Landman, R. Pretorius, B.E. Buitendach, P.H. van Rooyen, J. Conradie, *Organometallics* **2013** (32) 549 1-5503 "Synthesis, Structure, and Electrochemistry of Fischer Alkoxy- and Aminocarbene Complexes of Tungsten: The Use of DFT To Predict and Understand Oxidation and Reduction Potentials".

During the cyclic voltammetry experiments the oxidation of the metal and a red uction of the carbene ligand were observed, see **Figure 2.10**. When more than one isomer of the Cr-carbene exist, more than one chromium centered oxidization peak is sometimes observed, see **Figure 2.11**.[86]
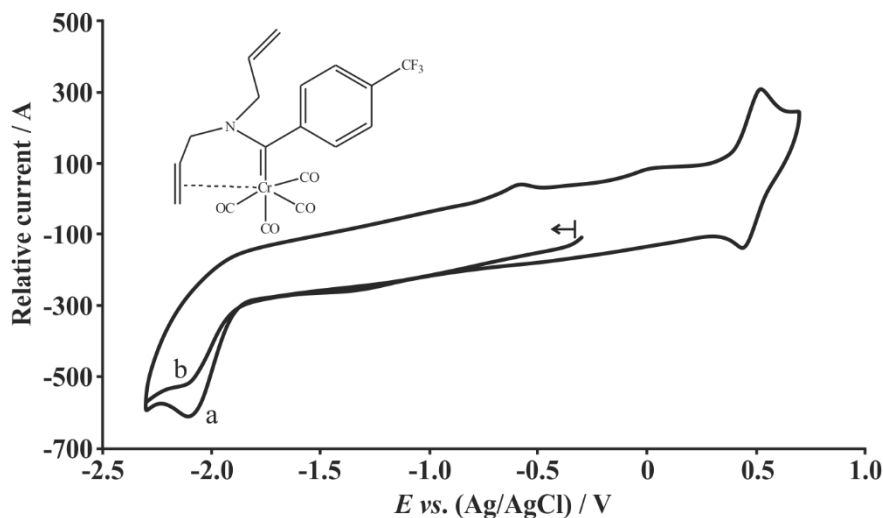
Figure 2.10: Cyclic voltammogram of Fischer carbene in DMF on platinum, scan rate 400 mV.s^{-1} versus Ag/AgCl. a) First scan b) Second scan.[91]
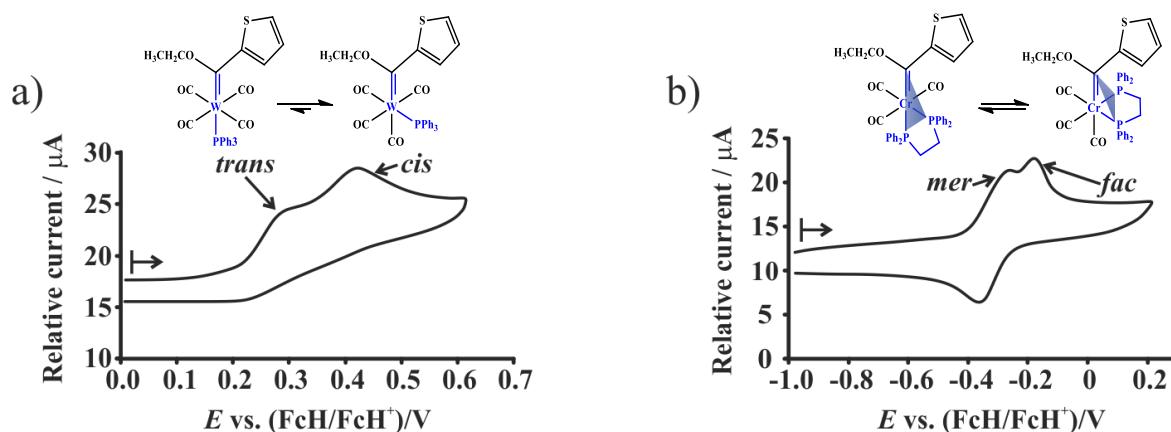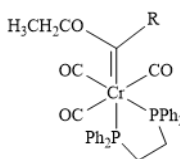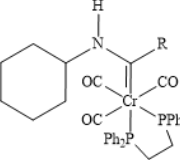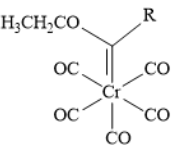
Figure 2.11: Cyclic voltammogram of a) *trans/cis* isomers and b) *mer/fac* isomers.

Selected cyclic voltammetry results published on Cr-carbene complexes, are summarized in **Table 2.3** and **Table 2.4**. The results clearly show that both the Cr-oxidation potential, as well as the carbene carbon reduction potential, is influenced by:

---

[91] I. Hoskovcová, J. Roháčová, L. Meca, T. Tobrman, D. Dvořák, J. Ludvík, *Electrochimica Acta* **2005** (50) 4911-4955 "Electrochemistry of chromium(0)–aminocarbene complexes The use of intramolecular interaction LFER for characterization of the oxidation and reduction centre of the complex".
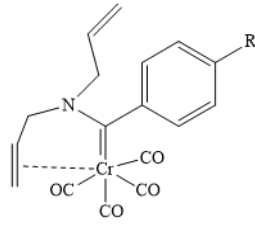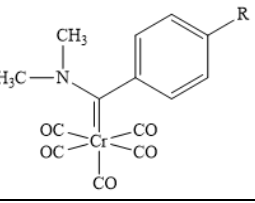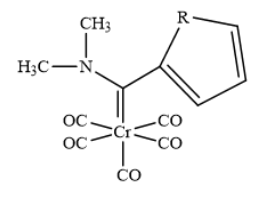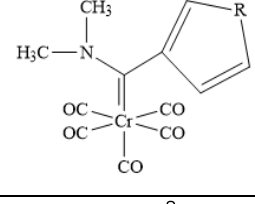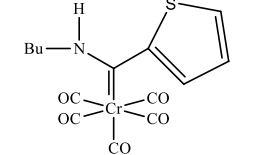
- Different heteroarene ligands (*e.g.* 2-thienyl versus 2-furyl; differently substituted phenyl rings etc.)

- Different heteroatoms (N versus O)

- Different substituents on the metal (*e.g.* dppe versus CO; *N,N*-dimethylamino versus chelated 2-*N*-allyl-*N*allylamino)

Table 2.3: Summary of Cr-carbene complex cyclic voltammetry results

Complex			First oxidation				Reduction				Ref.
	Isomer	R	E_{pa} (V)	E_{pc} (V)	ΔE	$E^{0'}$	E_{pc} (V)	E_{pa} (V)	ΔE	$E^{0'}$	
	mer	2-thienyl	-0.275	-0.353	0.078	-0.314	-	-	-	-	
	fac	2-thienyl	-	-	-	-	-2.162	-	-	-	
	mer	2-furyl	-0.356	-0.410	0.054	-0.383	-2.269				
	fac	2-furyl	-0.235	-	-	-	-2.124	-	-	-	
	mer	2-thienyl	-0.500	-0.569	0.069	-0.534	-2.800	-	-	-	**86**
	fac	2-thienyl	-0.306	-	-	-	-2.545	-	-	-	
	mer	2-furyl	-0.545	-0.600	0.055	-0.573	-2.615	-	-	-	
	fac	2-furyl	-0.368	-	-	-	-	-	-	-	
	-	2-thienyl	0.538	0.453	0.085	0.496	-1.625	-1.552	0.073	-1.552	**78**
	-	2-furyl	0.494	0.414	0.080	0.454	-1.719	-1.649	0.070	-1.649	
	-	2-(N-methylpyrrolyl)	0.463	0.396	0.067	0.430	-2.019	-1.938	0.081	-1.938	
	-	N-methyl-2-(2'-thienyl)pyrrole)	0.558	0.420	0.138	0.489	-1.594	-1.514	0.080	-1.554	
	-	2,2'-thienylfuran	0.531	0.444	0.087	0.488	-1.501	-1.435	0.066	-1.468	

Cyclic voltammograms were measured in 0.1M (^{n}(Bu$_4$)N][PF$_6$]/CH$_3$CN on a glassy carbon working electrode and reported *vs*. FcH/FcH$^+$

Table 2.4: Summary of Cr-carbene complex cyclic voltammetry.

Complex			First oxidation				Reduction	Ref.
	R	Temp	E_{ox} (V)[a]	E_{pa} (V)	E_{pc} (V)	ΔE	E_{red} (V)[b]	
	OCH$_3$		0.210[d]	-	-	-	-1.945	
	H		0.240[d]	-	-	-	-1.905	
	Cl		0.250[d]	-	-	-	-1.865	
	CF$_3$		0.275[d]	-	-	-	-1.765	
	OCH$_3$		0.540[d]	-	-	-	-1.975	
	CH$_3$		0.545[d]	-	-	-	-1.975	
	H		0.560[d]	-	-	-	-1.925	**91**
	Cl		0.575[d]	-	-	-	-1.800	
	CF$_3$		0.590[d]	-	-	-	-1.730	
	H		0.826	0.862	-	0.072	-	
	O	25 °C	0.899	0.959	0.838	0.121	-1.591	
		0 °C	0.897	0.940	0.853	0.087	-	
	S	25 °C	-	0.944	-	-	-1.601	
		0 °C	0.856	0.914	0.808	0.106	-	
	NMe	25 °C	-	0.894	-	-	-1.894	
		0 °C	0.826	0.858	0.793	0.065	-	
	O	25 °C	-	0.954	-	-	-1.909	
		0 °C	0.874	0.924	0.823	0.101	-	
	S	25 °C	-	0.954	-	-	-1.915	**92**
		0 °C	0.832	0.872	0.792	0.080	-	
	NMe	25 °C	-	0.792	-	-	-2.036	
		0 °C	-	0.823	-	-	-	
	-	20 °C	0.565	-	-	85	-1.762	**93**

[a] $E_{red} = E_{1/2}$, DC-Polarography
[b] $E_{ox} = \frac{1}{2}(E_{pa} + E_{pc})$
[89] DC-polarography, dropping mercury electrode (DME) *vs.* standard Ag/AgCl, CV platinum working electrode *vs.* standard Ag/AgCl
[92] Oxidation on a GC-disk electrode, either rotating (voltammetry, controlled-potential electrolyses) or stationary (cyclic voltammetry) in nonaqueous acetonitrile. Reduction was studied by DC polarography on dropping mercury electrode (DME) and by cyclic voltammetry (CV) on hanging mercury drop electrode (HMDE). Results reported *vs.* SCE.
[92] Cyclic voltammograms were measured in 0.1M ((^{n}Bu$_4$)N][PF$_6$]/CH$_2$Cl$_2$) on a glassy carbon working electrode and reported *vs.* FcH/FcH$^+$, with analyte concentration of 0.5 mmol.dm^{-3}

92 R. Metelková, T. Tobrman, H. Kvapilová, I. Hoskovcová, J. Ludvík, *Electrochimica Acta* **2012** (82) 470-477 "Synthesis, characterization and electrochemical investigation of hetaryl chromium(0) aminocarbene complexes".

93 B. van der Westhuizen, P.J. Swarts, I. Strydom, D.C. Liles, I. Fernandez, J.C. Swarts, D.I. Bezuidenhout, *Dalton Transactions* **2013** (42) 5367-5378 "Electrochemical illumination of thienyl and ferrocenyl chromium(0) Fischer carbene complexes". DOI: 10.1039/c3dt32913e

Computational chemistry results on a series of W-carbenes obtained under the same experimental conditions were successfully used to compare the experimentally obtained metal oxidation potential (E_{pa}) and the carbene ligand reduction potential (E_{pc}) with the HOMO (highest occupied molecular orbital) energy and LUMO (lowest unoccupied molecular orbital) energy respectively illustrated in **Figure 2.12**.[94]
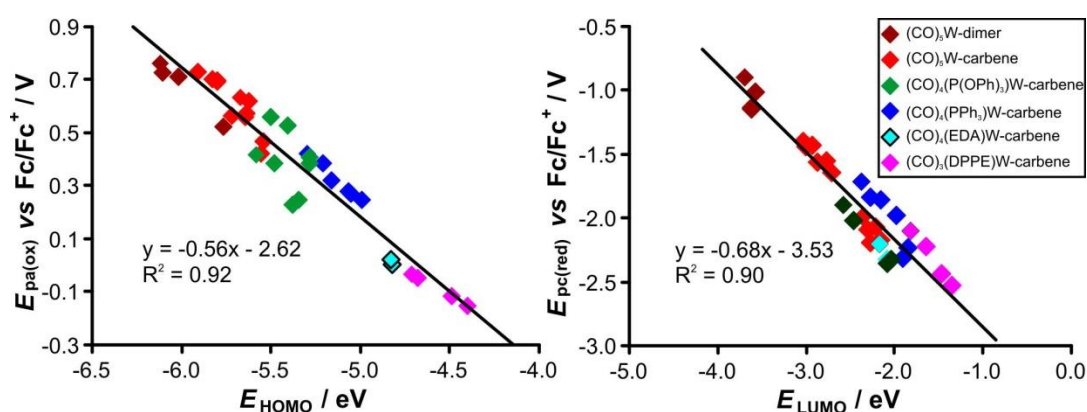
Figure 2.12: Computationally calculated molecular orbital energies against cyclic voltammetry results. (Reprinted from *Journal of Electroanalytical Chemistry* (739), M. Landman, B.E. Buitendach, M.M. Conradie, R. Fraser, P.H. van Rooyen. J. Conradie, "Fischer mono and biscarbene complexes of tungsten with mono and dimeric heteroaromatic substituents", 202-210 **2015**, with permission from Elsevier).

94 M. Landman, B.E. Buitendach, M.M. Conradie, R. Fraser, P.H. van Rooyen. J. Conradie, *Journal of Electroanalytical Chemistry* **2015** (739) 202-210, "Fischer mono and biscarbene complexes of tungsten with mono and dimeric heteroaromatic substituents".

3 Results and Discussion

3.1 Tris(β-diketonato)metal(III) / [M (β-diketonato)₃]

Nine (**1-9**)[1,2,3] [Mn(β-diketonato)₃] [β-diketonato = dipivaloymethanato (dpm), **1**; acetylacetonato (acac), **2**; benzoylacetonato (ba), **3**; dibenzoylmethanato (dbm), **4**; trifluoroacetylacetonato (tfaa), **5**; thenoyltrifluoroacetonato (tfth), **6**; trifluorofuroylacetonato (tffu), **7**; trifluorobenzoylacetonato (tfba), **8** and hexaflouroacetylacetonato, **9**] complexes were synthesized by the use of adapted methods, see **Section 3.1.1**. The structures of the complexes are illustrated in **Scheme 3.1**. [Mn(β-diketonato)₃] complexes **2-9** and a selection of [M(acac)₃] complexes ([Co(acac)₃], **12**; [Rh(acac)₃], **13**, and [Ir(acac)₃], **14**) were grafted onto two dimensional (2-D) Si-wafer supports (**S5**-**S12** and **S29**-**S31** respectively). [Mn(β-diketonato)₃] complexes **1-8** and selection of [M(acac)₃] complexes ([Cr(acac)₃], **10**; [Fe(acac)₃], **11**; [Co(acac)₃], **12**; [Rh(acac)₃], **13**, and [Ir(acac)₃], **14**) were wet impregnated onto various three dimensional (3-D) solid supports (forming **S13**-**S28** and **S32**-**S36** respectively) to form model catalysts. The model 2-D and 3-D catalysts were studied and characterized by the means of XPS, TGA and computational chemistry calculations. Selected 2-D and 3-D catalysts were tested for the catalytic self-solvating reaction between ethanol and hexamethylenediisocyanate (HDI) to form hexamethylenediurethane (HDU) as model of the industrial production of polyurethane.

[1] M.N. Bhattacharjee, M.K. Chaudhuri, D.T Khathing, *Dalton Trans*. **1982** (3) 669-670, "Direct synthesis of tris(acetylacetonato)manganese(III)". DOI: 10.1039/DT9820000669

[2] R. Freitag, J. Conradie, *Electrochimica Acta* **2015** (158) 418-426, "Electrochemical and Computational Chemistry Study of Mn(β-diketonato)₃ complexes". DOI: 10.1016/j.electacta.2015.01.147

[3] P. Magnus, A.H. Payne, M.J. Waring, D.A. Scott, V. Lynch, *Tetrahedron Lett.* **2000** (41) 9725–9730, "Conversion of α,β-unsaturated ketones into α-hydroxy ketones using an MnIII catalyst, phenylsilane and dioxygen: acceleration of conjugate hydride reduction by dioxygen". DOI:10.1016/S0040-4039(00)01727-5

[Mn(dpm)$_3$], **1**   [Mn(acac)$_3$], **2**   [Mn(ba)$_3$], **3**   [Mn(dbm)$_3$], **4**

[Mn(tfaa)$_3$], **5**   [Mn(tfth)$_3$], **6**   [Mn(tffu)$_3$], **7**   [Mn(tfba)$_3$], **8**

[Mn(hfaa)$_3$], **9**
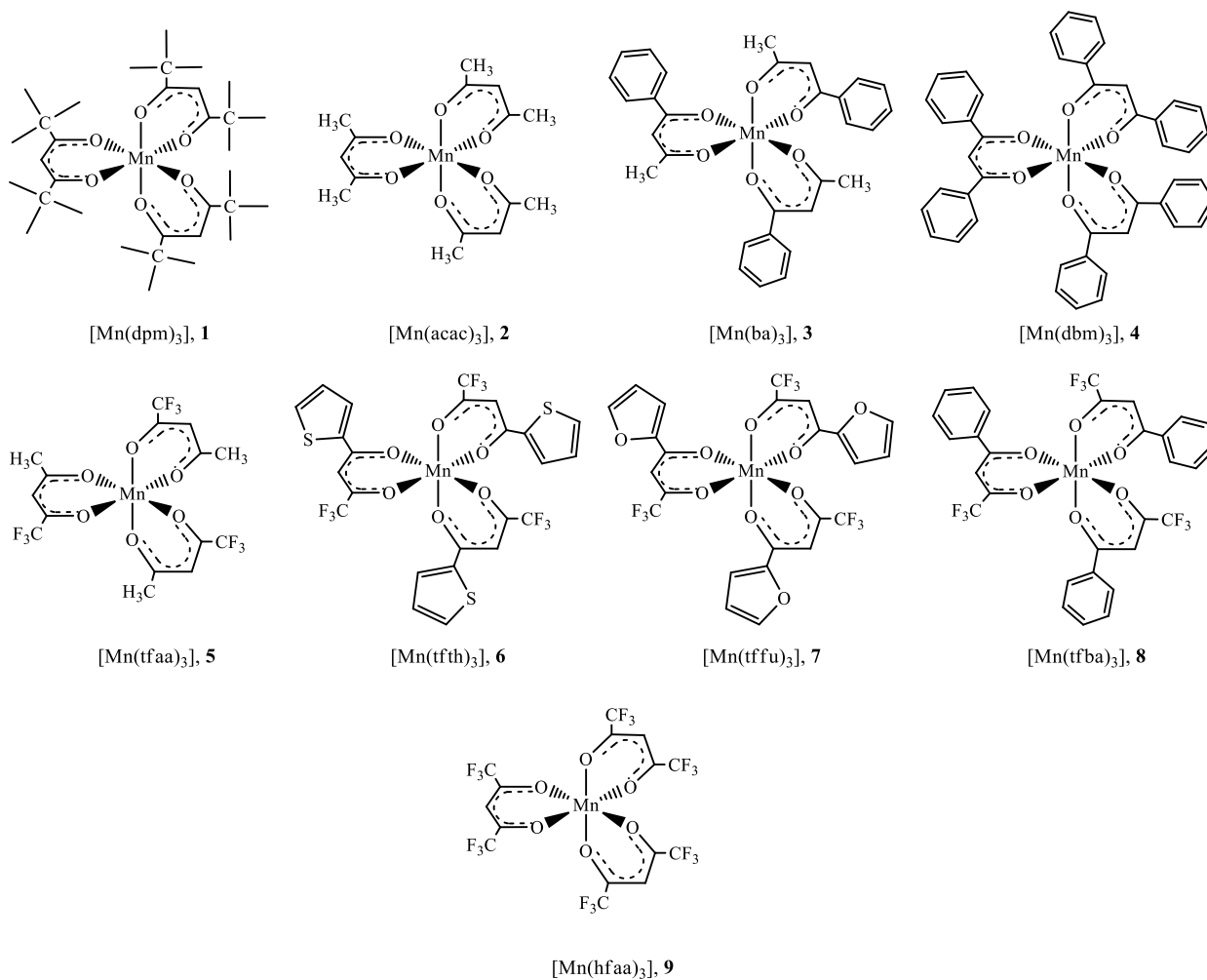
Scheme 3.1: Structures of the [Mn(β-diketonato)$_3$]complexes (**1-9**).

For the [Mn(β-diketonato)$_3$] complexes containing unsymmetrical β-diketonato ligands (RCOCHCOR′)$^-$ with R ≠ R′, *i.e.* complexes **3**, **5–8**., two isomers, namely facial (*fac*) or meridional (*mer*), are possible. The illustration of these isomers can be seen in **Scheme 3.2**.

54
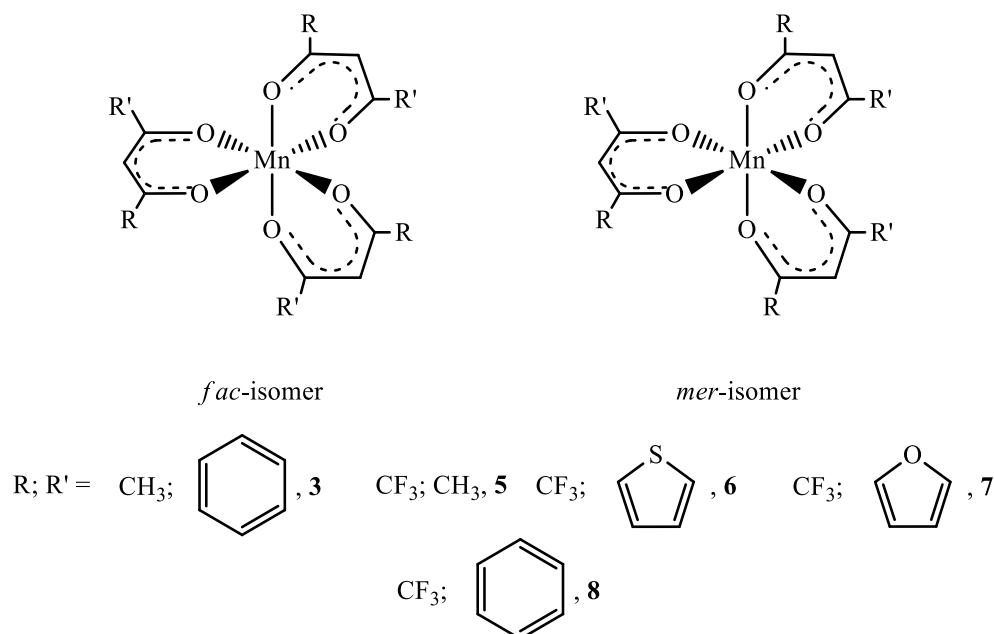
Scheme 3.2: The two possible isomers when unsymmetrical β-diketonato ligands (RCOCHCOR′)⁻ with R ≠ R′, are present in [Mn(β-diketonato)₃] complexes.

3.1.1 Synthesis

Using an adapted method[1,2] [Mn(dpm)₃], **1**, [Mn(acac)₃], **2**; [Mn(ba)₃], **3**; [Mn(dbm)₃], **4**; [Mn(tfaa)₃], **5**; [Mn(tfth)₃], **6**; [Mn(tffu)₃], **7**, [Mn(tfba)₃], **8**, and [Mn(hfaa)₃], **9**, were synthesized. The preparation method used to synthesize the [Mn(β-diketonato)₃] complexes depends on the phase (liquid or solid) of the β-diketone. Group 1 complexes which were synthesized from liquid β-diketones (**1**, **2**, **5**, **6**, **7**, and **8**) were prepared by a synthesis method according to **Scheme 3.3**, while group 2 complexes prepared from solid β-diketones (**3** and **4**), were synthesized according to **Scheme 3.3.b)** were ethanol was used in the aid of dissolving the β-diketone ligands.

R; R' = C(CH₃)₃; C(CH₃)₃, **1**   CH₃; CH₃, **2**

CF₃; CH₃, **5**   CF₃; [thiophene] , **6**

CH₃; [benzene] , **3**   [benzene] ; [benzene] , **4**

CF₃; [furan] , **7**   CF₃; [benzene] , **8**
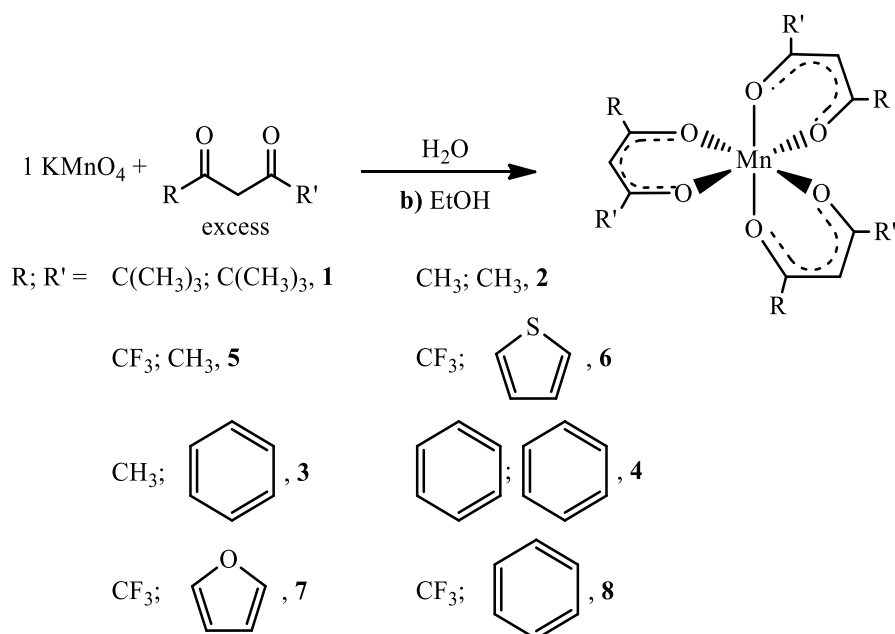
Scheme 3.3: Preparation method for [Mn(β-diketonato)₃] [**1-8**] complexes, **b)** ethanol was used to dissolve the β-diketone ligands in the preparation of **3** and **4**.

During the synthesis the reduction of Mn^{7+} in $[MnO_4]^-$ to Mn^{3+} in the tris chelate complex was achieved by unreacted β-diketone molecules. This reduction was observed through a colour change of the reaction mixture from purple (Mn^{7+}) to a brown-black (Mn^{3+}) mixture. The β-diketones used in the synthesis of the group 2 complexes are solids, which does not dissolve in H_2O. The solid β-diketones were first dissolved in EtOH before mixing it with the $KMnO_4$ water solution. The complexes precipitated out and were collected through filtration.

Due to the hygroscopic nature of the hexafluoroecetylacetone (Hhfaa), the [Mn(hfaa)₃], **9**, complex was prepared under argon atmosphere as illustrated in **Scheme 3.4**.
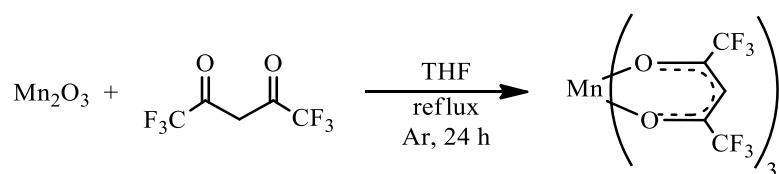
Scheme 3.4: Preparation method for [Mn(hfaa)₃], **9** complex.

After refluxing the reaction mixture of Mn_2O_3, Hhfaa and tetrahydrofurane (THF) for 24 hours, the excess tetrahydrofuran (THF) and Hhfaa was removed under vacuum. The resulting product [Mn(hfaa)₃] was obtained through sublimation.

Due to the paramagnetic properties of the $[Mn^{III}(\beta\text{-diketonato})_3]$ complexes,[4] NMR could not be used as a characterization method, instead elemental analysis, mass spectroscopy and crystal collections were used (**Section 4.3.1, chapter 4**). The summary of the $[Mn(\beta\text{-diketonato})_3]$ complexes' characteristics are given in **Table 3.1**.

Table 3.1: The $[Mn(\beta\text{-diketonato})_3]$ complexes' characteristics.

Complex	R	R'	Yield	Colour	Melting point
$[Mn(dpm)_3]$, **1**	$C(CH_3)_3$	$C(CH_3)_3$	24%	Dark brown-black	173.4 ℃
$[Mn(acac)_3]$, **2**	CH_3	CH_3	21%	black	156.5 ℃
$[Mn(ba)_3]$, **3**	CH_3	Ph	72%	green	186.2 ℃
$[Mn(dbm)_3]$, **4**	Ph	Ph	83%	black	234.8 ℃
$[Mn(tfaa)_3]$, **5**	CF_3	CH_3	66%	dark brown-black	117.3 ℃
$[Mn(tfth)_3]$, **6**	CF_3	C_4H_3S	94%	brown	157.2 ℃
$[Mn(tffu)_3]$, **7**	CF_3	C_4H_3O	70%	black	171.4 ℃
$[Mn(tfba)_3]$, **8**	CF_3	Ph	95%	black	88.9 ℃
$[Mn(hfaa)_3]$, **9**	CF_3	CF_3	-	yellow	-

General good yields of 69-98 % were achieved, with exception of $[Mn(dpm)_3]$, **1**, and $[Mn(acac)_3]$, **2**, which gave poor yields of 21-24%. The yield and melting point of $[Mn(hfaa)_3]$ could not be determined due to the hygroscopic nature of $[Mn(hfaa)_3]$. The volatility at room temperature of the liquid β-diketone ligands used for the synthesis of complex **1** and **2** could possibly be the cause of the low yields obtained, even though an excess of β-diketone (β-diketone : $KMnO_4$ = 10: 1) were used in the synthesis.

---

[4] S.L. Dexheimer, J.W. Gohdes, M.K. Chan, K.S. Hagen, W.H. Armstrong, M.P. Klein, *J. Am. Chem. Soc.* **1989** (111) 8923-8926, "Detection of EPR Spectra in S = 2 States of Trivalent Manganese Complexes". DOI: 10.1021/ja00206a028

3.1.2 Electrochemistry study

In this section the cyclic voltammetry of the tris(dipivaloymethanato)manganese(III), [Mn(dpm)$_3$], **1**, complex will be explained in detail and briefly compared to the cyclic voltammetry data of the other eight complexes (**2-9**)[5] in **Section 3.1.4.**

During the oxidation and reduction of the [Mn(dpm)$_3$] complex, **1**, the reduction of the (dpm)$^-$ ligand was not observed. Two redox processes were observed during a cyclic voltammetry (CV) experiment, this is in accordance with previous studies done on [Mn(acac)$_3$], **2**; [Mn(ba)$_3$], **3**, and [Mn(dbm)$_3$], **4**.[2,5] The resulting cyclic voltammorgram is illustrated in **Figure 3.1**. The redox process observed at positive potential is assigned to the Mn^{III}/Mn^{IV} couple where the Mn^{III} centre gets oxidized to Mn^{IV} during the forward scan and then reduced from Mn^{IV} back to Mn^{III} during the backward scan. At more negative potential another redox process was observed, that is allocated to the Mn^{III}/Mn^{II} couple. Data collected during the CV experiment is summarized in **Table 3.2**.
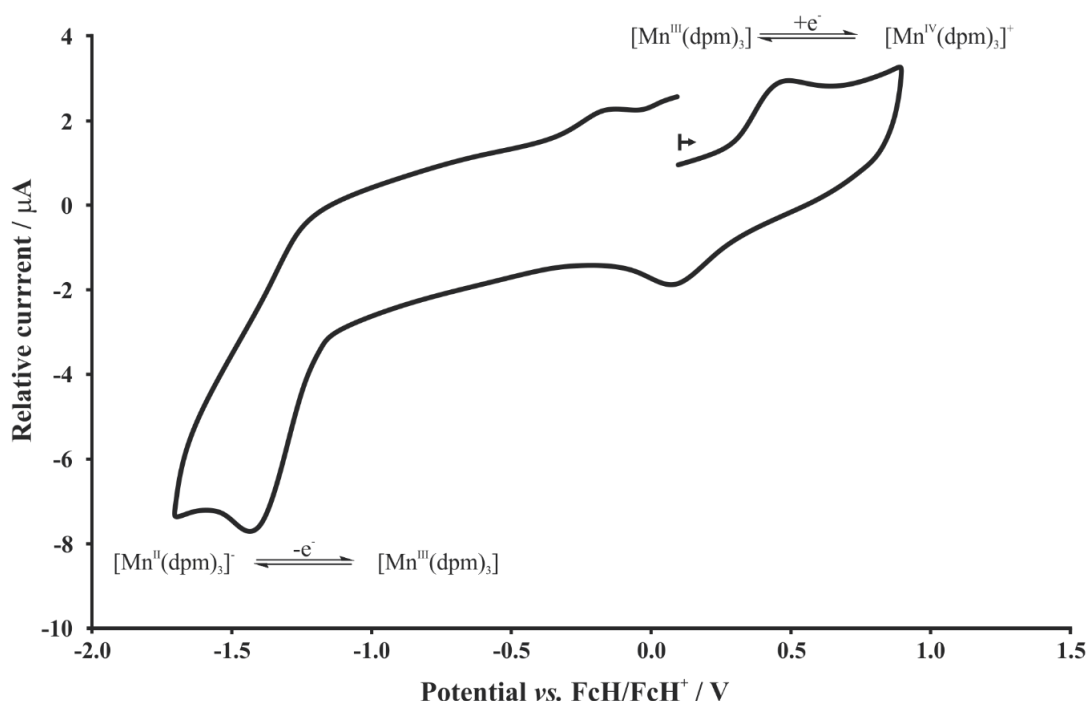
Figure 3.1: Cyclic voltammogram of [Mn(dpm)$_3$], **1**, at a scan rate of 0.10 V.s^{-1}. Measurements were performed on 0.5 mM analyte in 0.1 M [^{n}(Bu$_4$)N][PF$_6$]/DCM on a glassy carbon working electrode; the CV initiated in the direction of the arrow. The CV is referenced against ferrocene as an internal standard.

---

[5] R. Freitag, MSc study, "COMPUTATIONAL, STRUCTURAL AND ELECTROCHEMICAL PROPERTIES OF METAL(III) TRIS-BETADIKETONATO COMPLEXES", 2012, University of the Free State, Bloemfontein, South Africa.

Form the data presented in **Table 3.2** it is clear that the Mn^{III}/Mn^{II} couple with potential separation (ΔE) of more than 0.9 V is electrochemically irreversible ($\Delta E > 0.09V$ is considered as electrochemically irreversible) and with current ratio (i_{pa}/i_{pc}) of 0.10 - 0.11 it is also chemically irreversibly ($i_{pa}/i_{pc} = 1$ is considered as chemically reversible).[6] The Mn^{III}/Mn^{IV} couple with potential separation (ΔE) of more than 0.38 V and a current ratio (i_{pc}/i_{pa}) of $0.67 - 0.71$ is electrochemically irreversible and chemically partially reversible. The figure containing the CVs of the [Mn(dpm)$_3$] complex at $0.05 - 5.0$ V.s^{-1} scan rates can be seen in Appendix A (**Figure A.1**).

Table 3.2: Electrochemical data^i of [Mn(dpm)$_3$], **1**, obtained at different scan rates.

Scan Rate (V.s^{-1})	Mn^{III} / Mn^{II}							Mn^{III} / Mn^{IV}						
	E_{pa} (V)	E_{pc} (V)	ΔE (V)	$\frac{E_{pc} + E_{pa}}{2}$ (V)	i_{pa} (µA)	i_{pc} (µA)	i_{pa}/i_{pc}	E_{pa} (V)	E_{pc} (V)	ΔE (V)	$\frac{E_{pc} + E_{pa}}{2}$ (V)	i_{pa} (µA)	i_{pc} (µA)	i_{pc}/i_{pa}
0.05	-0.510	-1.422	0.913	-0.966	0.33	3.21	0.10	0.478	0.089	0.389	0.283	1.04	0.69	0.67
0.10	-0.500	-1.427	0.926	-0.964	0.40	3.60	0.11	0.502	0.080	0.422	0.291	1.04	0.69	0.67
0.15	-0.501	-1.432	0.931	-0.966	0.52	4.25	0.12	0.502	0.078	0.424	0.290	1.05	0.73	0.70
0.20	-0.481	-1.435	0.954	-0.958	0.52	4.41	0.12	0.523	0.076	0.447	0.299	1.20	0.83	0.69
0.25	-0.461	-1.499	1.039	-0.980	0.60	5.29	0.11	0.547	0.108	0.439	0.327	1.67	1.19	0.71
0.30	-0.452	-1.507	1.055	-0.980	0.60	5.33	0.11	0.560	0.105	0.455	0.332	1.69	1.19	0.70
0.50	-0.447	-1.525	1.078	-0.986	0.71	6.64	0.11	0.579	0.097	0.482	0.338	2.14	1.43	0.67

i Solvent DCM, supporting electrolyte tetrabutylammonium hexafluorophosphate, working electrode glassy carbon, concentration of 0.5 mM [Mn(dpm)$_3$] with all potential values given *vs.* FcH/FcH$^+$

[6] P.T. Kissinger, W.R. Heineman, *J. Chem. Educ.* **1983** (60) 702-706, "Cyclic Voltammetry" DOI: 10.1021/ed060p702; G.A. Mabbott, *J. Chem. Educ.* **1983** (60) 697-702, "An introduction to Cyclic Voltammetry". DOI: 10.1021/ed060p697; J.J. van Benschoten, J.Y. Lewis, W.R. Heineman, D.A. Roston, P.T. Kissinger, *J. Chem. Educ.* **1983** (60) 772-776, "Cyclic voltammetry experiment". DOI: 10.1021/ed060p772

3.1.3 Computational study

3.1.3.1 Computational study of [Mn(dpm)₃]

The [Mn(dpm)₃], **1**, is an octahedral complex with four unpaired *d*-electrons[4] and therefore, two *d*-orbital fillings are possible, namely $t^3_{2g}d^1_{z2}$ or $t^3_{2g}d^1_{x2-y2}$. DFT (ADF,[7] OLYP,[8] TZP data base) was used to optimize [Mn(dpm)₃], **1**. The orbital filling of the lowest energy optimized complex was $t^3_{2g}d^1_{z2}$. The highest occupied molecular orbital (HOMO) of the OLYP/TZP optimized [Mn(dpm)₃] structure is visualized in **Figure 3.2**.
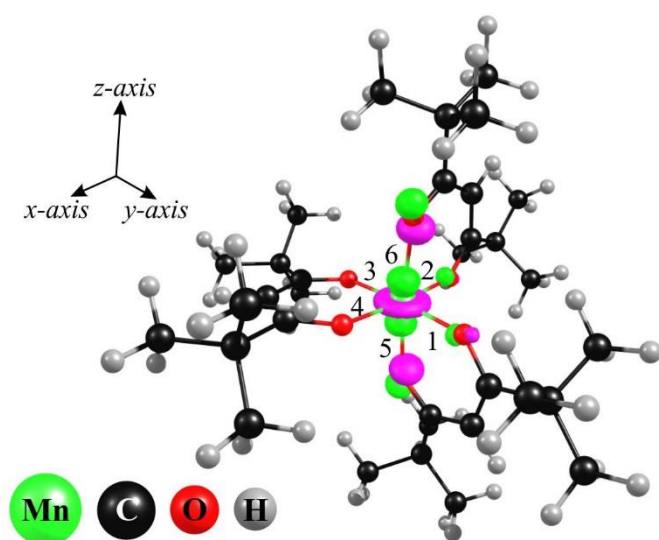
Figure 3.2: ADF/OLYP HOMO orbital of the optimized [Mn(dpm)₃] complex.

From **Figure 3.2** the HOMO clearly has d_{z2} character. The [Mn(dpm)₃] complex where the HOMO consists of d_{z2} character is associated with an elongation Jahn-Teller distortion. The elongation of the bonds along the *z*-axis is due to the large electrostatic repulsion caused between the d_{z2} HOMO

[7] G. te Velde, F.M. Bickelhaupt, E.J. Baerends, C.F. Guerra, S.J.A. van Gisbergen, J.G. Snijders, T.J. Ziegler, *J. Comput. Chem.* **2001** (22) 931-967, "Chemistry with ADF". DOI: 10.1002/jcc.1056

[8] N.C. Handy, A.J. Cohen, *Mol. Phys.* **2001** (99) 403-412, "Left-right correlation energy". DOI: 10.1080/00268970010018431; C. Lee, W. Yang, R.G. Parr, *Phys. Rev. B: Condens. Matter* **1988** (37) 785-789, "Development of the Colle-Salvetti correlation-energy formula into a functional of the electron density". DOI: 10.1103/PhysRevB.37.785; B.G. Johnson, P.M.W. Gill, J.A. Pople, *J. Chem. Phys.* **1993** (98) 5612-5626, "The performance of a family of density functional methods". DOI: 10.1063/1.464906; T.V. Russo, R.L. Martin, P.J. Hay, *J. Chem. Phys.* **1994** (101) 7729-7737, "Density Functional Calculations on First Row Transition Metals". DOI: 10.1063/1.468265

of the Mn centre and p_z orbital of the O on the *z*-axis (Mn-O bond 5 and 6), see **Figure 3.2** and **Table 3.3**. In **Table 3.3** the elongated Mn-O bond 5 has a length of 2.213 Å which is 0.231-0.296 Å longer than the Mn-O bond lengths numbered 1–4 in **Figure 3.2** along the *xy*-plane.

Table 3.3: Mn-O bond lengths of the OLYP/TZP optimized [Mn(dpm)₃] complex (refer to **Figure 3.2** for Mn-O numbering).

Complex	Bond length (Mn-O) (Å)					
	1	**2**	**3**	**4**	**5**	**6**
[Mn(dpm)₃], **1**	1.917	1.917	1.982	1.982	2.213	2.213

The structure of [Mn(dpm)₃] with the $t^3_{2g}d^1_{x2\text{-}y2}$ filling of the *d*-orbital was also calculated and was found to be 3.442 kJ.mol⁻¹ (OLYP value) higher in energy than the lowest energy $t^3_{2g}d^1_{z2}$ state. The HOMO of the $t^3_{2g}d^1_{x2\text{-}y2}$ state that is illustrated in **Figure 3.3** clearly consists mainly out of $d_{x2\text{-}y2}$ character. Repulsion between the p_x and p_y orbitals of the O and the $d_{x2\text{-}y2}$ on the Mn centre results in the elongation of the Mn-O bond in *xy*-plane, see **Table 3.4**.
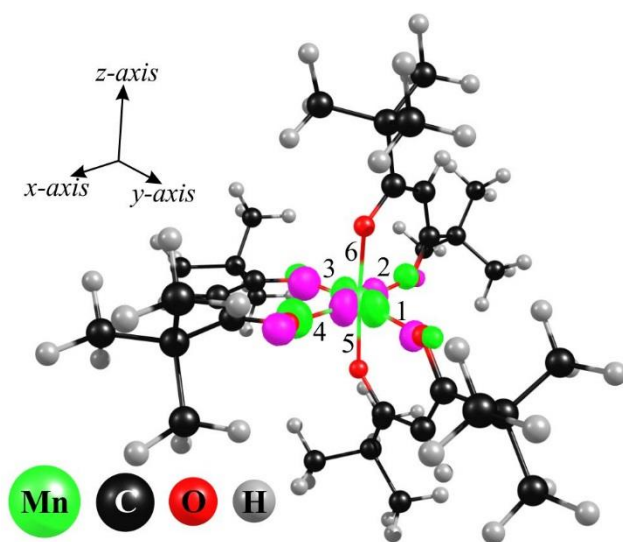
Figure 3.3: ADF/OLYP/TZP HOMO orbital of the optimized alternative electron filling [Mn(dpm)₃] complex

The Mn-O bond lengths along the *z*-axis is 0.162-0.207 Å shorter than the Mn-O bond lengths in the *xy*-plane. Therefore, this occurrence is classified as compression Jahn-Teller distortion.

Table 3.4: Mn-O bond lengths of the alternative optimized [Mn(dpm)$_3$] complex (refer to **Figure 3.3** for numbering).

Complex	Bond length (Mn-O) (Å)					
	1	**2**	**3**	**4**	**5**	**6**
[Mn(dpm)$_3$], **1**	2.104	2.103	2.112	2.112	1.905	1.941

Using the Boltzmann equation (**Equation 3.1**) the percentage (%) population of the two structures with the *d*-orbital filling possibilities were calculated to be 80% $t^3_{2g}d^1_{z2}$ (elongation Jahn-Teller distortion) and 20% $t^3_{2g}d^1_{x2-y2}$ (compression Jahn-Teller distortion). [Mn(dpm)$_3$], **1**, with the elongation Jahn-Teller distortion, is thus the main form of the [Mn(dpm)$_3$], **1**, complex.

$$\ln\frac{n_j}{n_i} = -\frac{(E_j - E_i)}{kT}$$

Equation 3.1

3.1.3.2 Computational study of [Mn(β-diketonato)$_3$]

[Mn(dpm)$_3$], **1**, presented in **Section 3.1.3.1** above, as well as complexes [Mn(acac)$_3$], **2**; [Mn(dbm)$_3$], **4**, and [Mn(hfaa)$_3$], **9**, have symmetrical β-diketonato ligands = (RCOCHCOR)$^-$ coordinated to Mn(III). However, for complexes **3**, **5-8**, containing unsymmetrical β-diketonato ligands = (RCOCHCOR')$^-$ with R ≠R', two isomers are possible, a *fac-* and a *mer-* isomer, see **Figure 3.4**. Although both *fac* and *mer* isomers are possible for complexes **3**, **5-8**, it was not possible to distinguish experimentally between the *fac* and *mer* isomers. Since it was shown for the related diamagnetic [Co^{III}(β-diketonato)$_3$] complexes that the *fac* and *mer* isomers are in equilibrium with each other,[9] we assume than both the *fac* and *mer* isomers of the [Mn^{III}(β-diketonato)$_3$] complexes exist in equilibrium with each other. Therefore, DFT computational chemistry calculations are presented to determine the geometry and energies of the *fac* and *mer* isomers. Using the Boltzmann equation (**Equation 3.1**) the *fac* : *mer* ratio for complexes **3**, **5-8**, is determined.

---

[9] R.F. Fay, T.S. Piper, *Journal of American Chemical Society* **1963** (85) 500-504, "Coordination Compounds of Trivalent Metals with Unsymmetrical Bidentate Ligands. 11. Trifluoroacetylacetonates". DOI: 10.1021/ja00888a002

f ac-isomer   *mer*-isomer
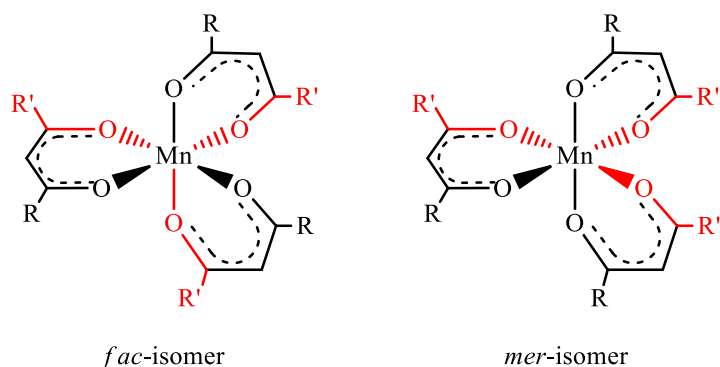
Figure 3.4: The *fac*- and *mer*-isomer of [Mn(β-diketonato)$_3$] complexes containing unsymmetrical β-diketonato ligands (RCOCHCOR')$^-$ with R ≠R'.

The relative energies obtained by DFT calculations using a selection of GGA (Generalized Gradient Approximation) functionals, namely PW91 (Perdew-Wang 1991),[10] BP86 (Becke-Perdew),[11,12] and OLYP (Handy-Cohen and Lee-Yang-Parr),[8] as well as the hybrid functional B3LYP (Becke 1993 and Lee-Yang-Parr),[13,14] of [Mn^{III}(β-diketonato)$_3$] complexes **1-9** are given in **Table 3.5**. The optimized coordinates of the calculations are provided in **Appendix C**. A spin state of S = 4/2, in agreement with previous DFT studies[5] and experimental

10 J.P. Perdew, J.A. Chevary, S.H. Vosko, K.A. Jackson, M.R. Pederson, D.J. Singh and C. Fiolhais, Phys. Rev. B 1992 (46) 6671-6687, "Atoms, molecules, solids, and surfaces: Applications of the generalized gradient approximation for exchange and correlation" DOI: 10.1103/PhysRevB.46.6671; Erratum: J.P. Perdew, J.A. Chevary, S.H. Vosko, K.A. Jackson, M.R. Perderson, D.J. Singh and C. Fiolhais, Phys. Rev. B 1993 (48) 4978, "Erratum: Atoms, molecules, solids, and surfaces: Applications of the generalized gradient approximation for exchange and correlation". DOI: 10.1103/PhysRevB.48.4978.2

11 A.D. Becke, Phys. Rev. A 1988 (38) 3098-3100, "Density-functional exchange-energy approximation with correct asymptotic behavior". DOI: 10.1103/PhysRevA.38.3098

12 J.P. Perdew, Phys. Rev. B 1986 (33) 8822-8824, "Density-functional approximation for the correlation energy of the inhomogeneous electron gas". DOI: 10.1103/PhysRevB.33.8822; Erratum: J.P. Perdew, Phys. Rev. B 1986 (34) 7406, "Erratum: Density-functional approximation for the correlation energy of the inhomogeneous electron gas". DOI: 10.1103/PhysRevB.34.7406

13 A.D. Becke, J. Chem. Phys. 1993 (98) 5648-5652, "Density-functional thermochemistry. III. The role of exact exchange". DOI: 10.1063/1.464913

14 P.J. Stephens, F.J. Devlin, C.F. Chabalowski and M.J. Frisch, J. Phys. Chem. 1994 (98) 11623-11627, "Ab Initio Calculation of Vibrational Absorption and Circular Dichroism Spectra Using Density Functional Force Fields". DOI: 10.1021/j100096a001

data was used.[15] The lowest energy geometry of all isomers of $[Mn^{III}(\beta\text{-diketonato})_3]$ complexes **1**-**9** exhibit elongation Jahn-Teller distortion. The *fac:mer* ratio of complexes **3**, **5**-**8**, ccalculated by the Boltzmann equation for the different functionals, are also given in **Table 3.5**. It is interesting to note that all functionals predict the *mer* isomer as the main isomer for complexes **5** – **8**. The $[Mn(tfth)_3]$ crystal studied by R. Gostynski *et al.* was found in the *mer* isomer, which is in agreement with the computational study.[16] The relative energies in **Table 3.5** of the symmetrical $[Mn^{III}(\beta\text{-diketonato})_3]$ complexes (**1**, **2**, **4** and **9**) are calculated between the different functionals, where the unsymmetrical $[Mn^{III}(\beta\text{-diketonato})_3]$ complexes' (**3** and **5-8**) relative energies are calculated between the *fac* and *mer* isomer of a functional.

Table 3.5: DFT calculated relative energies (kJ.mol⁻¹) of the lowest energy ground state of $[Mn(\beta\text{-diketonato})_3]$ complexes **1**–**9**, calculated with a selection of functionals. The lowest energy is indicated as a 0 in bold.

Complex	Isomer	R	R'	$E_{ground\ state}$ (kJ.mol⁻¹)				*fac:mer* (%)				
				PW91	BP86	OLYP	B3LYP	PW91	BP86	OLYP	B3LYP	Average
[Mn(dpm)₃], **1**		C(CH₃)₃	C(CH₃)₃	-	**-**	-	-	-	-	-	-	-
[Mn(acac)₃], **2**		CH₃	CH₃	-	-	-	**-**	-	-	-	-	-
[Mn(ba)₃], **3**	*fac*	CH₃	Ph	**0.00**	0.772	1.62	**0.00**	97.8:2.2	0:100	21.4:78.6	0:100	29.8:70.2
	mer			0.097	**0.00**	**0.00**	4.34					
[Mn(dbm)₃], **4**		Ph	Ph	-	-	-	**-**	-	-	-	-	-
[Mn(tfaa)₃], **5**	*fac*	CF₃	CH₃	2.60	3.10	3.00	2.90	11.9:88.1	11.1:88.9	22.3:77.7	12.7:87.3	15:85
	mer			**0.00**	**0.00**	**0.00**	**0.00**					
[Mn(tfth)₃], **6**	*fac*	CF₃	C₄H₃S	3.00	2.60	**0.00**	2.10	9.2:90.8	10.7:89.3	100:0	17.8:82.2	18:82
	mer			**0.00**	**0.00**	1.04	**0.00**					
[Mn(tffu)₃], **7**	*fac*	CF₃	C₄H₃O	3.80	3.70	7.50	-	7.2:92.8	7.2:92.7	2.4:97.6	-	6:94
	mer			**0.00**	**0.00**	**0.00**	-					
[Mn(tfba)₃], **8**	*fac*	CF₃	Ph	5.30	4.00	6.23	4.70	4.7:95.3	7.3:92.7	4.2:95.8	5.0:95.0	5.3:94.7
	mer			**0.00**	**0.00**	**0.00**	**0.00**					
[Mn(hfac)₃. **9**		CF₃	CF₃	-	-	-	**-**	-	-	-	-	-

Since the oxidation and reduction of $[Mn^{III}(\beta\text{-diketonato})_3]$ complexes **1**-**9** involve an electron to be added to the HOMO (that can be α or β) or removed from the LUMO (that can be α or β) of the complex, the DFT calculated energies of the frontier orbitals of **1**-**9** is given in **Table 3.6** in

---

[15] I. Diaz-Acosta, J. Baker, J.F. Hinton, P. Pulay, *Spectrochemica Acta Part A* **2003** (59) 363-377, "Calculated and experimental geometries and infrared spectra of metal tris-acetylacetonates: vibrational spectroscopy as a probe of molecular structure for ionic complexes. Part II". DOI: 10.1016/S1386-1425(02)00166-X

[16] R. Gostynski, P.H. van Rooyen, J. Conradie, *Journal of Moleculaar Structure* **2016** (1119) 48-53, "Jahn-Teller distortion in tris[4,4,4-trifluoro-1-(2-thienyl)-1,3-butanedionato]manganese(III) isomers: An X-ray and computational study". DOI: 10.1016/j.molstruc.2016.04.048

order to relate frontier orbital energies with experimental oxidation and reduction values, see **Section 3.1.4.1(ii)**. The energy that is released when an electron is added to a complex (reduction process) is known as the electron affinity (EA). The EA can be computationally obtained by calculating the energy difference between the neutral and the reduced species, see **Equation 3.2**.

$$[Mn^{III}(\beta\text{-diketonato})_3] + e^- \rightleftharpoons [Mn^{II}(\beta\text{-diketonato})_3]^- + EA$$

$$EA = E_{[Mn^{III}(\beta-\text{diketonato})_3]} - E_{[Mn^{II}(\beta-\text{diketonato})_3]^-} \qquad \textbf{Equation 3.2}$$

The Density Functional Theory (DFT) calculated EA of $[Mn^{III}(\beta\text{-diketonato})_3]$ complexes **1**-**9** are summarized in **Table 3.7**.

Table 3.6: DFT calculated energies (kJ.mol^{-1}) of the frontier orbitals of the lowest energy ground state of $[Mn(\beta\text{-diketonato})_3]$ complexes **1–9**, calculated with a selection of functionals.

Complex	Isomer	R	R'	E_{HOMO} (kJ.mol^{-1})				E_{LUMO} (kJ.mol^{-1})			
				PW91	BP86	OLYP	B3LYP	PW91	BP86	OLYP	B3LYP
[Mn(dpm)₃], **1**		C(CH₃)₃	C(CH₃)₃	-	-406.2	-361.8	-	-	-343.3	-312.2	-
[Mn(acac)₃], **2**		CH₃	CH₃	-393.8	-400.3	-382.6	-560.3	-329.9	-336.2	-328.9	-266.2
[Mn(ba)₃], **3**	*fac*	CH₃	Ph	-371.9	-380.4	-391.6	-540.9	-305.3	-313.7	-336.4	-244.3
	mer			-371.8	-382.7	-392.4	-538.7	-305.0	-311.4	-334.8	-238.6
[Mn(dbm)₃], **4**		Ph	Ph	-383.4	-392.8	-385.1	-557.4	-322.0	-326.8	-350.3	-256.0
[Mn(tfaa)₃], **5**	*fac*	CF₃	CH₃	-495.9	-502.7	-505.1	-672.5	-430.8	-436.1	-452.5	-378
	mer			-499.7	-506.5	-522.8	-677.9	-431.6	-437.6	-446.7	-376.2
[Mn(tfth)₃], **6**	*fac*	CF₃	C₄H₃S	-484.4	-490.9	-486.4	-657.6	-418.6	-426.4	-430.1	-364.9
	mer			-485.3	-490.3	-487.1	-656.1	-420.5	-425.7	-430	-366.0
[Mn(tffu)₃], **7**	*fac*	CF₃	C₄H₃O	-479.6	-486.6	-476.2	-	-412.6	-419.3	-418.5	-
	mer			-478.2	-485.9	-469.9	-657.3	-412.5	-419	-417.1	-357.4
[Mn(tfba)₃], **8**	*fac*	CF₃	Ph	-485.5	-493.5	-512.3	-666.2	-421.3	-428.4	-458.0	-366.2
	mer			-488.5	-495.1	-512.2-	-663.5	-423.2	-428.9	-451.0	-364.2
[Mn(hfac)₃. **9**		CF₃	CF₃	-	-	-593.7	-783.2	-	-	-541	-489.2

Table 3.7: DFT calculated ground state and anionic energies of [Mn(β-diketonato)₃] complexes **1–9**, calculated with OLYP/TZP. The electron affinity is also given.

Complex	Isomer	R	R'	$E_{ground\ state}$ (kJ.mol⁻¹)	$E_{reduced\ specie}$ (kJ.mol⁻¹)	EA (kJ.mol⁻¹)	*fac/mer* (%)	Effective EA[a] (kJ.mol⁻¹)
[Mn(dpm)₃], **1**	-	C(CH₃)₃	C(CH₃)₃	-51940.3	-52148.41	208.11	-	-
[Mn(acac)₃], **2**	-	CH₃	CH₃	-24524.3	-24722.95	198.65	-	-
[Mn(ba)₃], **3**	*fac*	CH₃	Ph	-38922.1	-39140.41	218.31	21.4	217.67
	mer			-38923.7	-39141.24	217.5	78.6	
[Mn(dbm)₃], **4**	-	Ph	Ph	-53317.8	-53553.59	235.79	-	-
[Mn(tfaa)₃], **5**	*fac*	CF₃	CH₃	-24747.3	-25031.44	284.14	22	281.98
	mer			-24750.3	-25031.66	281.36	78	
[Mn(tfth)₃], **6**	*fac*	CF₃	C₄H₃S	-33040.3	-33342.71	302.41	100	303.49
	mer			-33039.3	-33343.35	304.05	0	
[Mn(tffu)₃], **7**	*fac*	CF₃	C₄H₃O	-33778.9	-34075.09	296.19	2	293.54
	mer			-33786.4	-34079.88	293.48	98	
[Mn(tfba)₃], **8**	*fac*	CF₃	Ph	-39119.7	-39438.28	318.58	4.2	298.83
	mer			-39142.6	-39440.56	297.96	95.8	
[Mn(hfac)₃. **9**	-	CF₃	CF₃	-24910.1	-25302.17	392.07	-	-

a In calculating the effective EA of [Mn(β-diketonato)₃] complexes containing unsymmetrical β-diketonato ligands the Boltzmann equation was used on the ground state species.

3.1.4 Comparison study of [Mn(β-diketonato)₃] complexes

Large parts of the following data are published and reprinted from *Electrochimica Acta* (158), R. Freitag, J. Conradie, "Electrochemical and Computational Chemistry Study of [Mn(β-diketonato)₃] complexes", 418-426 2015, with permission from Elsevier and republished with permission of [Trans Tech Publications Ltd], from [Electronic Influence of Different β-Diketonato Ligands on the Electrochemical Behaviour of Tris(β-Diketonato)M(III) Complexes, M = Cr, Mn and Fe, R. Gostynski, M. M. Conradie, R. Y. Liu, J. Conradie, Journal of Nano Research, volume 44, 2016 of copyright]; permission conveyed through Copyright Clearance Center, Inc. In this section the newly obtained data from the [Mn(dpm)₃], **1**, complex will be compared to eight other [Mn(β-diketonato)₃] complexes (β-diketonato = acetylacetonato (acac), **2**; benzoylacetonato (ba), **3**; dibenzoylmethanato (dbm), **4**; trifluoroacetylacetonato (tfaa), **5**; thenoyltrifluoroacetonato (tfth), **6**; trifluorofuroylacetonato (tffu), **7**; trifluorobenzoylacetonato (tfba), **8**; hexafluoroacetylacetonato (hfaa), **9**).

3.1.4.1 Electrochemical results

Four of the [Mn(β-diketonato)₃] complexes exhibits both the Mn^{III}/Mn^{IV} and the Mn^{III}/Mn^{II} redox couples in the potential window of the solvent used, namely, [Mn(dpm)₃], **1**; [Mn(acac)₃], **2**; [Mn(ba)₃], **3**, and [Mn(dbm)₃], **4**. It was observed in **Figure 3.5** that with an increasing amount of phenyl (Ph) groups present in the β-diketonato ligand attached to the [Mn(β-diketonato)₃]

complex, the difference in the peak potential (ΔE_p) of both the Mn^{III}/Mn^{IV} and the Mn^{III}/Mn^{II} redox couples decreased, while the i_{pa}/i_{pc} ratio of the Mn^{III}/Mn^{II} redox couple increased, see **Table 3.8** and **Table 3.10**.
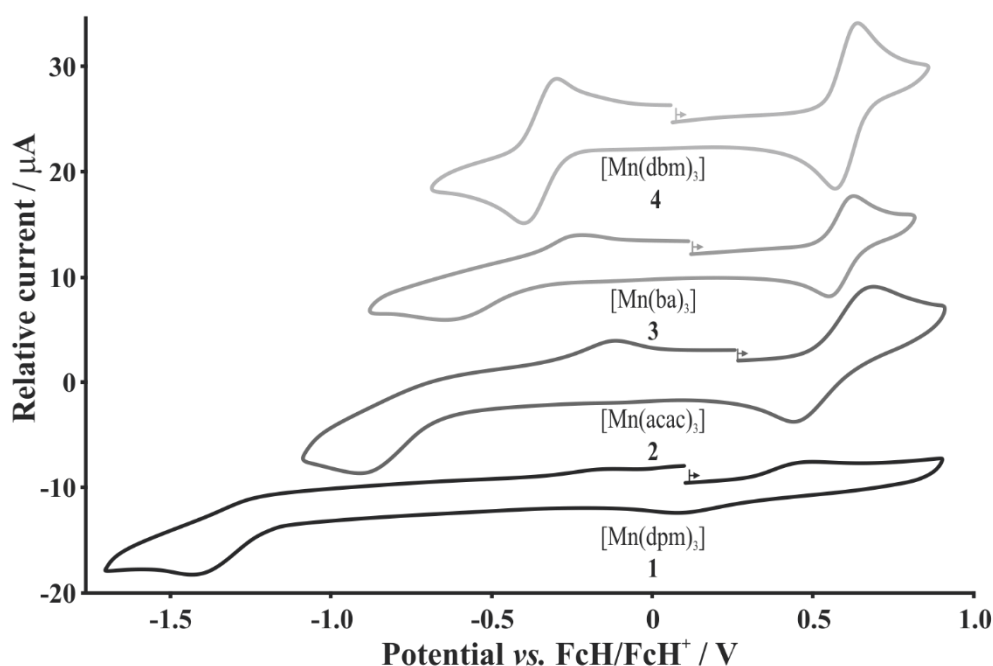
Figure 3.5: Cyclic voltammogram of the different [Mn(β-diketonato)$_3$] complexes **1** – **4** at scan rate of 0.10 V.s^{-1}. Measurements were performed on 0.5 mM analyte in 0.1 M [^{n}(Bu$_4$)N][PF$_6$]/CH$_3$CN(**1** in DCM) on a glassy carbon working electrode; the CV initiated in the direction of the arrows.

The increase of the i_{pa}/i_{pc} ratio of the Mn^{III}/Mn^{II} redox couple (**Table 3.10**) indicates that the reduced species [Mn^{II}(β-diketonato)$_3$]$^-$ are more stable in ascending order from [Mn(dpm)$_3$], **1**; to [Mn(acac)$_3$], **2**; to [Mn(ba)$_3$], **3**, and to [Mn(dbm)$_3$], **4**. For the Mn^{III}/Mn^{IV} redox couple it is observed that the peak potential difference (ΔE_p) of the [Mn(β-diketonato)$_3$] complexes with phenyl substituents (**3-4**) are electrochemically reversible with $\Delta E_p < 0.080$ V, as well as chemically reversible with i_{pa}/i_{pc} ratio *ca.* 1, see **Table 3.8**.

[Mn(acac)$_3$], **2**, was studied both in acetonitrile (CH$_3$CN) and dichloromethane (DCM) and it was found that the mean of E_{pc} and E_{pa} *vs*. FcH/FcH$^+$ of the Mn^{III}/Mn^{II} redox couple are -0.520 V and -0.632 V *vs*. FcH/FcH$^+$ in CH$_3$CN and DCM respectively. Referencing these values against SCE, using $E^{\circ\prime}$ (FcH/FcH$^+$) = 0.66(5) V *vs* SHE in [^{n}(Bu$_4$)N][PF$_6$]/CH$_3$CN, and E$^{\circ\prime}$

Results and discussion

(FcH/FcH$^+$) = 0.77(5) V *vs* SHE in [^{n}(Bu$_4$)N][PF$_6$]/DCM,[17] they are found to be within experimental accuracy the same (-0.100 V and -0.106 V *vs*. SHE, in CH$_3$CN and DCM respectively). This is in agreement with previously published work.[18] The CV of [Mn(dpm)$_3$], **1**, obtained in DCM, can thus be compared to the CVs of **2-8** obtained in CH$_3$CN when referenced *vs*. SCE.

Table 3.8: Electrochemical data of the of Mn^{III}/Mn^{IV} redox couple of 0.5 mM [Mn(β-diketonato)$_3$] complexes **1**–**4** in acetonitrile (**1** in DCM), with supporting electrolyte tetrabutylammonium hexafluorophosphate, and glassy carbon working electrode, at a scan rate of 0.1 V s^{-1}, with potential *vs* FcH/FcH$^+$.

Complex	R	R'	E_{pa} / V	E_{pc} / V	Mean of E_{pc} and E_{pa} *vs* FcH/FcH$^+$ / V	ΔE_p	i_{pa} / μA	i_{pc} / μA	i_{pc}/i_{pa}	Mean of E_{pc} and E_{pa} *vs* SCE/V^a
[Mn(dpm)$_3$], **1**	C(CH$_3$)$_3$	C(CH$_3$)$_3$	0.502	0.080	0.291	0.422	1.0	0.7	0.7	0.817
[Mn(acac)$_3$], **2**	CH$_3$	CH$_3$	0.697	0.445	0.571	0.253	5.0	4.9	1.0	0.987
[Mn(ba)$_3$], **3**	CH$_3$	Ph	0.633	0.553	0.593	0.080	4.2	4.1	1.0	1.009
[Mn(dbm)$_3$], **4**	Ph	Ph	0.647	0.580	0.614	0.067	4.1	4.0	1.0	1.030

^{a} SCE = 0.244 V *vs* NHE, E°' (FcH/FcH$^+$) = 0.66(5) V *vs* NHE in [^{n}(Bu$_4$)N][PF$_6$]/CH$_3$CN and 0.77(5) V *vs* NHE in [^{n}(Bu$_4$)N][PF$_6$]/DCM, from ref.[17].

The Mn^{III}/Mn^{IV} redox couple of complexes **5-9** could not be detected in the acetonitrile (CH$_3$CN) solvent window and are thus expected to be at a potential greater than 1.7 V *versus* FcH/FcH$^+$. However, the Mn^{III}/Mn^{II} redox couple could be detected in acetonitrile during the cyclic voltammetry experiments of all the [Mn(β-diketonato)$_3$] complexes **1**–**9** , see **Figure 3.6**. From **Figure 3.6** it is observed that the Mn^{III}/Mn^{II} peak separation between E$_{pc}$ and E$_{pa}$ is smaller when an aromatic group [Ph, C$_5$H$_4$O (Fu), C$_5$H$_4$S (Th)] is on the β-diketonato backbone.

[17] A.J.L. Pombeiro, *J. Organomet. Chem.* **2005** (690) 6021-6040, "Electron-donor/acceptor properties of carbynes, carbenes, vinylidenes, allenylidenes and alkynyls as measured by electrochemical ligand parameters". DOI: 10.1016/j.jorganchem.2005.07.111

[18] G. Gritzner, H. Murauer, V. Gutmann, *J. Electroanal. Chem. and Interfacial Electrochem.* **1979** (101) 185-200, "Solvent and salt effects on the redox behaviour of trisacetylacetonato Manganese(III) ".
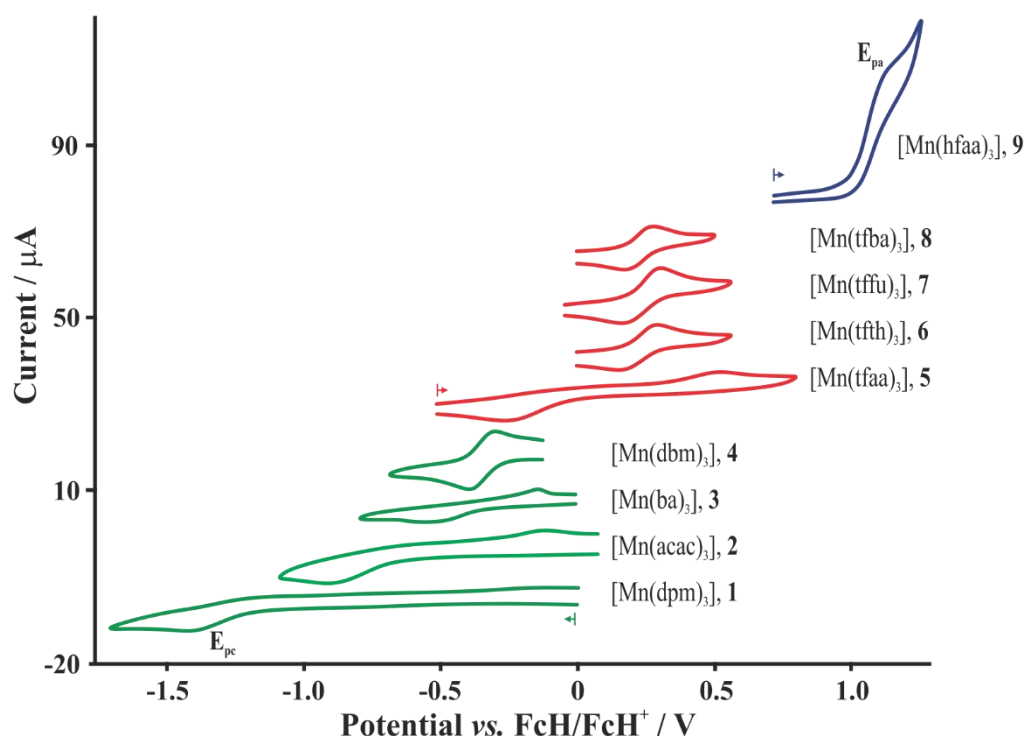
Figure 3.6: Cyclic voltammogram of Mn^{III}/Mn^{II} redox couple obtained from the different $[Mn(\beta\text{-diketonato})_3]$ complexes **1–9** at scan rate of 0.10 $V.s^{-1}$. Measurements were performed on 0.5 mM analyte in 0.1 M $[^n(Bu_4)N][PF_6]/CH_3CN$ (**1** in DCM) on a glassy carbon working electrode; the CV initiated in the direction of the arrows.

It was not possible to distinguish between the redox potentials of the *fac* and *mer* isomers for complexes **3**, **5**-**8** containing unsymmetrical β-diketonato ligands.

(i)   *Relationships between electrochemical results and electronic parameters*

The process where $[Mn^{III}(\beta\text{-diketonato})_3]$ gets reduced to $[Mn^{II}(\beta\text{-diketonato})_3]^-$ involves the addition of an electron to the complex. The more electrophilic the Mn centre (more positive) of the complex the easier an electron can be added. Therefore, it was expected that β-diketonato ligands $(RCOCHCOR')^-$ that contains R and R' groups that withdraw the electron density further away from the Mn centre (more electron withdrawing) would thus be easier to reduce. With this a relationship between any electronic parameter, describing electron withdrawing properties of R and R' groups, and the reduction potential (E_{pc}) of the Mn^{III}/Mn^{II} redox couple is expected. The $[Mn(\beta\text{-diketonato})_3]$ complexes **1–9** can be divided into three groups, group 1 with no CF_3 on β-diketonato backbone (complexes **1–4**), group 2 with one CF_3 on β-diketonato backbone (complexes **5–8**), and group 3 with two CF_3 on β-diketonato backbone (complex **9**). These groups are indicated in **Figure 3.6** in green, red and blue respectively. The

electronic parameters namely Gordy scale group electronegativity of the R groups (χ_R), Hammet sigma *meta* constant of the R groups (σ_R), and and the Lever ligand electrochemical parameter (E_L) of the β-diketonato ligand and the acid dissociation constant (pK_a) of the β-diketone are tabulated in **Table 3.9**. The electrochemical data obtained from **Figure 3.6** is summarized in **Table 3.10**.

Table 3.9: Electronic parameters of [Mn(β-diketonato)$_3$] complexes **1–9**.

Complex	R	R'	Electronic parameters [Mn(RCOCHCOR')$_3$]							
			$\chi_R{}^a$	$\chi_{R'}{}^a$	$3(\chi_R + \chi_{R'})^a$	$\sigma_R{}^b$	$\sigma_{R'}{}^b$	$3(\sigma_R + \sigma_{R'})^b$	p$K_a{}^c$	$\Sigma E_L{}^d$
[Mn(dpm)$_3$], **1**	C(CH$_3$)	C(CH$_3$)	2.27	2.27	13.62	-0.01	-0.01	-0.06	11.77	-0.78
[Mn(acac)$_3$], **2**	CH$_3$	CH$_3$	2.34	2.34	14.04	-0.069	-0.069	-0.41	8.95	-0.48
[Mn(ba)$_3$], **3**	CH$_3$	Ph	2.34	2.21	13.65	-0.069	0.06	-0.03	8.7	-0.36
[Mn(dbm)$_3$], **4**	Ph	Ph	2.21	2.21	13.26	0.06	0.06	0.36	8.89	-0.24
[Mn(tfaa)$_3$], **5**	CF$_3$	CH$_3$	3.01	2.34	16.05	0.43	-0.069	1.08	6.3	0.18
[Mn(tfth)$_3$], **6**	CF$_3$	C$_4$H$_3$S	3.01	2.1	15.33	0.43	0.09	1.56	6.50	0.3
[Mn(tffu)$_3$], **7**	CF$_3$	C$_4$H$_3$O	3.01	2.23	15.39	0.43	0.06	1.47	-	0.3
[Mn(tfba)$_3$], **8**	CF$_3$	Ph	3.01	2.21	15.66	0.43	0.06	1.47	6.3	0.3
[Mn(hfac)$_3$]. **9**	CF$_3$	CF$_3$	3.01	3.01	18.06	0.43	0.43	2.58	4.35	1.02

^{a} The Gordy scale group electronegativities χ_R, from ref. **26**, [19], [20], [21], and [22]

^{b} Hammet sigma meta constant σ_R, from ref. [23], [24] and [25]

^{c} Acid dissociation constant of β-diketone, pK_a, from ref. [26], [27] and [28]

^{d} ΣE_L (in V *vs* NHE) = 3 (three β-diketonato ligands) x 2 (each ligand has 2 arms) x E_L (β-diketonato ligand). Lever electrochemical ligand parameter E$_L$ of the β-diketonato ligand, from ref. [29], [30] and [31]

[19] W.C. du Plessis, T.G. Vosloo, J.C. Swarts, *J. Chem. Soc., Dalton Trans.* **1998** (15) 2507-2514, "β-Diketones containing a ferrocenyl group: synthesis, structural aspects, pK_a values, group electronegativities and complexation with rhodium(I) ".

[20] R.E. Kagarise, *J. Am. Chem. Soc.* **1955** (77) 1377-1379, "Relation between the Electronegativities of Adjacent Substituents and the Stretching Frequency of the Carbonyl Group".

[21] P. Klaas, *M.Sc. Thesis, University of the Free State*, *RSA*, **2002**, "Synthesis, electrochemical, kinetic and thermodynamic properties of new ferrocene-containing *beta*-diketonato rhodium(I) complexes with biomedical applications".

[22] M.M. Conradie, J. Conradie, *Electrochim. Acta* **2015** (152) 512-519, "Electrochemical behaviour of Tris(β-diketonato)iron(III) complexes: A DFT and experimental study".

[23] L.P. Hammett, *Chem. Rev.* **1935** (17) 125-136, "Some Relations between Reaction Rates and Equilibrium Constants".

[24] L.P. Hammett, *J. Am. Chem. Soc.* **1937** (59) 96-103, "The Effect of Structure upon the Reactions of Organic Compounds. Benzene Derivatives".

[25] C. Hansch, A. Leo, R.W. Taft, *Chem. Rev.* **1991** (91) 165-195, "A Survey of Hammett Substituent Constants and Resonance and Field Parameters".

[26] M.M. Conradie, A.J. Muller, J. Conradie, *S. Afr. J. Chem.* **2008** (61) 13-21, "Thienyl-containing β-diketones: Synthesis, characterization, crystal structure, keto-enol kinetics".

[27] J. Starý, *The Solvent Extraction of Metal Chelates*, MacMillan Company, New York, 1964, Appendix.

[28] M. Ellinger, H. Duschner, K. Starke, *J. Inorg. Nucl. Chem.* **1978** (40) 1063-1067, "The gem diol-enolate equilibrium constant of hexafluoroacetylacetone in aqueous solution".

[29] M.M. Conradie, J. Conradie, *Electrochim. Acta* **2015** (152) 512-519, "Electrochemical behaviour of Tris(β-diketonato)iron(III) complexes: A DFT and experimental study".

[30] A.B.P. Lever, *Inorg. Chem.* **1990** (29) 1271-1285, "Electrochemical Parametrization of Metal Complex Redox Potentials, Using the Ruthenium(III)/Ruthenium(II) Couple To Generate a Ligand Electrochemical Series".

[31] J.J.C. Erasmus, J. Conradie, *Electrochim. Acta* **2011** (565) 9287-9294, "Electrochemical study of β-Diketonatobis(triphenylphosphite) rhodium(I) complexes".

Results and discussion

Table 3.10: Electrochemical data of the Mn^{III}/Mn^{II} redox couple of $[Mn(\beta\text{-diketonato})_3]$ complexes **1–9**. Solvent DCM for $[Mn(dpm)_3]$, **1**, and acetonitrile for complexes **2-9**, supporting electrolyte tetrabutylammonium hexafluorophosphate, working electrode glassy carbon, concentration of 0.5 mM $[Mn(\beta\text{-diketonato})_3]$ with potential vs. FcH/FcH^+.

Complex	R	R'	E_{pa} /V	E_{pc} /V	ΔE_p	Mean of E_{pc} and E_{pa} vs FcH/FcH^+/V	Mean of E_{pc} and E_{pa} Vs SCE/V [a]	Mean of E_{pc} and E_{pa} vs NHE/V [a]	i_{pa}/i_{pc}
						Electrochemical data of Mn^{II}/Mn^{III}			
$[Mn(dpm)_3]$, **1**	$C(CH_3)_3$	$C(CH_3)_3$	-0.500	-1.427	0.926	-0.964	-0.438	-0.194	0.11
$[Mn(acac)_3]$, **2**	CH_3	CH_3	-0.117	-0.924	0.807	-0.520	-0.104	0.140	0.40
$[Mn(ba)_3]$, **3**	CH_3	Ph	-0.226	-0.635	0.409	-0.431	-0.015	0.229	0.58
$[Mn(dbm)_3]$, **4**	Ph	Ph	-0.302	-0.400	0.098	-0.351	0.065	0.309	0.96
$[Mn(tfaa)_3]$, **5**	CF_3	CH_3	0.520	-0.256	0.776	0.132	0.548	0.792	0.51
$[Mn(tfth)_3]$, **6**	CF_3	C_4H_3S	0.296	0.149	0.147	0.223	0.639	0.883	0.97
$[Mn(tffu)_3]$, **7**	CF_3	C_4H_3O	0.309	0.162	0.147	0.236	0.652	0.896	0.98
$[Mn(tfba)_3]$, **8**	CF_3	Ph	0.279	0.171	0.108	0.225	0.641	0.885	0.96
$[Mn(hfac)_3]$. **9**	CF_3	CF_3	1.149	1.041	0.108	1.095	1.511	1.755	0.49

[a] SCE = 0.244 V *vs* NHE, E°' (FcH/FcH^+) = 0.66(5) V *vs* NHE in $[^n(Bu_4)N][PF_6]/CH_3CN$ and 0.77(5) V *vs* NHE in $[^n(Bu_4)N][PF_6]/DCM$ from ref. **32**

The relationship between the mean of E_{pc} and E_{pa} of the Mn^{III}/Mn^{II} redox couple of $[Mn(RCOCHCOR')_3]$ complexes **1–9** and the pK_a (acid dissociation constants of the free un-coordinated β-diketone ligands), $3(\chi_R + \chi_{R'})$ (total group electronegativities), $3(\sigma_R + \sigma_{R'})$ (total Hammett sigma *meta* constants) of the R and R' groups, and the ΣE_L (sum of the Lever electrochemical ligand parameter values of the complexes) are illustrated in **Figure 3.7**.

32 G. Gritzner, J. Kuta, *Pure Appl. Chem.* **1984** (56) 461-466, "Recommendations on reporting electrode potentials in nonaqueous solvents".
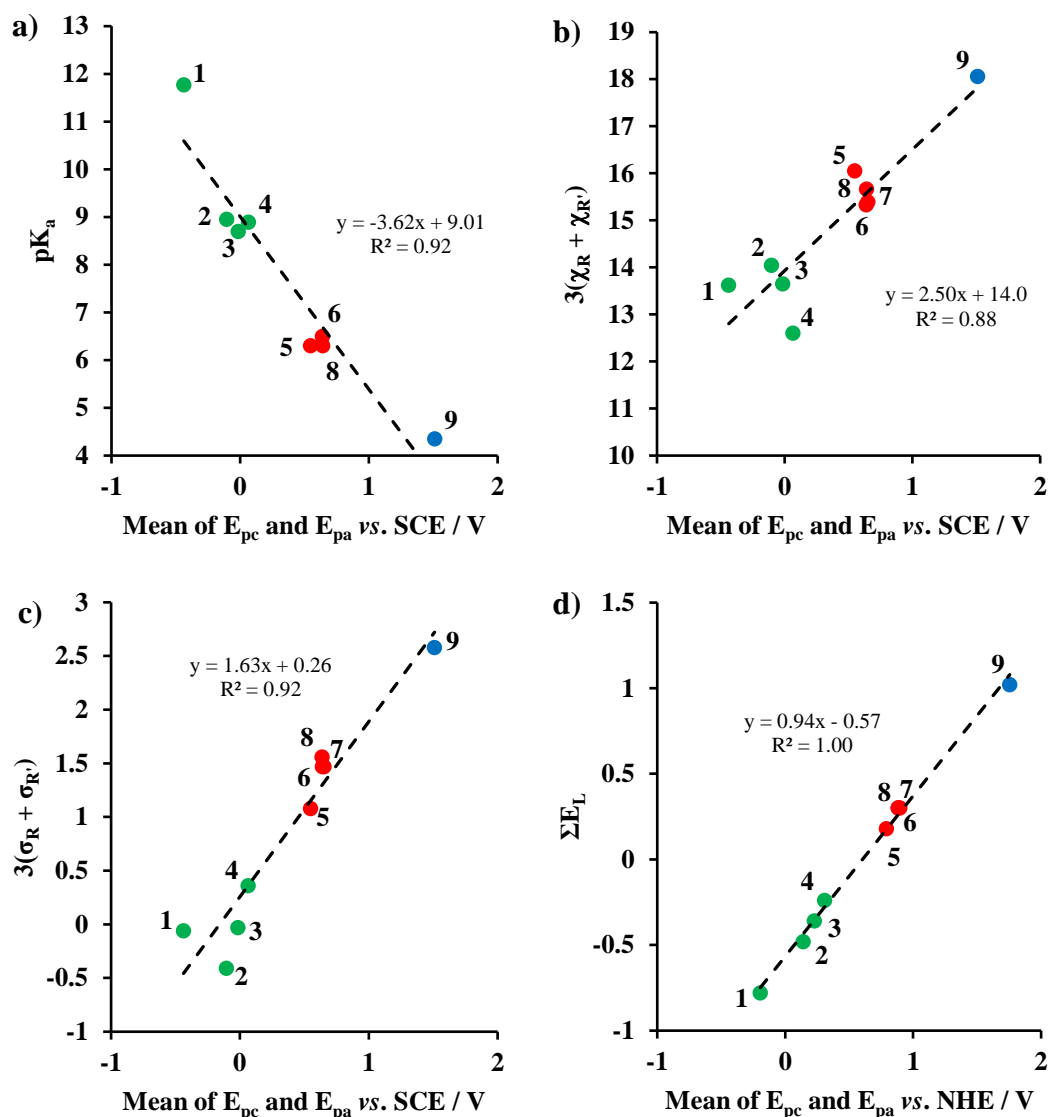
Figure 3.7: The correlation of the experimental mean of E_{pa} and E_{pc} of the Mn^{III}/Mn^{II} redox couple of the [Mn(β-diketonato)$_3$] complexes (where β-diketonato = (RCOCHCOR')$^-$ = dpm, **1**; acac, **2**; ba, **3**; dbm, **4**; tfaa, **5**; tfth, **6**; tffu, **7**; tfba, **8**; and hfaa, **9**), with **a)** the acid dissociation constants (pK_a) of the un-coordinated β-diketones (RCOCH$_2$COR'), **b)** with the total group electronegativity $\Sigma(\chi_R + \chi_{R'})$, **c)** with the total Hammett sigma *meta* constants $\Sigma(\sigma_R + \sigma_{R'})$ of the R and R' groups, and **d)** with ΣE_L, the sum of the Lever electrochemical ligand parameter values for the complexes. The β-diketonato ligands shown in green, red and blue, are the ligand groups which contain none, one and two CF$_3$ R-groups respectively.

Results and discussion

The correlation of the mean E_{pa} and E_{pc} of the Mn^{III}/Mn^{II} redox couple in **Figure 3.7**, showed the following trends:

1) As pK_a decrease the mean of E_{pa} and E_{pc} increases. Higher pK_a makes the manganese metal centre relatively more electron-rich (harder to reduce). The $[Mn^{III}(\beta\text{-diketonato})_3]$ complex with higher pK_a display a more negative reduction potential E_{pc} implying it needs more energy to undergo reduction. The linear equation defining the pK_a relationship with the mean of E_{pa} and E_{pc} (in V) is given by:

$$pK_a= (3.62)(E_{pc} + E_{pa})/2 \text{ } vs. \text{ SCE} + 9.01 \qquad\qquad R^2 = 0.92$$

2) The increase of total group electronegativity of the R-groups, $3(\chi_R + \chi_{R'})$, lead to more positive mean of E_{pa} and E_{pc}. An inverse effect was however found in the three groups (containing none, one or two CF_3 side groups). Within each group an increase of the total group electronegativities causes a slight decrease for the mean of E_{pa} and E_{pc}, see **Figure 3.7 b)**. The linear equation defining the overall $3(\chi_R + \chi_{R'})$ relationship with the mean of E_{pa} and E_{pc} (in V) is given by:

$$3(\chi_R + \chi_{R'}) = (2.50)(E_{pc} + E_{pa})/2 \text{ } vs. \text{ SCE} + 14.0 \qquad\qquad R^2 = 0.88$$

3) With an increase observed in the mean of E_{pa} and E_{pc} an increase of the total Hammett sigma *meta* constants, $3(\sigma_R + \sigma_{R'})$, followed. The manganese metal centre becomes more electron withdrawing with larger Hammett sigma *meta* constants of the R-groups, and as a result reduction of the $[Mn^{III}(\beta\text{-diketonato})_3]$ complexes takes place easier. The linear equation defining the relationship with the mean of E_{pa} and E_{pc} (in V), is given by:

$$3(\sigma_R + \sigma_{R'}) = (1.63)(E_{pc} + E_{pa})/2 \text{ } vs. \text{ SCE} + 0.257 \qquad\qquad R^2 = 0.92$$

4) Through the use of known redox potentials, statistically obtained ΣE_L, on the basis of redox potential-structure relationships, also gives a good fit with the experimental mean of E_{pa} and E_{pc} (in V) of the $[Mn^{III}(\beta\text{-diketonato})_3]$ complexes:

$$\Sigma E_L \text{ } (vs \text{ NHE}) = (0.938)(E_{pc} + E_{pa})/2 \text{ } vs. \text{ NHE} - 0.567 \qquad\qquad R^2 = 1.00$$

(ii)   *Relationships between electrochemical results and DFT calculated data (electron affinity and LUMO energy)*

The Density Functional Theory (DFT) calculated effective EA and energy of the LUMOs of **1**-**9** obtained in **Section 3.1.3.2** and given **Table 3.7** is summarized in **Table 3.11**.

Table 3.11: Summary of the electrochemical and DFT data of [Mn(β-diketonato)$_3$] complexes **1–9**. The E$_{LUMO}$ is obtained from the optimized neutral species of the complexes.

Complex	R	R'	Electrochemical data	DFT data [b]	
			Mean of E_{pc} and E_{pa} *vs* SCE/V [a]	Effective EA /kJ mol^{-1}	(neutral) E$_{LUMO}$ [c] /kJ mol^{-1}
[Mn(dpm)$_3$], **1**	C(CH$_3$)$_3$	C(CH$_3$)$_3$	-0.438	208.1	-312.2
[Mn(acac)$_3$], **2**	CH$_3$	CH$_3$	-0.104	198.6	-328.9
[Mn(ba)$_3$], **3**	CH$_3$	Ph	-0.015	182.3	-336.4
[Mn(dbm)$_3$], **4**	Ph	Ph	0.065	235.8	-350.3
[Mn(tfaa)$_3$], **5**	CF$_3$	CH$_3$	0.548	282.0	-452.5
[Mn(tfth)$_3$], **6**	CF$_3$	C$_4$H$_3$S	0.639	303.5	-430.0
[Mn(tffu)$_3$], **7**	CF$_3$	C$_4$H$_3$O	0.652	293.5	-418.5
[Mn(tfba)$_3$], **8**	CF$_3$	Ph	0.641	298.0	-458.0
[Mn(hfac)$_3$]. **9**	CF$_3$	CF$_3$	1.511	392.1	-541.0

a from **Table 3.10**

b from **Table 3.6** and **Table 3.7**, OLYP/TZP values

c α or β LUMOs

.

The relationship between the mean of E_{pa} and E_{pc} of the Mn^{III}/Mn^{II} redox couple of [Mn(RCOCHCOR')$_3$] complexes **1–9**, and the DFT calculated effective electron affinity (EA) and E$_{LUMO}$ is graphically shown in **Figure 3.8**.

a)
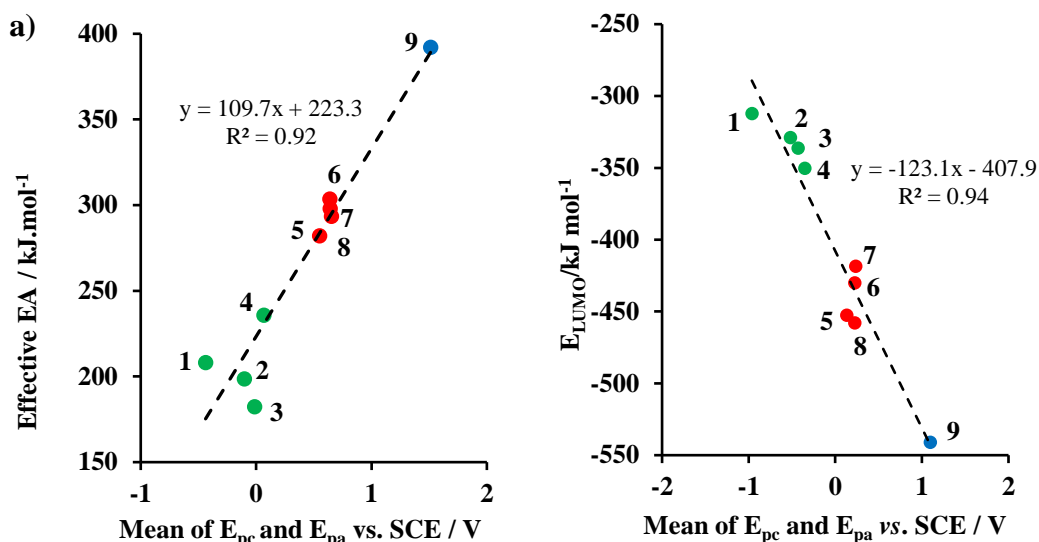
Figure 3.8: The correlation of the experimental mean of E_{pa} and E_{pc} of the Mn^{III}/Mn^{II} redox couple of the [Mn(β-diketonato)$_3$] complexes (where β-diketonato = dpm, **1**; acac, **2**; ba, **3**; dbm, **4**; tfaa, **5**; tfth, **6**; tffu, **7**; tfba, **8**; and hfaa, **9**), with **a)** DFT calculated effective electron affinity (EA) **b)** the LUMO energy (E_{LUMO}) of the neutral [Mn(β-diketonato)$_3$] species

From **Table 3.11** it is observed that with the increase of the reduction potential (E_{pc}) the calculated electron affinity (EA) also increases. A complex with larger electron affinity (EA, greater affinity to accept electron) would thus be easier to reduce than that of a [Mn(β-diketonato)$_3$] complex with lower EA, see **Figure 3.8 a)**. The linear equation describing the correlation between the calculated EA with the mean of E_{pa} and E_{pc} (in V), is given by:

$$EA = (109.7)(E_{pc} + E_{pa})/2 \; vs. \; SCE + 223.3 \hspace{2cm} R^2 = 0.92$$

When a [Mn(β-diketonato)$_3$] complex species is reduced, an electron is added to the lowest unoccupied molecular orbital (the LUMO). A linear correlation between the calculated LUMO energy (E_{LUMO}) and the Mn^{III}/Mn^{II} mean of E_{pa} and E_{pc} was obtained, showing that a decrease in the LUMO energy correlates the mean of E_{pa} and E_{pc} to increase. This relationship can be seen in **Figure 3.8 b)**. The linear equation that describes this correlation is, with the mean of E_{pa} and E_{pc} (in V):

$$E_{LUMO} = (-123.2) (E_{pc} + E_{pa})/2 \; vs. \; SCE - 407.9 \hspace{2cm} R^2 = 0.94$$

3.1.5 X-ray photoelectron spectroscopy (XPS) study of [Mn(β-diketonato)₃] complexes

The eight [Mn(β-diketonato)₃] complexes ([Mn(dpm)₃, **1**;[Mn(acac)₃], **2**; [Mn(ba)₃], **3**; [Mn(dbm)₃], **4**; [Mn(tfaa)₃], **5**; [Mn(tfth)₃], **6**; [Mn(tffu)₃], **7**; [Mn(tfba)₃], **8**, and [Mn(hfaa)₃], **9**) that were synthesized in **Section 3.1.1**, were further characterized by XPS. Firstly the neat samples [Mn(β-diketonato)₃] complexes **1**-**9** (**Section 3.1.5.1**), secondly complexes **2**-**9** bound to amino-functionalized Si-wafers (2-D support, **Section 3.1.5.2**) and thirdly the complexes **2**-**9** which was wet impregnated onto various 3-D supports (see **Section 0**) will be presented.

3.1.5.1   XPS study of neat [Mn(β-diketonato)₃] complexes

Large parts of the data presented in this section were published in *RSC Advances* 2017 (7) 27718-27728, R. Gostynski, J. Conradie and E. Erasmus - Published by The Royal Society of Chemistry. The [Mn(β-diketonato)₃] complexes (**1**-**9**) were characterized by XPS. The wide scan XPS of the [Mn(tfba)₃], **8**, complex is illustrated in **Figure 3.9** as an example.
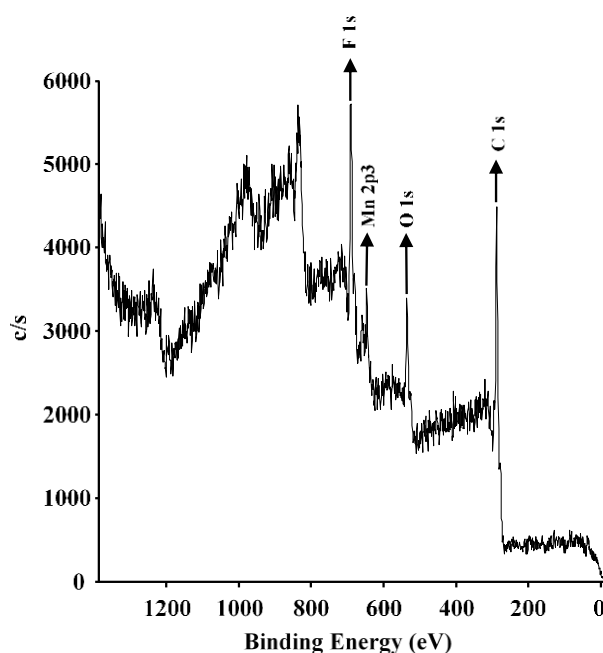
Figure 3.9: Wide XPS scan of [M(tfba)₃], **8**

The atomic ratios obtained from the XPS of [Mn(tfaa)₃], **5**; [Mn(tfth)₃], **6**; [Mn(tffu)₃], **7**; [Mn(tfba)₃], **8**, and [Mn(hfaa)₃], **9** are tabulated in **Table 3.12**. It is expected that the [Mn(β-diketonato)₃] complexes with one CF₃ group on the backbone of the β-diketonato ligand will have a Mn:F ratio of 1:9 (three CF₃ groups in each complex). The Mn:F ratios seen in **Table**

3.12 of the four complexes with one CF_3 group on the backbone of the β-diketonato ligand ([Mn(tfaa)$_3$], **5**; [Mn(tfth)$_3$], **6**; [Mn(tffu)$_3$], **7** and [Mn(tfba)$_3$], **8**) are approximately 1:9 which is in accordance with the expected Mn:F ratio. The [Mn(tfth)$_3$], **6**, complex has one thiol group on each of the backbone of the β-diketonato ligands, therefore in addition to the 1:9 Mn:F ratio a 1:3 Mn:S ratio is also expected. The Mn:S ratio of the [Mn(tfth)$_3$], **6** complex is *ca.* 1:3 which is in accordance with the expected Mn:S ratio. The [Mn(hfaa)$_3$], **9**, complex has two CF_3 groups on the backbone of the β-diketonato ligands (6 x CF_3 groups in total), in **Table 3.12** a Mn:F of 1:18.1 is observed which is in agreement with the expected 1:18 Mn:F ratio. The tabulated atomic percentages of C and O are more than the atomic percentages of C and O in the complexes, since adventitious C[33] and O contamination (samples were exposed to air) is present.

Table 3.12: Atomic ratios obtained from the wide XPS scans of [Mn(tfaa)$_3$], **5**; [Mn(tfth)$_3$], **6**; [Mn(tffu)$_3$], **7**; [Mn(tfba)$_3$], **8**, and [Mn(hfaa)$_3$], **9**.

Complex	Atomic % (%)					Atomic ratio	
	S	F	Mn	C	O	Mn:F	Mn:S
[Mn(tfaa)$_3$], **5**	-	29.5	3.4	38.9	28.2	1:8.7	-
[Mn(tfth)$_3$], **6**	6.9	18.2	2.1	58.3	14.6	1:8.7	1:3.3
[Mn(tffu)$_3$]. **7**	-	20.9	2.3	55.4	21.3	1:9.1	-
[Mn(tfba)$_3$], **8**	-	24.4	2.7	61.5	11.4	1:9.0	-
[Mn(hfaa)$_3$], **9**	-	30.7	1.7	45.7	21.9	1:18.1	-

The summary of the binding energies obtained from the detailed XPS scans of the Mn and F peaks are tabulated in **Table 3.13**.

---

[33] S. Evens, *Surface and Interface Analysis* **1997** (25) 924-930, "Correction for the Effects of Adventitious Carbon Overlayers in Quantitative XPS Analysis". DOI: 10.1002/(SICI)1096-9918(199711)25:12<924::AID-SIA317>3.0.CO;2-

Table 3.13: The binding energies (BE) in eV of F, and Mn obtained of neat [Mn(β-diketonato)₃] complexes (**1-9**) from XPS measurements.

Complex	R	R'	$3(\chi_R + \chi_{R'})^a$	BE F 1s$_{main}$ (eV)	BE F 1s$_{satel}$ (eV)	$\Delta BE_1{}^b$ (eV)	$I_{ratio(F)}{}^c$	BE Mn 2p$_{3/2main}$ (eV)	BE Mn 2p$_{3/2satel}$ (eV)	$\Delta BE_2{}^d$ (eV)	$I_{ratio(Mn)}{}^e$
[Mn(dpm)₃], **1**	C(CH₃)₃	C(CH₃)₃	13.62	-^{f}	-^{f}	-^{f}	-^{f}	641.67	645.87	4.20	0.16
[Mn(acac)₃], **2**	CH₃	CH₃	14.04	-^{f}	-^{f}	-^{f}	-^{f}	641.73	646.09	4.36	0.17
[Mn(ba)₃], **3**	CH₃	Ph	13.65	-^{f}	-^{f}	-^{f}	-^{f}	641.69	645.98	4.29	0.16
[Mn(dbm)₃], **4**	Ph	Ph	13.26	-^{f}	-^{f}	-^{f}	-^{f}	641.67	645.99	4.32	0.17
[Mn(tfaa)₃], **5**	CF₃	CH₃	16.05	688.42	683.4	5.02	0.43	642.05	645.81	3.76	0.11
[Mn(tfth)₃], **6**	CF₃	C₄H₃S	15.33	688.28	683.75	4.56	0.45	641.93	645.73	3.9	0.13
[Mn(tffu)₃], **7**	CF₃	C₄H₃O	15.39	688.31	684.62	3.69	0.41	641.97	645.84	3.87	0.13
[Mn(tfba)₃], **8**	CF₃	Ph	15.66	688.35	682.51	5.84	0.77	641.99	645.83	3.84	0.11
[Mn(hfac)₃]. **9**	CF₃	CF₃	18.06	688.59	685.55	3.04	0.52	642.38	645.73	3.35	0.05

a Sum of R-group electronegativities, $3(\chi_R + \chi_{R'})$

b $\Delta BE_1 = BE_{F1s\ satel} - BE_{F1s\ main}$

c $I_{ratio(F)} = (I_{F1s\ satel})/(I_{F1s\ main})$

d $\Delta BE_2 = BE_{Mn2p3/2satel} - BE_{Mn2p3/2main}$

e $I_{ratio(Mn)} = (I_{Mn2p3/2satel})/(I_{Mn2p3/2main})$

f Complexes containing no CF₃ groups on the β-diketonato ligands

(i)   *Mn 2p peaks*

The binding energies at the maximum peak height of the main Mn 2p$_{3/2}$ photoelectron line of the [Mn(β-diketonato)₃], **1-9**, complexes are observed at *ca.* 642 eV with a satellite peak at *ca.* 4 eV higher. The main Mn 2p$_{3/2}$ photoelectron lines are *ca.* 3 eV higher than that of manganese(0) (638.7 eV),[34,35] confirming the III oxidation state of the Mn centres. The Mn 2p$_{3/2}$ and Mn 2p$_{1/2}$ peak deconvolution of the neat [Mn(tfaa)₃], **5**, complex is illustrated in **Figure 3.10 a)** and that of complexes **7** and **8** in **Appendix B**. The Mn 2p peaks gave broad unsymmetrical single peaks, which displayed a full width half maximum (FWHM) larger than 4.3 eV and a spin orbit splitting of *ca.* 11.7 eV. It has been shown that the larger the pass energy used

[34] D. Banerjee, H.W. Nesbitt, *Geochimica et Cosmochimica Acta* **1999** (63) 3025-3038, "XPS study of reductive dissolution of birnessite by oxalate: rates and mechanistic aspects of dissolution and redox processes".

[35] H.W. Nesbitt, D. Banerjee, *American Mineralogist* **1998** (83) 305–315, "Interpretation of XPS Mn(2p) spectra of Mn oxyhydroxides and constraints on the mechanism of MnO₂ precipitation".

during the experiment, the larger the FWHM will be.[36, 37] Since a large pass energy had to be used to obtain well defined peaks (the same pass energy of 93.90 eV was used for all the [Mn(β-diketonato)$_3$] complexes for the Mn 2p region), the FWHM of the obtained peaks are rather large in comparison to the 2.2 eV reported for cubic alloy $Al_{60}Pd_{25}Mn_{15}$, which was measured at a pass energy of 29 eV[38] and elemental Mn which showed FWHM of 2.52 eV measured at the pass energy of 35.75 eV[39]. The larger than expected FWHM could be attributed to final state effects like the coupling of the angular momenta of the unpaired electrons of the core level electrons after photoionization with one of the four unpaired 3d electrons (Mn^{III} exist in the high-spin paramagnetic state) of the outer orbitals (causing multiplet splitting), crystal field- and electrostatic interactions.[40, 41]

An increase in the total Gordy group electronegativity of the R-groups on the β-diketonato ligands, $3(\chi_R + \chi_{R'})$, is accompanied by an increase in the binding energy of the Mn 2p$_{3/2}$ peaks (**Figure 3.10 b)**, **Table 3.13**). With an increase of β-diketonato ligands' electronegativity the electrophilicity or δ^+ charge on the metal (Mn) centre will accordingly also be higher (Mn centre will be more positively charged). This causes the Mn^{3+} nucleus to bind stronger to its core electrons which in turn increases the amount of energy needed to emit a Mn 2p electron to the Fermi level.[42] The linear relationship obtained between the binding energy (BE) of the Mn 2p$_{3/2main}$ peaks and $3(\chi_R + \chi_{R'})$ fits the equation:

[36] M.C. Biesinger, B.P. Payne, A.P. Grosvenor, L.W.M. Lau, A.R. Gerson, R.St.C. Smart, *Appl. Surf. Sci.* **2011** (257) 2717-2730, "Resolving surface chemical states in XPS analysis of first row transition metals, oxides and hydroxides: Cr, Mn, Fe, Co and Ni". DOI: 10.1016/j.apsusc.2010.10.051

[37] M.C. Biesinger, C. Brown, J.R. Mycroft, R.D. Davidson, N.S. McIntyre, *Surf. Interface Anal.* **2004** (36) 1550-1563, "X-ray photoelectron spectroscopy studies of chromium compounds". DOI: 10.1002/sia.1983

[38] C.J. Jenks, S.-L. Chang, J.W. Anderegg, P.A. Thiel, D.W. Lynch, Phys. Rev. **1996** (B 54) 6301, "Photoelectron spectra of an $Al_{70}Pd_{21}Mn_9$ quasicrystal and the cubic alloy $Al_{60}Pd_{25}Mn_{15}$". DOI: 10.1103/PhysRevB.54.6301

[39] A.R. Chourasia, D.R. Chopra, Surf. Sci. Spectra 1994 (3) 74, "Elemental Manganese Studied by X-ray Photoemission Spectroscopy Using Mg and Zr Radiations". DOI: 10.1116/1.1247766

[40] R.P. Gupta, S.K. Sen, *Phys. Rev. B*, **1974** (10) 71, "Calculation of multiplet structure of core p-vacancy levels". DOI: 10.1103/PhysRevB.10.71

[41] R.P. Gupta, S.K. Sen, *Phys. Rev. B*, **1975** (12) 15, "Calculation of multiplet structure of core p -vacancy levels. II". DOI: 10.1103/PhysRevB.12.15

[42] A.P. Grosvenor, B.A. Kobe, M.C. Biesinger, N.S. McIntyre, *Surf. Interface Anal.* **2004** (36) 1564-1574, "Investigation of multiplet splitting of Fe 2p XPS spectra and bonding in iron compounds". DOI: 10.1002/sia.1984

$$BE_{\text{Mn 2p3/2 main}} = 0.153[3(\chi_R + \chi_{R'})] + 639.6 \qquad\qquad R^2 = 0.99$$

As mentioned earlier, the Mn $2p_{3/2}$ satellite peak is located at *ca.* 3.7 eV higher binding energy than the main Mn $2p_{3/2}$ peak. The intensity of the satellite and main peaks are of importance in paramagnetic compounds. It has been shown that there exists a correlation between the ratio of the intensities of the satellite towards the main Mn $2p_{3/2}$ peak, $I_{\text{ratio(Mn)}} = (I_{\text{Mn2p3/2satel}})/(I_{\text{Mn2p3/2main}})$, and the spin density (magnetic moment, *i.e.* increasing number of unpaired electrons) of the compound.[43,44] From **Figure 3.10 c)** it can be seen that there exists an inversely proportional relationship between $I_{\text{ratio(Mn)}}$ (and therefore also spin density) and $3(\chi_R + \chi_{R'})$. However, the same number of unpaired electrons are present in all of the Mn^{III} in the [Mn(β-diketonato)$_3$] complexes **1**-**9**. Thus to clarify the relationship, between $I_{\text{ratio(Mn)}}$ and $3(\chi_R + \chi_{R'})$, the increase in magnetic moment or spin density could be considered proportional to the increase in polarity (electron density shift to one side of the β-diketonato ligand) of the valence electrons due to increased $3(\chi_R + \chi_{R'})$. This relationship thus shows that an increase in polarity (electron density shift to one side of the β-diketonato ligand) and by implication $3(\chi_R + \chi_{R'})$ is accompanied by a larger satellite peak.

These satellite peaks detected for first row transition metal complexes with an octahedral symmetry is assigned to the $e_g - e_g*$ and/or $t_{2g} - t_{2g}*$ charge transfer process from the ligand-to-metal.[45] As more charge is transferred from the ligand to the metal *via* a σ-donor mechanism, the larger the satellite charge transfer peak (shake-up peak) becomes. The inversely proportional relationship between $3(\chi_R + \chi_{R'})$ and $I_{\text{ratio(Mn)}}$ (**Figure 3.10 c)**) affirms that β-diketonato ligands with higher $3(\chi_R + \chi_{R'})$ values (e.g. $3(\chi_R + \chi_{R'}) = 18.06$ for [Mn(hfaa)$_3$], **9**), which possesses stronger electron withdrawing properties than the other [Mn(β-diketonato)$_3$] complexes, would obviously transfer less charge to the Mn metal centre than

[43] Yu. G. Borod'ko, Yu. I. Vetchinkin, S. L. Zimont, I.N. Ivleva, Y.M. Shul'ga, *Chem. Phys. Lett.* **1976** (42) 264-267, "Nature of satellites in x-ray photoelectron spectra XPS of paramagnetic cobalt (II) compounds". DOI: 10.1016/0009-2614(76)80360-0

[44] M.S. Ioffe, Y.G. Borod'Ko, *J. Elec. Spec. Rel. Phen.* **1977** (11) 235-238, "Dependence of satellite intensity in X-ray photoelectron spectra of Cu(II) complexes on the spin density on copper". DOI: 10.1016/0368-2048(77)85114-1

[45] J.S.H.Q. Perera, D.C. Frost, C.A. McDowell, *Journal of Chemical Physics* **1980** (72) 5151, "X-ray photoelectron spectroscopy of Co(II), Ni(II), and Cu(II) acetylacetonate vapors". DOI: dx.doi.org/10.1063/1.439749

the ligands of, for example, [Mn(dbm)$_3$], **4**, with $3(\chi_R + \chi_{R'}) = 13.62$. The linear relationship obtained between $I_{\text{ratio(Mn)}}$ and $3(\chi_R + \chi_{R'})$ fits the equation:

$$I_{\text{ratio(Mn)}} = -0.025[3(\chi_R + \chi_{R'})] + 0.506 \qquad\qquad R^2 = 0.96$$

The overlap of the Mn atomic orbitals with the atomic orbitals of the ligand, is responsible for the formation of the bonding and anti-bonding orbitals. The molecular orbital energy of a covalent bond depends on the level of overlap between these orbitals. A larger overlap of the orbitals will lead to a lower energy of the bonding orbital and a higher energy of the anti-bonding orbital. Since the satellite Mn 2p$_{3/2}$ photoelectron line denotes the charge-transfer from the ligand to the metal, the difference between the maximum binding energies of the satellite and the main Mn 2p$_{3/2}$ photoelectron line, $\Delta BE_2 = BE_{\text{Mn2p3/2satel}} - BE_{\text{Mn2p3/2main}}$, can be used as a measure of the degree of covalence of the ligand-metal bond. The relationship obtained from the plot between $3(\chi_R + \chi_{R'})$ and $\Delta BE_{2(\text{Mn})}$, shows that the degree of covalency (ΔBE_2) of the ligand-metal bond decreases as $3(\chi_R + \chi_{R'})$ increases. This is consistent with reported data from a series of Mn-halides, where MnF$_2$ (Pauling $\chi_{Cl} = 3.98$)[46] showed a lower degree of covalency than MnBr$_2$ (Pauling $\chi_{Br} = 2.96$). The linear relationship between the difference between the maximum binding energy of the satellite Mn 2p$_{3/2}$ photoelectron line and the main Mn 2p$_{3/2}$ photoelectron line (ΔBE_2) and the sum of β-diketonato ligand Gordy scale R-group electronegativities, $3(\chi_R + \chi_{R'})$, and the linear relationship found between the main Mn 2p$_{3/2}$ photoelectron envelope (BE$_{\text{Mn2p3/2main}}$), the ratio of the intensities of the satellite and main Mn 2p$_{3/2}$ photoelectron line ($I_{\text{ratio(Mn)}}$) (**Figure 3.10 d)**, **Figure 3.10 e)**) fits the equations respectively:

$$\Delta BE_2 = -0.212[3(\chi_R + \chi_{R'})] + 7.174 \qquad\qquad R^2 = 0.96$$

$$I_{\text{ratio(Mn)}} = -0.0162[3\,BE_{\text{Mn 2p3/2 main}}] + 104.4 \qquad\qquad R^2 = 0.97$$

[46] L. Pauling, *Journal of American Chemical Society* **1932** (54) 3570-3582, "THE NATURE OF THE CHEMICAL BOND. IV. THE ENERGY OF SINGLE BONDS AND THE RELATIVE ELECTRONEGATIVITY OF ATOMS". DOI: 10.1021/ja01348a011
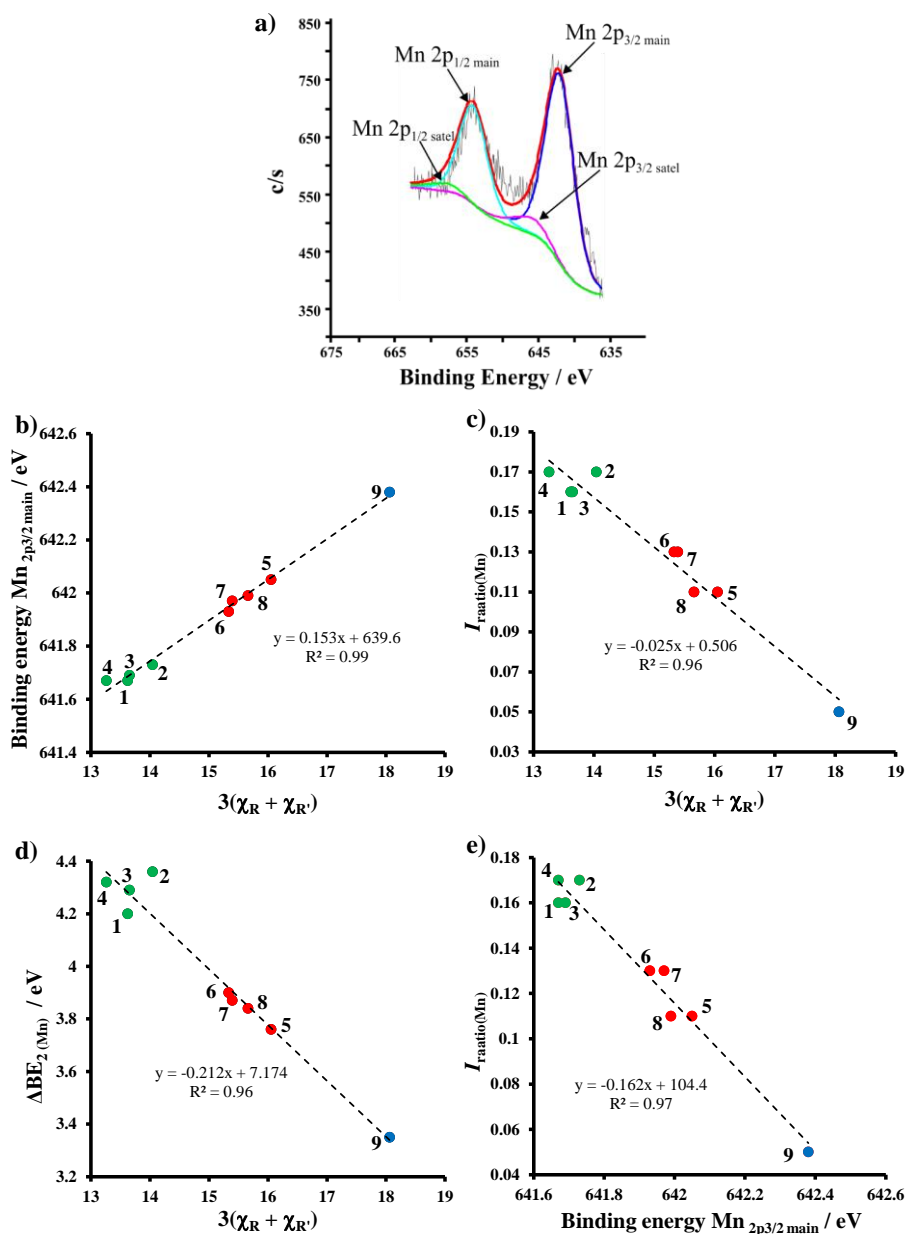
Figure 3.10: a) The fitting (deconvolution) of the [Mn(tfaa)$_3$], **5**, Mn 2p XPS peak. **b)** Relationship between the binding energy of the main Mn 2p$_{3/2}$ photoelectron envelope and $3(\chi_R + \chi_{R'})$, of **1-9**. **c)** Relationship between the $I_{ratio(Mn)}$ and $3(\chi_R + \chi_{R'})$, of **1-9**. **d)** Relationship between the $\Delta BE_{2(Mn)}$ and $3(\chi_R + \chi_{R'})$, of **1-9**. **e)** Relationship between $I_{ratio(Mn)}$ and the binding energy of the main Mn 2p$_{3/2}$ photoelectron envelope, of **1-9**.

The relationships presented above for the series of non-ferrocene-containing [Mn(β-diketonato)$_3$] complexes **1**- **9** of this study, compare well with relationships obtained for a series of Mn^{III}(ferrocenyl-β-diketonato)$_3$ complexes published in Molecules 2016 (21) 1427, B.E. Buitendach, E. Erasmus, J.W.H. Niemantsverdriet, J.C. Swarts - Published by MDPI Open Access

Journals.[47] The linear relationships of this study will be given in black while the linear relationships obtained by Buitendach and *et al.* are given in blue:

$$BE_{Mn\ 2p3/2main} = 0.153[3(\chi_R + \chi_{R'})] + 639.6 \qquad R^2 = 0.99$$

$$BE_{Mn2p3/2main} = 0.152[3(\chi_R + \chi_{R'})] + 639.6 \qquad R^2 = 0.99^{[47]}$$

$$I_{ratio(Mn)} = -0.025[3(\chi_R + \chi_{R'})] + 0.506 \qquad R^2 = 0.96$$

$$I_{ratio(Mn)} = -0.026[3(\chi_R + \chi_{R'})] + 0.515 \qquad R^2 = 0.91^{[47]}$$

$$\Delta BE_2 = -0.212[3(\chi_R + \chi_{R'})] + 7.174 \qquad R^2 = 0.96$$

$$\Delta BE_2 = -0.201[3(\chi_R + \chi_{R'})] + 6.99 \qquad R^2 = 0.96^{[47]}$$

The similarities between the linear relationships of the two studies (the [Mn(β-diketonato)$_3$] complexes and the [Mn^{III}(ferrocenyl-β-diketonato)$_3$] complexes[47]), show that the equations can be used to a high degree of accuracy to determine the binding energies of Mn 2p$_{3/2}$ main photoelectron line and amount of charge transfer *via* a σ-donor mechanism of related [Mn(β-diketonato)$_3$] complexes, if the electronegativity χ_R of the R groups on the backbone of the the β-diketonato ligands (RCOCHCOR')$^-$, is known.

(ii)   *F 1s peak*

Similar to the satellite peaks observed in the Mn 2p spectra representing the charge transfer from the ligand to metal, a similar charge transfer peak representing the ligand could be detected. Since all the [Mn(β-diketonato)$_3$] complexes, **5-9**, contains CF$_3$-fragments, the F 1s peak can be seen as a representative of the ligand. For complexes **5-9**, the F 1s peak has a maximum binding energy at *ca.* 684 eV, with a very distinct shoulder at *ca.* 4.4 eV lower than the main F 1s peak. This satellite peak which represents the charge transfer from the ligand to the metal, is formed by a shake-down mechanism.

---

[47] B.E. Buitendach, E. Erasmus, J.W.H. Niemantsverdriet, J.C. Swarts, *Molecules* **2016** (21) 1427, "Properties of Manganese(III) Ferrocenyl-β-Diketonato Complexes Revealed by Charge Transfer and Multiplet Splitting in the Mn 2p and Fe 2p X-Ray Photoelectron Envelopes". DOI: 10.3390/molecules21111427

The F 1s peak fitting of the [Mn(tfaa)₃], **5**, complex is illustrated in **Figure 3.11**. Unlike the good correlations obtained for the Mn 2p peaks, no meaningful relationships could be established for the F 1s peaks.
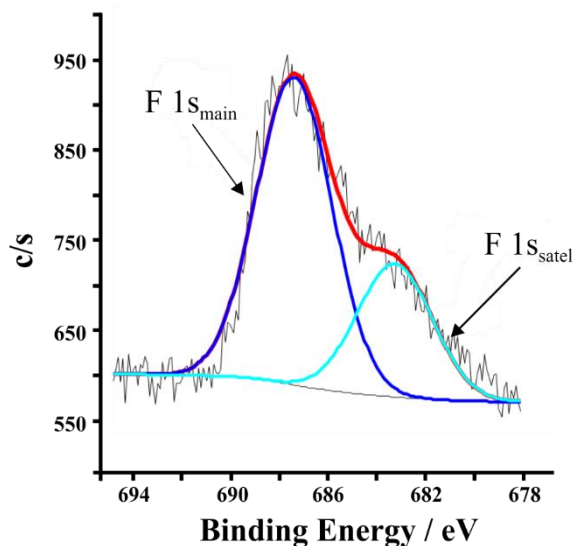
Figure 3.11: The fitting (deconvolution) of the [Mn(tfaa)₃], **5**, F 1s XPS peak.

3.1.5.2 Study of [Mn(β-diketonato)₃] complexes grafted on amino-functionalized Si-wafers

In this part of the study the eight [Mn(β-diketonato)₃] complexes **2–9** were grafted onto the 2-D amino-functionalized Si-wafers. But first the preparation and characterisation of the 2-D silicon wafer support will be discussed.

(i) *Preparation and characterisation of the 2-D silicon wafer support*

Silicon wafers (Si-wafers) with a (100) surface orientation was used as a flat 2-D support in this study. This silicon surface was modified before any metal containing complex (potential catalyst) was anchored onto it.

The Si-wafer was calcined to form a thin silicon oxide (-O-Si-O-) layer. The thickness of this bridged -O-Si-O- network was previously reported to be *ca.* 90 nm.[48,49,50] The -O-Si-O- was then

[48] P. C. Thune, J. Loos, A. M. de Jong, P. J. Lemstra, J. W. Niemantsverdriet, *Top. Catal.* **2000** (13) 67-74, "Planar model system for olefin polymerization: the Phillips CrOx/SiO₂ catalyst". DOI: 10.1023/A:1009084922459

[49] Z. H. Lu, J. P. McCaffrey, B. Brar, G. D. Wilk, R. M. Wallace, L. C. Feldman, S. P. Tay, *Appl. Phys. Lett.* **1997** (71) 2764-2766, "SiO₂ film thickness metrology by x-ray photoelectron spectroscopy". DOI: 10.1063/1.120438

[50] T. Eickhoff, V. Medicherla, W. Drube, *J. Elec. Spec. Rel. Phenom.* **2004** (137-140) 85-88, "Final state contribution to the Si 2p binding energy shift in SiO₂/Si(1 0 0)". DOI: 10.1016/j.elspec.2004.02.026

hydroxylated to form -Si-OH groups on the surface. Finally, the 3-aminopropyltrimethoxysilane was anchored onto the -OH groups. This 3-step process is illustrated from frontal view of the Si-wafer (wafer goes into the paper plane), in **Scheme 3.5**.
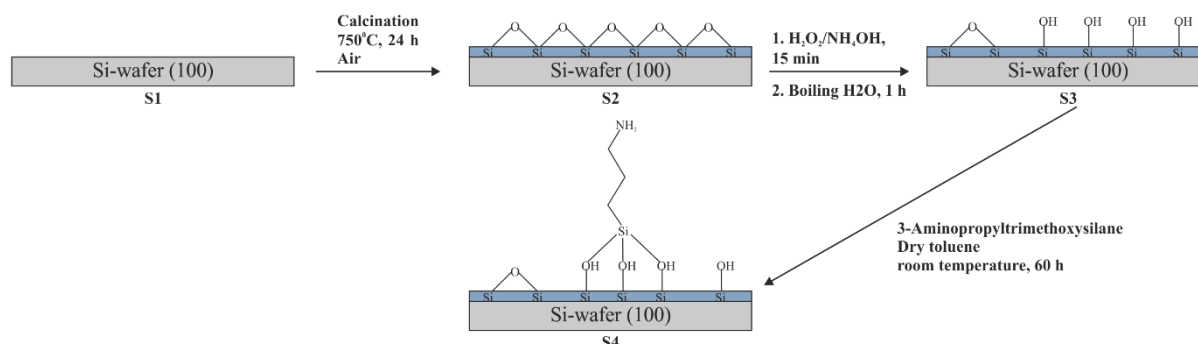
Scheme 3.5: Activation steps of the Si-wafer to form the surfaces **S1**, **S2**, **S3** and **S4**.

The calcined Si-wafer with a layer of -O-Si-O- was immediately hydroxylated without further characterization. The hydroxylated Si-wafer, **S3**, and the amino-functionalized Si-wafer, **S4**, were characterized by XPS and the characterization data is presented in the following sections.

(a)   C 1s peak

XPS measurements of samples often contain adventitious carbon contamination, due to deposition of carbon species present in the atmosphere. The C 1s XPS peak of this adventitious carbon overlaps with the carbon backbone of the silane in the C 1s area of the anchored species of interest during a XPS study.[51] The appearance of a peak at ~ 286.8 eV in **Figure 3.12 b)**, which is assigned to the -C-N- of the 3-aminopropyltrimethoxysilane, see **Scheme 3.6**, is a confirmation that the silanation process was successful.

---

[51] S. Evens, *Surface and Interface Analysis* **1997** (25) 924-930, "Correction for the Effects of Adventitious Carbon Overlayers in Quantitative XPS Analysis". DOI: 10.1002/(SICI)1096-9918(199711)25:12<924::AID-SIA317>3.0.CO;2-
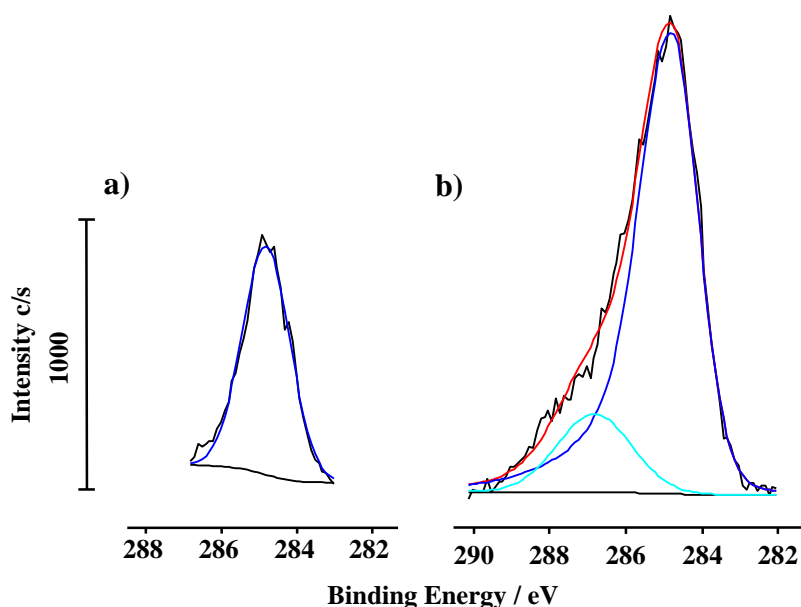
Figure 3.12: Comparison of the XPS measured C 1s peak of **a)** hydroxylated Si-wafer, **S3**, **b)** amino-functionalized Si-wafer, **S4**. The black line represents the experimentally measured peak, red line is the theoretically fitted curve formed by the theoretically introduced peaks (light blue and dark blue lines).

(b) <u>**Si 2p peak**</u>

The Si 2p peaks of the **S4** sample were fitted into 3 peaks between 101 – 103.16 eV, see **Figure 3.13** and **Table 3.14**. Starting from the lowest binding energy the first peak is assigned to the silicon atom in -O-Si-CH$_2$- of the silane (connected to the amino group). The second peak is assigned to the silanol silicon atom in -O-Si-OH, while the third peak is allocated to the silicon atom in -O-Si-O- on the surface. This is in agreement with the PhD studies completed by C.C. Joubert and previously published work.[52,53] The ratios between these three peaks are approximately 1: 1.85: 0.35 (silane: -O-Si-OH: -O-Si-O) which implies that for every silicon (Si) bound to an amine group, there are ~2 unbound Si-OH groups. Since it is known that the procedure used for hydroxylation yields 4-6 OH groups per nm^2, there are 2-3 silane molecules per nm^2. This is further confirmed by the ratio between the atomic percentage of the <u>C</u>-N peak the -O-Si-CH$_2$- of the silane, as well as the N peak (discussed in the next paragraph), which are the same.

---

52 C.C. Joubert, PhD dissertation **2017**, "Copper-Ferrocenyl complexes supported on silicon wafers for heterogeneous catalysis application"

53 M.M. Conradie, J. Conradie, E. Erasmus, *Polyhedron* 2014 (79) 52-59," Immobilisation of iron tris(β-diketonates) on a two-dimensional flat amine functionalised silicon wafer: A catalytic study of the formation of urethane, from ethanol and a diisocyanate derivative " DOI: 10.1016/j.poly.2014.04.054.

Table 3.14: The binding energies in eV of N and Si obtained for the amino-functionalized Si-wafer, **S4**.

Element	N 1s	Si 2p
Amino functionalized Si-wafer **S4**	399.18 (65.73%)	101.91 (31.22%)
	400.27 (26.20%)	102.46 (57.79%)
	401.12 (8.07%)	103.16 (10.99%)
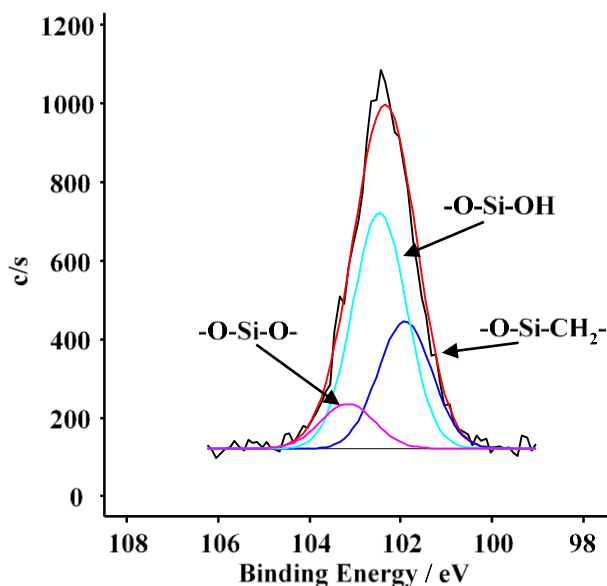
Figure 3.13: The fitting (deconvolution) of the Si 2p XPS peak of the amino-functionalized Si-wafer, **S4**.

(c)   N 1s peak

The 3-aminopropyltrimethoxysilane can be bound in three different ways[54] onto the hydroxylated Si-wafer, **S3**, illustrated in **Scheme 3.6**.

---

[54] R.G. Acres, A.V. Ellis, J. Alvino, C.E. Lenahan, D.A. Khodakov, G.F. Metha, G.G. Anderson, The Journal of Physical Chemistry C 2012 (116) 6289-6297, "Molecular Structure of 3-Aminopropyltriethoxysilane Layers Formed on Silanol-Terminated Silicon Surfaces". DOI: 10.1021/jp212056s
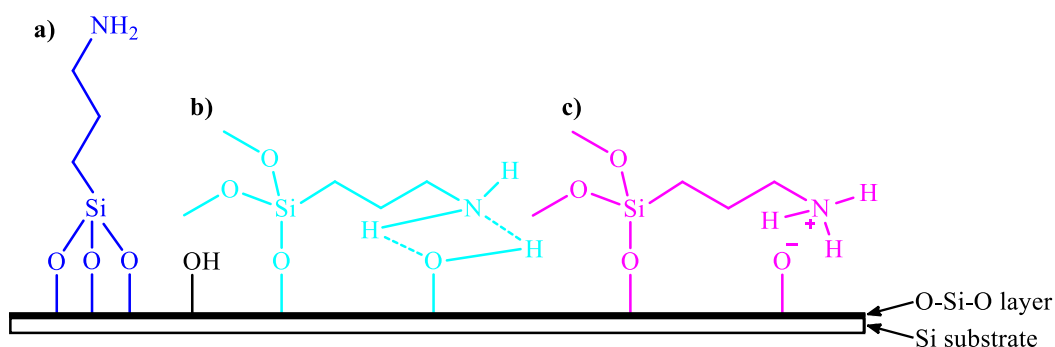
Scheme 3.6: Binding possibilities of 3-aminopropyltrimethoxysilane on to the hydroxylated Si-wafer, **a)** binding that will allow covalent binding of metal contain complexes, **b)** interaction between the amine group and the hydroxylated Si-wafer and **c)** positively charge nitrogen. The different colours indicate correlation to the peak position in **Figure 3.14**.

The N 1s peak of the amino functionalized Si-wafer, **S4**, was therefore fitted with three distinct peaks, shown in **Figure 3.14**. The free amine (-C-NH$_2$, **Scheme 3.6 a)**) was assigned to the peak at 399.18 eV. The hydrogen-bonded amine in **Scheme 3.6 b)** is associated with the peak fitted at 400.27 eV. The positively charged N (with O influence) illustrated in **Scheme 3.6 c)** is assigned to the fitted peak at 401.12 eV.[55,56,57] The data obtained during the XPS measurement is summarized in **Table 3.15**. From the discussion in the previous paragraph, there are 2-3 silane molecules per nm^2, consequently there will also be 2-3 nitrogen molecules per nm^2.

[55] L.D. White, C.P. Tripp, *Journal of Colloid and Interface Science* **2000** (232) 400-407, "Reaction of (3-Aminopropyl)dimethylethoxysilane with Amine Catalysts on Silica Surfaces." DOI: 10.1006/jcis.2000.7224.

[56] F. Zhang, M.P. Srinivasan, *Langmuir* **2004** (20) 2309-2314, "Self-Assembled Molecular Films of Aminosilanes and Their Immobilization Capacities" DOI: 10.1021/la0354638.

[57] S. Gilles, "*Chemical modification of silicon surfaces for the application in soft lithography*", Berichte des Forschungszentrums Jülich, Germany, **2007**, p55-56 & 79-80.
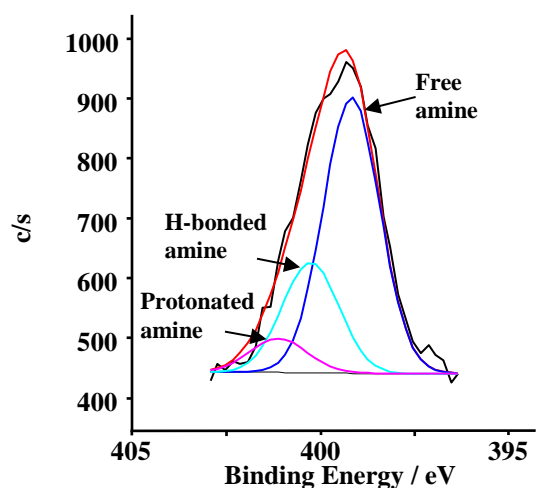
Figure 3.14: The fitting (deconvolution) of the amino-functionalized Si-wafer N 1s XPS peak. The black line represents the experimentally measured peak, red line is the theoretically fitted curve formed by the theoretically introduced peaks (magenta, light blue and dark blue lines), Si-wafer, **S4**.

Table 3.15: The XPS data of the N 1s peak obtained from the amino-functionalized Si-wafer, **S4**.

Band	Position	Position Separation	% Area
1	399.18	0	65.73
2	400.27	1.09	26.2
3	401.12	1.94	8.07

(ii)   *Grafting of [Mn(β-diketonato)₃] complexes onto amino-functionalized Si-wafers*

In this study the eight Mn(β-diketonato)₃ complexes ([Mn(acac)₃], **2**; [Mn(ba)₃], **3**; [Mn(dbm)₃], **4**; [Mn(tfaa)₃], **5**; [Mn(tfth)₃], **6**; [Mn(tffu)₃], **7**; [Mn(tfba)₃], **8**, and [Mn(hfaa)₃], **9**) were grafted onto the amino-functionalized Si-wafers, see **Scheme 3.7** to form surfaces **S5**, **S6**, **S7**, **S8**, **S8**, **S9**, **S10**, **S11** and **S12** respectively.

90

R; R' =

CH₃; CH₃, **2**

CH₃; ⬡ , **3**   ⬡ ; ⬡ , **4**

CF₃; CH₃, **5**   CF₃; ⬠S , **6**

CF₃; ⬠O , **7**   CF₃; ⬡ , **8**

CF₃; CF₃, **9**

Formation of **S5** | Formation of **S6-S12**
in toluene, | in toluene, gentle reflux
Gentle stirring ca. 24 hours | Stirring ca. 16 hours
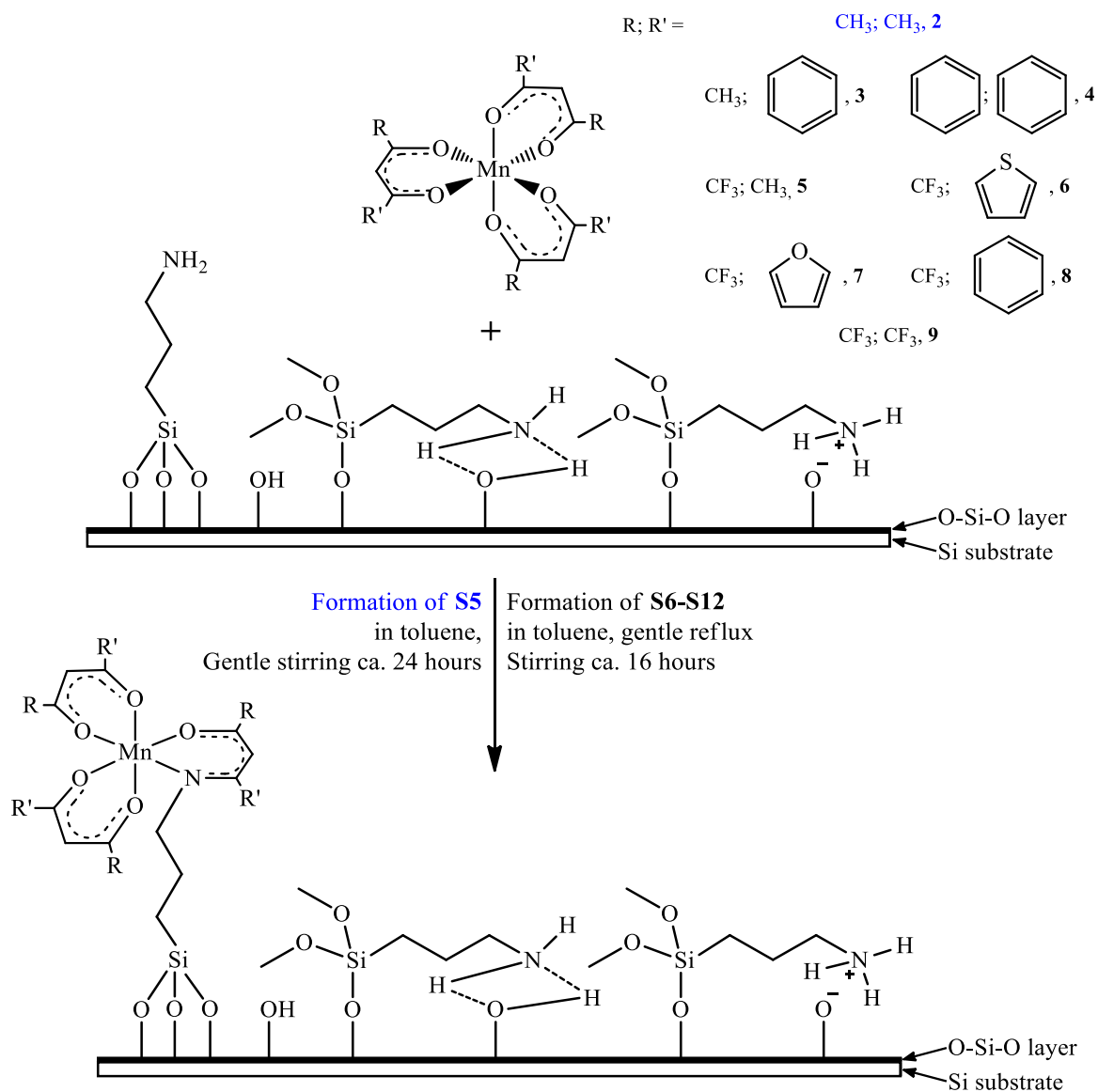
Scheme 3.7: The chemical grafting of [Mn(acac)₃], **2**; [Mn(ba)₃], **3**; [Mn(dbm)₃], **4**; [Mn(tfaa)₃], **5**; [Mn(tfth)₃], **6**; [Mn(tffu)₃], **7**; [Mn(tfba)₃], **8**, and [Mn(hfaa)₃], **9** complexes onto an amino-functionalized Si-wafer to form Mn-grafted Si-wafers **S5**, **S6**, **S7**, **S8**, **S9**, **S10**, **S11** and **S12** respectively.

The XPS data obtained from the eight [Mn(β-diketonato)₃] complexes chemically grafted onto amino-functionalized Si-wafer is summarized in **Table 3.16**.

91

Table 3.16: The binding energies in eV of N, F, S and Mn obtained of the [Mn(β-diketonato)$_3$] complexes grafted onto amino-functionalized Si-wafers from XPS measurements.

Complex	N 1s	Mn 2p$_{3/2}$	Mn 2p$_{1/2}$	F 1s	S 2p$_{3/2}$	S 2p$_{1/2}$
[Mn(acac)$_3$] + amino-functionalized Si-wafer, **S5**	399.47 (59.25%)[a] 399.55 (6.48%)[b] 400.70 (26.20%)[c] 401.43 (8.07%)[d]	641.55 (55.58%)[f] 645.95 (11.09%)[g]	653.37 (27.79%)[f] 657.37 (5.54%)[g]	- - - -	- - -	
[Mn(ba)$_3$] + amino-functionalized Si-wafer, **S6**	399.07 (28.48%)[a] 399.51 (6.02%)[e] 400.02 (31.23%)[b] 400.81 (26.20%)[c] 402.25 (8.07%)[d]	641.90 (51.59%)[f] 645.79 (15.08%)[g]	653.62 (25.79%)[f] 657.48 (7.54%)[g]	- -	 -	
[Mn(dbm)$_3$] + amino-functionalized Si-wafer, **S7**	399.04 (4.26%)[a] 399.43 (61.47%)[b] 400.47 (26.20%)[c] 401.55 (8.07%)[d]	641.71 (48.73%)[f] 645.79 (17.93%)[g]	653.79 (24.37%)[f] 657.48 (8.97%)[g]	- -	- -	
[Mn(tfaa)$_3$] + amino-functionalized Si-wafer, **S8**	397.75 (6.26%)[e] 398.73 (16.83%)[a] 399.55 (42.63%)[b] 400.61 (26.20%)[c] 401.30 (8.07%)[d]	641.77 (50.90%)[f] 645.63 (15.76%)[g]	653.55 (25.45%)[f] 657.32 (7.88%)[g]	684.85 (13.72%)[h] 687.92 (86.28%)[i]	- - -	
[Mn(tfth)$_3$] + amino-functionalized Si-wafer, **S9**	397.54 (1.46%)[e] 398.86 (24.68%)[a] 399.75 (39.60%)[b] 400.81 (26.20%)[c] 402.31 (8.07%)[d]	641.58 (50.04%)[f] 645.86 (16.63%)[g]	653.14 (25.02%)[f] 657.41 (8.31%)[g]	685.07 (12.76%)[h] 688.17 (87.24%)[i]	164.20 (35.25%)[j] 168.04 (31.42%)[k]	165.25 (17.62%)[j] 169.84 (15.71%)[k]
[Mn(tffu)$_3$] + amino-functionalized Si-wafer, **S10**	397.25 (0.38%)[e] 397.99 (8.61%)[a] 399.84 (56.74%)[b] 401.31 (26.20%)[c] 403.47 (8.07%)[d]	642.01 (45.20%)[f] 645.79 (21.47%)[g]	653.90 (22.60%)[f] 657.48 (10.73%)[g]	688.13 (100.00%)[h]	- - -	
[Mn(tfba)$_3$] + amino-functionalized Si-wafer, **S11**	397.75 (1.24%)[e] 398.41 (4.27%)[a] 399.91 (60.21%)[b] 401.15 (26.20%)[c] 402.83 (8.07%)[d]	641.59 (44.17%)[f] 645.79 (22.50%)[g]	653.37 (22.08%)[f] 657.48 (11.25%)[g]	685.60 (11.85%)[h] 688.19 (88.15%)[i]	- - -	
[Mn(hfaa)$_3$] + amino-functionalized wafer, **S12**	399.57 (55.31%)[a] 399.84 (10.42%)[b] 400.77 (26.20%)[c] 401.47 (8.07%)[d]	642.29 (52.02%)[f] 646.19 (14.64%)[g]	654.07 (26.01%)[f] 657.88 (7.32%)[g]	685.21 (32.43%)[h] 688.36 (67.57%)[i]	- -	

[a] Bound nitrogen (-N-C-CH$_3$, for **S5** & **S6**; -N-C-Ph, for **S7** and -N-C-CF$_3$, for **S8, S9, S10, S11** & **S12**)

[b] Unbound nitrogen (-C-NH$_2$)

[c] Hydrogen bonded nitrogen

[d] Protonated nitrogen

[e] Bound nitrogen (-N-C-CH$_3$, for **S8**; -N-C-Th, for **S9**; -N-C-Fu, for **S10** and -N-C-Ph, for **S11** & **S6**)

[f] Mn 2p main peak

[g] Mn satellite peak (Mn satel peak)

[h] F peak of fluorine containing [Mn(β-diketonato)$_3$] complexes (F $_{main}$)

[i] F satellite peak (F $_{satel}$)

[j] S peak of sulphur containing [Mn(β-diketonato)$_3$] complexes (S $_{main}$)

[k] S satellite peak (S $_{satel}$)

From the atomic ratios of the fluorine containing [Mn(β-diketonato)$_3$] complexes (see **Table 3.17**) the expected Mn:F ratio of 1:9 for complexes with one CF_3 group and Mn:F ratio of 1:18 for [Mn(hfaa)$_3$] was not observed. This means that during the grafting process the [Mn(β-diketonato)$_3$] complexes undergo either decomposition (oxidation) or the binding mode is different from excepted. It has also been reported that an amine functionality (such as the amine-silane bound to the surface) facilitates the cleavage of the β-diketonato ligand by the removal of CO_2,[58] possibly explaining why there is less F (from the β-diketonato-ligand) than expected.

Table 3.17: The Mn:F and Mn:N ratio of the fluorine containing [Mn(β-diketonato)$_3$] complexes ([Mn(tfaa)$_3$], **S8**; [Mn(tfth)$_3$], **S9**; [Mn(tffu)$_3$], **S10**; [Mn(tfba)$_3$], **S11** and [Mn(hfaa)$_3$], **S12**) grafted on amino-functionalized Si-wafers.

Complex	Mn:F ratio	Mn:N ratio
[Mn(tfaa)$_3$] + amino-functionalized Si-wafer, **S8**	1:1.1	1:2.3
[Mn(tfth)$_3$] + amino-functionalized Si-wafer, **S9**	1:1.4	1:2.5
[Mn(tffu)$_3$] + amino-functionalized Si-wafer, **S10**	1:4.1	1:8.2
[Mn(tfba)$_3$] + amino-functionalized Si-wafer, **S11**	1:8.8	1:11.9
[Mn(hfaa)$_3$] + amino-functionalized Si-wafer, **S12**	1:1.1	1:1.2

(a)   Mn 2p peaks

Since there are more than one expected Mn-species on the surface (the intended grafted species as depicted in **Scheme 3.7** and some other decomposition complexes, most likely being a manganese oxide) and not being certain what these species are, no attempt was made to deconvolute separate peaks for these species in the XPS spectra. On average 80% of the Mn detected by XPS are that of the oxide form of Mn, except that of **S11** where only 2.9% was observed, when taking the Mn:F ratios in to account in **Table 3.17**, where [Mn(tfba)$_3$] grafted on amino functionalized Si-wafer, **S11**, had a ratio of 1:8.8. The peak fitting of the other grafted [Mn(β-diketonato)$_3$] complexes can be seen in **Appendix B**.

---

[58] Yang Li, Mohammad Afzaal and Paul O'Brien, Journal of Materials Chemistry **2006** (16) 2175–2180, "The synthesis of amine-capped magnetic (Fe, Mn, Co, Ni) oxide nanocrystals and their surface modification for aqueous dispersibility". DOI: 10.1039/B517351E
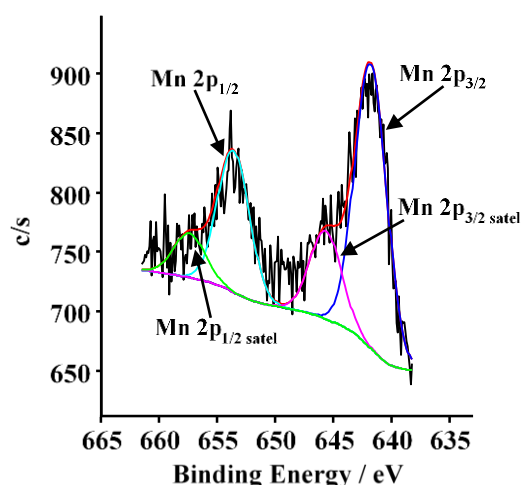
Figure 3.15: The fitting (deconvolution) of the [Mn(β-diketonato)₃] complex grafted onto the amino-functionalized Si-wafer Mn 2p XPS peak, showing [Mn(tfaa)₃] + amino-functionalized Si-wafer, **S8**, as an example.

To confirm that the photoelectron line consist mostly of Mn_2O_3, XPS data was collected of Mn_2O_3 deposited onto the hydroxylated surface (**S3**, to form **S13**) and amino-functionalized Si-wafer surface (**S4**, to form **S14**). [Mn(tfaa)₃], **5**, was also heated in toluene, to mimic the same conditions used to graft the complexes onto the amino-functionalized Si-wafers. The Mn 2p peaks were fitted (see **Figure 3.16**) and summarized in **Table 3.18**.
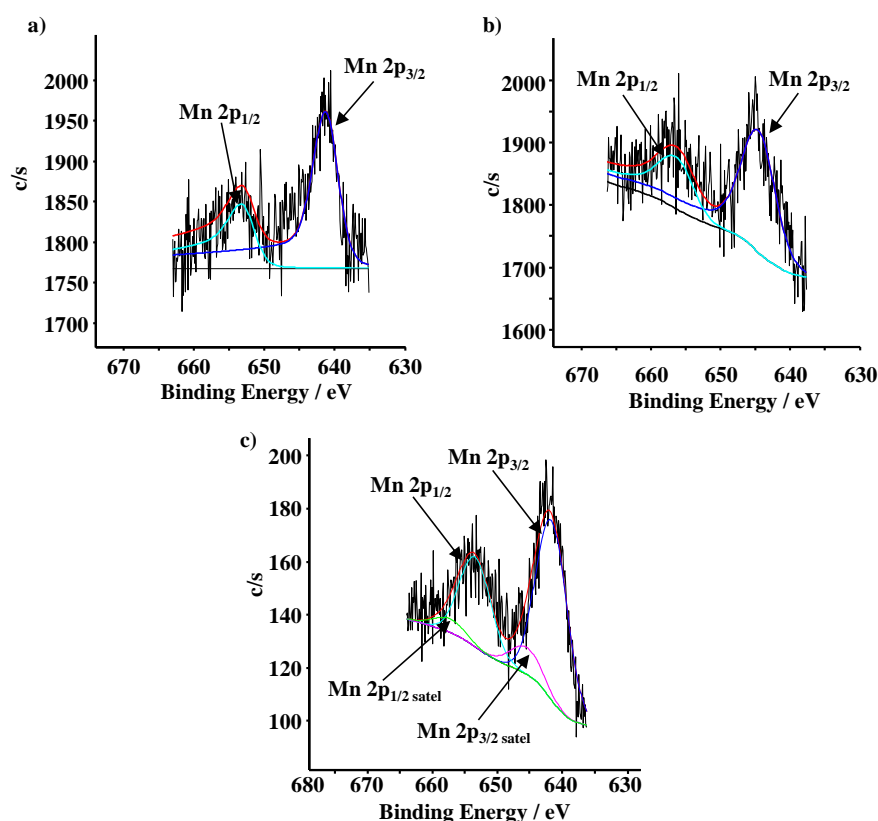
Figure 3.16: The fitting (deconvolution) of the Mn 2p XPS peak of **a)** Mn_2O_3 grafted onto the hydroxylated Si-wafer and **b)** Mn_2O_3 grafted onto the amino-functionalized Si-wafer **c)** [Mn(tfaa)₃] heated in toluene.

Table 3.18: The binding energies in eV of Mn obtained of Mn_2O_3 after grafting conditions with hydroxylated Si-wafer and amino-functionalized Si-wafer, and $[Mn(tfaa)_3]$ heated in toluene.

Complex	Mn 2p$_{3/2}$	Mn 2p$_{1/2}$	Mn:F ratio
Mn_2O_3 + hydroxylated Si-wafer, **S13**	641.90	653.20	-
Mn_2O_3 + amino-functionalized Si-wafer, **S14**	644.60	656.40	-
$[Mn(tfaa)_3]$ heated in toluene	642.08 (57.92%) [b] 645.93 (8.75%) [a]	654.93 (28.96%) [a] 657.77 (4.38%) [b]	1:2

[a] Mn 2p peak
[b] Mn satellite peak (Mn satel peak)

The Mn 2p peaks of the Mn_2O_3 after grafting conditions with the hydroxylated Si-wafer (Mn 2p$_{3/2}$ 641.90 eV peak) is *ca.* 3 eV lower in binding energy than that of the Mn_2O_3 after grafting conditions with the amino-functionalized Si-wafer (Mn 2p$_{3/2}$ 644.60 eV peak). The Mn 2p$_{3/2}$ peaks of the Mn_2O_3 observed form $[Mn(\beta\text{-diketonato})_3]$ complexes ($[Mn(acac)_3]$, **S5**; $[Mn(ba)_3]$, **S6**; $[Mn(dbm)_3]$, **S7**; $[Mn(tfaa)_3]$, **S8**; $[Mn(tfth)_3]$, **S9**; $[Mn(tffu)_3]$, **S10**; $[Mn(tfba)_3]$, **S11**, and $[Mn(hfaa)_3]$, **S12**) grafted on amino-functionalized Si-wafers, are found at binding energies of 641.9 eV and therefore correlates to the Mn_2O_3 on the Si-OH surface and not that of the Mn_2O_3 that has interactions with the amino-functional group. $[Mn(tfaa)_3]$ that was heated in toluene to determine if the conditions used to graft the $[Mn(\beta\text{-diketonato})_3]$ complexes onto the amino-functionalized wafers will cause the complex to decompose. The Mn:F ratios (1:2) obtained from the XPS data confirmed that *ca.* 80% of the $[Mn(tfaa)_3]$ complex decomposed to Mn_2O_3 when exposed to the grafting conditions.

(b) N 1s peak

Even though the Mn peaks were not deconvoluted, an attempt was made to deconvolute the N peaks. The nitrogen (N 1s) peak has been fitted with either four or five distinct peaks. Four peaks were fitted for $[Mn(\beta\text{-diketonato})_3]$ complex (bound to the surface *via* amine-silane) containing the symmetrical ligands (where R- and R'-groups are the same, $[Mn(acac)_3]$, **S5**; $[Mn(dbm)_3]$, **S7** and $[Mn(hfaa)_3]$, **S12**) with no CF_3 or two CF_3 R-groups. The N 1s peak of $[Mn(\beta\text{-diketonato})_3]$ complexes (bound to the surface *via* the amine-silane) containing unsymmetrical ligands (where R- and R'-groups are not the same, $[Mn(tfaa)_3]$, **S8**; $[Mn(tfth)_3]$, **S9**; $[Mn(tffu)_3]$, **S10** and $[Mn(tfba)_3]$, **S11**) with one CF_3 R-group is fitted with five peaks. See **Figure 3.17** for the N 1s peak fitting of $[Mn(acac)_3]$, **S5** and $[Mn(tfaa)_3]$, **S8**, the rest of the N 1s peak fittings are included in **Appendix B**.
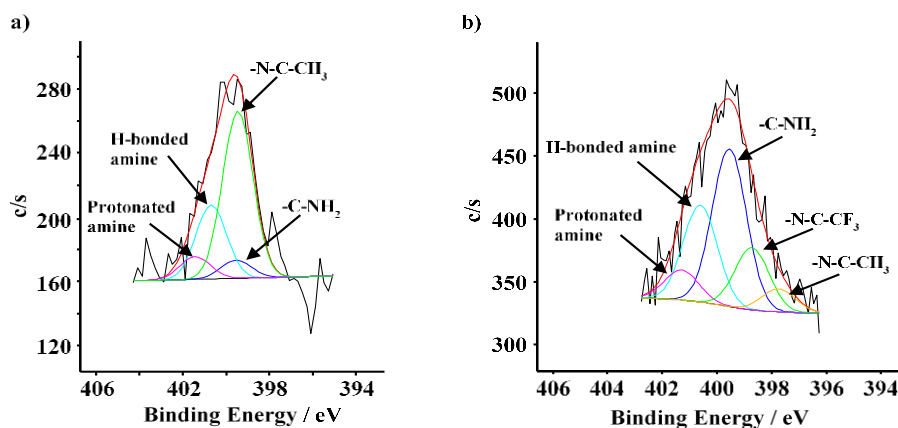
Figure 3.17: The fitting (deconvolution) of the N 1s peak of [Mn(β-diketonato)₃] complexes (**a**) [Mn(acac)₃], **S5** and **b**) [Mn(tfaa)₃], **S8**) grafted onto the amino-functionalized Si-wafer. The black line represents the experimentally measured peak, red line is the theoretically fitted curve formed by the theoretically introduced peaks (magenta, light blue, dark blue, green and yellow lines).

When looking at the [Mn(β-diketonato)₃] complexes (bound to the surface *via* the amine-silane) containing the symmetrical ligands (R = R') the N1s peak fitted at lowest binding energy (399.04-399.57 eV) corresponds to the nitrogen (N) atom bound to [Mn(β-diketonato)₃] complexes[59] on the surface. The second peak (399.43-399.84 eV) is attributed to the unreacted nitrogen atom -C-NH₂ in the silane on the surface. The hydrogen bonded nitrogen atom of the silane on the surface and the protonated nitrogen atom is assigned to the third (400.47-400.77 eV) and fourth (401.43-401.55 eV) N 1s peaks. The nitrogen peaks that is not bound to the [Mn(β-diketonato)₃] complexes have similar binding energies discussed in **Section 3.1.5.2 (i) (c)**.

The deconvolution of the N 1s photoelectron line of [Mn(β-diketonato)₃] complexes (bound to the surface *via* the amine-silane) containing unsymmetrical ligands (R≠R') were simulated to have five distinct peaks. The N 1s peak at the lowest binding energy that was assigned to the nitrogen bound to the [Mn(β-diketonato)₃] complexes with symmetrical β-diketonato ligands is now split in two peaks due to the great influence the electronegativity (Gordy group electronegativity scale) of the different R-groups have on the chemical surroundings. The N 1s peak at the lowest binding energy (397.25-397.75 eV) for complexes with one CF₃ R-group and 399.07 eV for [Mn(ba)₃], **S7** with no CF₃ R-group) corresponds to the nitrogen (N) atom bound to the R-group side of the

[59] M.M. Conradie, J. Conradie, E. Erasmus, *Polyhedron* **2014** (79) 52-59, "Immobilisation of iron tris(β-diketonates) on a two-dimensional flat amine functionalised silicon wafer: A catalytic study of the formation of urethane, from ethanol and a diisocyanate derivative " DOI: 10.1016/j.poly.2014.04.054.

β-diketonato ligand with more electron donating groups, where R = CH$_3$(χ_{CH3}=2.34), Ph(χ_{Ph}=2.21), Th(χ_{Th}=2.10) and Fu(χ_{Fu}=2.23). The second peak (399.51 eV for [Mn(ba)$_3$], **S7** with no CF$_3$ R-group and 397.99-398.41 eV for **S8**-**S11** with one CF$_3$ R-group) is allocated to the nitrogen atom bound to the more electronegative R-group side of the β-diketonato ligand, where R = CF$_3$ for **S8**-**S11** and CH$_3$ for **S7** (χ_{CF3}=3.01 and χ_{CH3}=2.34). The third (399.75-400.47 eV), fourth (400.16-401.31 eV) and fifth (401.30-403.47 eV) peaks are assigned to the unreacted -C-NH$_2$, hydrogen bonded nitrogen and the protonated nitrogen on the surface respectively. The nitrogen peaks that is not bound to the [Mn(β-diketonato)$_3$] complexes have similar binding energies discussed in **Section 3.1.5.2 (i) (c)**.

The % of the unreacted nitrogen atom (-C-NH$_2$), hydrogenated nitrogen and the protonated nitrogen of the silane on the surface can be determined from the difference between the measured % N and the %N atoms that is bound to [Mn(β-diketonato)$_3$] complexes (which is the same as the % Mn atoms in [Mn(β-diketonato)$_3$]), see **Table 3.19**. From these values we observe that the success of anchoring the [Mn(β-diketonato)$_3$] complexes onto the amino-functionalized Si-wafer *via* an amine bond is between 5 and 13 %.

Table 3.19: Percentage nitrogen (N) bound to grafted [Mn(β-diketonato)$_3$] complexes ([Mn(acac)$_3$], **S5**; [Mn(ba)$_3$], **S6**; [Mn(dbm)$_3$], **S7**; [Mn(tfaa)$_3$], **S8**; [Mn(tfth)$_3$], **S9**; [Mn(tffu)$_3$], **S10**; [Mn(tfba)$_3$], **S11** and [Mn(hfaa)$_3$], **S12**).

Complex	% N$_{bound}$	% N$_{not\ bound}$ (-C-NH$_2$)	Ratio N$_{bound}$:N$_{not\ bound}$
[Mn(acac)$_3$] + amino-functionalized Si-wafer, **S5**	12.61	87.39	1:6.93
[Mn(ba)$_3$] + amino-functionalized Si-wafer, **S6**	3.23	96.77	1:29.96
[Mn(dbm)$_3$] + amino-functionalized Si-wafer, **S7**	8.48	91.52	1:10.79
[Mn(tfaa)$_3$] + amino-functionalized Si-wafer, **S8**	5.02	94.98	1:18.92
[Mn(tfth)$_3$] + amino-functionalized Si-wafer, **S9**	6.16	93.84	1:15.23
[Mn(tffu)$_3$] + amino-functionalized Si-wafer, **S10**	5.52	94.48	1:17.12
[Mn(tfba)$_3$] + amino-functionalized Si-wafer, **S11**	8.15	91.85	1:11.27
[Mn(hfaa)$_3$] + amino-functionalized Si-wafer, **S12**	5.2	94.8	1:18.23

(c) **F 1s peak**

The broad and asymmetric fluorine F 1s peaks suggest that more than one closely overlapping peak may be present. Different binding environments of fluorine (F) atom in the [Mn(β-diketonato)₃] complexes are possible as illustrated in **Scheme 3.8**. The peaks due to these different environments, however, are to closely overlapping to be deconvoluted and therefore the maximum BE of the F 1s peaks are reported in **Table 3.16**. A similar charge transfer peak (satellite peak) seen in the neat complexes is observed in the XPS spectra of the F containing [Mn(β-diketonato)₃] complexes impregnated on to the amino-functionalized Si-wafer surfaces. The satellite peak (charge transfer from ligand to the metal) is formed by the shake-down mechanism. The F 1s peak deconvolution of the grafted [Mn(tfaa)₃], **S8**, onto a amino-functionalized Si-wafer is illustrated in **Figure 3.18**.
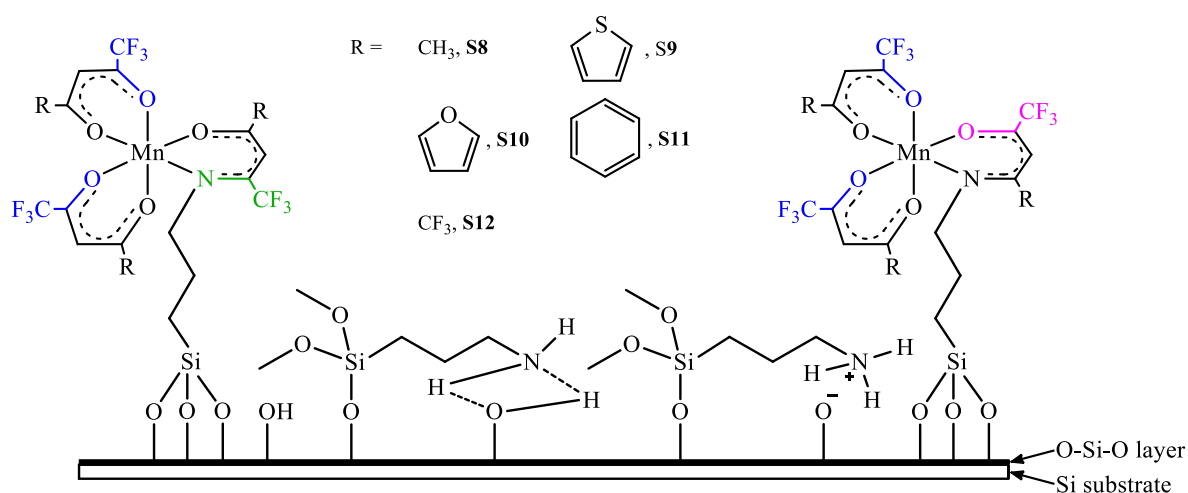
Scheme 3.8: The different binding environments of fluorine (F) atom found in [Mn(β-diketonato)₃] complexes ([Mn(tfaa)₃], **S8**; [Mn(tfth)₃], **S9**; [Mn(tffu)₃], **S10**; [Mn(tfba)₃], **S11** and [Mn(hfaa)₃], **S12**) that is grafted onto a amino-functionalized Si-wafer.
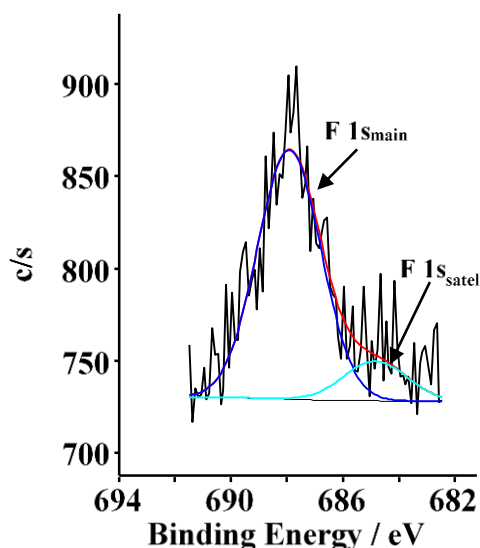
Figure 3.18: The F 1s peak deconvolution of the [Mn(tfaa)$_3$] grafted onto the amino-functionalized Si-wafer, **S8**.

(iii)   *Computational calculations of [Mn(β-diketonato)$_3$] complexes grafted on amino-functionalized Si-wafers*

Since it was not possible to distinguish between the different electronic environments of the [Mn(β-diketonato)$_3$] complexes by XPS, a DFT study is presented here to mimic the electronic environment of the [Mn(β-diketonato)$_3$] complexes bound to the Si-wafer through amine-silane. A simplified model of the [Mn(β-diketonato)$_3$] complexes grafted on amino-functionalized Si-wafers, namely [Mn(β-diketonato)$_3$] complexes containing an amine group have been optimized. Eight isomers are possible when the [Mn(β-diketonato)$_3$] complexes ([Mn(tfaa)$_2$(CH$_3$COC(NH)HCF$_3$)],   **13**;   [Mn(tfth)$_2$(ThCOC(NH)HCF$_3$)],   **14**; [Mn(tffu)$_2$(FuCOC(NH)HCF$_3$)], **15**; [Mn(tfba)$_2$(PhCOC(NH)HCF$_3$)], **16**) containing an unsymmetrical β-diketonato ligand due to the different position of the amine in the [Mn(β-diketonato)$_3$] complexes, see **Scheme 3.9**. All isomers have been optimized and the results are presented in **Table 3.20**. All isomers optimized to an elongation (in the *z*-direction) Jahn-Teller geometry with the amine in the *xy*-plane, see **Figure 3.19** for selected examples.
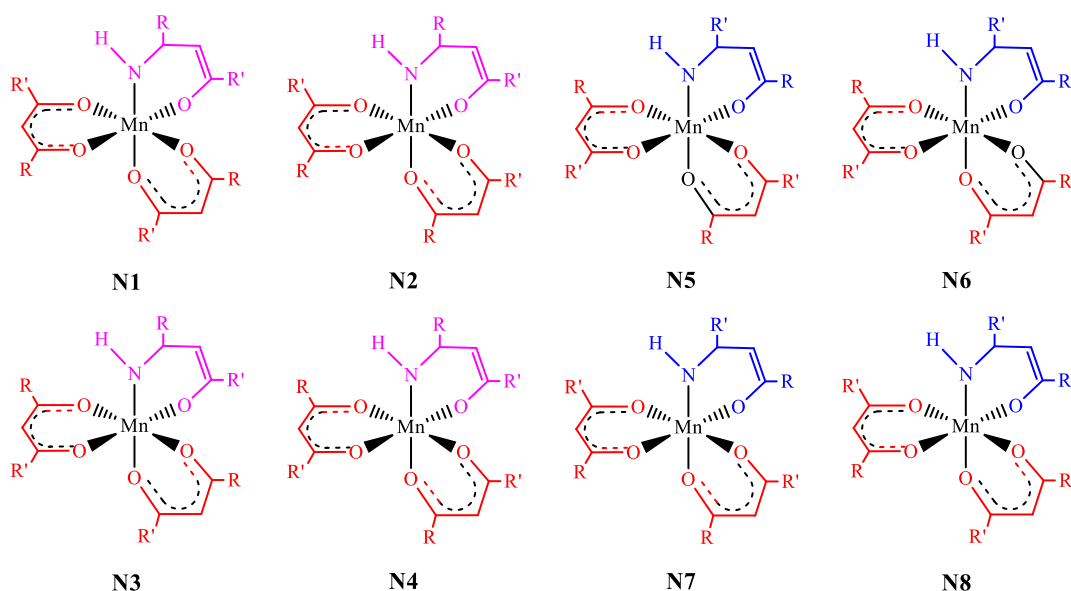
Scheme 3.9: Amine-containing [Mn(β-diketonato)₃] complexes (**13-16**). Eight isomers, **N1 – N8**, are possible when R ≠ R'.
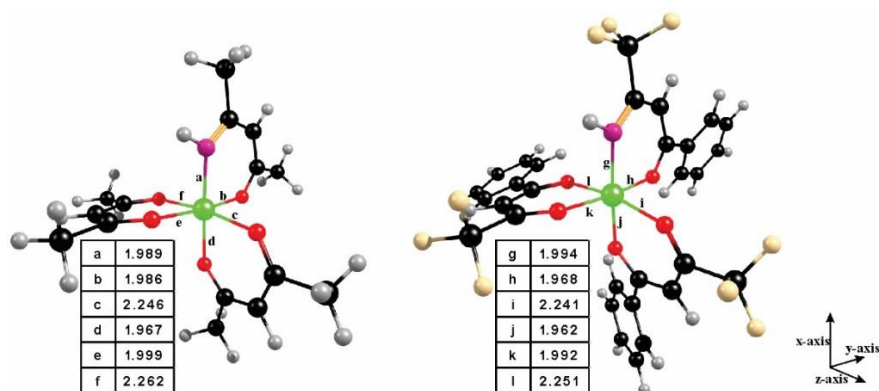
Figure 3.19: Selected examples of optimized amine-containing [Mn(β-diketonato)₃] complexes, left [Mn(acac)₂(CH₃COC((NH)HCH₃)], **10**, and right the lowest energy isomer of [Mn(tfba)₂(PhCOC((NH)HCF₃)], **16**. Colour code of atoms: Mn (lime), C (black), O (red), N (magenta), F (cream), H (grey).

Table 3.20: DFT data of the theoretical [Mn(β-diketonato)$_3$] complexes containing an amino-bond.

Compound	Isomer	E (kJ.mol^{-1})	Relative E (kJ.mol^{-1})	Population (%)[a]	E$_{HOMO}$	E$_{HOMO}$ (Boltzmann)
[Mn(acac)$_2$(CH$_3$COC(NH)HCH$_3$)], **10**		-25002.03	-	100	-3.909	-3.909
[Mn(ba)$_2$(PhCOC(NH)HCH$_3$)], **11**	N1	-39401.473	0.852	12.8	-4.015	-3.334
	N2	-39402.325	0.000	18.1	-4.035	
	N3	-39399.956	2.370	6.9	-4.022	
	N4	-39401.939	0.387	15.5	-4.023	
	N5	-39401.827	0.499	14.8	-4.015	
	N6	-39399.928	2.397	6.9	-4.013	
	N7	-39402.106	0.220	16.5	-4.021	
	N8	-39400.473	1.852	8.6	-4.021	
[Mn(dbm)$_2$(PhCOC(NH)HPh)], **12**		-53802.58	-	100	-4.104	-4.104
[Mn(tfaa)$_2$(CH$_3$COC(NH)HCF$_3$)], **13**	N1	-25228.223	1.608	21.6	-5.002	-5.068
	N2	-25213.119	16.712	0.0	-4.899	
	N3	-25229.830	0.000	41.3	-5.121	
	N4	-25226.414	3.417	10.4	-5.003	
	N5	-25222.551	7.279	2.2	-5.018	
	N6	-25227.023	2.807	13.3	-5.135	
	N7	-25207.243	22.588	0.0	-4.828	
	N8	-25226.596	3.235	11.2	-4.993	
[Mn(tfth)$_2$(ThCOC(NH)HCF$_3$)], **14**	N1	-33529.740	2.793	21.0	-4.872	-4.965
	N2	-33513.627	18.906	0.0	-4.797	
	N3	-33532.533	0.000	64.8	-4.994	
	N4	-33528.447	4.086	12.5	-4.972	
	N5	-33517.673	14.860	0.2	-5.046	
	N6	-33522.097	10.437	1.0	-5.027	
	N7	-33504.199	28.335	0.0	-4.773	
	N8	-33521.049	11.484	0.6	-4.916	
[Mn(tffu)$_2$(FuCOC(NH)HCF$_3$)], **15**	N1	-34254.645	21.162	0.0	-4.785	-5.002
	N2	-34242.312	33.495	0.0	-4.691	
	N3	-34275.807	0.000	99.3	-5.003	
	N4	-34263.197	12.610	0.6	-4.844	
	N5	-34254.833	20.974	0.0	-4.918	
	N6	-34257.222	18.585	0.1	-4.959	
	N7	-34236.317	39.490	0.0	-4.657	
	N8	-34250.993	24.814	0.0	-4.829	
[Mn(tfba)$_2$(PhCOC(NH)HCF$_3$)], **16**	N1	-39628.370	2.622	17.4	-4.952	-5.017
	N2	-39613.997	16.995	0.1	-4.825	
	N3	-39630.992	0.000	50.1	-5.063	
	N4	-39627.494	3.497	12.2	-4.959	
	N5	-39620.600	10.391	0.8	-4.975	
	N6	-39626.998	3.993	10.0	-5.056	
	N7	-39604.168	26.824	0.0	-4.774	
	N8	-39626.885	4.106	9.5	-4.937	
[Mn(hfaa)$_2$(CF$_3$COC(NH)HCF$_3$)], **17**		-25410.77	-	100	-6.086	-6.086

a Boltzman equation used with the assumption that all possibilities have accessible transition states that will produce the desired products

3.1.5.3 Study of [Mn(β-diketonato)₃] complexes impregnated onto 3-D solid supports

In this section seven [Mn(β-diketonato)₃] complexes ([Mn(acac)₃], **2**; [Mn(tfaa)₃], **5**) was wet impregnated onto various three dimensional (3-D) solid supports namely SiO_2, TiO_2, MgO, acidic zeolite and basic zeolite. While the [Mn(β-diketonato)₃] complexes ([Mn(dpm)₃], **1**; [Mn(ba)₃], **3**; [Mn(dbm)₃], **4**; [Mn(tfth)₃], **6**; [Mn(tffu)₃], **7** and [Mn(tfba)₃], **8**) was wet impregnated onto SiO_2.

(i) *[Mn(β-diketonato)₃]complexes ([Mn(dpm)₃], **1**; [Mn(acac)₃], **2**; [Mn(ba)₃], **3**; [Mn(dbm)₃], **4**; [Mn(tfaa)₃], **5** [Mn(tfth)₃], **6**; [Mn(tffu)₃], **7** and [Mn(tfba)₃], **8**) impregnated onto SiO₂ 3-D support*

Eight [Mn(β-diketonato)₃] complexes ([Mn(dpm)₃], **1**; [Mn(acac)₃], **2**; [Mn(ba)₃], **3**; [Mn(dbm)₃], **4**; [Mn(tfaa)₃], **5** [Mn(tfth)₃], **6**; [Mn(tffu)₃], **7** and [Mn(tfba)₃], **8**) were wet impregnated onto silica (SiO_2) to form surfaces **S13**, **S14**, **S15**, **S16**, **S17**, **S18**, **S19** and **S20** respectively. The binding mode of the Mn-complexes onto the SiO_2 is through hydrogen bonding between the OH-groups on the SiO_2 surface and the carbonyl oxygens of the β-diketonato ligand, in correlation with published results.[60] These surfaces were characterized by XPS and thermogravimetric analysis (TGA). The peak deconvolutions is included in **Appendix B**. The summary of the XPS result can be seen in **Table 3.21**. The charge transfer observed for the [Mn(β-diketonato)₃] complexes on the SiO_2 are similar than that of the neat [Mn(β-diketonato)₃] complexes.

---

[60] L. Davydenko, B. Mischanchuk, V. Pokrovskiy, *Chemical Vapor Deposition* **2011** (17) 123-127, "TPD-MS and spectroscopic studies of Cr(acac)₃binding at silica and alumina surface". DOI: 10.1002/cvde.201006885

Table 3.21: The binding energies in eV of Mn, F, S, O and Si obtained of the [Mn(β-diketonato)$_3$] complexes wet impregnated onto to SiO$_2$ obtained from XPS measurements.

Complex	$3(\chi_R + \chi_{R'})^a$	Mn 2p$_{3/2}$	Mn 2p$_{1/2}$	F 1s	S 2p$_{3/2}$	S 2p$_{1/2}$
[Mn(dpm)$_3$], **S13**	13.62	641.46 (55.55%)[b] 645.16 (11.11%)[c]	652.86 (27.78%)[b] 656.58 (5.57%)[c]	-	-	
[Mn(acac)$_3$], **S14**	14.04	641.68 (56.87%)[b] 645.48 (9.79%)[c]	653.32 (28.43%)[b] 657.08 (4.91%)[c]	-	-	
[Mn(ba)$_3$], **S15**	13.65	641.68 (33.59%)[b] 645.43 (33.05%)[c]	653.36 (16.79%)[b] 657.04 (16.57%)[c]	-	-	
[Mn(dbm)$_3$], **S16**	12.6	641.32 (45.61%)[b] 645.04 (21.04%)[c]	653.03 (22.80%)[b] 656.72 (10.55%)[c]	-	-	
[Mn(tfaa)$_3$], **S17**	16.05	642.14 (58.08%)[b] 645.99 (8.58%)[c]	653.85 (29.04%)[b] 657.58 (4.30%)[c]	684.48 (27.45%)[d] 688.19 (72.55%)[e]	-	
[Mn(tfth)$_3$], **S18**	15.33	641.86 (58.93%)[b] 645.55 (7.73%)[c]	653.50 (29.47%)[b] 657.25 (3.87%)[c]	684.35 (34.11%)[d] 688.25 (65.89%)[e]	163.58 (36.34%)	165.34 (63.66%)
[Mn(tffu)$_3$], **S19**	15.39	641.95 (64.23%)[b] 645.68 (2.43%)[c]	653.23 (32.12%)[b] 656.90 (1.22%)[c]	684.92 (32.18%)[d] 688.66 (67.82%)[e]	-	
[Mn(tfba)$_3$], **S20**	15.66	641.98 (47.83%)[b] 645.68 (18.82%)[c]	653.77 (23.92%)[b] 657.50 (9.43%)[c]	684.48 (34.63%)[d] 688.25 (65.37%)[e]	-	

a The Gordy scale group electronegativities χ_R, from ref. [61],[62],[63],[64] and [65]

b [Mn(β-diketonato)$_3$] complexes Mn peak (Mn $_{main}$ peaks)

c Mn satellite peak (Mn $_{satel}$ peak)

d F peak of fluorine containing [Mn(β-diketonato)$_3$] complexes (F $_{main}$)

e F satellite peak (F $_{satel}$)

(a)   <u>Mn 2p peaks</u>

The orbit splitting between the Mn 2p$_{3/2\ main}$ and Mn 2p$_{1/2\ main}$ of [Mn(β-diketonato)$_3$] on the SiO$_2$ 3-D support range from 11.28-11.79 eV with an average of 11.61 eV which is comparable to the spin orbit splitting (11.7 eV and 1.75 eV respectively) observed for the neat [Mn(β-diketonato)$_3$] complexes as well as the [Mn(β-diketonato)$_3$] complexes grafted onto amino-

---

[61] M.M. Conradie, A.J. Muller, J. Conradie, *S. Afr. J. Chem.* **2008** (61) 13-21, "Thienyl-containing β-diketones: Synthesis, characterization, crystal structure, keto-enol kinetics".

[62] W.C. du Plessis, T.G. Vosloo, J.C. Swarts, *J. Chem. Soc., Dalton Trans.* **1998** (15) 2507-2514, "β-Diketones containing a ferrocenyl group: synthesis, structural aspects, pK_a values, group electronegativities and complexation with rhodium(I) ".

[63] R.E. Kagarise, *J. Am. Chem. Soc.* **1955** (77) 1377-1379, "Relation between the Electronegativities of Adjacent Substituents and the Stretching Frequency of the Carbonyl Group".

[64] P. Klaas, *M.Sc. Thesis, University of the Free State*, *RSA*, **2002**, "Synthesis, electrochemical, kinetic and thermodynamic properties of new ferrocene-containing *beta*-diketonato rhodium(I) complexes with biomedical applications".

[65] M.M. Conradie, J. Conradie, *Electrochim. Acta* **2015** (152) 512-519, "Electrochemical behaviour of Tris(β-diketonato)iron(III) complexes: A DFT and experimental study".

functionalized silicon wafers. The Mn 2p photoelectron lines were fitted into the two sets of Mn $2p_{3/2}$ and Mn $2p_{1/2}$ photoelectron peaks, one set belongs to the main photoelectron peaks while the other set is assigned to the satellite photoelectron peaks. The deconvolution of the Mn 2p photoelectron lines of [Mn(dpm)$_3$], **S13**, surface is illustrated in **Figure 3.20**.
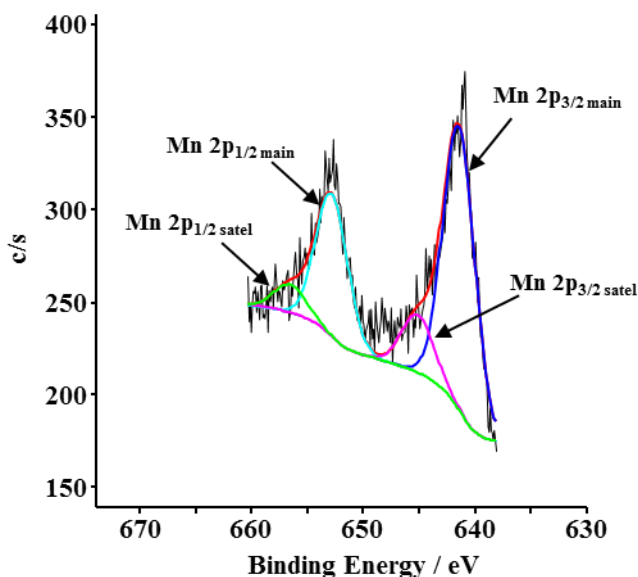
Figure 3.20: The fitting (deconvolution) of the [Mn(dpm)$_3$], **S13**, Mn 2p photoelectron peaks.

The Mn $2p_{3/2\ main}$ photoelectron peaks of were observed at a narrow range of binding energies between 641.32 - 642.14 eV. The Mn $2p_{3/2\ main}$ of the [Mn(β-diketonato)$_3$] complexes impregnated onto SiO_2 solid support is *ca.* 3 eV higher than that of the Mn $2p_{3/2}$ (638.7 eV) peak of Mn^0.[66,67] The *ca.* 3 eV shift to higher binding energy of the Mn 2p photoelectron peaks confirms that a Mn^{3+} species is present on the 3-D supports, confirming that during impregnation no oxidation of the Mn centre took place and that the binding mode is through hydrogen bonding.

The comparison between the total Gordy group electronegativity of the R-groups on the ligand, $3(\chi_R + \chi_{R'})$, and the Mn $2p_{3/2\ main}$ of the [Mn(β-diketonato)$_3$] complexes impregnated onto SiO_2, is shown in **Figure 3.21**. An increase in the total Gordy group electronegativity is accompanied by an increase in the binding energy of the Mn 2p peaks. This relationship is similar to that seen from

[66] D. Banerjee, H.W. Nesbitt, *Geochimica et Cosmochimica Acta* **1999** (63) 3025-3038, "XPS study of reductive dissolution of birnessite by oxalate: rates and mechanistic aspects of dissolution and redox processes". DOI: 10.1016/S0016-7037(99)00230-6

[67] H.W. Nesbitt, D. Banerjee, *American Mineralogist* **1998** (83) 305–315, "Interpretation of XPS Mn(2p) spectra of Mn oxyhydroxides and constraints on the mechanism of MnO_2 precipitation". DOI: 10.2138/am-1998-3-414

the neat [Mn(β-diketonato)$_3$] complexes discussed in **Section 3.1.5.1(i)**. The linear relationship obtained between the BE of the Mn 2p$_{3/2 \text{ main}}$ peaks and the total Gordy group electronegativity is described by the following equation:

$$(BE_{Mn\ 2p3/2\ main}) = 0.233[3(\chi_R + \chi_{R'})] + 638.3 \qquad\qquad R^2 = 0.94$$
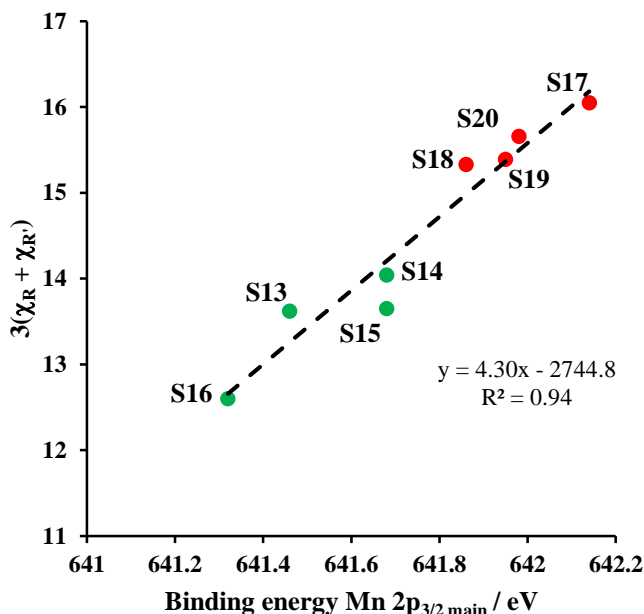
Figure 3.21: The relationship between the Mn 2p$_{3/2 \text{ main}}$ of the [Mn(β-diketonato)$_3$] complexes on a SiO$_2$ binding energies and the total Gordy group electronegativity.

(b) <u>**F 1s peak**</u>

The [Mn(β-diketonato)$_3$] complexes containing one CF$_3$ R-group on the β-diketonato ligand backbone immobilized onto a SiO$_2$ 3-D support system is expected to have an atomic Mn:F ratio of 1:9 (same as expected for these complexes grafted onto 2-D amino-functionalized Si-wafers in **Section 3.1.5.1**). From **Table 3.22** it is clear that the Mn:F ratios of all the fluorine containing [Mn(β-diketonato)$_3$] complexes immobilized onto a 3-D SiO$_2$ support are approximately 1:9, it could therefore be concluded that these complexes most probably did not decompose during the wet impregnation process onto the 3-D support and that the binding mode is through hydrogen bonding. The conditions that the two methods used to prepare the 2-D and 3-D is completely different, wet impregnation process takes place with no heat or breaking of any bonds (and the formation of hydrogen bonds) where the grafting process of the [Mn(β-diketonato)$_3$] complexes onto amino-functionalized wafers takes place under gentle reflux in dry toluene where one of the oxygens of a β-diketonato ligand is replaced by the nitrogen of the

silane linker on the Si-wafer. These differences between the two methods could be the reason why the wet impregnation method is seen as a more successful immobilization method of the [Mn(β-diketonato)$_3$] complexes onto the surface compared to the grafting process of the [Mn(β-diketonato)$_3$] complexes onto amino-functionalized Si-wafers in this study.

Table 3.22: The Mn:F of the fluorine containing [Mn(β-diketonato)$_3$] complexes ([Mn(tfaa)$_3$], **S17**; [Mn(tfth)$_3$], **S18**; [Mn(tffu)$_3$], **S19**, and [Mn(tfba)$_3$], **S20**) immobilized onto SiO$_2$.

Complex	Mn:F ratio
[Mn(tfaa)$_3$], **S17**	1:9.4
[Mn(tfth)$_3$], S**18**	1:9.0
[Mn(tffu)$_3$], **S19**	1:8.5
[Mn(tfba)$_3$], **S20**	1:9.5

The fluorine (F 1s) photoelectron peak of the [Mn(β-diketonato)$_3$] complexes containing one CF$_3$ R-group ([Mn(tfaa)$_3$], **S17**; [Mn(tfth)$_3$], **S18**; [Mn(tffu)$_3$], **S19**, and [Mn(tfba)$_3$], **S20**) is deconvoluted with two distinct peaks (same as the neat complexes described in **Section 3.1.5.1(ii)**). A similar charge transfer peak (satellite peak) seen in the neat complexes is observed in the XPS spectra of the [Mn(β-diketonato)$_3$] complexes impregnated on to the 3-D SiO$_2$ surface. The F 1s peak has a maximum peak binding energy range from 684.35 eV to 684.92 eV for the [Mn(β-diketonato)$_3$] complexes impregnated onto SiO$_2$, with a very distinct shoulder at *ca.* 3.8 eV lower than the maximum F 1s peak. The satellite peak (charge transfer from ligand to the metal) is formed by the shake-down mechanism. The F 1s photoelectron peak deconvolution of [Mn(tfaa)$_3$] complex impregnated onto SiO$_2$, **S17**, is illustrated in **Figure 3.22**.
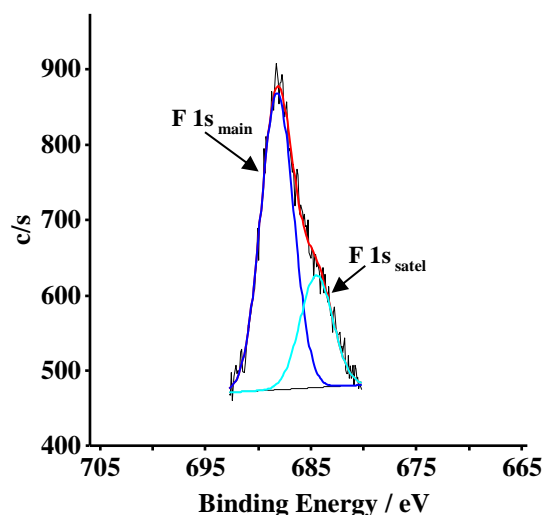
Figure 3.22: The fitting (deconvolution) of the [Mn(tfaa)₃] wet impregnated onto SiO₂, **S17**, F 1s XPS peak.

(ii)   *[Mn(β-diketonato)₃] complexes ([Mn(acac)₃], 2; [Mn(tfaa)₃], 5) impregnated onto SiO₂, TiO₂, MgO, acidic zeolite and basic zeolite 3-D supports*

[Mn(acac)₃], **2**, and [Mn(tfaa)₃], **5**, was wet impregnated onto five different 3-D solid supports and characterized by XPS. The XPS peak deconvolution of the SiO₂ 3-D solid support containing [Mn(acac)₃] and [Mn(tfaa)₃] will be illustrated in this section and the rest will be included in the **Appendix B**.

(a)   [Mn(acac)₃]

The XPS data obtained of [Mn(acac)₃] on SiO₂, **S14**; TiO₂, **S21**; MgO, **S22**; acidic zeolite, **S23** and basic zeolite, **S24** is summarized in **Table 3.23**. The spin orbit splitting between the Mn $2p_{3/2}$ and Mn $2p_{1/2}$ of [Mn(acac)₃] on the five different 3-D supports range from 11.59-11.86 eV with an average of 11.69 eV, which is comparable to the spin orbit splitting (11.7 eV and 1.75 eV respectively) observed for the neat [Mn(β-diketonato)₃] complexes as well as the [Mn(β-diketonato)₃] complexes grafted onto amino-functionalized silicon wafers. The *ca.* 3 eV shift to higher binding energy for the Mn 2p peaks compared to that of Mn⁰, [68,69] again confirms that a Mn³⁺ species is present on the 3-D supports and that no oxidation of the Mn centre occured. Once again the [Mn(acac)₃] on the 3-D supports showed similar charge transfer as the neat [Mn(β-

68 D. Banerjee, H.W. Nesbitt, *Geochimica et Cosmochimica Acta* **1999** (63) 3025-3038, "XPS study of reductive dissolution of birnessite by oxalate: rates and mechanistic aspects of dissolution and redox processes". DOI: 10.1016/S0016-7037(99)00230-6

69 H.W. Nesbitt, D. Banerjee, *American Mineralogist* **1998** (83) 305–315, "Interpretation of XPS Mn(2p) spectra of Mn oxyhydroxides and constraints on the mechanism of MnO₂ precipitation". DOI: 10.2138/am-1998-3-414

diketonato)$_3$] complexes, which gives rise to the satellite peaks seen in the Mn 2p photoelectron lines.

Table 3.23: The XPS results of [Mn(acac)$_3$] supported on different 3-D support materials.

Support	Mn 2p$_{3/2}$	Mn 2p$_{1/2}$
SiO$_2$, **S14**	641.68 (56.87%) [a] 645.48 (9.79%) [b]	653.32 (28.43%) [a] 657.08 (4.91%) [b]
TiO$_2$, **S21**	642.05 (54.88%) [a] 645.73 (11.77%) [b]	653.64 (27.44%) [a] 657.33 (5.90%) [b]
MgO, **S22**	641.41 (48.12%) [a] 645.16 (18.53%) [b]	653.13 (24.06%) [a] 656.87 (9.29%) [b]
Acidic Zeolite, **S23**	642.07 (50.75%) [a] 645.77 (15.90%) [b]	653.71 (25.37%) [a] 657.41 (7.97%) [b]
Basic Zeolite, **S24**	641.09 (46.54%) [a] 644.89 (20.11%) [b]	652.95 (23.27%) [a] 656.72 (10.08%) [b]

a [Mn(acac)$_3$] complexes Mn peak (Mn $_{main}$ peaks)

b Mn satalite peak (Mn $_{satel}$ peak)

The XPS deconvolution of the [Mn(acac)$_3$] impregnated onto SiO$_2$ Mn 2p peaks is illustrated in **Figure 3.23**.
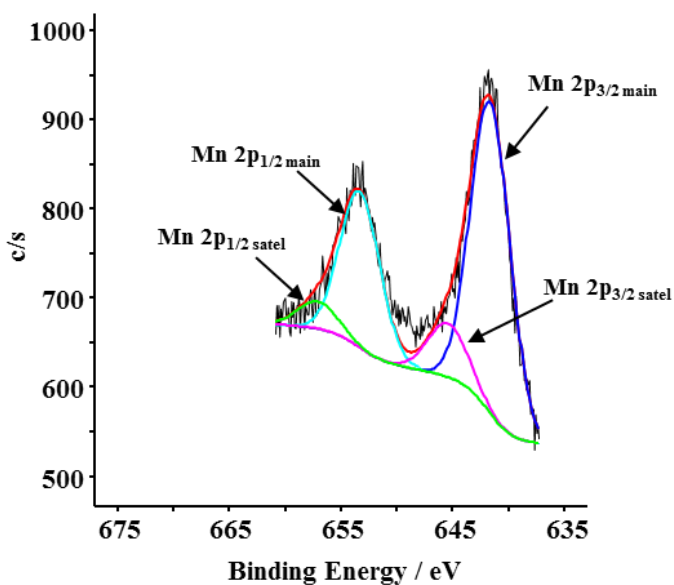
Figure 3.23: Mn 2p peak fitting (deconvolution) of [Mn(acac)$_3$] impregnated onto SiO$_2$ 3-D surface, **S14**.

(b) <u>**[Mn(tfaa)$_3$]**</u>

Since [Mn(tfaa)$_3$] is a [Mn(β-diketonato)$_3$] complex with one CF$_3$ R-group on the β-diketonato ligand backbone, the [Mn(tfaa)$_3$], complex immobilized onto the different 3-D supports system is expected to have an atomic Mn:F ratio of 1:9. From **Table 3.24** it can be seen that the Mn:F ratios of the [Mn(tfaa)$_3$] complex immobilized on the different 3-D supports are approximately 1:9, which indicates that the [Mn(tfaa)$_3$] did not decompose during the immobilization process and that the binding mode onto the different supports is most probably also through hydrogen bonding. As stated in **Section 3.1.5.3(i) (b)** the [Mn(tfaa)$_3$] complex most probably did not decompose due to the milder conditions/process taking place to immobilize the [Mn(tfaa)$_3$] complex onto the 3-D supports compared to grafting it onto an amio-functionalized Si-wafer. The XPS data obtained of [Mn(tfaa)$_3$] on SiO$_2$, **S17**; TiO$_2$, **S25**; MgO, **S26**; acidic zeolite, **S27** and basic zeolite, **S28** is summarized in **Table 3.25**. The orbit splitting between the Mn 2p$_{3/2}$ and Mn 2p$_{1/2}$ of [Mn(tfaa)$_3$] on the five different 3-D supports range from 11.40-11.90 eV with an average of 11.70 eV this is the same as the spin orbit splitting (11.70 eV) observed for the neat [Mn(β-diketonato)$_3$] complexes, the binding energy position of *ca.* 642.2 eV for the Mn 2p$_{3/2}$ photoelectron line (similar to all the previous results) confirm that a Mn^{3+} species is present on the 3-D supports. The [Mn(tfaa)$_3$] impregnated onto the 3-D supports showed similar charge transfer as the neat [Mn(β-diketonato)$_3$] complexes. The charge transfer between the Mn metal centre and the ligands gives rise to the satellite peaks seen in the Mn 2p and F 1s photoelectron lines.

Table 3.24: The Mn:F of [Mn(tfaa)$_3$] complex immobilized on a selection of 3-D supports (SiO$_2$, **S17**; TiO$_2$, **S25**; MgO, **S26**; acidic zeolite, **S27** and basic zeolite, **S28**).

Support	Mn:F ratio
SiO$_2$,**S17**	1:9.4
TiO$_2$, **S25**	1:9.8
MgO, **S26**	1:9.2
Acidic Zeolite, **S27**	1:9.3
Basic Zeolite, **S28**	1:8.9

Table 3.25: The XPS results of [Mn(tfaa)$_3$] wet impregnated onto different 3-D support materials.

Support	Mn 2p$_{3/2}$	Mn 2p$_{1/2}$	F 1s
SiO$_2$,**S17**	642.14 (58.08%) [a] 645.99 (8.58%) [b]	653.85 (29.04%) [a] 657.58 (4.3%) [b]	684.48 (27.45%) [c] 688.19 (72.55%) [d]
TiO$_2$, **S25**	642.71 (61.50%) [a] 646.45 (5.16%) [b]	654.11 (30.75%) [a] 657.80 (2.59%) [b]	685.73 (15.45%) [c] 688.99 (84.55%) [d]
MgO, **S26**	641.82 (38.95%) [a] 645.56 (27.69%) [b]	653.54 (19.48%) [a] 657.23 (13.88%) [b]	684.98 (32.74%) [c] 688.64 (67.26%) [d]
Acidic Zeolite, **S27**	642.77 (55.31%) [a] 646.47 (11.34%) [b]	654.54 (27.66%) [a] 658.24 (5.69%) [b]	684.40 (16.78%) [c] 688.46 (83.22%) [d]
Basic Zeolite, **S28**	641.67 (48.67%) [a] 645.41 (17.98%) [b]	653.59 (24.34%) [a] 657.31 (9.01%) [b]	683.37 (24.19%) [c] 687.38 (75.81%) [d]

[a] [Mn(tfaa)$_3$] complexes Mn peak (Mn $_{main}$ peaks)　　　[c] F peak of [Mn(tfaa)$_3$] complex (F $_{main}$)

[b] Mn satalite peak (Mn $_{satel}$ peak)　　　　　　　　　　　[d] F satallite peak (F $_{satel}$)

The XPS deconvolution of the Mn 2p and the F 1s peaks of [Mn(tfaa)$_3$] impregnated onto a SiO$_2$ support are illustrated in **Figure 3.24** and **Figure 3.22** (**Section 3.1.5.3 (i) (b)**) respectively.
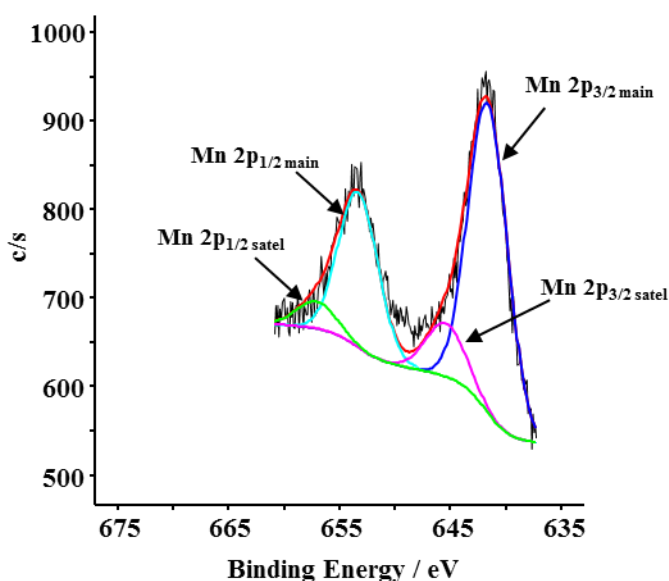
Figure 3.24: Mn 2p peak fitting (deconvolution) of [Mn(tfaa)$_3$] on SiO$_2$ 3-D surface, **S17**.

3.1.5.4 Study of [M(acac)$_3$] complexes grafted on amino-functionalized Si-wafers (M = Co, Rh and Ir) S29-S31

Three [M(acac)$_3$] complexes ([Co(acac)$_3$], **12**; [Rh(acac)$_3$], **13**, and [Ir(acac)$_3$], **14**) was grafted onto 2-D amino-functionalized Si-wafers, see **Scheme 3.10** to form surfaces **S29**, **S30** and **S31** respectively. The binding mode for the different metal tris(acetylacetonato) complexes is expected to be similar to that described for Mn(β-diketonato)$_3$ in **Section 3.5.1.2**, with the aimed binding mode as shown in **Scheme 3.10**.
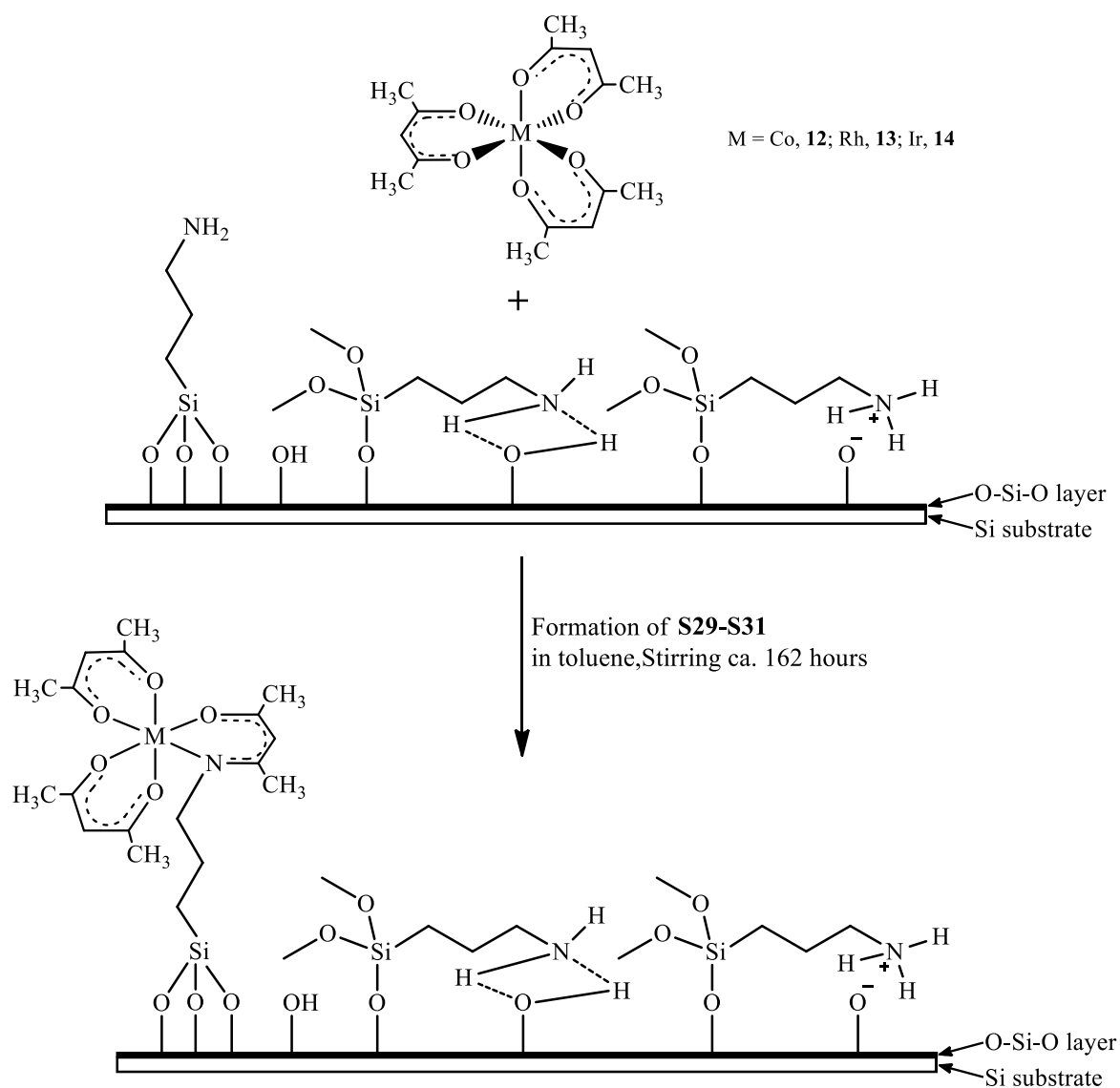
Scheme 3.10: The chemical grafting of [Co(acac)$_3$], **12**; [Rh(acac)$_3$], **13**, and [Ir(acac)$_3$], **14**, complexes onto an amino-functionalized Si-wafer to form [M(acac)$_3$]-grafted Si-wafers **S29**, **S30** and **S31** respectively.

The XPS data obtained from the three [M(acac)$_3$] complexes grafted onto amino-functionalized Si-wafers is summarized in **Table 3.26** and discussed in the following sub-sections.

Table 3.26: The binding energies in eV of N and metal peaks obtained of the [M(acac)$_3$] complexes grafted onto amino-functionalized Si-wafers from XPS measurements.

Complex	Co 2p$_{3/2}$	Co 2p$_{1/2}$	Rh 3d$_{5/2}$	Rh 3d$_{3/2}$	Ir 4f$_{7/2}$	Ir 4f$_{5/2}$	N 1s
							399.40 (37.40%) [e]
[Co(acac)$_3$],	781.53 (48.40%) [a]	796.60 (24.20%) [a]					399.83 (28.33%) [f]
S29	786.76 (18.27%) [b]	803.12 (9.14%) [b]	-	-	-	-	400.45 (26.20%) [g]
							401.84 (8.07%) [h]
							399.23 (2.53%) [e]
[Rh(acac)$_3$],			309.13 (47.76%) [c]	313.93 (31.52%) [c]			399.68 (63.20%) [f]
S30	-	-	310.59 (12.48%) [d]	315.34 (8.23) [d]	-	-	400.94 (26.2%) [g]
							402.16 (8.07%) [h]
							398.79 (8.05%) [e]
[Ir(acac)$_3$],							399.91 (57.68%) [f]
S31	-	-	-	-	63.21 (57.14%)	66.11 (42.86%)	400.87 (26.20%) [g]
							401.89 (8.07%) [h]

a Co $_{main}$ peaks
b Co satalite peak (Co $_{satel}$ peak)
c Rh$_2$O$_3$ peaks
d [Rh(acac)$_3$] peaks

e Nitrogen bound to [M(acac)$_3$] complexes (-N-C-CH$_3$)
f Unbound nitrogen (-C-NH$_2$)
g Hydrogen bonded nitrogen
h Protonated nitrogen

(i)   *Metal peaks*

The sub-sections contain the illustration and discussion of the XPS peak deconvolutions of the M-atoms of [M(acac)$_3$] complexes grafted onto amino-functionalized Si-wafers.

(a)   <u>Co 2p peaks</u>

The Co 2p$_{3/2}$ and Co 2p$_{1/2}$ binding energies (of the peak maxima) of the [Co(acac)$_3$] complex grafted onto amino-functionalized Si-wafer are 781.53 and 796.60 eV respectively with satellite peaks caused by shake-up mechanism at 786.76 and 803.12 eV respectively. These binding energies are *ca.* 1 eV higher than Chen *et al.* found for a C-Co^{II}(acac)$_2$-H$_2$O specie.[70] This confirms that the Co specie found on the amino-functionalized Si-wafer is in the Co^{3+} oxidation state. The [Co(acac)$_3$] grafted onto the amino-functionalized Si-wafer is similar to the charge transfer observed by Chen *et al.* where the binding energy of the Co 2p$_{3/2satel}$ and the Co 2p$_{1/2satel}$ is *ca.* 5.2 and 5.5 eV higher than the binding energy of Co 2p$_{3/2\ main}$ and Co 2p$_{1/2\ main}$ respectively. The spin

---

[70] X. Chen, X. Li, S. Liu, Z. Li, *Industrial & Engineering Chemistry Research* **2015** (54) 4756-4762, "Effects of Cobalt Compounds on the Morphology and Structure of Carbonaceous Materials Prepared by Hydrothermal/Solvothermal Carbonization of Furfural" DOI: 10.1021/acs.iecr.5b00230

orbit splitting between the Co $2p_{3/2\ main}$ and Co $2p_{1/2\ main}$ is 16.07 eV which is comparable to the 15.98 eV found for C-Co(acac)$_2$-H$_2$O by Chen *et al.*
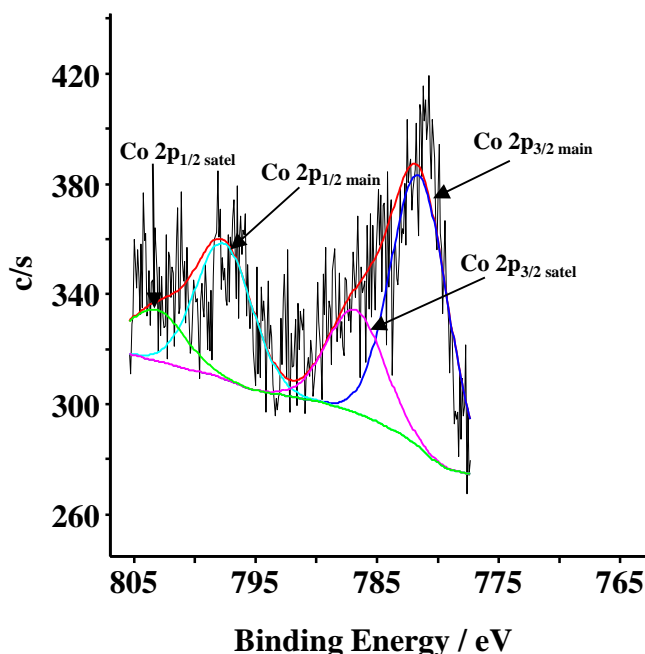
Figure 3.25: The fitting (deconvolution) of the [Co(acac)$_3$] complex grafted onto the amino-functionalized Si-wafer, **S29**, Co 2p XPS peak.

(b) <u>**Rh 3d peaks**</u>

The first set of photoelectron Rh $3d_{7/5}$ and Rh $3d_{2/5}$ peaks with binding energies at 309.13 eV and 313.93 eV are in agreement with previously published values (309 eV and 314 eV respectively) for Rh$_2$O$_3$.[71] This gives an indication that oxidation on the Rh centre took place. The [Rh(acac)$_3$] complex grafted onto the amino-functionalized Si-wafer's, **S30,** Rh $3d_{7/5}$ and Rh $3d_{2/5}$ peak binding energies are located at 310.59 eV and 315.34 eV respectively, which is *ca.* 3 eV higher in binding energy of elemental Rh^0.[72, 73] The spin orbit splitting observed in this study (4.75 eV) of the [Rh(acac)$_3$] grafted onto amino-functionalized Si-wafer, **S30**, is comparable to the splitting

71 L. Li, S. Niu, Y. Qu, Q. Zhang, H. Li, Y. Li, W. Zhao, J. Shi, *Journal of Maretial Chemistry* **2012** (22) 9263-9267, "One-pot synthesis of uniform mesoporous rhodium oxide/alumina hybrid as high sensitivity and low power consumption methane catalytic combustion micro-sensor" DOI: 10.1039/C2JM15870A

72 J.S. Brinen, A. Malera, *The Journal of Physical Chemistry* **1972** (76) 2525-2526, "Electron spectroscopy for chemical analysis (ESCA) studies on catalysts. Rhodium on charcoal" DOI: 10.1021/j100662a007

73 Y.V. Larichev, O.V. Netskina, O.V. Komova, V.I. Simagina, *International Journal of Hydrogen Energy* **2010** (35) 6501-6507 "Comparative XPS study of Rh/Al$_2$O$_3$ and Rh/TiO$_2$ as catalysts for NaBH$_4$ hydrolysis". DOI: 10.1016/j.ijhydene.2010.04.048

observed by Suhonen *et al.* where the spin split orbit of Rh-Al (L) of ~4.7 eV is seen.[74] The Rh 3d spectrum of [Rh(acac)$_3$] grafted onto amino-functionalized Si-wafer's, **S30**, deconvolution is illustrated in **Figure 3.26**.
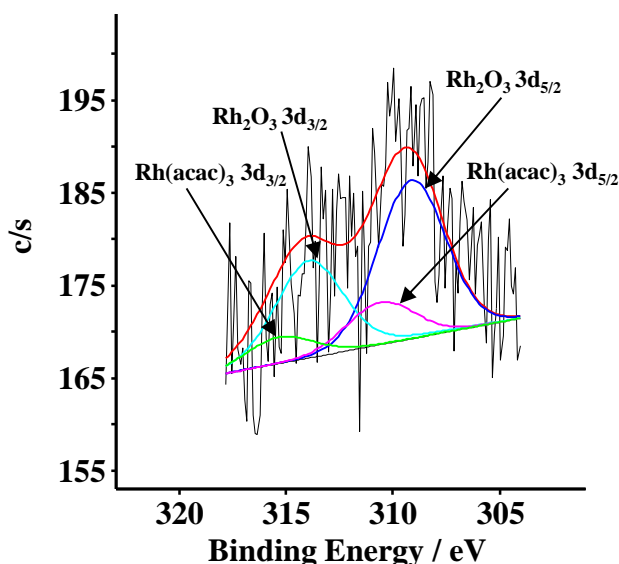
Figure 3.26: The fitting (deconvolution) of the [Rh(acac)$_3$] complex grafted onto the amino-functionalized Si-wafer, **S30**, Rh 3d XPS peak.

(c)   Ir 4f peaks

The [Ir(acac)$_3$] complex grafted onto amino-functionlized Si-wafer, **S31**, exhibits an Ir 4f$_{7/2}$ peak at a binding energy of 63.21 eV, which is *ca.* 3 eV higher than the 4f$_{7/2}$ peak of elemental Ir(0) (60.8 eV). [75] The shift to *ca.* 3 eV higher binding energy confirms that the iridium specie that is observed on the surface is that of an Ir^{3+} oxidation state. Fuggle *et al.* reported the spin orbit splitting of the Ir 4f$_{7/2}$ and Ir 4f$_{5/2}$ peaks of an Ir(0) to be 3 eV. The spin orbit splitting observed in this study is 2.9 eV and comparable to what Fuggle *et al.* reported. The deconvolution of the Ir 4f spectrum obtained through XPS of the [Ir(acac)$_3$] grafted onto amino-functioinalized Si-wafer, **S31**, is illustrated in **Figure 3.27**.

[74] S. Suhonen, R. Polvinen, M. Vladen, K. Kallinen, M. Härkönen, *Applied Surface Science* **2002** (200) 48-54, "Surface oxides on supported Rh particles: thermal decomposition of Rh oxide under high vacuum conditions". 10.1016/S0169-4332(02)00607-4

[75] J.C. Fuggle, N. Mårtensson, *Journal of Electron Spectroscopy and Related Phenomena* **1980** (21) 275-281, "Core-level binding energies in metals". DOI: 10.1016/0368-2048(80)85056-0
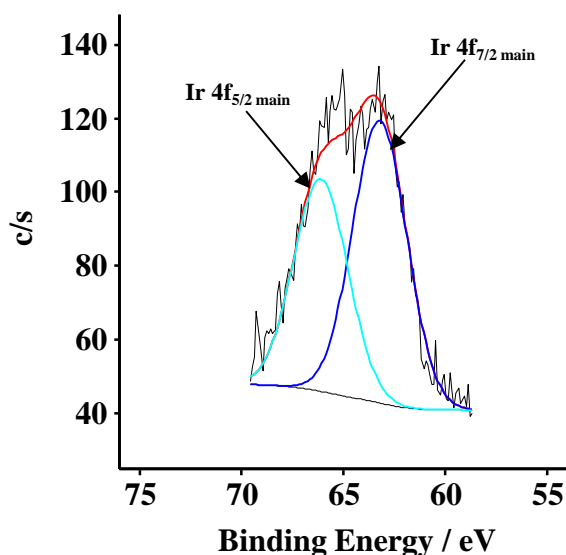
Figure 3.27: The fitting (deconvolution) of the [Ir(acac)₃] complex grafted onto the amino-functionalized Si-wafer, **S31**, Ir 4f XPS peak.

(ii)   *N 1s peak*

The N 1s peaks of the [M(acac)₃] complexes grafted onto amino-functionalized Si-wafer ([Co(acac)₃], **S29**; [Rh(acac)₃], **S30**, and [Ir(acac)₃], **S31**) is simulated with four peaks. The three peaks at highest binding energies correlates to the different amine environments observed on the clean amino-functionalized Si-wafer surface discussed in **Section 3.1.5.2 (i) (c)**. The three peaks are assigned as follows from highest to lowest binding energies *i.e.* the protonated amine (401.84 eV), the hydrogen-bonded amine (400.45 eV) and the free amine (399.83 eV). The fourth peak (at the lowest binding energy) is assigned to the nitrogen atom bound to the [M(acac)₃] complexes (399.40, 399.23 and 398.79 eV) for [Co(acac)₃], **S29**; [Rh(acac)₃], **S30**, and [Ir(acac)₃], **S31**, respectively. The deconvolution of the N 1s spectrum obtained through XPS of the [Co(acac)₃] grafted onto amino-functioinalized Si-wafer, **S29**, can be seen in **Figure 3.28**.
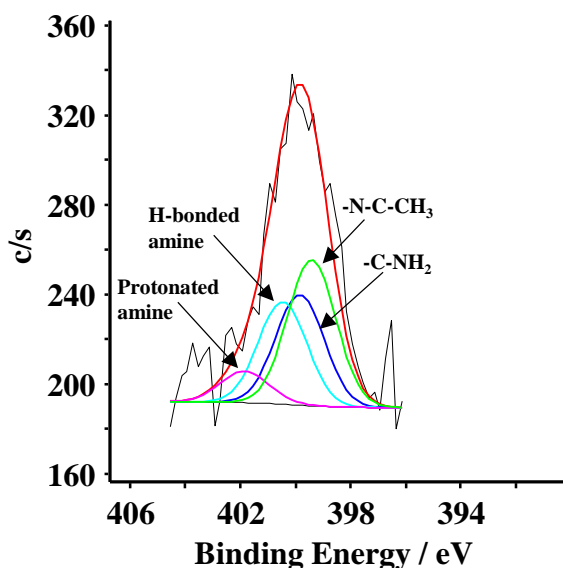
Figure 3.28: The fitting (deconvolution) of the [Co(acac)$_3$] complex grafted onto the amino-functionalized Si-wafer, **S29**, N 1s XPS peak.

Similar to **Section 3.1.5.2 (ii)(b)** the percentage of nitrogen (N) atoms bound to [M(acac)$_3$] complexes ([Co(acac)$_3$], **S29**; [Rh(acac)$_3$], **S30,** and [Ir(acac)$_3$], **S31**) are equal to the percentage metal atoms found to be part of [M(acac)$_3$] complexes, see **Table 3.27**. From these values we observe that the success of anchoring the [M(acac)$_3$] complexes onto the amino-functionalized Si-wafer *via* an amine bond, ranges from as low as 3.85 % for [Rh(acac)$_3$], **S30**, to as high as 43.1 % for [Co(acac)$_3$], **S29**, grafted onto the amino-functionalized Si-wafer.

Table 3.27: Percentage nitrogen (N) bound to grafted [M(acac)$_3$] complexes ([Co(acac)$_3$], **S29**; [Rh(acac)$_3$], **S30**, and [Ir(acac)$_3$], **S31**) onto amino-functionalized Si-wafer.

Complex	% N$_{bound}$	% N$_{not\ bound}$ (-C-NH$_2$)	Ratio N$_{bound}$:N$_{not\ bound}$
[Co(acac)$_3$] + amino-functionalized Si-wafer, **S29**	43.10	56.90	1:1.32
[Rh(acac)$_3$] + amino-functionalized Si-wafer, **S30**	3.85	96.15	1:24.97
[Ir(acac)$_3$] + amino-functionalized Si-wafer, **S31**	12.24	87.76	1:7.17

3.1.5.5 Study of [M(acac)$_3$] complexes impregnated onto SiO$_2$ 3-D solid support

Five [M(acac)$_3$] complexes ([Cr(acac)$_3$], **10**; [Fe(acac)$_3$], **11**; [Co(acac)$_3$], **12** [Rh(acac)$_3$], **13**; [Ir(acac)$_3$], **14**), were wet impregnated onto a 3-D solid support surface silica (SiO$_2$), forming 3-D supported catalyst surfaces **S32**, **S33**, **S34**, **S35** and **S36** respectively. These surfaces were characterized by XPS. In the sub-sections the O 1s peak deconvolution of the [Cr(acac)$_3$] complex impregnated onto SiO$_2$, **S32**, will be illustrated, with the rest of the surfaces included in **Appendix B**.

Table 3.28: The binding energies in eV of N, O and metal peaks obtained of the [M(acac)$_3$] complexes impregnated onto 3-D SiO$_2$.

Complex	Cr 2p$_{3/2}$	Cr 2p$_{1/2}$	Fe 2p$_{3/2}$	Fe 2p$_{1/2}$	Co 2p$_{3/2}$	Co 2p$_{1/2}$	Rh 3d$_{5/2}$	Rh 3d$_{3/2}$	Ir 4f$_{7/2}$	Ir 4f$_{5/2}$	O 1s
[Cr(acac)$_3$], **S32**	577.59 (66.67%)	586.97 (33.33%)	-	-	-	-	-	-	-	-	528.74 (11.22%) [c] 531.07 (23.41%) [d] 532.87 (65.36%) [e]
[Fe(acac)$_3$], **S33**	-	-	710.24 (66.67%)	723.86 (33.33%)	-	-	-	-	-	-	529.73 (36.46%) [c] 531.40 (27.76%) [d] 533.29 (35.78%) [e]
[Co(acac)$_3$], **S34**	-	-	-	-	780.10 (49.91%) [a] 786.93 (16.76%) [b]	796.11 (24.95%) [a] 800.97 (8.38%) [b]	-	-	-	-	529.38 (19.55%) [c] 531.47 (22.62%) [d] 533.23 (57.83%) [e]
[Rh(acac)$_3$], **S35**	-	-	-	-	-	-	310.27 (60.24%)	315.04 (39.76%)	-	-	530.16 (11.22%) [c] 531.92 (23.41%) [d] 534.30 (65.36%) [e]
[Ir(acac)$_3$], **S36**	-	-	-	-	-	-	-	-	63.81 (57.14%)	67.02 (42.86%)	529.34 (15.22%) [c] 531.37 (26.96%) [d] *533.00 (57.83%) [e]*

[a] Co $_{main}$ peaks
[b] Co satalite peak (Co $_{satel}$ peak)
[c] Oxygen bound to the metal (M) center (M-O)
[d] Oxygen bound to carbons (C-O)
[e] Oxygen that forms part of the solid surface (SiO$_2$)

(i)   *Metal peaks*

The sub-sections contain XPS peak deconvolutions of the M-atoms of SiO_2 surface containing [M(acac)$_3$] complexes which will be illustrated and discussed below.

(a)   Cr 2p peaks

The binding energy of the Cr 2p$_{3/2}$ of the [Cr(acac)$_3$] impregnated onto SiO_2, **S32**, is found at 577.59 eV which is *ca.* 3 eV higher than the binding energy of the Cr 2p$_{3/2}$ of the free chromium metal Cr(0) of 574.2 eV.[76] The 3 eV shift to higher binding energy indicates that a Cr^{3+} specie is present on the SiO_2 surface and that no oxidation of the Cr occurred during the wet impregnation process. The spin orbit splitting between the Cr 2p$_{1/2}$ and the Cr 2p$_{3/2}$ peaks are 9.38 eV, which is similar to the observed 9.6 eV spin orbit splitting of $Cr^{III}Cl_3$ complex.[77] **Figure 3.29** shows the Cr 2p peak deconvolution of the [Cr(acac)$_3$] complex impregnated onto SiO_2, **S32**.
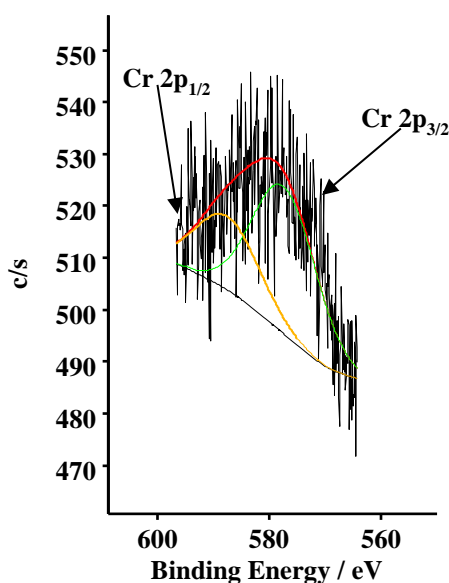
Figure 3.29: Cr 2p peak fitting (deconvolution) of [Cr(acac)$_3$] impregnated onto SiO_2 3-D surface, **S32**.

[76] M.C. Biesinger, C. Brown, J.R. Mycroft, R.D. Davidson, N.S. McIntyre, *Surf. Interface Anal.* **2004** (36) 1550-1563, "X-ray photoelectron spectroscopy studies of chromium compounds". DOI: 10.1002/sia.1983

[77] T.L. Daulton, B.J. Little, *Ultramicroscopy* **2006** (106) 561-573, "Determination of chromium valence over the range Cr(0)-Cr(VI) by electron energy loss spectroscopy". DOI: 10.1016/j.ultramic.2006.02.005.

(b) <u>**Fe 2p peaks**</u>

The binding energy of the Fe $2p_{3/2}$ peak of the [Fe(acac)$_3$] impregnated onto SiO$_2$, **S33**, is at 710.24 eV which is *ca.* 3 eV higher than the corresponding peak of the metal Fe(0) at a binding energy of 706.7 eV.[78] The value of the Fe $2p_{3/2}$ peak of the [Fe(acac)$_3$] impregnated onto SiO$_2$, **S33**, compares well to the value of [Fe(acac)$_3$] bound to a Si-wafer through an amine link, which had an Fe $2p_{3/2}$ binding energy of 710.46 eV.[79] The spin orbit splitting between the Fe $2p_{3/2}$ and Fe $2p_{1/2}$ peaks of the [Fe(acac)$_3$] impregnated onto SiO$_2$ is 13.62 eV which, is comparable to the splitting of the peaks found for Fe^{3+} specie Fe$_2$O$_3$ of 13.6 eV.[80] **Figure 3.30** shows the Fe 2p peak deconvolution of the [Fe(acac)$_3$] complex impregnated onto SiO$_2$, **S33**.
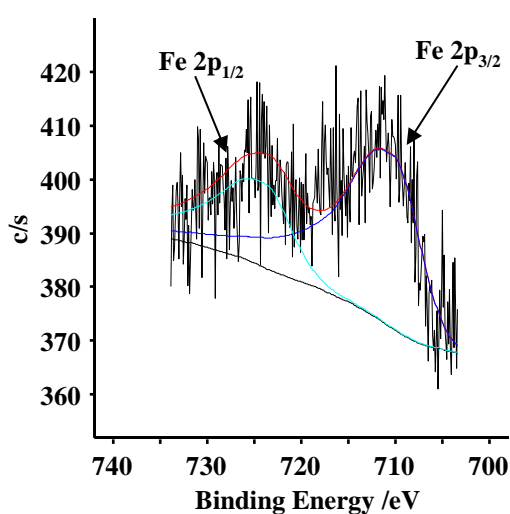
Figure 3.30: Fe 2p peak fitting (deconvolution) of [Fe(acac)$_3$] impregnated onto SiO$_2$ 3-D surface, **S33**.

[78] N.S. McIntyre, D.G. Zetaruk, *Analytical Chemistry* **1977** (49) 1521-1629, "X-ray Photoelectron Spectroscopic Studies of Iron Oxides". DOI: 10.1021/ac50019a016.

[79] M.M. Conradie, J. Conradie, E. Erasmus, *Polyhedron* 2014 (79) 52-59," Immobilisation of iron tris(β-diketonates) on a two-dimensional flat amine functionalised silicon wafer: A catalytic study of the formation of urethane, from ethanol and a diisocyanate derivative " DOI: 10.1016/j.poly.2014.04.054.

[80] T. Yamashita, P. Hayes, *Applied Surface Science* **2008** (254) 2441-2449, "Analysis of XPS spectra of Fe^{2+} and Fe^{3+} ions in oxide materials". DOI: 10.1016/j.apsusc.2007.09.063.

(c) <u>**Co 2p peaks**</u>

The Co $2p_{3/2}$ binding energy (780.10 eV) of the [Co(acac)$_3$] impregnated onto SiO$_2$, **S34**, is *ca.* 3 eV higher than the corresponding peak of the metal Co(0), which is observed at 777.3 eV.[81] The Co $2p_{3/2}$ binding energy (780.10 eV) of the [Co(acac)$_3$] impregnated onto SiO$_2$, **S34**, compares well to the binding energy of CO^{3+} specie Co$_2$O$_3$ (780.20 eV) reported by Tan *et al.*[81] The spin orbit splitting that is observed by B.J. Tan *et al.* of 15.8 eV for the Co$_2$O$_3$ complex is similar to the spin orbit splitting found for the [Co(acac)$_3$] impregnated onto SiO$_2$ (16.0 eV), **S34**. **Figure 3.31** shows the Co 2p peak deconvolution of the [Co(acac)$_3$] complex impregnated onto SiO$_2$, **S34**.
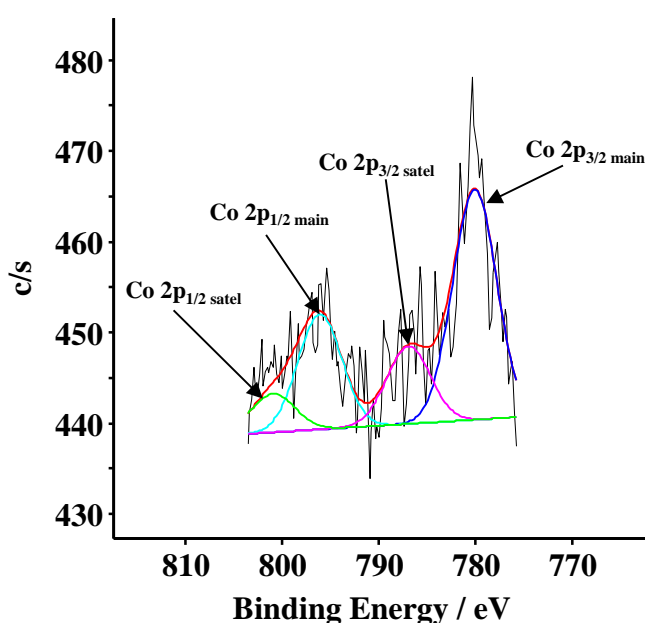
Figure 3.31: Co 2p peak fitting (deconvolution) of [Co(acac)$_3$] impregnated onto SiO$_2$ 3-D surface, **S34**.

[81] B.J. Tan, K.J. Klabunde, P.M.A. Sherwood, J. Am. Chem. Soc. 1991 (113) 855-861, "XPS Studies of Solvated Metal Dispersed Catalysts. Evidence for Layered Cobalt-Manganese Particles on Alumina and Silica". DOI: 10.1021/ja00003a019.

(d)   Rh 3d peaks

The Rh $3d_{5/2}$ binding energy (310.27 eV) of the [Rh(acac)$_3$] impregnated onto SiO$_2$, **S35**, is *ca.* 3 eV higher than that of the corresponding Rh $3d_{5/2}$ peak (307.1 eV)[82] of the metal Rh(0). This increase in the binding energy indicates that a Rh^{3+} specie is present on the SiO$_2$ surface, which is expected since the rhodium in the [Rh(acac)$_3$] complex is Rh^{3+}. The Rh $3d_{5/2}$ peak of the [Rh(acac)$_3$] impregnated onto SiO$_2$, **S35**, compares well to the binding energy of Rh^{III}Cl$_3$ of 310.0 eV.[82] The spin orbit splitting observed in this study (4.77 eV) of the [Rh(acac)$_3$] impregnated onto SiO$_2$, **S35**, is comparable to the splitting observed by Suhonen *et al.* where the spin orbit splitting of Rh-Al (L) of ~4.7 eV is seen.[83] **Figure 3.32** shows the Rh 3d peak deconvolution of the [Rh(acac)$_3$] complex impregnated onto SiO$_2$, **S35**.
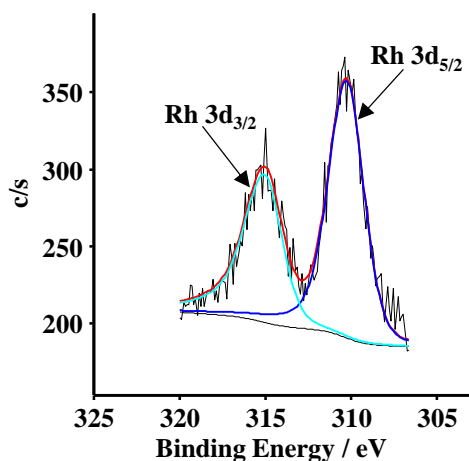
Figure 3.32: Rh 3d peak fitting (deconvolution) of [Rh(acac)$_3$] impregnated onto SiO$_2$ 3-D surface, **S35**.

---

[82] Y.V. Larichev, O.V. Netskina, O.V. Komova, V.I. Simagina, *International Journal of Hydrogen Energy* **2010** (35) 6501-6507 "Comparative XPS study of Rh/Al$_2$O$_3$ and Rh/TiO$_2$ as catalysts for NaBH$_4$ hydrolysis". DOI: 10.1016/j.ijhydene.2010.04.048

[83] S. Suhonen, R. Polvinen, M. Vladen, K. Kallinen, M. Härkönen, *Applied Surface Science* **2002** (200) 48-54, "Surface oxides on supported Rh particles: thermal decomposition of Rh oxide under high vacuum conditions". 10.1016/S0169-4332(02)00607-4

(e) <u>**Ir 4f peaks**</u>

The Ir $4f_{7/2}$ binding energy (63.81 eV) of [Ir(acac)$_3$] impregnated onto SiO$_2$, **S36**, is 3 eV higher than the corresponding peak of the metal Ir(0) which is observed at 60.8 eV.[84] This confirms that an Ir^{3+} specie is observed on the SiO$_2$ surface attributed to the [Ir^{III}(acac)$_3$] complex. The spin orbit splitting between the Ir $4f_{7/2}$ and Ir $4f_{5/2}$ peaks that Fuggle and Mårtensson observed for the Ir(0) metal (3 eV) is comparable to the spin orbit splitting that is seen in this study of 3.21 eV for the [Ir(acac)$_3$] impregnated onto SiO$_2$, **S36**. **Figure 3.33** shows the Ir 4f peak deconvolution of the [Ir(acac)$_3$] complex impregnated onto SiO$_2$, **S36**.
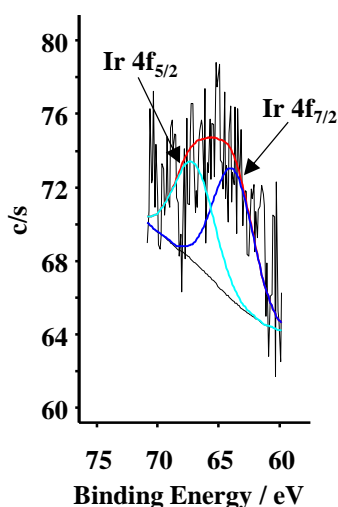
Figure 3.33: Ir 4f peak fitting (deconvolution) of [Ir(acac)$_3$] impregnated onto SiO$_2$ 3-D surface, **S36**.

(ii) *O 1s peak*

The O 1s peak deconvolution is simulated with 3 distinctive peaks. The peaks in increasing binding energies are assigned to oxygen bound to the metal center (M-O, ranging from 528.74 – 530.16 eV)[85], oxygen bound to carbon (C-O, ranging from 531.07-531.92 eV) and the oxygen that is part of the solid support (SiO$_2$, ranging from 532.87-534.30 eV).[86] The O 1s peak deconvolution of the SiO$_2$ surface containing the [Cr(acac)$_3$] complex, **S32**, can be seen in **Figure 3.34**.

[84] J.C. Fuggle, N. Mårtensson, *Journal of Electron Spectroscopy and Related Phenomena* **1980** (21) 275-281, "Core-level binding energies in metals". DOI: 10.1016/0368-2048(80)85056-0

[85] J.C. Dupin, D. Gonbeau, P. Vinatier, A. Levasseur, *Physical Chemistry Chemical Physics* **2000** (2) 1319-1324, "Systematic XPS studies of metal oxides, hydroxides and peroxides". DOI: 10.1039/A908800H

[86] R. Hofman, J.G.F. Westheim, I. Pouwel, T. Fransen, P.J. Gellings, *Surface and Interface Analysis* **1996** (24) 1-6, "FTIR and XPS Studies on Corrosion-resistant SiO$_2$ Coatings as a Function of the Humidity during Deposition". DOI: 10.1002/(SICI)1096-9918(199601)24:1<1::AID-SIA73>3.0.CO;2-I
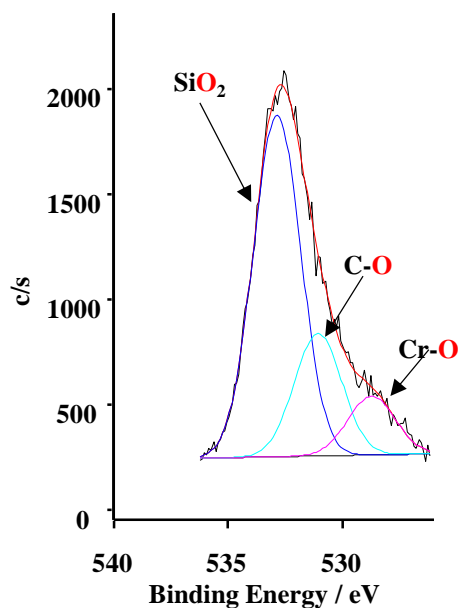
Figure 3.34: The O 1s fitting (deconvolution) of the SiO_2 surface containing $[Cr(acac)_3]$, **S32**.

3.1.6 Thermogravimetric analysis (TGA)

In this section the thermogravimetric analysis on neat $[M(\beta\text{-diketonato})_3]$ complexes and $[M(\beta\text{-diketonato})_3]$ complexes impregnated onto 3-D supports will be discussed. An understanding of the decomposition with heating of the neat $[M(\beta\text{-diketonato})_3]$ complexes is needed to understand the decomposition of the $[M(\beta\text{-diketonato})_3]$ complexes impregnated onto 3-D supports. The thermogravimetric analyses were performed at a temperature range of 30-700 °C with a 10 °C.min^{-1} heating rate under Ar atmosphere.

3.1.6.1 [M(β-diketonato)₃] complexes

(i)   *[Mn(acac)₃], 2*

The TGA of $[Mn(acac)_3]$ is given in **Figure 3.35**. Decomposition occurred according to a five step mass loss process, which started at a temperature of 124.12 °C and was only measured up to *ca.* 669.82 °C. It has been reported that $[Mn(acac)_3]$ under ambient air atmosphere, upto *ca.* 160°C decomposed with the loss as an acac radical (31.62% mass loss).[87] However, under an Ar atmosphere (upto *ca.* 160 °C) in this study, a mass loss of only 5.62% has been found, which

---

[87] A. Galukhin, M.A. Khelkhal, A. Gerasimov, T. Biktagirov, M. Gafurov, A. Rodionov, S. Orlinskii, *Energy and Fuels* **2016** (30) 7731−7737, "Mn-Catalyzed Oxidation of Heavy Oil in Porous Media: Kinetics and Some Aspects of the Mechanism". DOI: 10.1021/acs.energyfuels.6b01234

indicates that decomposition proceeds differently under an inert atmosphere. The total mass loss of [Mn(acac)$_3$] up to *ca.* 700 °C amounts to *ca.* 62.6 %, but it can be seen that decomposition is not yet complete. The calculations of the theoretical mass loss of [Mn(acac)$_3$] ($Mr_{[Mn(acac)_3]}$ = 352.26 g.mol^{-1}) will be illustrated by using $Mn^{VI}O_3$ ($Mr_{Mn^{VI}O_3}$ = 102.94 g.mol^{-1})and $Mn_2^{III}O_3$ ($Mr_{Mn_2^{III}O_3}$ = 157.87 g.mol^{-1}) as examples.

%Mass loss of [Mn(acac)$_3$] if $Mn^{VI}O_3$ is a decomposition product (note that one [Mn(acac)$_3$] can form the $Mn^{VI}O_3$ decomposition product and therefore only 1 x $Mr_{[Mn(acac)_3]}$ is used):

$$\text{\%Mass loss} = 100\% - \left(\frac{Mr_{Mn^{VI}O_3}}{Mr_{[Mn(acac)_3]}} \; x \; 100 \right) = 100\% - \left(\frac{102.94 \; g.mol^{-1}}{352.26 \; g.mol^{-1}} \; x \; 100 \right) = 70.8 \%$$

%Mass loss of [Mn(acac)$_3$] if $Mn_2^{III}O_3$ is decomposition product (note that two [Mn(acac)$_3$] is needed to form the $Mn_2^{III}O_3$ decomposition product and therefore only 2 x $Mr_{[Mn(acac)_3]}$ is used):

$$\text{\%Mass loss} = 100\% - \left(\frac{Mr_{Mn_2^{III}O_3}}{2 \; x \; Mr_{[Mn(acac)_3]}} \; x \; 100 \right) = 100\% - \left(\frac{157.87 \; g.mol^{-1}}{2 \; x \; 352.26 \; g.mol^{-1}} \; x \; 100 \right) = 77.6 \%$$

The calculated theoretical mass loss values of possible products that could form are:

Mn	84.4%
MnO(OH)	75.0%
$Mn^{II}O$	79.7%
$Mn^{IV}O_2$	75.3%
$Mn^{VI}O_3$	70.8%
$Mn_2^{III}O_3$	77.6%
$Mn_3^{II,III}O_4$	78.4%
$Mn_2^{VII}O_7$	68.5%

Considering that decomposition is not complete yet and that mass loss up to 700 °C amounts to *ca.* 62.6 %, $Mn_2^{VII}O_7$ (with mass loss of 68.5 % needed) is the most probable decomposition product up to 700 °C. Decomposition in air atmosphere resulted in a 76.67% mass loss (up to 300 °C),[87] which shows that other oxides might also be possible, but the exact composition of the decomposition product cannot be predicted with certainty using only TGA.
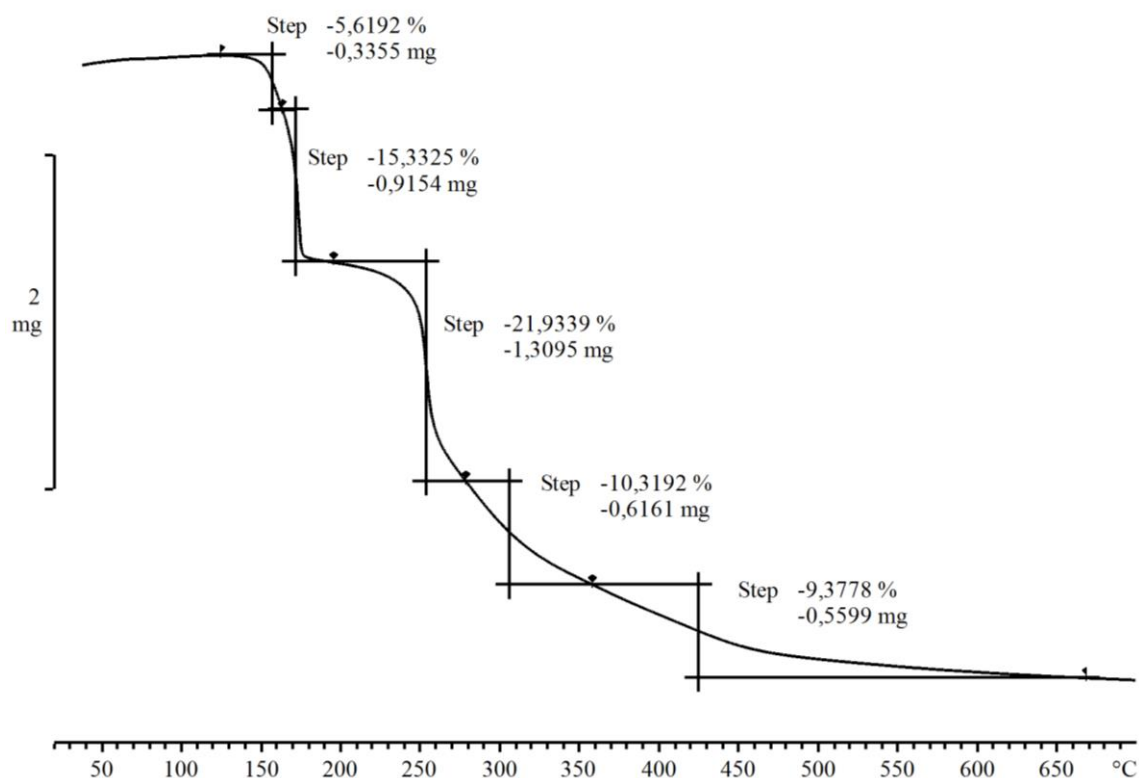
Figure 3.35: TGA of [Mn(acac)$_3$], **2**, with a sample size of 5.97 mg.

ATR FTIR of Mn(acac)$_3$ after heating it in ambient air at various temperature was measured, see **Figure 3.36**. Here it can clearly be seen how the acac ligand is removed with increase in temperature.
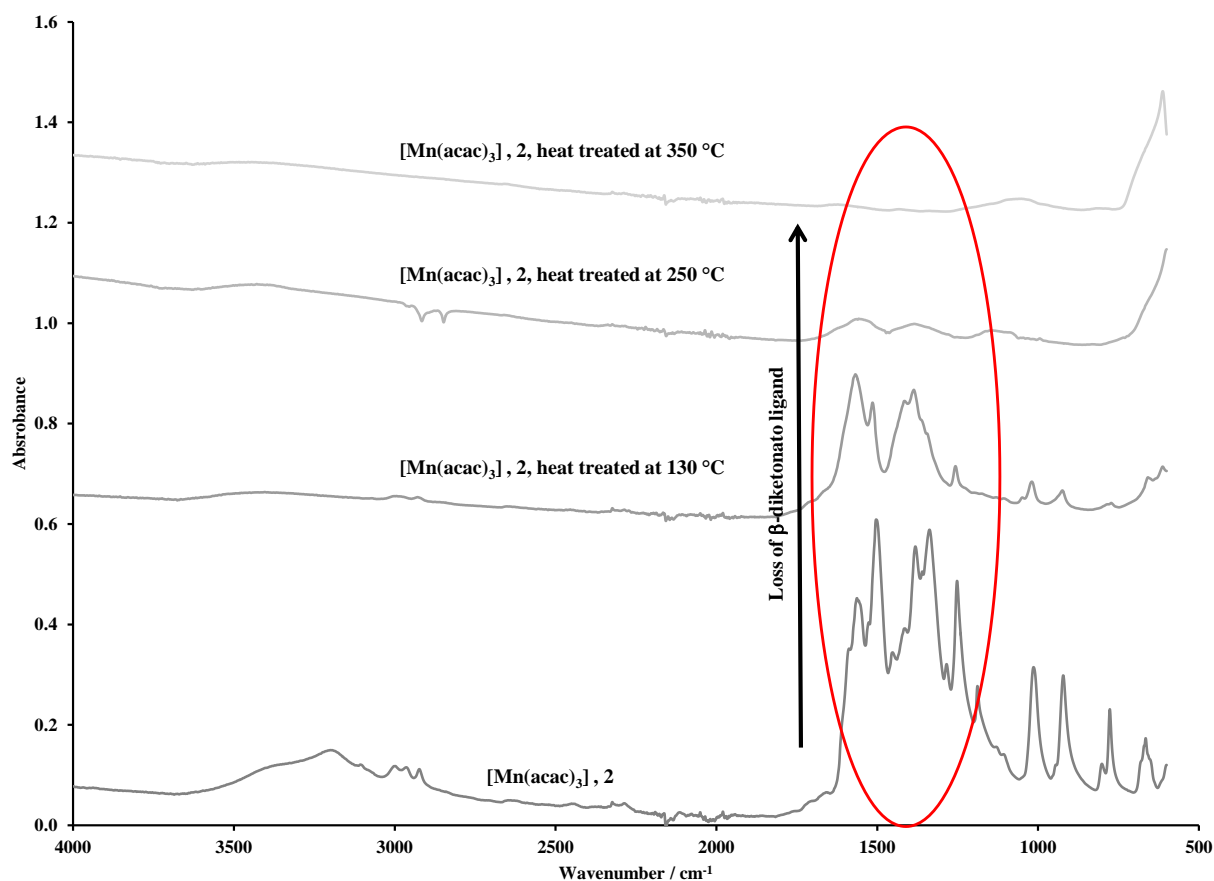
Figure 3.36: ATR FTIR spectra showing the loss of β-diketonato ligands of [Mn(acac)$_3$], 2, when heat treated.

(ii)   *[Mn(tfaa)$_3$], 5*

The TGA of [Mn(tfaa)$_3$] is given in **Figure 3.37**. The five step mass loss started at a temperature of 90.26 °C and was only measured up to *ca.* 683.40 °C. The total mass loss of [Mn(tfaa)$_3$] amounts to *ca.* 50.56 %. The calculated theoretical mass loss values of possible products that could form are:

Mn	89.3%
MnO(OH)	82.9%
Mn^{II}O	86.2%
Mn^{IV}O$_2$	83.1%
Mn^{VI}O$_3$	79.9%
Mn$_2$^{III}O$_3$	84.6%
Mn$_3$^{II,III}O$_4$	85.2%
Mn$_2$^{VII}O$_7$	78.4%
Mn(CH$_3$COCHCOCF$_3$)	59.5%

Considering that decomposition is not complete yet and that mass loss up to 700 °C amounts to *ca.* 50.56 %, Mn(CH$_3$COCHCOCF$_3$) is the most probable decomposition product up to 700 °C.
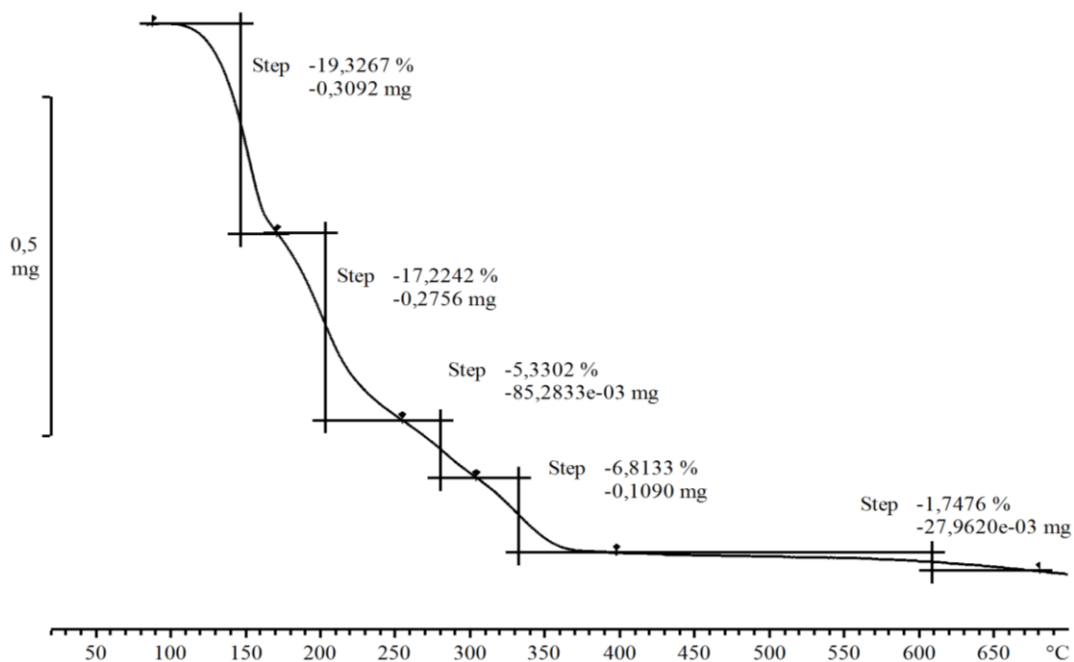
Figure 3.37: TGA of [Mn(tfaa)₃], **5**, with a sample size of 1.6 mg.

(iii)   *[Cr(acac)₃], **10***

The TGA of [Cr(acac)₃] is given in **Figure 3.38**. The two step mass loss started at a temperature of 121.21 °C and was only measured up to *ca.* 629.04 °C. The total mass loss of [Cr(acac)₃] amounts to *ca.* 94.84 %. The calculated theoretical mass loss values of possible products that could form are:

Cr	85.1%
$Cr^{II}O$	80.5%
$Cr^{IV}O_2$	76.0%
$Cr^{VI}O_3$	71.4%
$Cr^{VI}O_5$	62.2%
$Cr_2^{III}O_3$	78.2%

This indicates that the most probable decomposition product is chromium metal. However, since it is known that metal acetylacetonato complexes are used in chemical vapour deposition,[88] the global mass loss recorded here is a combination of decomposition as well as sublimation of the [Cr(acac)₃]. Thus the exact composition of the remaining product could not be predicted using

---

[88] L. Davydenko, B. Mischanchuk, V. Pokrovskiy, I. Babich, Y. Plyuto, Chemical Vapor Deposition 2011 (17) 123-127, "TPD-MS and IR Studies of Cr(acac)₃ Binding Upon CVD at Silica and Alumina Surfaces". DOI: 10.1002/cvde.201006885

TGA alone. The reported heat of sublimation and calculated temperature of sublimation of [Cr(acac)$_3$] is ΔH_{sub} = 91 kJ mol^{-1} and T_{sub} = 148 °C.[89]

Step   -92,8903 %
       -8,2208 mg

Step   -1,9503 %
       -0,1726 mg
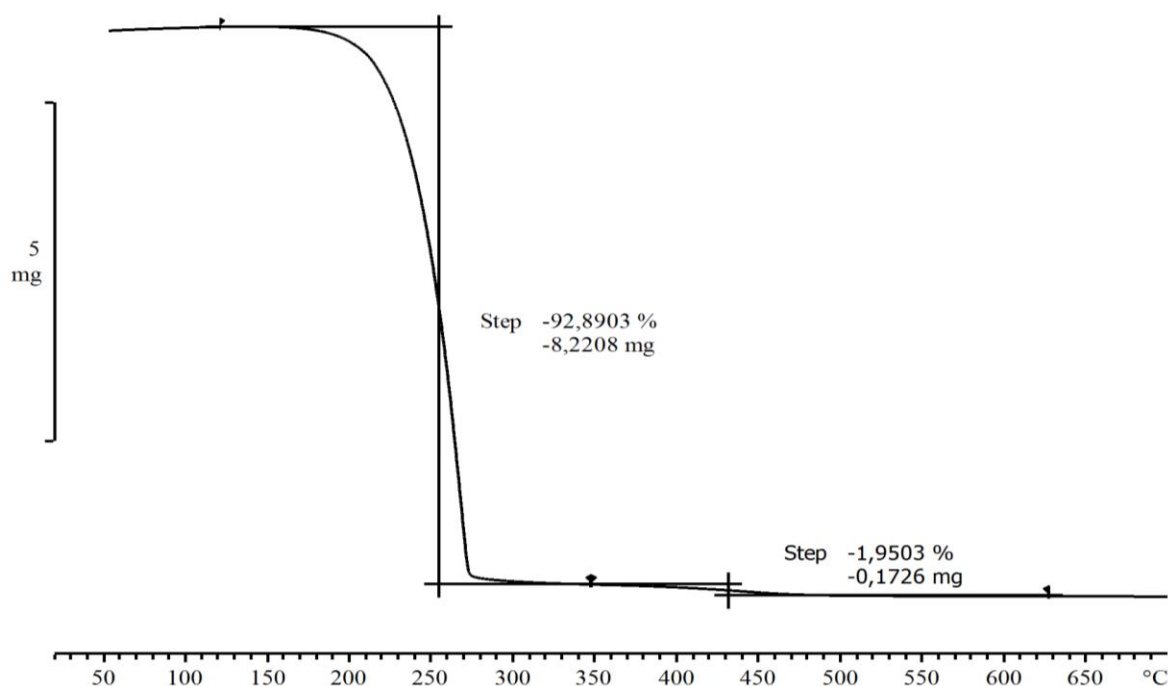
Figure 3.38: TGA of [Cr(acac)$_3$], **10**, with a sample size of 8.85 mg.

(iv)   *[Fe(acac)$_3$], 11*

The TGA of [Fe(acac)$_3$] is given in **Figure 3.39**. The two step mass loss started at a temperature of 115.79 °C and was only measured up to *ca.* 642.75 °C. The total mass loss of [Fe(acac)$_3$] amounts to *ca.* 89.04 %. The calculated theoretical mass loss values of possible products that could form are:

Fe	85.1%
Fe^{II}O	79.7%
Fe$_3$^{II,III}O$_4$	78.1%
Fe$_4$^{II,III}O$_5$	78.5%
Fe$_5$^{II,III}O$_6$	78.8%
Fe$_5$^{II,III}O$_7$	77.8%

This indicates that the most probable decomposition product is iron metal. However, similar to the [Cr(acac)$_3$], iron acetylacetonato are used in chemical vapour deposition,[88] the global mass loss

[89] B.D. Fahlman, A.R. Barron, *Advanced Materials for optics and Electronics* **2000** (10) 223-232, "Substituent effects on the volatility of metal β-diketonates". DOI: 10.1002/1099-0712(200005/10)10:3/5<223::AID-AMO411>3.0.CO;2

recorded here is a combination of decomposition as well as sublimation of the $[Fe(acac)_3]$. Thus the exact composition of the remaining product could not be predicted using TGA alone. The reported heat of sublimation and calculated temperature of sublimation of $[Fe(acac)_3]$ is $\Delta H_{sub} = 112$ kJ mol^{-1} and $T_{sub} = 161$ °C.[89]
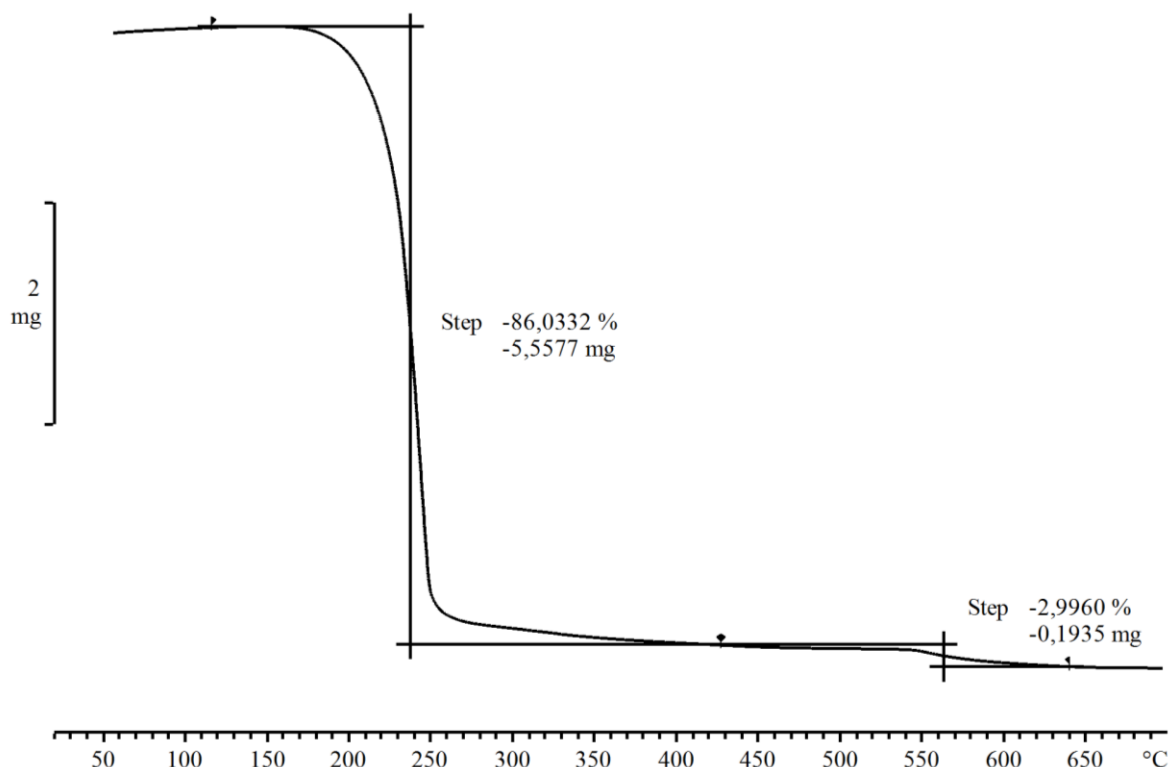
Figure 3.39: TGA of $[Fe(acac)_3]$, **11**, with a sample size of 6.46 mg.

(v)   *[Co(acac)₃], 12*

The TGA of $[Co(acac)_3]$ is given in **Figure 3.40**. The three step mass loss started at a temperature of 144.21 °C and was only measured up to *ca.* 660.51 °C. The total mass loss of $[Co(acac)_3]$ amounts to *ca.* 83.11 %. The calculated theoretical mass loss values of possible products that could form are:

Co	83.5%
Co^{II}O	79.0%
Co$_2^{III}$O$_3$	76.7%
Co$_3^{II,III}$O$_4$	77.5%

This indicates that the most probable decomposition product is cobalt metal. However, similar to the $[Cr(acac)_3]$ and $[Fe(acac)_3]$, cobalt acetylacetonato is used in chemical vapour deposition,[88] the global mass loss recorded here is a combination of decomposition as well as sublimation of the $[Co(acac)_3]$. Thus the exact composition of the remaining product could not be predicted using

TGA alone. The reported heat of sublimation and calculated temperature of sublimation of [Co(acac)$_3$] is ΔH_{sub} = 149 kJ mol^{-1} and T_{sub} = 181 °C.[89]
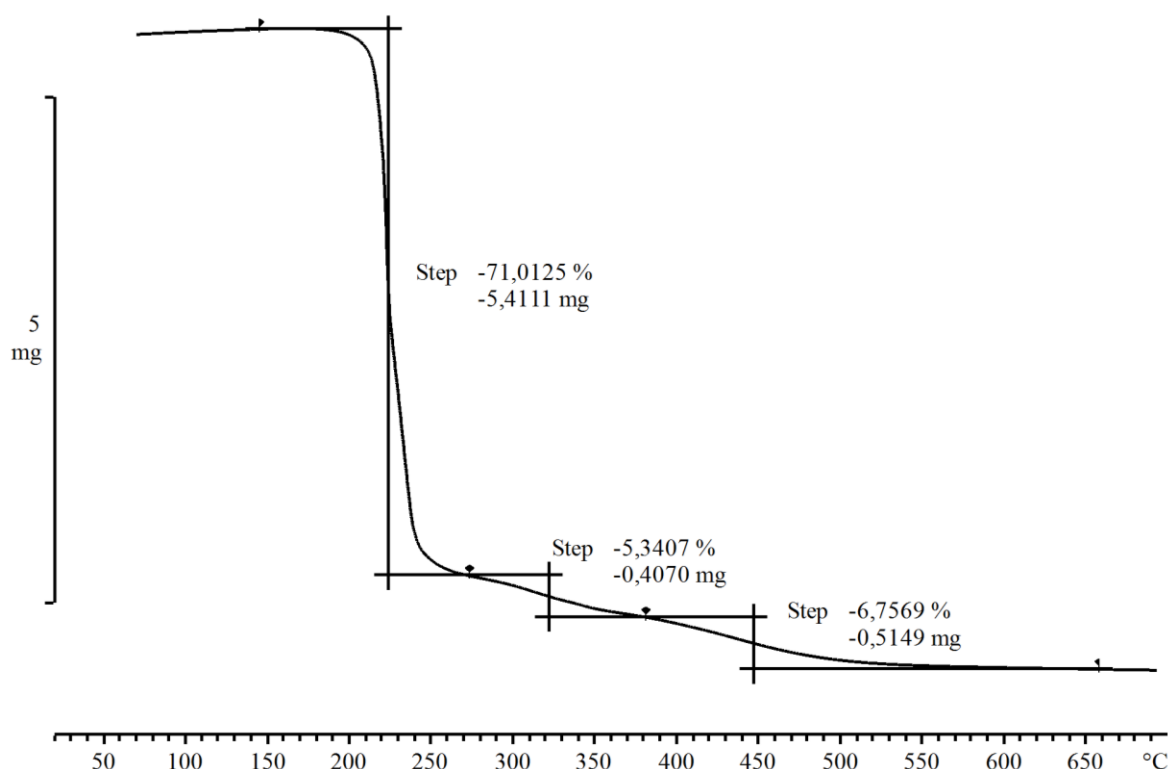
Figure 3.40: TGA of [Co(acac)$_3$], **12**, with a sample size of 7.62 mg.

3.1.6.2 [M(β-diketonato)$_3$] complexes impregnated onto 3-D supports

The 3-D supports used in this study are not expected to decompose during the TGA analyses as they all have melting points higher than the maximum temperature of 700 °C is used in the TGA study. SiO$_2$ has a melting point of 1996 K (±50 K, *ca.* 1723 °C)[90] therefore it can be expected that SiO$_2$ will be stable at the temperatures that is used in the TGA analyses. During the synthesis of nano-TiO$_2$ powders it was found that the calcination temperature during the process can influence the particle sizes of the nano-TiO$_2$ powder, B. Li and *et al.* looked at calcination temperatures of 350, 500 and 1000 °C during their studies and found that at higher calcination temperature larger particle sizes were observed.[91] MgO is known to be important in the high-temperature insulation

---

[90] E.A. Gulbransen, S.A. Jansson, *Oxidatin of Metals* **1972** (4) 181-201, "The High-Temperature Oxidation, Reduction, and Volatilization Reactions of Silicon and Silicon Carbide". DOI: 10.1007/BF00613092

[91] B. Li, X. Wang, M. Yan, L. Li, *Materials Chemistry and Physics* **2002** (78) 184-188, "Preparation and characterization of nano-TiO$_2$ powder". DOI: 10.1016/S0254-0584(02)00226-2

in the form of compacted powder. Fused MgO (prepared from calcined MgO by fusion in an electric furnace at *ca.* 2800 °C) are used when operating temperatures up to 1100 °C.[92] The temperature during the TGA studies in this section of [Mn(acac)$_3$] and [Mn(tfaa)$_3$] immoblized onto TiO$_2$ and MgO did not exceed 700 °C. Previous high temperature studies performed on TiO$_2$ and MgO indicates that it is safe to say that the TiO$_2$ and MgO supports will not decompose during the TGA investigation. The TGA of the supported metal tris(β-diketonato)$_3$ complexes were conducted to compare it to the neat complexes as well as to determine the optimum temperature to "activate" the catalyst.

(i)   *[Mn(acac)$_3$] immobilized on 3-D supports*

The TGA results of [Mn(acac)$_3$], **2**, immobilized onto SiO$_2$, **S14**; TiO$_2$, **S21**; MgO, **S22**; acidic zeolite, **S23** and basic zeolite, **S24** will be presented in this paragraph. The mass loss for the surfaces immobilized with [Mn(acac)$_3$] takes place in a 5, 3, 4, 2 and 2 step process respectively, see **Table 3.29** and **Figure 3.41**. It is clear that the Mn(acac)$_3$ complex decomposes differently on different supports and also different from the neat complexes as described in **Section 3.1.6.1**.

Table 3.29: The % mass loss during the different decomposing steps of [Mn(acac)$_3$] immobilized onto 3-D supports (**S14**, **S21-S24**)

3-D support	% Mass loss during the:					
	1st step	2nd step	3rd step	4th step	5th step	Total mass loss
SiO$_2$, **S14**	1.49 %	1.53 %	2.93 %	5.66 %	1.59 %	13.17 %
TiO$_2$, **S21**	0.27 %	1.26 %	0.26 %	-	-	1.79 %
MgO, **S22**	7.03 %	17.40 %	6.19 %	5.11 %	-	35.73 %
Acidic zeolite, **S23**	10.13 %	2.93 %	-	-	-	13.06 %
Basic Zeolite, **S24**	3.98 %	7.61 %	-	-	-	11.59 %

[92] I.O. Wilson, *IEE Proc* **1981** (128) 159-164, "Magnesium oxide as a high-temperature insulant". DOI: 10.1049/ip-a-1.1981.0026
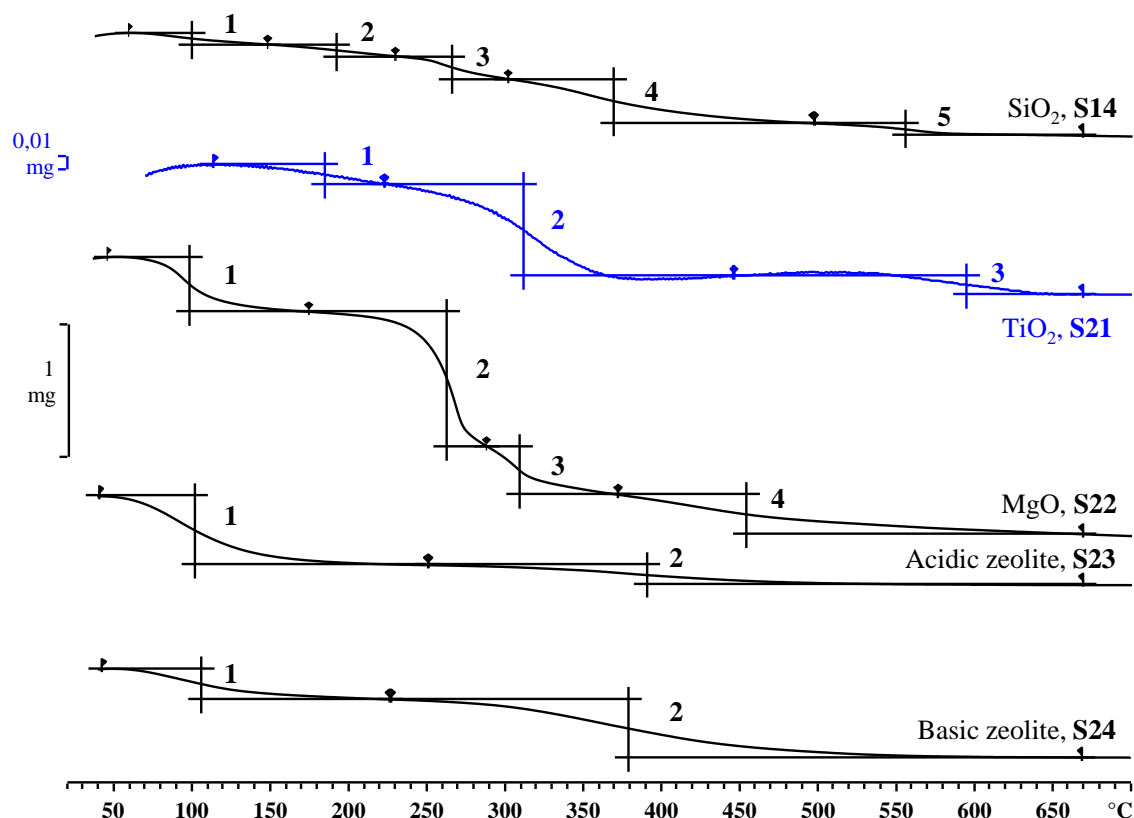
Figure 3.41: TGA curves of [Mn(acac)$_3$] immobilized on 3-D supports (**S14**, **S21-S24**)

Since in **Section 3.1.6.1 (i)** it was showed that the mass loss of [Mn(acac)$_3$] started at 124.12 °C, the mass loss before 124.12 °C during the thermogravimetric analysis of [Mn(acac)$_3$] immobilized on SiO$_2$, **S14**; TiO$_2$, **S21**; MgO, **S22**; acidic zeolite, **S23** and basic zeolite, **S24**, can be assigned to the loss of H$_2$O (% mass$_{H_2O}$ loss). With this in mind, the mass loss that can be assigned to the decomposition of [Mn(acac)$_3$] can be calculated (% mass$_{total}$ loss subtracted by the % mass$_{H_2O}$ loss). The % mass loss of each of the supports (**S14**, **S21-S24**) is summarized in **Table 3.30**.

Table 3.30: The % mass loss summary of the [Mn(acac)$_3$] immobilized on 3-D supports (**S14**, **S21-S24**).

3-D support	% mass$_{total}$ loss	% mass$_{H_2O}$ loss	% mass$_{[Mn(acac)_3]}$ loss
SiO$_2$, **S14**	13.17 %	1.25 %	11.92 %
TiO$_2$, **S21**	1.79 %	0.016 %	1.77 %
MgO, **S22**	35.73 %	5.96 %	29.77 %
Acidic Zeolite, **S23**	13.06 %	7.39 %	5.67 %
Basic Zeolite, **S24**	11.59 %	2.71 %	8.88 %

During immobilization, it was aimed to prepare a 13 wt% metal immobilization per weight of the support. This implies a 0.237 mmol (13 mg) Mn per 100 mg of support, thus 83.5 mg [Mn(acac)$_3$] per 100 mg support. Thus 45.5% [83.5x100/(83.5 + 100)] of the total mass is [Mn(acac)$_3$]. Using

only the mass of [Mn(acac)$_3$] in the sample, the % mass of the complexes was determined, see **Table 3.31**. From this it can be seen that only the decomposition of [Mn(acac)$_3$] on the MgO support is similar to the neat complex. Thus for the other supports there is a definite interaction between the support and the complex.

Table 3.31: TGA results of [Mn(acac)$_3$] immobilized on 3-D supports (**S14**, **S21-S24**)

3-D support	% mass$_{supported[Mn(acac)_3]}$ loss	Mass$_{sample}$	Mass$_{[Mn(acac)_3]}$ present on sample	Mass$_{loss(excluding\ water)}$ ^{a}	% mass$_{[Mn(acac)_3]}$ loss
SiO$_2$, **S14**	11.92 %	5.58 mg	2.54 mg	0.67 mg	26.4 %
TiO$_2$, **S21**	1.77 %	5.76 mg	2.62 mg	0.10 mg	3.8 %
MgO, **S22**	29.77 %	5.86 mg	2.67 mg	1.74 mg	65.2 %
Acidic Zeolite, **S23**	5.67 %	5.16 mg	2.35 mg	0.29 mg	12.3 %
Basic Zeolite, **S24**	8.88 %	5.68 mg	2.58 mg	0.51 mg	19.8 %

^{a} Mass$_{loss(excluding\ water)}$ = Mass$_{sample}$ x % mass$_{[Mn(acac)_3]}$ loss/100

According to the FTIR and published results of the mass loss of the neat [Mn(acac)$_3$] in air, up to 130 °C the acac$^-$ ligand is lost. With the [Mn(acac)$_3$] supported on the SiO$_2$, we propose that as prepared, the [Mn(acac)$_3$] is "bound" to the surface through hydrogen bonding. When the sample is heated to 130°C, one acac$^-$ ligand is lost and the Mn coordinates to the OH-groups on the SiO$_2$ surface. Further heat treatment results in the loss of the other acac$^-$ ligands forming Mn-oxides, see the FTIR Spectra below in **Figure 3.42**.
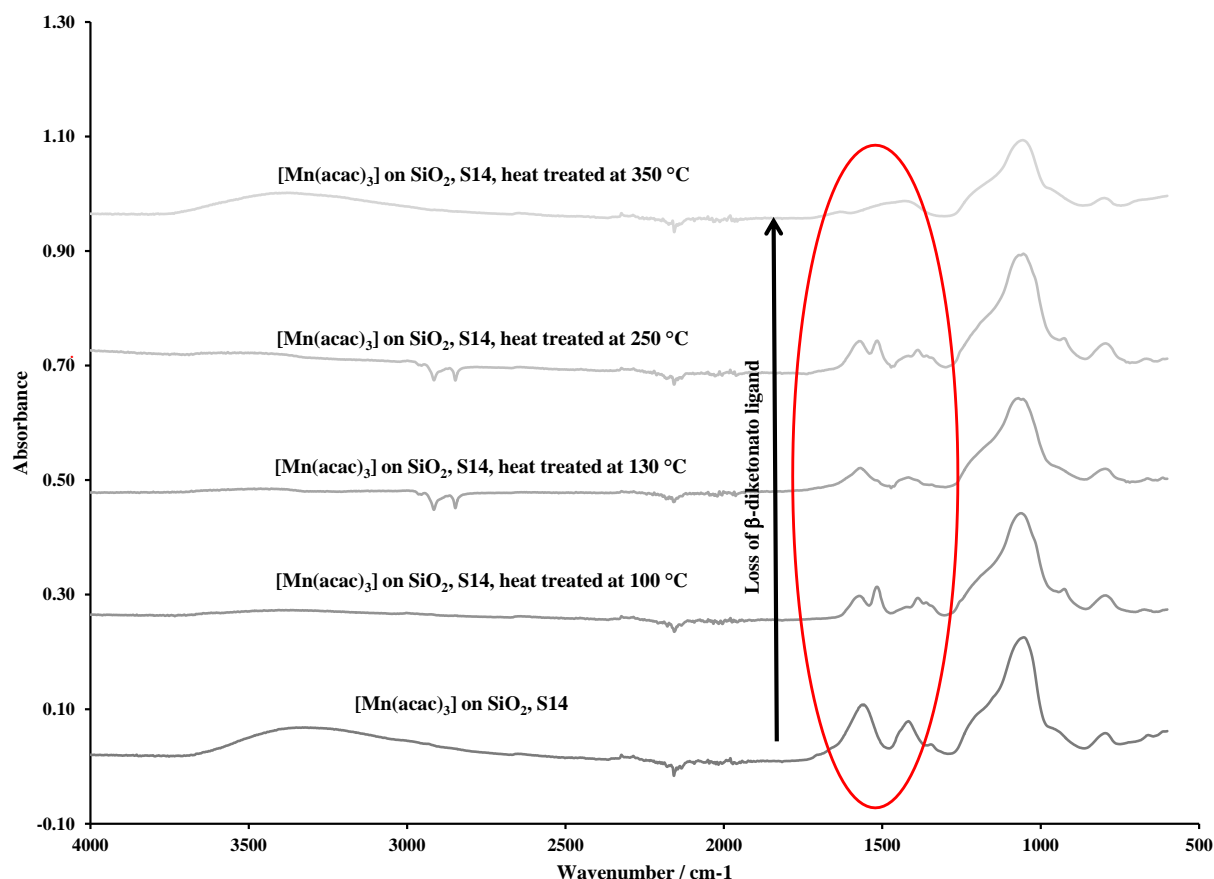
Figure 3.42: ATR FTIR spectra showing the loss of β-diketonato ligands of [Mn(acac)$_3$] on SiO$_2$, **S14**, when heat treated.

(ii)   *[Mn(tfaa)$_3$] immobilized on 3-D supports*

The TGA results of [Mn(tfaa)$_3$], **5**, immobilized onto SiO$_2$, **S17**; TiO$_2$, **S25**; MgO, **S26**; acidic zeolite, **S27** and basic zeolite, **S28** will be presented in this paragraph. The mass loss for the surfaces immobilized with [Mn(tfaa)$_3$] takes place in a 4, 4, 7, 3 and 3 step process respectively, see **Table 3.32** and **Figure 3.43**.

Table 3.32: The % mass loss during the different decomposing steps of [Mn(tfaa)$_3$] immobilized onto 3-D supports (**S17**, **S25-S8**).

3-D support	% Mass loss during the:							Total mass loss
	1st step	2nd step	3rd step	4th step	5th step	6th step	7th step	
SiO$_2$, **S17**	1.08 %	4.95 %	9.32 %	2.56 %	-	-	-	17.91 %
TiO$_2$, **S25**	0.10 %	5.16 %	5.75 %	1.18 %	-	-	-	12.19 %
MgO, **S26**	4.07 %	4.84 %	1.47 %	8.56 %	9.73 %	2.93 %	12.09 %	43.69 %
Acidic Zeolite, **S27**	4.92 %	12.94 %	6.18 %	-	-	-	-	24.04 %
Basic Zeolite, **S28**	8.17 %	15.12 %	5.16 %	-	-	-	-	28.45 %
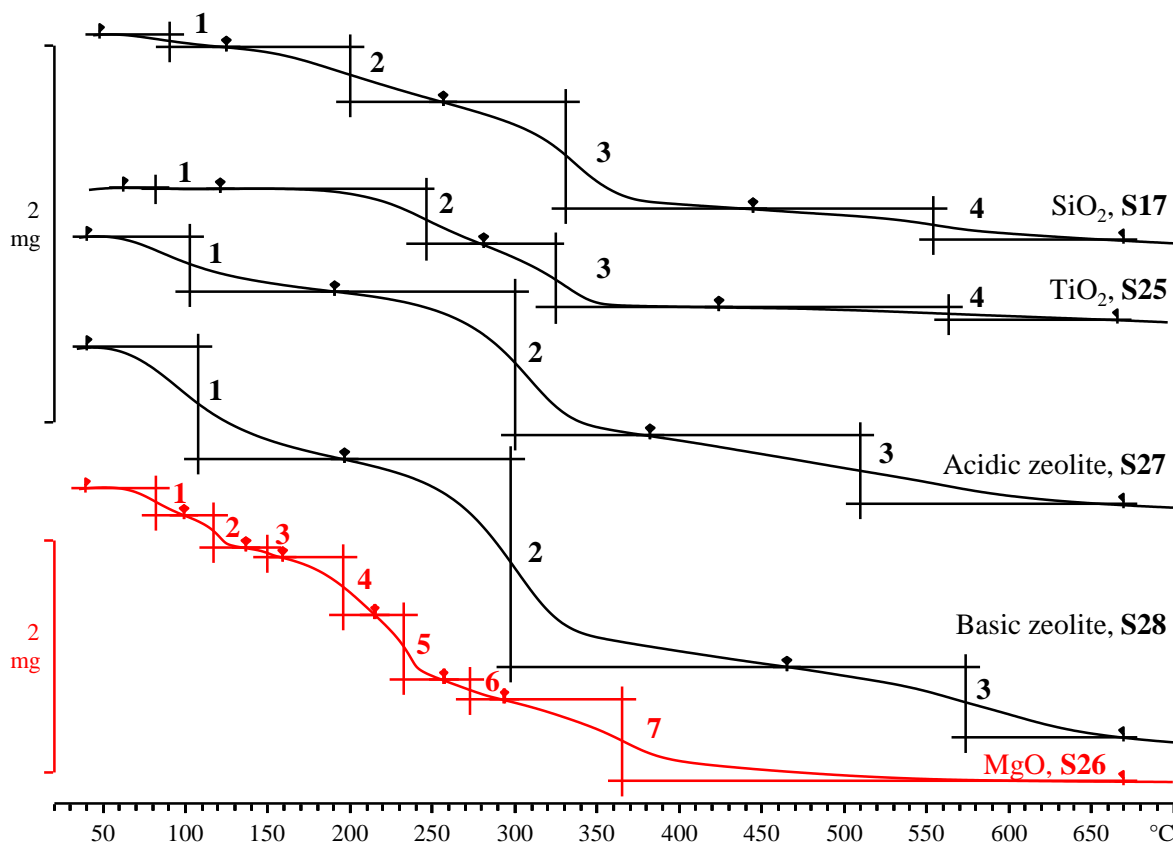
Figure 3.43: TGA curves of [Mn(tfaa)$_3$] immobilized on 3-D supports (**S17**, **S25-S28**)

These supports immobilized with [Mn(tfaa)$_3$] showed the loss of H$_2$O similar to the supports immobilized with [Mn(acac)$_3$]. Therefore, the mass loss before 124.12 °C during the thermogravimetric analysis can be assigned to the loss of H$_2$O (% mass$_{H_2O}$ loss). The determination of the decomposition of [Mn(tfaa)$_3$] is the same as in **Section 3.1.6.2(i)**. The % mass loss of each of the supports (**S17**, **S25-S28**) is summarized in **Table 3.33**.

Table 3.33: The % mass loss summary of the [Mn(tfaa)$_3$] immobilized on 3-D supports (**S17**, **S25-S28**).

3-D support	% mass$_{total}$ loss	% mass$_{H_2O}$ loss	% mass$_{[Mn(tfaa)_3]}$ loss
SiO$_2$, **S17**	17.94 %	1.11 %	16.83 %
TiO$_2$, **S25**	12.19 %	0.10 %	12.09 %
MgO, **S26**	43.54 %	8.30 %	35.24 %
Acidic Zeolite, **S27**	24.01 %	3.44 %	20.57 %
Basic Zeolite, **S28**	28.43 %	5.47 %	22.97 %

During immobilization, it was aimed to prepare a 13 wt% metal immobilization per weight on the support. This implies a 0.237 mmol (13 mg) Mn per 100 mg of support, thus 121.9 mg [Mn(tfaa)$_3$] per 100 mg support. A 120.4 % [Mn(tfaa)$_3$] per supported catalyst system was used in this study.

Table 3.34: TGA results of [Mn(tfaa)$_3$] immobilized on 3-D supports (**S17**, **S25-S28**)

3-D support	% mass$_{[Mn(tfaa)_3]}$ loss	Mass$_{sample}$	Mass$_{loss(excluding\ water)}$ ^{a}
SiO$_2$, **S17**	16.83 %	6.10 mg	1.03 mg
TiO$_2$, **S25**	12.09 %	7.28 mg	0.88 mg
MgO, **S26**	35.24 %	5.84 mg	2.06 mg
Acidic Zeolite, **S27**	20.57 %	5.92 mg	1.22 mg
Basic Zeolite, **S28**	22.97 %	7.28 mg	1.67 mg

^{a} Mass$_{loss(excluding\ water)}$ = Mass$_{sample}$ x % mass$_{[Mn(tfaa)_3]}$ loss/100

The %Mn loading on the surface are summarized in **Table 3.35**. From **Table 3.35** it is clear that the 3-D support with the highest % Mn$_{loaded}$ is MgO (3.77 %) followed by basic zeolite (2.45 %), acidic zeolite (2.20 %), SiO$_2$ (1.80 %) and TiO$_2$ (1.29 %). This is similar to the trend observed for [Mn(acac)$_3$] immobilized onto SiO$_2$, **S14**; TiO$_2$, **S21**; MgO, **S22**; acidic zeolite, **S23** and basic zeolite, **S24** supports however, the second highest %Mn loaded was on the SiO$_2$, **S14**, support.

Table 3.35: The calculated % manganese loaded onto the 3-D supports.

3-D support	% Mn$_{loaded}$
SiO$_2$, **S17**	1.80 %
TiO$_2$, **S25**	1.29 %
MgO, **S26**	3.77 %
Acidic Zeolite, **S27**	2.20 %
Basic Zeolite, **S28**	2.45 %

(iii)   *[M(acac)$_3$] immobilized onto SiO$_2$ (S32-S34)*

The TGA results of [M(acac)$_3$] (M = Cr, **S32**; Fe, **S33** and Co, **S34**) immobilized onto SiO$_2$ will be presented in this paragraph. The mass loss for the [M(acac)$_3$] complexes immobilized onto SiO$_2$ takes place in a 2, 3 and 3 step process respectively, see **Table 3.36** and **Figure 3.44**.

Table 3.36: The % mass loss during the different decomposing steps of [M(acac)$_3$] immobilized onto 3-D supports (**S32-S34**).

[M(acac)$_3$] immobilized onto SiO$_2$	% Mass loss during the:			Total mass loss
	1st step	2nd step	3rd step	
[Cr(acac)$_3$], **S32**	3.04 %	3.52 %	-	6.56 %
[Fe(acac)$_3$], **S33**	1.72 %	3.08 %	1.93 %	6.73 %
[Co(acac)$_3$], **S34**	1.99 %	0.94 %	0.84 %	3.77 %
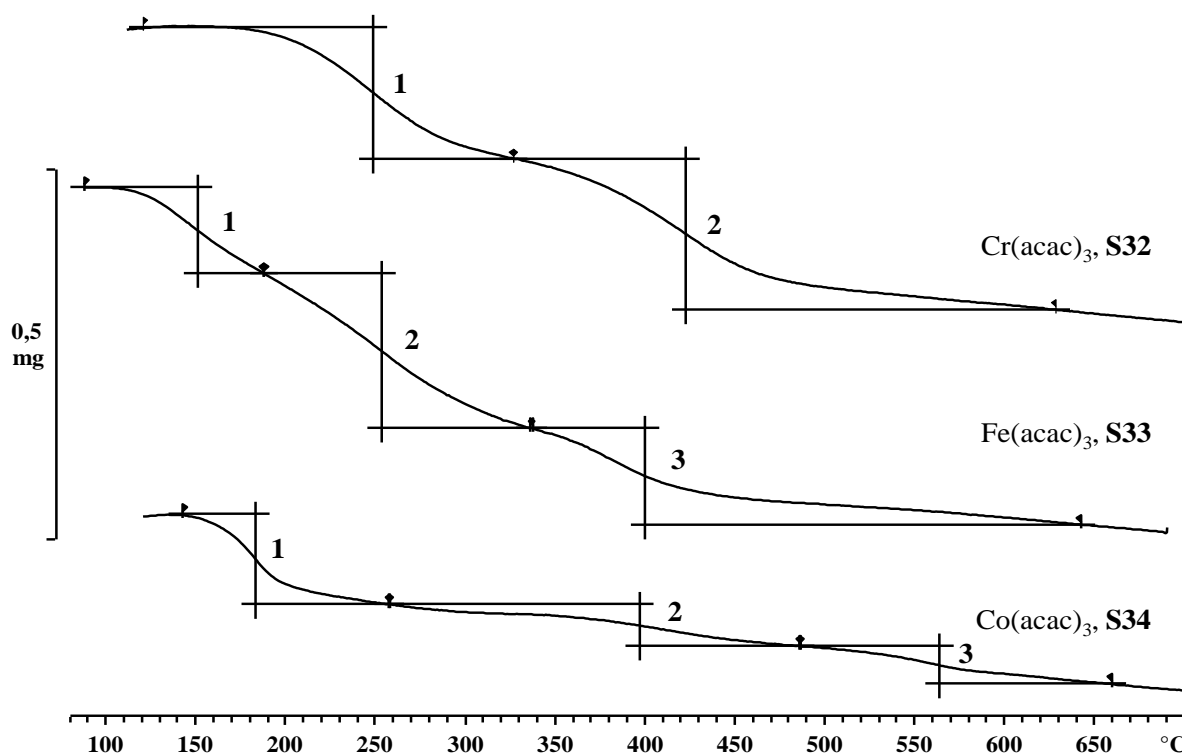
Figure 3.44: TGA curves of [M(acac)$_3$] immobilized on SiO$_2$ (**S32-S34**).

When comparing the neat complex's TGA with that of the complexes immobilized onto SiO$_2$ it can be seen that [Fe(acac)$_3$] immobilized onto SiO$_2$, **S33**, is the only support system that starts decomposing at lower temperature compared to their respective neat complex ([Fe(acac)$_3$], **11**, which started decomposing at 115.79 °C and [Fe(acac)$_3$] immobilized onto SiO$_2$, **S33**, which already started decomposing at 89.78 °C). The loss of H$_2$O during the TGA of [Fe(acac)$_3$] immobilized onto SiO$_2$, **S33**, is similar to what was found in [Mn(acac)$_3$] and [Mn(tfaa)$_3$] immobilized onto different 3-D supports, see **Section 3.1.6.1(i)** and **Section 3.1.6.1(ii)**. Therefore, the mass loss before 115.79 °C during the thermogravimetric analysis of [Fe(acac)$_3$] immobilized onto SiO$_2$, **S33**, can be assigned to the mass loss of H$_2$O (% mass$_{H_2O}$ loss). The determination of the decomposition of [M(acac)$_3$] (M = Cr, **S32**; Fe, **S33** and Co, **S34)** is calculated the same way as in **Section 3.1.6.1(i)**. The % mass loss of each of the supports (**S32-S34**) is summarized in **Table 3.37**.

Table 3.37: The % mass loss summary of the [M(acac)$_3$] immobilized on SiO$_2$ (**S32-S34**).

[M(acac)$_3$] immobilized onto SiO$_2$	% mass$_{total}$ loss	% mass$_{H_2O}$ loss	% mass$_{[M(acac)_3]}$ loss
[Cr(acac)$_3$], **S32**	6.56 %	-	6.56 %
[Fe(acac)$_3$], **S33**	6.73 %	1.64 %	5.09 %
[Co(acac)$_3$], **S34**	3.77 %	-	3.77 %

137

During immobilization, it was aimed to prepare a 13 wt% metal immobilization per weight on the support. This implies 13 mg (0.25 mmol, 0.23 mmol and 0.22 mmol respectively) of Cr, Fe and Co per 100 mg of support. Therefore, 87.3 mg, 82.2 mg, 78.6 mg [Cr(acac)$_3$], [Fe(acac)$_3$] and [Co(acac)$_3$] per 100 mg support respectively. A 100.2 %, 100.4 % and 100.3 % [Cr(acac)$_3$], [Fe(acac)$_3$] and [Co(acac)$_3$] per supported catalyst system respectively.

Table 3.38: TGA results of [M(acac)$_3$] immobilized on SiO$_2$ (**S32-S34**).

[M(acac)$_3$] immobilized onto SiO$_2$	% mass$_{[M(acac)_3]}$ loss	Mass$_{sample}$	Mass$_{loss(excluding\ water)}$ ^{a}
[Cr(acac)$_3$], **S32**	6.56 %	5.82mg	0.38 mg
[Fe(acac)$_3$], **S33**	5.09 %	6.79 mg	0.35 mg
[Co(acac)$_3$], **S34**	3.77 %	6.06 mg	0.23 mg

^{a} Mass$_{loss(excluding\ water)}$ = Mass$_{sample}$ x Total % mass$_{[M(acac)_3]}$ loss/100

The %M load on the SiO$_2$ surface are summarized in **Table 3.39**. From **Table 3.39** it is clear that the SiO$_2$ with the highest % M$_{loaded}$ is Mn (1.87 %) followed by Cr (0.98 %), Fe (0.80 %) and Co (0.62 %).

Table 3.39: The calculated % metal loaded onto SiO$_2$ (**S14**, **S32-S34**).

[M(acac)$_3$] immobilized onto SiO$_2$	% M$_{loaded}$	M$_{Electronegativity}$
[Cr(acac)$_3$], **S32**	0.98 %	1.66
[Mn(acac)$_3$], **S14**	1.87 %	1.55
[Fe(acac)$_3$], **S33**	0.80 %	1.83
[Co(acac)$_3$], **S34**	0.62 %	1.88

The relationship between the Pauling electronegativity of the metal centres and the % M$_{loaded}$ onto the SiO$_2$ support can be seen in **Figure 3.45**.
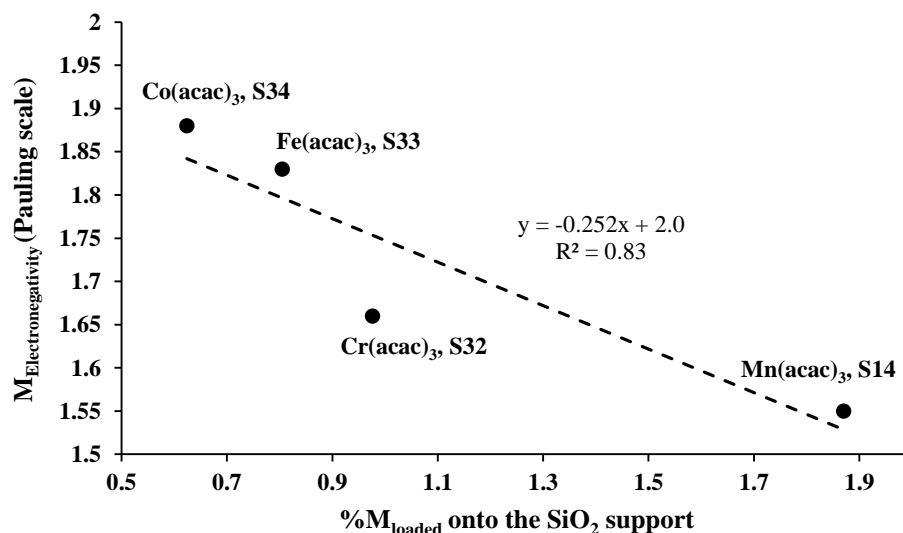
Figure 3.45: The correlation between the % metal loaded onto SiO$_2$ support and the electronegativity of the metal centres.

From **Figure 3.45** it is observed that with an increase in the electronegativity of the [M(acac)$_3$] metal centre, the percentage metal loaded onto the SiO$_2$ decreased. The linear equation describing the correlation between the Pauling electronegativity of the [M(acac)$_3$] metal centre and the % metal loaded onto the SiO$_2$, is given by:

$$M_{Electronegativity} = (-0.252)(\%M_{loaded}) + 2.0 \hspace{3cm} R^2 = 0.83$$

3.1.7 Catalytic testing of selected 2-D model catalyst

To determine if the [M(β-diketonato)$_3$] complexes grafted onto 2-D (two-dimentional) amino-functionalized Si-wafers can be used in organic reactions as catalysts, the catalytic self-solvating reaction to form diurethane (which mimics the industrial production of polyurethane) was monitored by the use of ATR FTIR. Seven of the prepared 2-D model catalyst ([Mn(acac)$_3$], **S5**; [Mn(dbm)]$_3$, **S7**; [Mn(tfaa)]$_3$, **S8**; [Mn(hfaa)$_3$], **S12**; [Co(acac)$_3$], **S29**; [Rh(acac)$_3$], **S30**, and [Ir(acac)$_3$], **S31**) were used in this catalytic activity study. The formation of hexamethylenediurethane (HDU, product) was monitored at carbonyl stretching frequency ranging between 1680-1698 cm^{-1}, and the disappearance of the cyanate (-N=C=O, reactant) stretching frequency of the hexamethylenediisocyanate (HDI) ranging between 2259-2264 cm^{-1}, see **Figure 3.46**. The reaction catalyzed by the use of the 2-D model catalysts is illustrated in **Scheme 3.11**. The hexamethlenediisocyanate and ethanol was used in a 1:10 equivalents ratio, having a [HDI] of 1.35 mmol.dm^{-3} as a result.
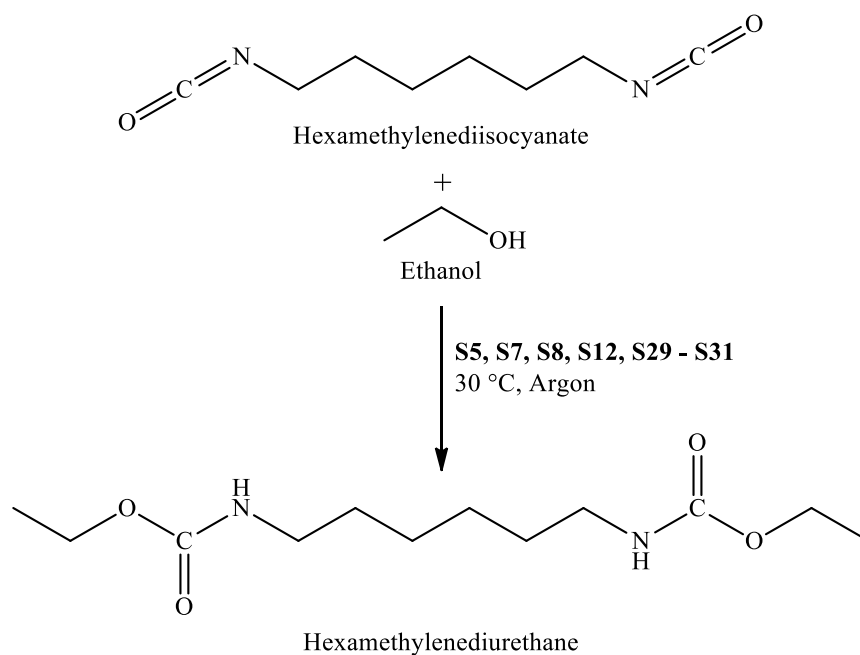
Scheme 3.11: The self-solvating reaction, where hexamethylenediisocyanate and ethanol form hexamethylenediurethane catalyzed by **S5, S7, S8, S12** and **S29**-**S31**.
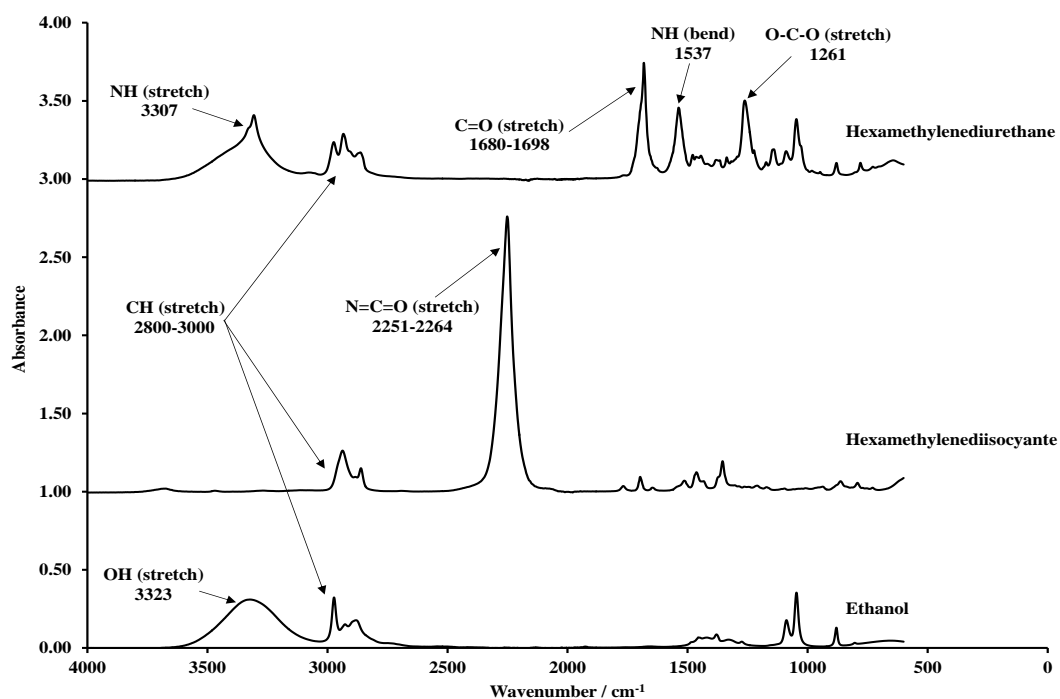
Figure 3.46: ATR FTIR spectra of ethanol (reactant, bottom), hexamethylenediisocyanate (reactant, middle) and the hexamethylenediurethane (product, top).

3.1.7.1 [Mn(β-diketonato)₃] on amino-functionalized Si-wafers (S5, S7, S8 and S12)

The performance of the four [Mn(β-diketonato)₃] 2-D model catalysts (*ca.* 4.5 mm²) during the reaction of HDI and ethanol to form HDU is summarized in **Table 3.40**. The ATR FTIR monitoring of the catalytic formation of hexamethylenediurethane in the presence of [Mn(acac)₃] immobilized on amino-functionalized Si-wafer, **S5**, is illustrated in **Figure 3.47**. In **Figure 3.47** the N=C=O stretching frequency decreases (2270 cm⁻¹) while the C=O stretching frequency (1680 cm⁻¹) appears (as hexamethylenediurethane is produced) and increase as the reaction takes place till completion.
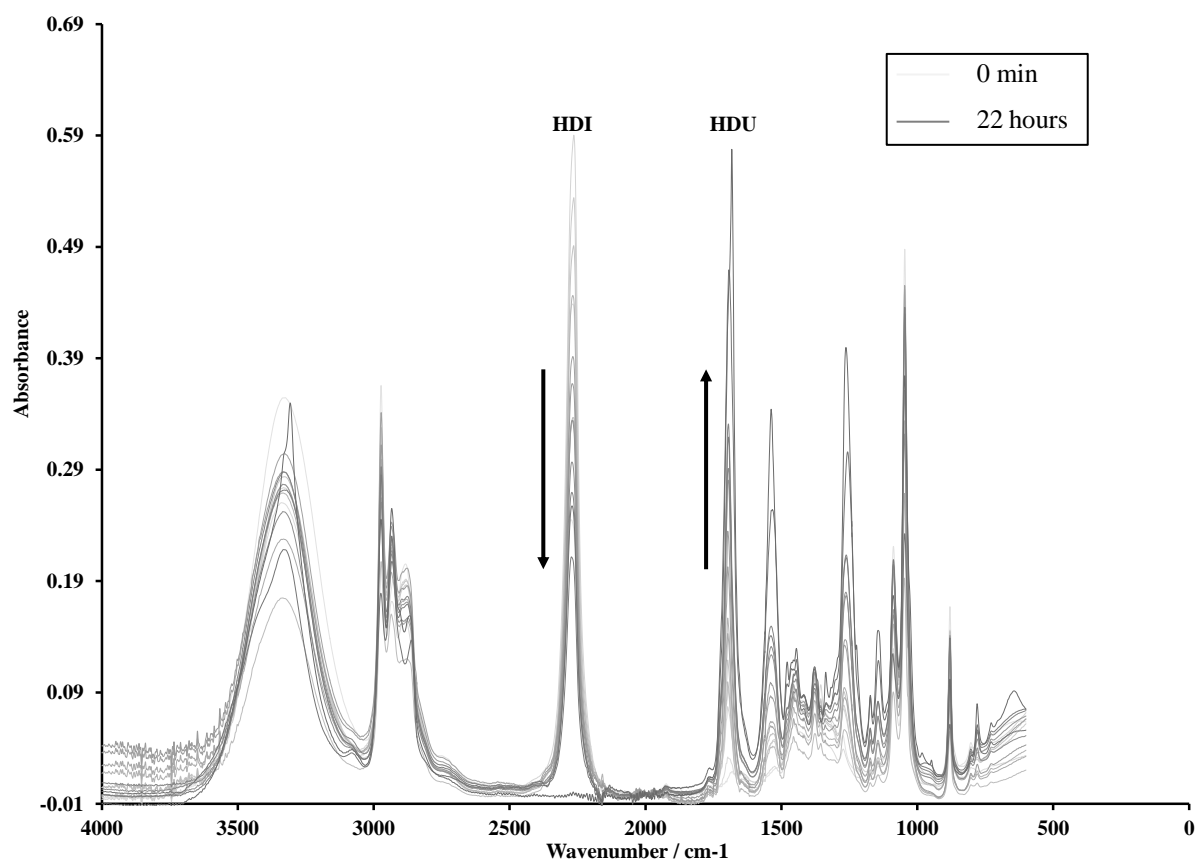
Figure 3.47: ATR FTIR monitoring of the catalytic formation of hexamethylenediurethane (HDU) in the presence of [Mn(acac)₃] immobilized on amino-functionalized Si-wafer, **S5**, over 22 hours.

In this section the [Mn(acac)₃] immobilized onto amino-functionalized Si-wafer surface, **S5**, will be used to explain how the data in **Table 3.40** was calculated. Since it is known that [Mn(β-diketonato)₃] complexes as well as Mn-oxides can catalyze reactions, the total amount of Mn on the surface will be used in the determination of the turnover frequencies (TOF) of the catalysts. From **Section 3.1.5.2 (i)** it was determined that there is 2-3 silane linker (amine) per nm². From the ratio between N and Mn, the amount of Mn molecules per nm² and subsequently the amount of Mn molecules per surface used in the catalytic testing can be calculated. For surface **S5**, for instance, the Mn:N ratio is 1:2.7, thus for every 1 N there is 0.38 Mn. Since it is known

that there are 2-3 N per nm^2, there are $(2 - 3)(0.38)$ Mn per nm^2 giving $0.74 - 1.11$ Mn per nm^2. The total amount of Mn molecules on the **S5** surface is calculated by multiplying the amount of Mn molecules per nm^2 with the total surface area in nm^2 [5.0×10^{12} nm^2 x ($0.74 - 1.11$ Mn molecules per nm^2) = $3.70 \times 10^{12} - 5.56 \times 10^{12}$ Mn molecules on the **S5** surface]. The surface areas of the [Mn(β-diketonato)$_3$] 2-D model catalysts are 5.0×10^{12}, 3.8×10^{12}, 4.4×10^{12} and 5.0×10^{12} nm^2 for surfaces [Mn(acac)$_3$], **S5**; [Mn(dbm)$_3$], **S7**; [Mn(tfaa)$_3$], **S8**; [Mn(hfaa)$_3$], **S12**, respectively.

Table 3.40: Performance of Mn on the amino-functionalized Si-wafer 2-D model catalysts (**S5**, **S7**, **S8** and **S12**).

2-D model catalysts	Mn:N ^{a}	Mn molecules per nm^2	Mn molecules x10^{+12} per surface	TOF / S^{-1}	% disappearance of HDI	$\chi_R + \chi_{R'}$ all three ligands
[Mn(acac)$_3$] + amino-functionalized wafer, **S5**	1:2.7	0.74 - 1.11	3.70 – 5.56	7.11 – 10.66	56.0	14.04
[Mn(dbm)$_3$] + amino-functionalized wafer, **S7**	1:2.1	0.95 – 1.43	3.62 – 5.43	6.74 – 10.11	51.9	12.60
[Mn(tfaa)$_3$] + amino-functionalized wafer, **S8**	1:2.3	0.87 – 1.30	3.83 – 5.74	5.51 – 8.27	44.9	16.05
[Mn(hfaa)$_3$] + amino-functionalized wafer, **S12**	1:1.9	1.05 – 1.58	5.31 – 7.96	4.68 – 7.03	52.9	18.06

^{a} The XPS determined Mn:N ratio

The % disappearance of the HDI frequency and turn over frequency (TOF) was determined after 240 min into the catalytic reaction. Very little to no product was produced in the presence of no catalyst and/or the non-functionalized Si-wafer.[93] The disappearance of the reactants (hexemethylenediisocyante (HDI) and ethanol) was observed (on FTIR at 2270 cm^{-1}) while formation of the product (hexamethylenediurethane (HDU)) is measured at 1680 cm^{-1}. The 1.27 cm^3 reaction mixture (1 cm^{-3} ethanol and 0.27 cm^{-3} HDI) with a concentration of 1.33 mol.dm^{-3} contains 1.69 mmol of HDI (1.02×10^{21} HDI molecules). For surface **S5**, 56% of the HDI molecules were converted after 240 minutes, implying 5.68×10^{20} HDI molecules were converted. The turn over frequency (TOF) is determined by using the following equation:

$$TOF = \frac{\left(\frac{amount\ of\ molecules\ converted}{amount\ of\ active\ sites}\right)}{time\ in\ sec} \qquad \textbf{Equation 3.4}$$

---

[93] M.M. Conradie, J. Conradie, E. Erasmus, *Polyhedron* **2014** (79) 52-59," Immobilisation of iron tris(β-diketonates) on a two-dimensional flat amine functionalised silicon wafer: A catalytic study of the formation of urethane, from ethanol and a diisocyanate derivative " DOI: 10.1016/j.poly.2014.04.054

The TOF of surface **S5** is calculated as 5733 – 8600 s^{-1} (5.733 x 10^3 s^{-1} – 8.60 x 10^3 s^{-1}). From **Table 3.40** and **Figure 3.48** it is clear that the TOF is dependent on the combined Gordy group electronegativity (3(χ_R + $\chi_{R'}$)) of the R-groups on the β-diketonato ligands of the manganese catalysts used to prepare the surface, even though a portion of the [Mn(β-diketonato)$_3$] complexes grafted on the wafers decomposed. As the total group electronegativity, 3(χ_R + $\chi_{R'}$), increases a general decrease in the TOF is observed in **Figure 3.48**. This observation is consistent with the catalytic activity testing of [Fe(β-diketonato)$_3$] immobilized catalyst on amino-functionalized Si-wafers.[93] This gives an indication that a more electron rich [Mn(β-diketonato)$_3$] manganese centre will be more active compared to an electron deficient [Mn(β-diketonato)$_3$] manganese centre. This can however not be said with certainty, since all the manganese on the surface is involved in the catalysis, which is a combination of the [Mn(β-diketonato)$_3$] immobilized catalyst as well as Mn oxides.
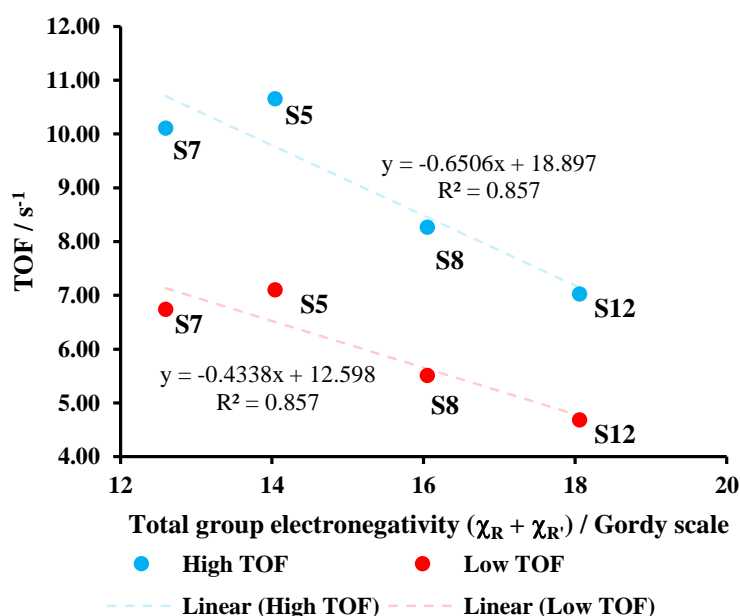
Figure 3.48: The calculated TOF of the four [Mn(β-diketonato)$_3$] 2-D model catalysts ([Mn(acac)$_3$], **S5**; [Mn(dbm)$_3$], **S7**; [Mn(tfaa)$_3$], **S8**; [Mn(hfaa)$_3$], **S12**) vs. the total Gordy group electronegativity (3(χ_R + $\chi_{R'}$)).

3.1.7.2   [M(acac)$_3$] on amino-functionalized Si-wafers (S29 – S31)

The performance of the four [M(acac)$_3$] 2-D model catalysts ([Mn(acac)$_3$], **S5**; [Co(acac)$_3$], **S29**; [Rh(acac)$_3$], **S30** and [Ir(acac)$_3$], **S31**) during the reaction of HDI and ethanol to form HDU is summarized in **Table 3.41**. The information was calculated as explained in the previous paragraph. Once again the total metal content on the surface was used in the determination of the turnover frequencies (TOF) of the catalysts since the XPS data cannot distinguish between [M(acac)$_3$] and M-oxides or other M decomposition products immobilized on the 2D model

catalyst. The surface areas of the [M(acac)$_3$] 2-D model catalysts ([Mn(acac)$_3$], **S5**; [Co(acac)$_3$], **S29**; [Rh(acac)$_3$], **S30** and [Ir(acac)$_3$], **S31**) are 5×10^{12} nm^2, 3.25×10^{12} nm^2, 3.36×10^{12} nm^2 and 3.75×10^{12} nm^2 respectively.

Table 3.41: Performance of four M-amino-functionalized Si-wafer 2-D model catalysts.

2-D model catalysts	M:N ^{a}	M molecules per nm^2	M molecules x10^{+12} per surface	TOF / s^{-1}	% dissaperence of HDI	χ_M ^{b}
[Fe(acac)$_3$] + amino-functionalized wafer ^{c}	1:1.1	0.7 – 1.1	17.0 – 26.0	33.0 – 46.0	50.6	1.83
[Mn(acac)$_3$] + amino-functionalized wafer, **S5**	1:2.7	0.74 - 1.11	3.70 – 5.56	7.11 – 10.66	56.0	1.55
[Co(acac)$_3$] + amino-functionalized wafer, **S29**	1:2.8	0.71 -1.07	3.71 – 5.57	9.11 – 13.67	72.0	1.88
[Rh(acac)$_3$] + amino-functionalized wafer, **S30**	1:15.4	0.13 – 0.19	0.55 – 0.82	65.77 – 98.65	76.3	2.28
[Ir(acac)$_3$] + amino-functionalized wafer, **S31**	1:8.5	0.24 – 0.35	1.98 – 2.96	17.43 – 26.14	73.3	2.20

^{a} The XPS determined % M attributed to [M(acac)$_3$] bound to amine on the Si-wafer surface
^{b} Electronegativity by Pauling scale
c Data obtained from [94]

From **Table 3.41** it is clear that surface **S30**, where [Rh(acac)$_3$] was immobilized onto amino-functionalized Si-wafer, is the most active 2-D model catalyst. The superior performance of the [Rh(acac)$_3$] (and possible Rh metal and oxides due to decomposition similar as was found for [Mn(acac)$_3$]) immobilized onto amino-functionalized Si-wafer, **S30**, could be attributed to the electronegativity of the rhodium centre, see **Figure 3.49**. The Pauling electronegativity of the rhodium centre of the [Rh(acac)$_3$] or Rh-oxides, etc immobilized onto amino-functionalized Si-wafer, **S30**, surface is greater compared to the other metal centres. The greater electronegativity of the metal centre indicates that the metal centre attracts electrons stronger and in turn will make the metal centre of the [M(acac)$_3$] complex, as well as the M-oxides etc, immobilized onto the amino-functionalized Si-wafer surface more electron rich. This is consistent with the catalytic activity testing of [Fe(β-diketonato)$_3$] immobilized catalyst on amino-functionalized Si-wafers,[94] as well as the conclusion of the previous section where it was determined that the more electron donating the β-diketonato ligands (more electron rich manganese centre) the more effective the 2-D model catalyst was in the formation of HDU (higher TOF). However, it must be noted that not

[94] M.M. Conradie, J. Conradie, E. Erasmus, *Polyhedron* **2014** (79) 52-59," Immobilisation of iron tris(β-diketonates) on a two-dimensional flat amine functionalised silicon wafer: A catalytic study of the formation of urethane, from ethanol and a diisocyanate derivative " DOI: 10.1016/j.poly.2014.04.054

all the metal on the surface is involved in the catalysis, is [M(acac)₃], due to possible decomposition to M-oxides etc.
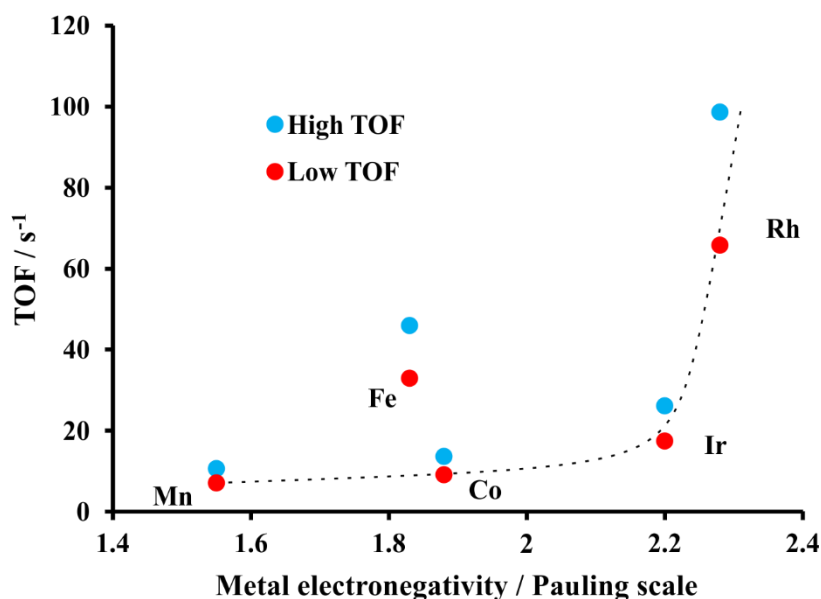
Figure 3.49: The calculated TOF of the four [M(acac)₃] 2-D model catalysts ([Mn(acac)₃], **S5**; [Fe(acac)₃]; [Co(acac)₃], **S29**; [Rh(acac)₃], **S30** and [Ir(acac)₃], **S31**) vs. the Pauling metal electronegativity.

3.1.8 Catalytic testing of [Mn(acac)₃] 3-D model catalyst

The catalytic activity of the [Mn(acac)₃] supported on the 3-D SiO_2 (heat treated at different temperatures) was evaluated for the reaction of HDI and ethanol to form HDU is summarized in **Table 3.42**.

Table 3.42: Catalytic data of [Mn(acac)₃] on SiO_2 heat treated at different temperatures and tested for the catalytic reaction between EtOH and HDI to form HDU. The amount of HDI used was 6.38×10^{20} molecules and the amount of Mn on the surface is 1.09×10^{16} molecules.

Tempwrature treatment	% dissaperence of HDI	Time/s	TOF
No treatment	89.5	19380	2.7
100 °C	100	5700	10.3
130 °C	76	8700	5.1
250 °C	74.2	8700	5.0
350°C	76.8	16680	2.3

The calculated TOF is not as good as the 2-D sample, which could probably be an indication that access to the active species is more important in the catalysis than the surface area or that the catalytic activity of the [Mn(acac)$_3$] and the different Mn-oxides that formed on the 2-D and 3-D samples differs. The ratio between [Mn(acac)$_3$] and the different Mn-oxides is unknown and not the same for the 2-D and the different 3-D catalysts. Of the 3-D catalysts, the one treated at 100 °C gave the highest TOF, probably since it only lost one acac ligand while the higher temperature treated samples started to form oxides.

3.2 Chromium(0) Fischer Carbene Complexes

The work that will be discussed was done in collaboration with the research group of Dr. M Landman at the University of Pretoria. The homogeneous alkoxy- and amino-Fischer carbene complexes were supplied by the research group in Pretoria. Four Fischer carbene complexes, [Cr(CO)$_4$(PPh$_3$)=C(OEt)(Fu)], **C1**; [Cr(CO)$_5$=C(NHCy)(Fu)], **C2**; [Cr(CO)$_5$=C(NHCy)(Th)], **C3** and [Cr(CO)$_5$=C(OEt)(ThTh)], **C4**, (see **Scheme 3.12**) were obtained and characterized by electrochemistry, X-ray photoelectron spectroscopy (XPS) and computational chemistry calculations at the University of the Free State as part of this study and this research is presented and discussed here. Penta-carbonyl complexes [Cr(CO)$_5$=C(OEt)(Fu)], **C5**, and [Cr(CO)$_5$=C(OEt)(Th)], **C6**, were also supplied and they were anchored onto an amino-functionalized Si-wafer to create an immobilized Fischer carbene (see **Section 3.2.4.3**).
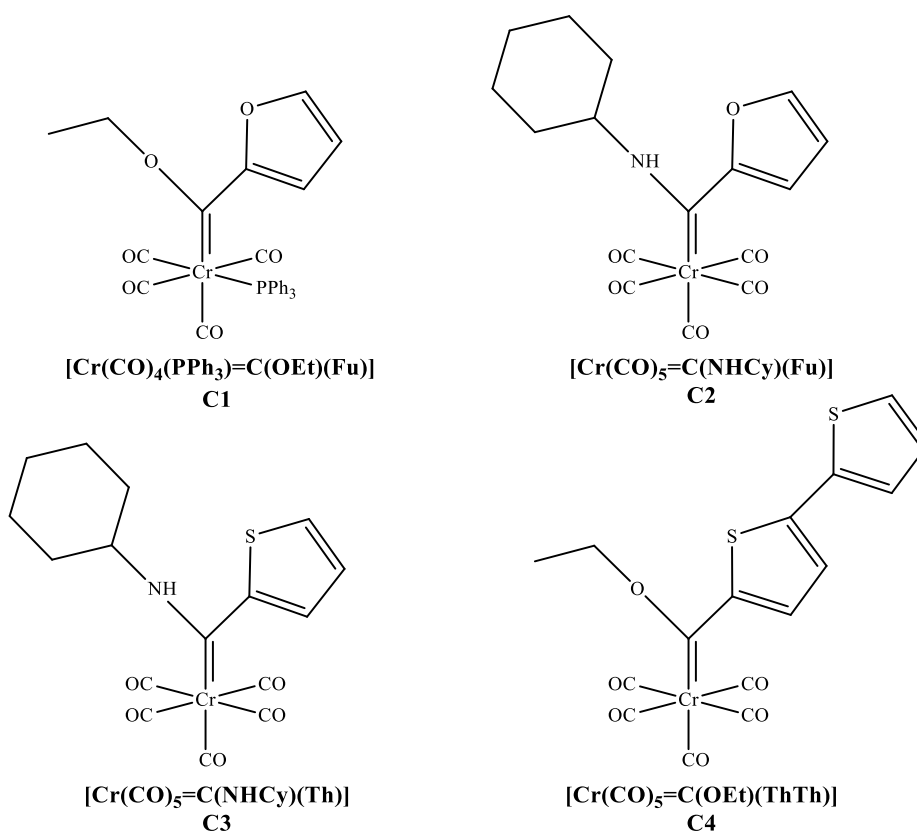
Scheme 3.12: Alkoxy- and amino-Fischer carbene complexes **C1 – C4** of this study.

3.2.1 Conformations of carbene complexes

The alkoxy- and amino-Fischer carbene complexes of this study can have different isomers and conformations, namely *syn/anti*, *Z/E*, *fac/mer*, and *cis/trans* as discussed in **Chapter 2 Section 2.10.1**. **Scheme 3.13** illustrates the different isomer combinations that are possible for the Fischer carbene complexes in this study.
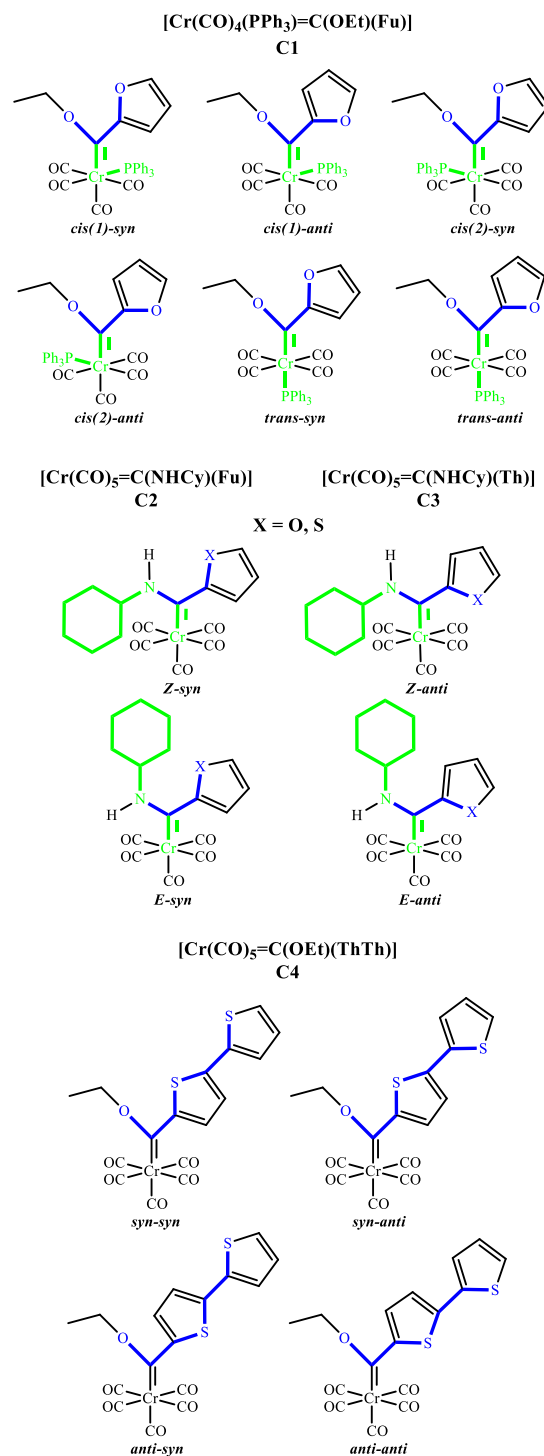
Scheme 3.13: Possible isomers and conformers of the different Fischer carbene complexes of this study.

3.2.2 Electrochemistry study

There are two redox active centres in the Cr-Fischer carbene complexes (**C1-C4**) namely the chromium metal centre and the carbene ligand. Due to formation of unwanted decomposition products during the cyclic voltammetry (CV) experiments the oxidation and the reduction peaks are reported separately. The CV over a wide potential range, as well as CV's at different scan

rates are given in **Appendix A**. This study only concentrates on the first oxidation- (Cr^0 to Cr^{+1}) and the first reduction (the reduction of the carbene carbon) process. The resulting voltammograms of the four Fischer carbene complexes **C1-C4** are showed in **Figure 3.50** (oxidation peaks) and **Figure 3.51** (reduction peaks).
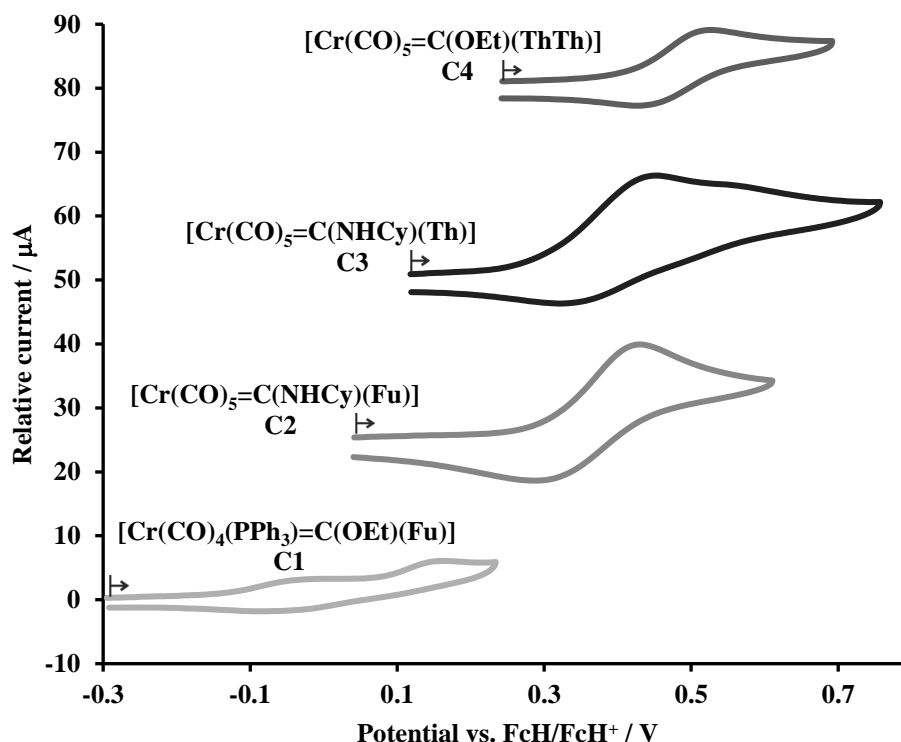
Figure 3.50: Cyclic voltammogram of oxidation process of the different Cr-Fischer carbene complexes **C1–C4** at scan rate of 0.10 V.s^{-1}. Measurements were performed on 1.0 mM analyte in 0.1 M [^{n}(Bu$_4$)N][PF$_6$]/CH$_3$CN on a glassy carbon working electrode and are reported versus ferrocene as an internal standard; the CV initiated in the direction of the arrows.

The oxidation waves all show a reduction peak coupled to the oxidation peak with a peak potential separation (ΔE) of 57 – 145 mV (see **Figure 3.50**). The oxidation process of [Cr(CO)$_4$(PPh$_3$)(OEt)(Fu)], **C1**, with ΔE = 57 mV is electrochemically reversible, but chemically quasi- or partially reversible, since i_{pc}/i_{pa} = 0.67. The oxidation process of complexes **C2–C4** with 102 mV < ΔE < 145 mV and i_{pc}/i_{pa} < 0.7 is electrochemically and chemically quasi-reversible. The reduction of three of the complexes, **C1–C3**, is irreversible (see **Figure 3.51**). No re-oxidation peak coupled to the reduction peak is observed, even at high scan rates up to 0.500 V.s^{-1} (see **Appendix A**). The reduction of [Cr(CO)$_5$=C(OEt)(ThTh)], **C4**, however, is electrochemically reversible and chemically quasi-reversible. The extended dimeric heteroarene five-membered ring systems lead to enhanced stabilization of the reduced radical anion, since the density of the electron

that is added upon reduction is distributed over the carbene carbon and both the heteroarene rings, see **Table 3.45** and the discussion in **Section 3.2.3.2**.

From **Figure 3.50** it is clear that the oxidation potential (E_{pa}) is influenced by the varied substituents on different sites of the Fischer carbene complex. The oxidation order of the Fischer carbenes is: $[Cr(CO)_5=C(OEt)(ThTh)]$, **C4** > $[Cr(CO)_5=C(NHCy)(Th)]$, **C3** > $[Cr(CO)_5=C(NHCy)(Fu)]$, **C2** > $[Cr(CO)_4(PPh_3)=C(OEt)(Fu)]$, **C1**. The reduction followed the same trend except for the $[Cr(CO)_4(PPh_3)=C(OEt)(Fu)]$, **C1**, complex that is reduced at a higher potential than the aminocarbene complexes, see **Figure 3.51**: $[Cr(CO)_5=C(OEt)(ThTh)]$, **C4** > $[Cr(CO)_4(PPh_3)=C(OEt)(Fu)]$, **C1** > $[Cr(CO)_5=C(NHCy)(Th)]$, **C3** > $[Cr(CO)_5=C(NHCy)(Fu)]$, **C2**.

Changing the hetero atom from O to N (by substitution of OEt with NHCy), leads to a lower oxidation and reduction potential. This result is in agreement with the electron donating properties of N and O. The Pauling electronegativity of N ($\chi_N = 3.04$) is lower than that of O ($\chi_O = 3.44$) implying that N is more electron donating than O. This leads to more electron density on the carbene C making it more difficult to add an electron, thus the reduction potential (E_{pc}) is at a lower more negative potential. Similar, for the Cr it will be easier to remove an electron, leading to an oxidation potential (E_{pa}) at a lower potential.

Substitution of one of the CO groups with the more electron donating PPh_3-group on the Cr-centre makes the metal easier to oxidize. **Figure 3.50** shows that $[Cr(CO)_4(PPh_3)=C(OEt)(Fu)]$, **C1**, complex has a lower oxidation potential than the penta-carbonyl complexes **C2**–**C4** of this study. CO is a better π-acceptor than PPh_3.[95] Therefore, five CO groups will accept more electron density from Cr-centre than that of four CO groups and one PPh_3 group. This in turn causes the Cr metal centre in the penta-carbonyl complexes **C2**–**C4** to have relatively less electron density available to be oxidized (the electrons are more difficult to remove, oxidation potential (E_{pa}) at a higher potential) than that of the Cr metal centre in the tetra carbonyl carbene **C1**.

[95] W.A. Schenk, W. Buchner, *Inorg. Chim. Acta*, **1983** (70) 189-196.; W Buchner, W.A. Schenk, *Inorg. Chem.* **1984** (23) 132-137, "Tetracarbonyl tungsten complexes containing two different donor ligands. III. [1] 31P-NMR spectra" DOI: 10.1016/S0020-1693(00)82801-7, "Carbon-13 NMR spectra of monosubstituted tungsten carbonyl complexes. NMR trans influence in octahedral tungsten (0) compounds" DOI: 10.1021/ic00170a004.
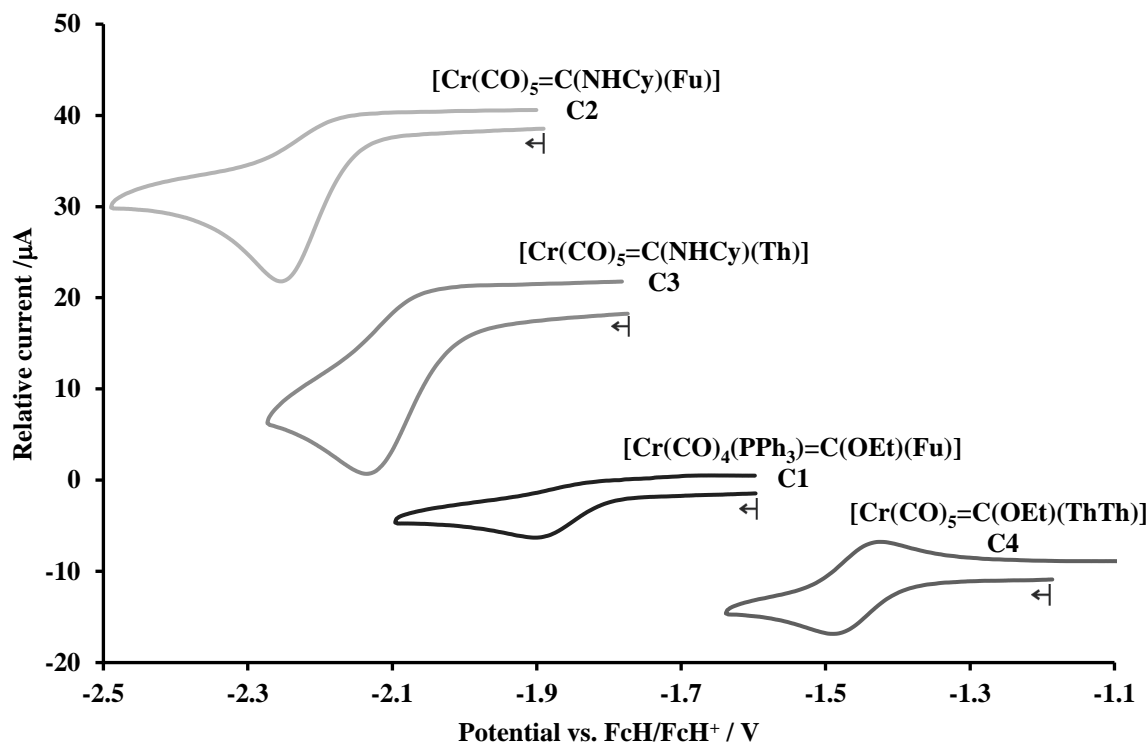
Figure 3.51: Cyclic voltammogram of reduction process of the different Cr-Fischer carbene complexes at scan rate of 0.10 V.s^{-1}. Measurements were performed in 1.0 mM analyte in 0.1 M [^{n}(Bu$_4$)N][PF$_6$]/CH$_3$CN on a glassy carbon working electrode with ferrocene as an internal standard; the CV initiated in the direction of the arrows.

The electrochemical data obtained from **Figure 3.50** and **Figure 3.51** are tabulated in **Table 3.43**. A summary of the electrochemical data at scan rates 0.05 – 0.500 V.s^{-1} is provided in **Appendix A**. The first oxidation of the [Cr(CO)$_4$(PPh$_3$)=C(OEt)(Fu)], **C1**, and [Cr(CO)$_5$=C(NHCy)(Th)], **C3**, carbene complexes are splitted into two peaks corresponding to the different isomers or conformers of the complexes.

Table 3.43: Summary of the electrochemical data obtained of the Fischer carbene complexes from **Figure 3.50** and **Figure 3.51**.

Complex	Oxidation						Reduction					
	1st					2nd	1st					2nd
	E_{pa} (V)	E_{pc} (V)	ΔE (V)	$E^{0'}$ (V)	i_{pc}/i_{pa}	E_{pa} (V)	E_{pc} (V)	E_{pa} (V)	ΔE (V)	$E^{0'}$ (V)	i_{pa}/i_{pc}	E_{pc} (V)
[Cr(CO)$_4$(PPh$_3$)=C(OEt)(Fu)] **C1**	-0.029	-0.086	0.057	-0.057	0.67	0.161	-1.900	-	-	-	-	-
[Cr(CO)$_5$=C(NHCy)(Fu)] **C2**	0.432	0.287	0.145	0.359	0.69	-	-2.278	-	-	-	-	-
[Cr(CO)$_5$=C(NHCy)(Th)] **C3**	0.456	0.323	0.133	0.389	0.50	0.569	-2.145	-	-	-	-	-
[Cr(CO)$_5$=C(OEt)(ThTh)] **C4**	0.531	0.429	0.102	0.480	0.65	-	-1.489	-1.423	0.066	-1.456	0.8	-2.098

3.2.2.1 *Cis* and *trans* isomers

The $[Cr(CO)_4(PPh_3)=C(OEt)(Fu)]$, **C1**, carbene complex has a PPh_3 substituent that is directly bound to the Cr metal centre. This substituent makes it possible for this complex to exist either as a *trans* or a *cis* isomer. From the density functional theory (DFT) computational chemistry results that will be presented in **Section 3.2.3**, it was observed that both *cis* and *trans* isomers are thermodynamically accessible due to the small energy difference between the *cis* and *trans* conformations (see **Table 3.44**). The energy of the highest occupied molecular orbital (HOMO) of the *cis* conformations is lower (more stable) than that of the *trans* conformations. More energy will thus be needed to remove an electron from the HOMO of a *cis* isomer, i.e. it will be more difficult to oxidize a *cis* isomer than a *trans* isomer. The oxidation peak of the *cis* isomer will therefore be found at higher potential than the oxidation peak of the *trans* isomer, see **Figure 3.52**, which evidence suggest that the two peaks are the oxidation of the two conformers respectivily. The two oxidation processes observed could also be interpreted as two different oxidation process of the same compound, but since only one oxidation process is observed for complex C4 (no conformers possible), see **Figure 3.50**, this interpretation is not favoured.
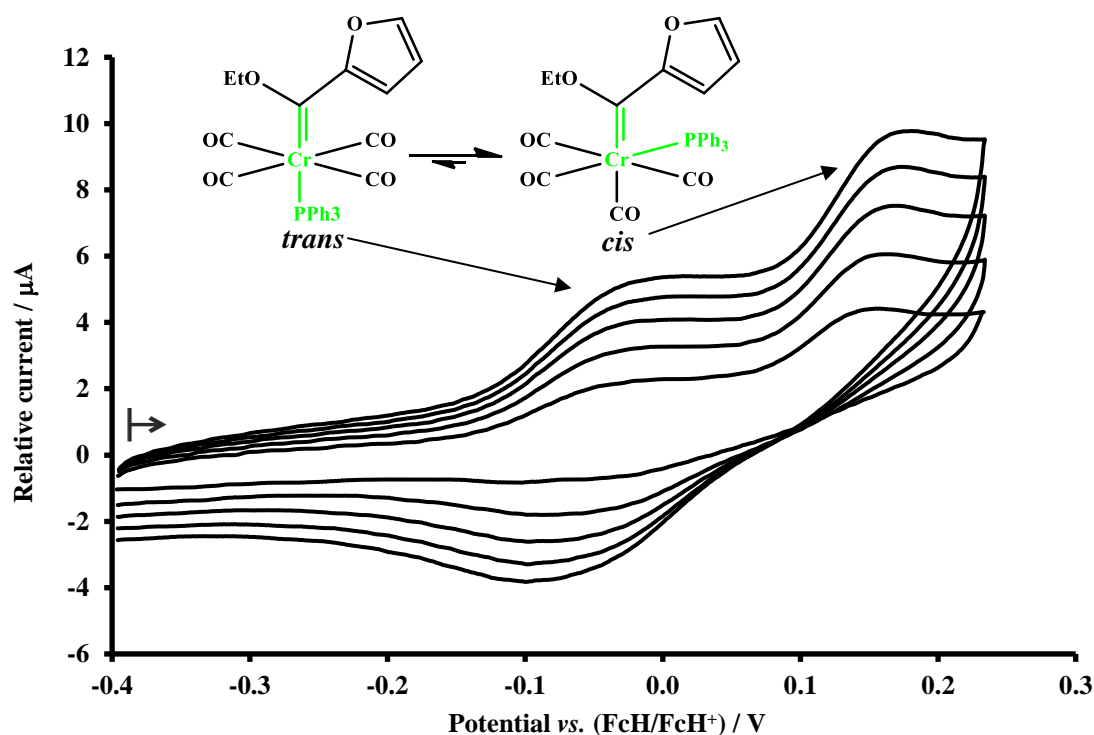
Figure 3.52: Cyclic voltammogram showing the trans and cis isomers of $[Cr(CO)_4(PPh_3)=C(OEt)(Fu)]$, **C1**, at scan rates of 0.05, 0.10, 0.15, 0.20 and 0.25 $V.s^{-1}$. Measurements were performed in 0.1 mM $[^n(Bu_4)N][PF_6]/CH_3CN$ on a

glassy carbon working electrode and are reported with ferrocene as an internal standard; the CV initiated in the direction of the arrow.

3.2.2.2 *E* and *Z* isomers

The cyclic voltammogram of [Cr(CO)$_5$=C(NHCy)(Th)], **C3**, showed the splitting of the oxidation peak which is ascribed to the *Z* and *E* isomers (the position of the cyclohexane substituent on the nitrogen with regards to the chromium metal centre). In the NMR spectra, both the *Z* and *E* isomers of [Cr(CO)$_5$=C(NHCy)(Th)], **C3**, are observed with *Z*: *E* (Experimental) = 64.4 : 35.6.[96] The two isomers, *Z* and *E,* arise from restricted rotation about the N-C$_{carbene}$ bond, that exhibit a double bond character due to π-donation from the nitrogen atom to the carbene carbon. Both the *Z* and *E* isomer exists of two conformers in fast equilibrium with each other, namely *Z*-syn with *Z*-anti and *E*-syn with *E*-anti.[96]

The higher the HOMO energy, the easier an electron can be removed (less energy needed to remove the electron) and thus it can be oxidized at a lower potential. The *E* conformation thus has a lower oxidation potential (E$_{pa}$) than the *Z* conformation. The cyclic voltammogram of the oxidation process is illustrated in **Figure 3.53**. However, for **C2**, the DFT calculated HOMO energy of the one *Z* isomer is higher than the HOMO energy of one of the *E* isomers. This result is consistent with the oxidation potential of the *Z* and *E* isomers of **C2** to be closely overlapping. This is in agreement with experimental observation of the [Cr(CO)$_5$=C(NHCy)(Fu)], **C2**, cyclic voltammogram, which did not show evidence of splitting of the oxidation peak, see **Figure 3.50**.

This is the first time that two distinct peaks, *E* isomers and *Z* isomers, for a carbene complex are observed in cyclic voltammetry. Similar W-carbene complexes [W(CO)$_5$=C(NHCy)(Fu)] and [W(CO)$_5$=C(NHCy)(Th)] did not show the splitting of the first oxidation peak.[97] Two very poorly resolved components of the CV oxidation peak of related aminocarbene [Cr(CO)$_5$=C(NHBu)Th] was previously reported ($E^{0'}$ = 0.258 and E$_{pa}$ = 0.435 V vs. FcH/FcH$^+$ in CH$_2$Cl$_2$ containing 0.1 M^{-3} [N(^{n}Bu)$_4$][PF$_6$] as supporting electrolyte). In that case the first peak is ascribed to the presence of two zwitterionic stabilized forms of the Cr(0)$^-$aminocarbene species of sufficient stability and

---

[96] M. Landman, R. Fraser, L. Twigge, J. Conradie, *Journal of Coordination Chemistry* **2015** (6814) 2388–2408, "Fischer aminocarbene conformers containing a 2-thienyl or 2-furyl ring: A crystallographic, NMR and DFT study" DOI: 10.1080/00958972.2015.1046852.

[97] M. Landman, R. Pretorius, R. Fraser, B.E. Buitendach, M.M. Conradie, P.H. van Rooyen, J. Conradie, *Electrochimica Acta* **2014** (130) 104-11, "Electrochemical behaviour and structure of novel phosphine- and phosphite substituted tungsten(0) Fischer carbene complexes" DOI: 10.1016/j.electacta.2014.02.127.

long enough existence time to allow detection on CV timescale and the second peak to the oxidation of the Cr(0)-aminocarbene [CrCO)$_5$=C(NHBu)Th] itself.[98]
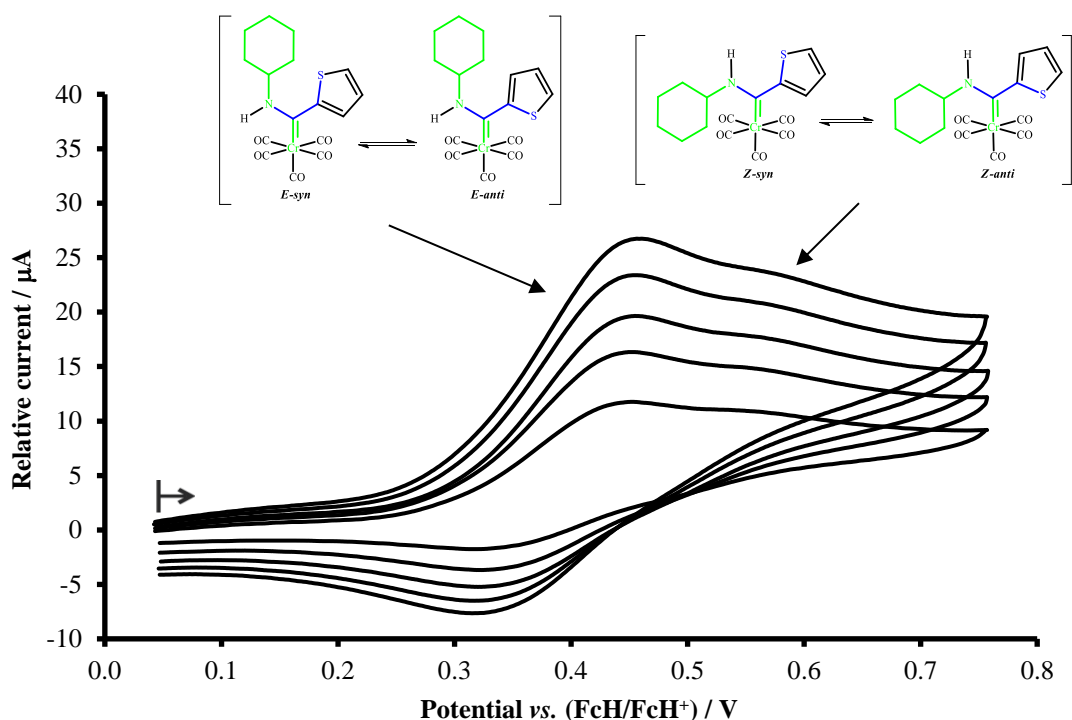
Figure 3.53: Cyclic voltammogram showing the *Z* and *E* isomers of [Cr(CO)$_5$=C(NHCy)(Th)], **C3**, at scan rates of 0.05, 0.10, 0.15, 0.20 and 0.25 V.s^{-1}. Measurements were performed in 0.1 mM [^{n}(Bu$_4$)N][PF$_6$]/CH$_3$CN on a glassy carbon working electrode and are reported with ferrocene as an internal standard; the CV initiated in the direction of the arrow.

3.2.3 Computational study

3.2.3.1 Conformational study

As illustrated in **Scheme 3.13** the [Cr(CO)$_4$(PPh$_3$)=C(OEt)(Fu)], **C1**, has six conformations namely *cis(1)-syn*, *cis(1)-anti*, *cis(2)-syn*, *cis(2)-anti*, *trans-syn* and *trans-anti*. [Cr(CO)$_5$=C(NHCy)(Fu)], **C2**, and [Cr(CO)$_5$=C(NHCy)(Th)], **C3**, both have the following four conformations: *Z-syn*, *Z-anti*, *E-syn* and *E-anti*. There are also four conformations, *syn-syn*, *syn-anti*, *anti-anti*, and *anti-syn*, possible for the [Cr(CO)$_5$=C(OEt)(ThTh)], **C4**, complex due to the different combinations of orientation of the two thiophene rings in the carbene substituent. Using

---

98 B. van der Westhuizen, P.J. Swarts, I. Strydom, D.C. Liles, I. Fernández, J.C. Swarts, D.I. Bezuidenhout, *Dalton Trans.* **2013** (42) 5367–5378, "Electrochemical illumination of thienyl and ferrocenyl chromium(0) Fischer carbene complexes" DOI: 10.1039/C3DT32913E.

computational chemistry the electronic energy of the optimized geometry was determined. Since the *cis* and *trans* isomers are in equilibrium with each other, the statistical distribution (population) of the *cis* and *trans* Cr-Fischer carbene complexes' isomers/conformations were calculated with the Maxwell-Boltzmann equation (**Equation 3.5**), see **Table 3.44**.

However, DFT and experimental results showed that the *Z* isomers exist of a fast equilibrium of *Z-syn* and *Z-anti*, while the *E* isomers exist of a fast equilibrium of *E-syn* and *E-anti*. [96] No dynamic equilibrium was found between the isomers *Z* and *E* during a temperature and concentration NMR study and different batches of complexes **C2** and **C3** exhibit different ratios of isomers *E* and *Z*.[96] Thus the *E* : *Z* ratio of each sample must be determined experimentally. The Boltzmann equation can only be used to determine the *Z-syn* : *Z-anti* and the *E-syn* and *E-anti* ratios. The experimental *Z* : *E* ratios of the **C2** and **C3** aminocarbene complexes of this study are *Z* : *E* (Experimental) = 55.7 : 44.3 and *Z* : *E* (Experimental) = 64.4 : 35.6 respectively.[96]

$$\ln \frac{n_j}{n_i} = -\frac{(E_j - E_i)}{kT}$$ **Equation 3.5**

Table 3.44: Summary of the energies of the optimized geometries (Gaussian, B3LYP, def2tzvpp) and calculated Boltzmann population percentage (%) of the different Fischer carbene complexes' isomers.

Complex	Conformation	$E_{complex}$ (eV)	E_j-E_i (eV)	%Pop	E_{HOMO}	E_{LUMO}	X-ray structure ref
[Cr(CO)$_4$(PPh$_3$)=C(OEt)(Fu)] **C1**	*cis(1)-anti*	-54373.11	0.00	48.9	-5.354	-2.203	
	cis(2)-anti	-54373.10	0.01	35.2	-5.288	-2.133	
	cis(1)-syn	-54373.03	0.08	2.0	-5.378	-2.165	
	cis(2)-syn	-54373.02	0.09	1.5	-5.335	-2.124	
	trans-anti	-54373.08	0.04	12.1	-5.220	-1.909	
	trans-syn	-54372.98	0.14	0.2	-5.273	-1.908	
[Cr(CO)$_5$=C(NHCy)(Fu)] **C2-Z**	*Z-syn*	-32960.97	0.00	99.2	-5.784	-2.141	**96**
	Z-anti	-32960.85	0.12	0.8	-5.709	-2.087	
Cr(CO)$_5$=C(NHCy)(Fu)] **C2-E**	*E-syn*	-32960.86	0.00	92.9	-5.759	-2.211	
	E-anti	-32960.80	0.07	7.1	-5.658	-2.120	
[Cr(CO)$_5$=C(NHCy)(Th)] **C3-Z**	*Z-syn*	-41749.62	0.00	82.5	-5.820	-2.181	**96**
	Z-anti	-41749.58	0.04	17.5	-5.796	-2.032	
Cr(CO)$_5$=C(NHCy)(Th)] **C3-E**	*E-syn*	-41749.56	0.00	65.3	-5.780	-1.934	
	E-anti	-41749.54	0.02	34.7	-5.767	-1.928	
[Cr(CO)$_5$=C(OEt)(ThTh)] **C4**	*syn-anti*	-53059.76	0.00	76.5	-5.967	-2.917	
	syn-syn	-53059.73	0.03	23.5	-5.943	-2.931	
	anti-syn	-53059.63	0.00	75.9	-5.948	-2.874	
	anti-anti	-53059.60	0.03	24.1	-5.954	-2.833	

From the electronic energies of the different conformations presented in **Table 3.44** it is clear that certain conformations are preferred over others. For complex **C1**, [Cr(CO)$_4$(PPh$_3$)=C(OEt)(Fu)], we observe that the ratio to *cis:trans* isomers is 88:12. This is in agreement with the fact that both *cis* and *trans* isomers were observed on CV.

The small energy differences found between the *E* and *Z* isomers for complexes **C3**, [Cr(CO)$_5$=C(NHCy)(Th)], and **C2**, [Cr(CO)$_5$=C(NHCy)(Fu)] suggests that both *E* and *Z* isomers should be observed experimentally, as was the case in NMR study.[96] For both aminocarbene complexes **C2** and **C3** the lowest energy isomer is the *Z-syn* isomer. The X-ray structure solved for both **C2** and **C3** revealed the *Z-syn* isomer, which is in agreement with the DFT calculated results in **Table 3.44**.[96] The *Z-syn* isomer was also determined to be the major isomer by experimental NMR studies.[96]

3.2.3.2 Molecular orbitals

The highest occupied molecular orbital (HOMO) and lowest unoccupied molecular orbital (LUMO) character gives information on where the oxidation and reduction will take place in the Cr-Fischer carbene complexes since the electron is removed upon oxidation from the HOMO and added to the LUMO during reduction of the complex. These orbitals are illustrated in **Table 3.45** for the complexes of this study. Here we can see that the HOMO of all the complexes are mostly over the metal centre confirming that the oxidation is metal based. The LUMO is located mostly on the carbene ligand confirming that the reduction occurs at the carbene carbon and that the added electron density is distributed over the carbene ligand. The LUMO of complex **C4** with the extended dimeric heteroarene five-membered ring systems is distributed over the carbene C and both the heteroarene rings. Therefore, the density of the electron that is added upon reduction of **C4** will be added to this LUMO, which will be distributed over the carbene C as well as both aromatic heteroarene five-membered rings. This leads to enhanced stabilization of the reduced radical anion to such an extent that the electrochemical reduction of [Cr(CO)$_5$=C(OEt)(ThTh)], **C4**, is electrochemically reversible and chemically quasi reversible. The electrochemically reversible and chemically quasi reversible reduction of C4 is contrary to what was observed for complex **C1–C3** that showed electrochemical irreversible behaviour, see **Section 3.2.2**.

Table 3.45: The visualization of the HOMO and LUMO orbitals of the neutral **C1**-**C4** Fischer carbenes by the use of computational chemistry.

Complex	HOMO	LUMO
[Cr(CO)$_4$(PPh$_3$)=C(OEt)(Fu)] **C1**		
[Cr(CO$_5$)=C(NHCy)(Fu)] **C2**		
[Cr(CO)$_5$=C(NHCy)(Th)] **C3**		
[Cr(CO)$_5$=C(OEt)(ThTh)] **C4**		

3.2.3.3 Relationships between electrochemical and computational results of structurally modified Cr-Fischer carbene complexes

When a complex is oxidized an electron is taken from the complex. This electron is normally taken from the highest occupied molecular (HOMO) orbital. The reduction of a complex consist of process where an electron is added to the complex. The electron is normally added to the lowest unoccupied molecular orbital (LUMO) of the complex. Therefore the energy of the HOMO (E$_{HOMO}$) and the LUMO (E$_{LUMO}$) can be compared to the oxidation potential (E$_{pa}$) and the reduction potential (E$_{pc}$) respectively. A summary of the electrochemical and computational data of this study is tabulated in **Table 3.46** and illustrated in **Figure 3.54**. Electrochemical data obtained

under the same experimental conditions (from references [99] and [100]) and computational data for the additional complexes (calculated with B3LYP / 6-311G(d,p), def-2TZVPP for this study) are also added to **Table 3.46** and **Figure 3.54**. The B3LYP / 6-311G(d,p), def-2TZVPP computational approach gave good trends and relationships between calculated and experimental data for related Mo and W carbenes (add some refs).

Table 3.46: Summary of electrochemical and computational data. (Gaussian, B3LYP, 6-311G(d,p), def2tzvpp), the E_{HOMO} and E_{LUMO} is calculated with the % population.

Complex	Isomer	R	First oxidation		Reduction		E_{HOMO} (eV)	E_{LUMO} (eV)	Ref
			E_{pa} (V)	E_{pc} (V)	E_{pc} (V)	E_{pa} (V)			
[Cr(CO)₄(PPh₃)=C(OEt)(Fu)] **C1**	*trans*	furyl	-0.029	-0.086	-1.900	-	-5.221	-1.909	This study
	cis		0.161	-	-	-	-5.328	-2.173	
[Cr(CO)₅=C(NHCy)(Fu)] **C2**	Z	furyl	0.432	0.287	-2.278	-	-5.784	-2.141	
[Cr(CO)₅=C(NHCy)(Th)] **C3**	E	thiophene	0.456	0.323	-2.145	-	-5.775	-1.932	
	Z		0.569	-	-	-	-5.816	-2.155	
[Cr(CO)₅=C(OEt)(ThTh)] **C4**	-	thiophene+ thiophene	0.531	0.429	-1.489	-1.423	-5.961	-2.920	
[Cr(CO)₃(dppe)=C(OEt)(R)]	*mer*	thiophene	-0.275	-0.353	-	-	-4.811	-1.812	100
	fac	thiophene	-	-	-2.162	-	-4.916	-1.792	
	mer	furyl	-0.356	-0.41	-2.269		-4.743	-1.632	
	fac	furyl	-0.235	-	-2.124	-	-4.90	-1.958	
[Cr(CO)₃(dppe)=C(NHCy)(R)]	*mer*	thiophene	-0.5	-0.569	-2.8	-	-4.658	-1.181	
	fac	thiophene	-0.306	-	-2.545	-	-4.73	-1.248	
	mer	furyl	-0.545	-0.6	-2.615	-	-4.523	-1.328	
	fac	furyl	-0.368	-	-	-	-4.671	-1.596	
[Cr(CO)₅=C(OEt)(R)]	-	thiophene	0.538	0.453	-1.625	-1.552	-6.074	-2.754	99
	-	furyl	0.494	0.414	-1.719	-1.649	-5.962	-2.583	
	-	NMe-pyrrole	0.463	0.396	-2.019	-1.938	-5.833	-2.204	
	-	thiophene + NMe-pyrrole	0.558	0.42	-1.594	-1.514	-5.726	-2.686	
	-	thiophene + furyl	0.531	0.444	-1.501	-1.435	-5.907	-2.854	

[99] M. Landman, R. Liu, P.H. van Rooyen, J. Conradie, *Electrochimica Acta* **2013** (114) 205-214, "Electrochemistry of Fischer alkoxycarbene complexes of chromium: The use of density functional theory to predict and understand oxidation and reduction potentials" DOI: 10.1016/j.electacta.2013.10.013.

[100] M. Landman, R. Liu, R. Fraser, P.H. van Rooyen, J. Conradie, *Journal of Organometallic Chemistry* **2014** (752) 171-182 "Fac and mer dppe-substituted Fischer carbene complexes of chromium: X-ray, DFT and electrochemical study" DOI: 10.1016/j.jorganchem.2013.12.003.

a)

b)

$y = -0.7518x - 3.910$
$R^2 = 0.97$

$y = -0.6869x - 3.500$
$R^2 = 0.94$

◆ **[Cr(CO)₃(dppe)=C(NHCy)(R)]** ◆ **[Cr(CO)₃(dppe)=C(OEt)(R)]** ◆ **[Cr(CO)₃(dppe)=C(OEt)(R)]**

◆ **[This study's Fischer carbene complexes]**
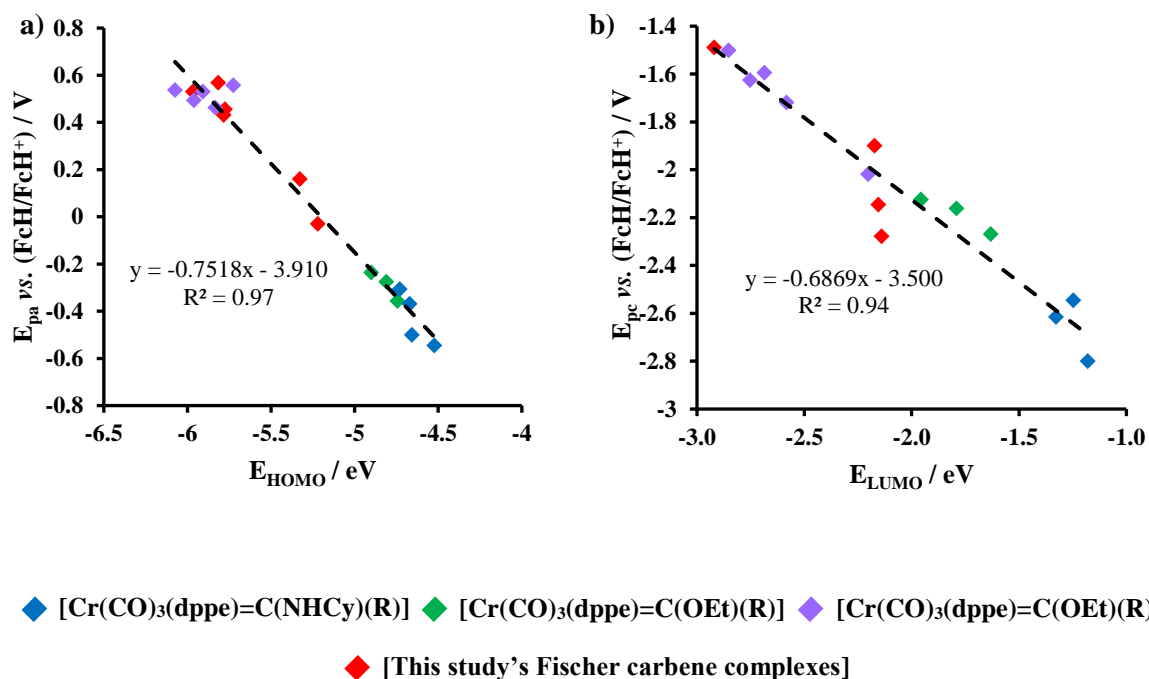
Figure 3.54: The comparison of a) oxidation potential (E_{pa}) and the HOMO energy (E_{HOMO}) b) reduction potential (E_{pc}) and LUMO energy (E_{LUMO}).

The correlation of the oxidation potential (E_{pa}) and reduction potential (E_{pc}) with the HOMO energy (E_{HOMO}) and LUMO energy (E_{LUMO}) respectively, showed that with decreasing molecular orbital energy an increase to more positive potentials are obtained. It is easier to remove an electron from complexes with higher, more positive, HOMO energy (E_{HOMO}), which gives rise to lower oxidation potentials (E_{pa}). When the LUMO energy (E_{LUMO}) of a complex is more positive, the more difficult it is for the complex to accept an electron, therefore a more negative reduction potential (E_{pc}) is observed.

3.2.4 X-ray photoelectron spectroscopy (XPS) data

Four Cr-Fisher carbenes were selected for further characterization by XPS. The penta-carbonyl complexes [Cr(CO)₅=C(OEt)(Fu)], **C5**, and [Cr(CO)₅=C(OEt)(Th)], **C6**, as well as the amino (NHCy) substituted complexes of **C5** and **C6**, namely [Cr(CO)₅=C(NHCy)(Fu)], **C2,** and [Cr(CO)₅=C(NHCy)(Th)], **C3**, were selected. Since the ethoxy (OEt) moiety in complex **C5** and **C6** can be substituted by an amino group, such as in complexes **C2** and **C3**, it is possible to anchor complex **C5** and **C6** onto Si-wafers, by covalently binding the complexes onto an amino-functionalized Si-wafer as described in **Section 3.1.5.2**. All XPS data were charge corrected with the main peak of the adventitious carbon set at 284.8 eV.

3.2.4.1 XPS study of Fischer carbene complexes

The wide scan XPS obtained for [Cr(CO)$_5$=C(NHCy)(Th)], **C3**, is shown in **Figure 3.55** with the wide scan data of **C2**, **C3**, **C5** and **C6** summarized in **Table 3.47**. The detailed XPS data obtained of the [Cr(CO)$_5$=C(OEt)(Fu)], **C5**, [Cr(CO)$_5$=C(OEt)(Th)], **C6**, [Cr(CO)$_5$=C(NHCy)(Fu)], **C2**, and [Cr(CO)$_5$=C(NHCy)(Th)], **C3**, Cr-Fischer carbene complexes are summarized in **Table 3.48**.
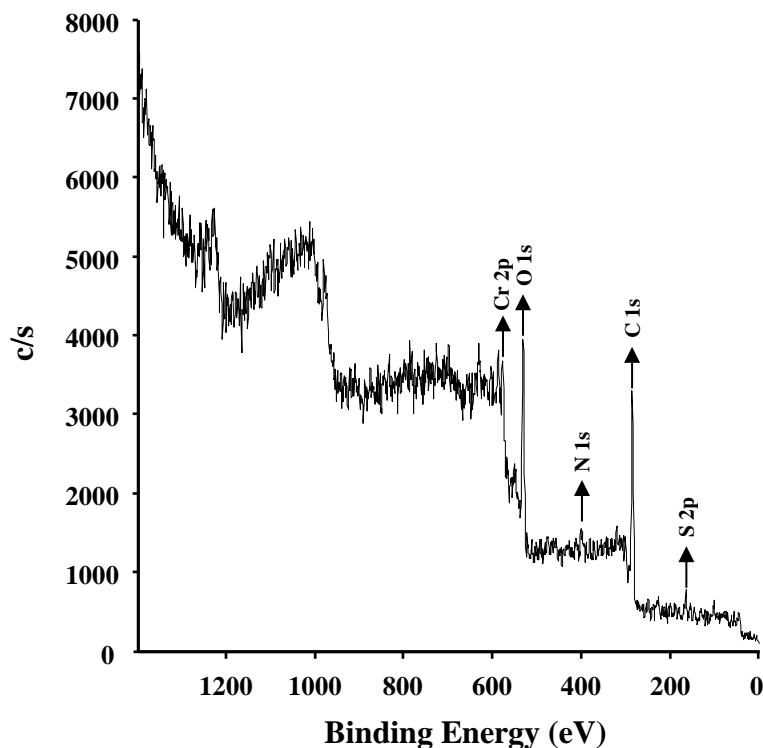
Figure 3.55: Wide XPS scan of [Cr(CO)$_5$=C(NHCy)(Th)], **C3**.

The atomic ratios that were obtained from the wide XPS scan of the [Cr(CO)$_5$=C(NHCy)(Th)], **C3**, carbene complex in **Figure 3.55** are summarized in **Table 3.47**. The expected ratio of 1 : 1 : 1 for the Cr : N: S atoms is observed for this complex since there is one N and one S for every Cr atom in the Cr-Fischer carbene complex **C3**. Similarly data of **C6** shows the ratio of 1:1 for the Cr : S atoms and **C2** shows the ratio of 1:1 for the Cr : N atoms. Since there are always adventitious oxygen and carbon present on all samples, and **C5** only contains Cr, C and O, no useful atomic ratio comparison between the different atoms could be made.

160

Table 3.47: The atomic percentage (%) obtained from the wide XPS scan of the [Cr(CO)$_5$=C(NHCy)(Fu)], **C2**; [Cr(CO)$_5$=C(NHCy)(Th)], **C3**, [Cr(CO)$_5$=C(OEt)(Fu)], **C5**,and [Cr(CO)$_5$=C(OEt)(Th)], **C6**, carbene complexes.

Complex	Atom	%
Cr(CO)$_5$=C(NHCy)(Fu)] **C2**	C 1s	67.1
	O 1s	24.7
	Cr 2p	4.1
	N 1s	4.1
[Cr(CO)$_5$=C(NHCy)(Th)] **C3**	C 1s	61.2
	O 1s	29.7
	Cr 2p	3.0
	S 2p	3.1
	N 1s	3.0
[Cr(CO)$_5$=C(OEt)(Fu)] **C5**	C 1s	87.4
	O 1s	10.7
	Cr 2p	1.9
[Cr(CO)$_5$=C(OEt)(Th)] **C6**	C 1s	86.9
	O 1s	8.9
	Cr 2p	2.1
	S 2p	2.1

Table 3.48: The binding energies in eV of the N 1s, S 2p$_{3/2}$, S 2p$_{1/2}$, Cr 2p$_{3/2}$ and Cr 2p$_{1/2}$ peak obtained from XPS measurements. The spin orbit splitting between the Cr 2p$_{3/2}$ and Cr 2p$_{1/2}$ peaks, as well as the full width at half maximum (FWHM).

Complex	N 1s	S 2p$_{3/2}$	S 2p$_{1/2}$	Cr 2p$_{3/2}$	Cr 2p$_{1/2}$	Cr 2p$_{1/2}$ - Cr 2p$_{3/2}$	FWHM Cr peaks
[Cr(CO)$_5$=C(NHCy)(Fu)] **C2**	400.07	-	-	576.64	586.38	9.74	5.18
[Cr(CO)$_5$=C(NHCy)(Th)] **C3**	399.17	163.52	166.20	576.52	586.23	9.71	5.36
[Cr(CO)$_5$=C(OEt)(Fu)] **C5**	-	-	-	574.68	583.25	8.57	3.45
[Cr(CO)$_5$=C(OEt)(Th)] **C6**	-	163.30	164.84	574.41	583.14	8.73	3.17

(i)   *Cr 2p peaks*

The detailed XPS scan of the Cr 2p peaks of [Cr(CO)$_5$=C(NHCy)(Th)], **C3**, and [Cr(CO)$_5$=C(OEt)(Th)], **C6,** complexes are shown in **Figure 3.56** and that of **C2** and **C5** in **Appendix B**. Full width at half maximum (FWHM) of ~3.31 eV is measured for the Cr 2p$_{3/2}$ and Cr 2p$_{1/2}$ peaks of **C6**. However, the Cr 2p peaks of [Cr(CO)$_5$=C(NHCy)(Th)], **C3**, gave a full width at half maximum of ~5.27 eV. The spin orbit splitting between Cr 2p$_{3/2}$ and Cr 2p$_{1/2}$ of *ca.* 8.65 eV (for **C5** and **C6**) and *ca.* 9.73 eV (for **C2** and **C3**). The broadness (large FWHM) of the Cr 2p$_{3/2}$ and Cr 2p$_{1/2}$ peaks of **C2** and **C3** is an indication that there is more than one species present in the sample, in this case it would represent the *E* and *Z* isomers (see **Scheme 3.13**). The asymmetric

tail towards the lower binding energy side for both the Cr $2p_{3/2}$ and Cr $2p_{1/2}$ peaks of **C3** and **C2** in **Figure 3.56** and in **Appendix B** are also consistent with more than one species present.

Comparison of the Cr $2p_{3/2}$ binding energies of [Cr(CO)$_5$=C(OEt)(Fu)], **C5**, and [Cr(CO)$_5$=C(OEt)(Th)], **C6**, revealed that **C5** had a binding energy of 0.27 eV higher than that of **C6**. Since the Pauling electronegativity of oxygen (χ_O = 3.44) is higher than that of sulphur (χ_S = 2.58),[101] it is expected that the Cr-Fischer carbene complex containing oxygen will have Cr 2p binding energies higher than that of the Cr-Fischer carbene complex containing sulphur. This trend was observed in the XPS results where the Cr $2p_{3/2}$ peak binding energy of the oxygen containing carbene is at 574.68 eV and the sulphur containing carbene is at 574.41 eV, see **Table 3.48**. The same trend is observed with the amino-containing complexes [Cr(CO)$_5$=C(NHCy)(Fu)], **C2**, and [Cr(CO)$_5$=C(NHCy)(Th)], **C3**. **C2** (oxygen-containing) complex has a higher binding energy (Cr $2p_{3/2}$ = 576.95 eV) than **C3** (sulphur-containing) complex (Cr $2p_{3/2}$ = 576.41 eV), see **Table 3.48**.

The influence of the amino-containing substituent (NHCy) on the complexes resulted in higher binding energies (~2.0 eV) of the Cr-peaks. Also, the spin orbit splitting of the complexes containing the amino substituent (NHCy, **C2**-**C3**) is ~1.1 eV larger than that of the ethoxy (OEt, **C5**-**C6**) variant. This could possibly be attributed to the higher electronegativity of the aminocyclohexane group over the ethoxy group (2.53 Pauling electronegativity). Thus more electron density is moved away from the Cr metal centre towards the nitrogen group. This causes the Cr centre to be closer to its own electron, hence the increased binding energy. The Cr $2p_{3/2}$ and Cr $2p_{1/2}$ peak fitting of the [Cr(CO)$_5$=C(NHCy)(Th)], **C3**, complex is shown in **Figure 3.56**.

---

[101] F.A. Cotton, G. Wilkinson, P.L. Gaus, *Basic Inorganic Chemistry*, 3rd edition, John Wiley & Sons Ltd, New York, **1995**, p 65
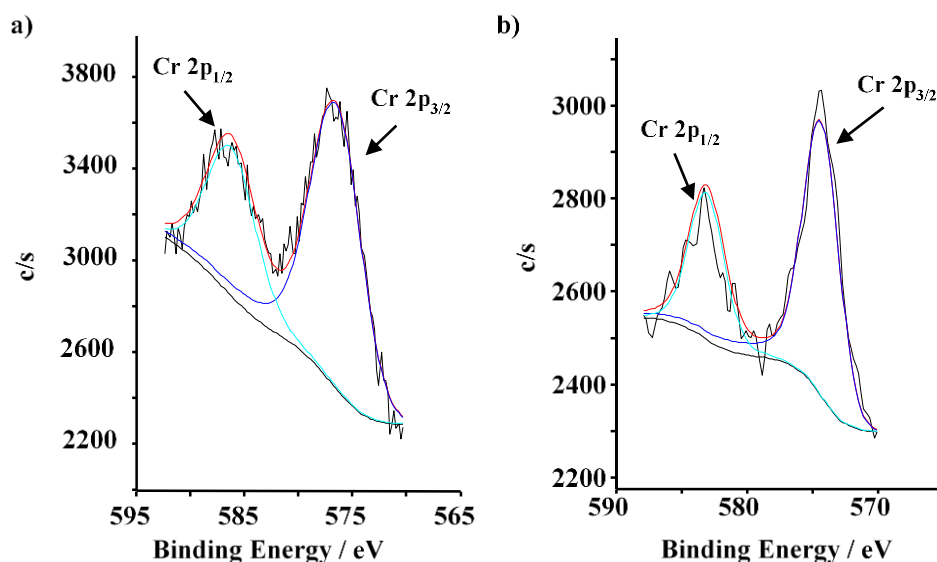
Figure 3.56: The fitting (deconvolution) of the **a)** [Cr(CO)$_5$=C(NHCy)(Th)], **C3**, and **b)** [Cr(CO)$_5$=C(OEt)(Th)], **C6**, Cr 2p XPS peaks.

(ii)   *S 2p peaks*

The two thiophene (Th) containing complexes [Cr(CO)$_5$=C(NHCy)(Th)], **C3**, and [Cr(CO)$_5$=C(OEt)(Th)], **C6**, showed S 2p peaks between 163.3-166.20 eV, see **Figure 3.57** with the data given in **Table 3.48**. The spin orbit splitting between the S 2p$_{3/2}$ and the S 2p$_{1/2}$ peaks for the **C3** and **C6** complexes was found to be 2.68 eV and 1.18 eV respectively. The spin orbit splitting difference between **C3** and **C6** complexes is 1.5 eV, which is comparable to that of the Cr 2p spin orbit difference (*ca.* 1.1 eV).

The S 2p$_{3/2}$ peak binding energy of [Cr(CO)$_5$=C(NHCy)(Th)], **C3**, is 0.22 eV higher than the S 2p$_{3/2}$ peak binding energy of the of the [Cr(CO)$_5$=C(OEt)(Th)], **C6**, Cr-Fischer carbene complex. The higher binding energy observed for the amino-containing complex over the ethoxy-containing complex is again attributed to the aminocyclohexane being more electronegative than the ethoxy group.

a)

b)
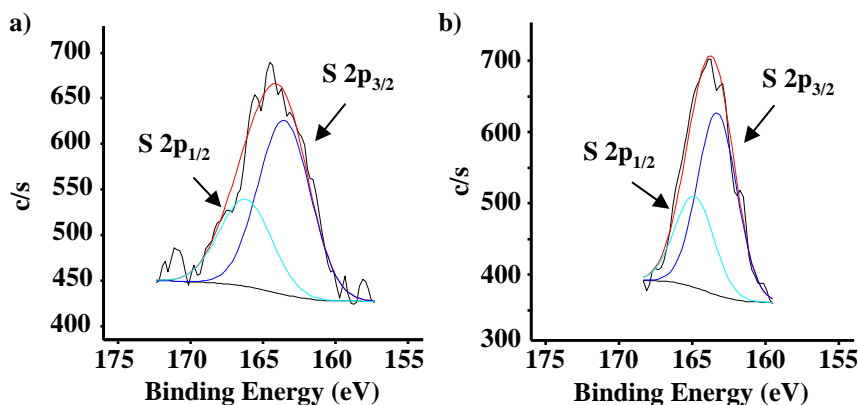
Figure 3.57: The fitting (deconvolution) of the a) [Cr(CO)$_5$=C(NHCy)(Th)], **C3**, and b) [Cr(CO)$_5$=C(OEt)(Th)], **C6**, S 2p XPS peak.

(iii)   *N 1s peaks*

The N 1s peak fitting of the [Cr(CO)$_5$=C(NHCy)(Fu)], **C2**, and [Cr(CO)$_5$=C(NHCy)(Th)], **C3**, is shown in **Figure 3.58**. The two amino-containing (NHCy) complexes [Cr(CO)$_5$=C(NHCy)(Fu)], **C2**, and [Cr(CO)$_5$=C(NHCy)(Th)], **C3**, show an N 1s peak at 399.8 eV and 399.34 V respectively, **Table 3.48**. The N 1s peak of the furyl (Fu) containing **C2** Cr-Fischer carbene complex is at higher binding energy due to the higher Pauling electronegativity of the oxygen atom (χ_O = 3.44) compared to the sulphur (χ_S = 2.58) of the thiophene (Th) containing **C3** Cr-Fischer carbene complex.

a)

b)
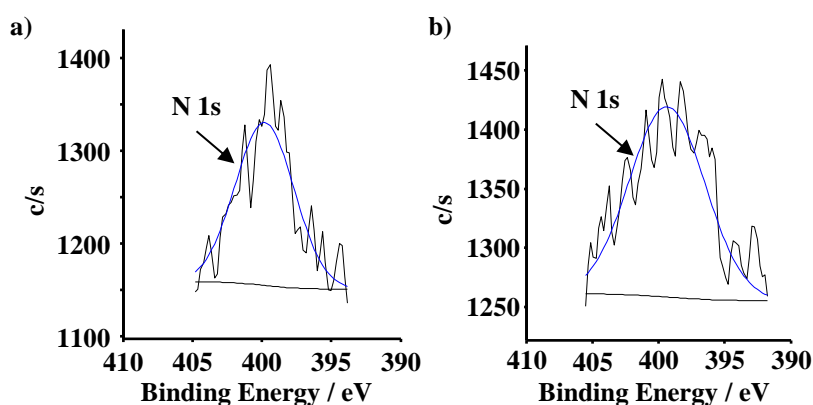
Figure 3.58: The fitting (deconvolution) of the **a)** Cr(CO)$_5$=C(NHCy)(Fu)], **C2**, and **b)** [Cr(CO)$_5$=C(NHCy)(Th)], **C3**, N 1s XPS peaks.

3.2.4.2 Relationships between computational data and XPS results of penta-carbonyl Cr-Fischer carbene complexes

During XPS measurements the sample is irradiated with x-rays, which causes core electrons to be emitted from the sample. Since Cr-electrons furthest away from the Cr-atom centre of the Cr-Fischer carbene complexes in question, are more easily emitted (uses less energy to be emitted), one can expect a relationship between the energy of the HOMO of the Cr-Fischer carbene complexes that is largely Cr based, and the binding energy obtained during a XPS measurement. The HOMO energy and the chromium binding energy is summarized in **Table 3.49**.

Table 3.49: Summary of HOMO energy and chromium binding energies in eV obtained from XPS results.

Complex	HOMO		Free complex		Bound complex	
	E_{HOMO} (eV)	Average[a] (eV)	Cr $2p_{3/2}$	Cr $2p_{1/2}$	Cr $2p_{3/2}$	Cr $2p_{1/2}$
[Cr(CO)$_5$=C(NHCy)(Fu)] **C2**	-5.658 -5.709 -5.759 -5.784	-5.783	576.95	586.30	-	-
[Cr(CO)$_5$=C(NHCy)(Th)] **C3**	-5.767 -5.796 -5.780 -5.820	-5.811	576.41	586.17	-	-
[Cr(CO)$_5$=C(OEt)(Fu)] **C5**	-5.962 -6.050	-5.963	574.64	583.33	577.14	586.89
[Cr(CO)$_5$=C(OEt)(Th)] **C6**	-6.074 -6.034	-6.074	574.38	583.34	576.57	586.36

[a] The average E_{HOMO} was calculated by the use of the % Boltzmann population, see **Table 3.44**.

The relationship between the average HOMO energy and the Cr $2p_{3/2}$ is illustrated in **Figure 3.59**.
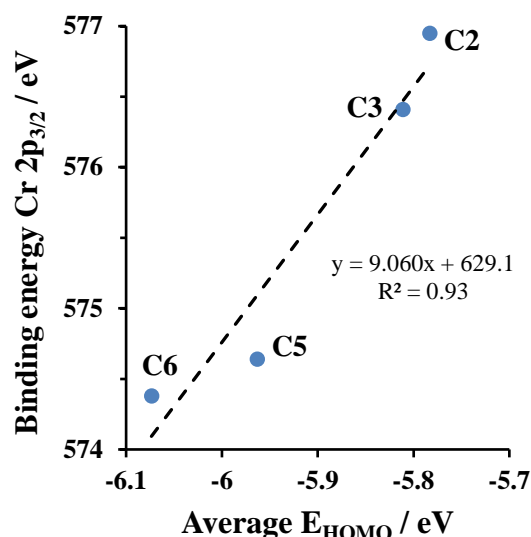
Figure 3.59: Relationship between the average HOMO energy (E_{HOMO}) calculated by the use of % Boltzmann equation and the Cr $2p_{3/2}$ binding energies measured by XPS.

As the average HOMO energy (E_{HOMO}) go to less negative eV the Cr $2p_{3/2}$ binding energy increase, see **Figure 3.59**. This is expected as the less negative the average E_{HOMO} the closer the HOMO is to the atom centre and more energy will be needed to emit an electron. This also correlates to the increase of the Cr $2p_{3/2}$ binding energy. A linear relationship was found between the HOMO energy and the binding energies (in eV) of the chromium metal centre, according to the following equation:

$$\text{Average } E_{HOMO} = 8.472(\text{Binding energy}) + 625.6 \qquad\qquad R^2 = 0.94$$

3.2.4.3 Study of Cr-Fischer carbene complexes grafted on amino-functionalized Si-wafers

Since the ethoxy-containing Cr-Fisher carbene complexes can easily be converted to their amino-containing counterparts, the ethoxy complexes **C5** and **C6** should also be able to bind to amino-functionalized Si-wafers. The $[Cr(CO)_5=C(OEt)(Fu)]$, **C5**, and $[Cr(CO)_5=C(OEt)(Th)]$, **C6**, complexes were grafted onto the amino-functionalized Si-wafers by placing an amino-functionalized wafer in a 1.2×10^{-8} mol.dm^{-3} solution of the Cr-Fischer carbene complex in tetrahydrofuran (THF) with gentle stirring for ~ 24 hours, see **Scheme 3.14**. The grafted $[Cr(CO)_5=C(OEt)(Fu)]$, **C5**, and $[Cr(CO)_5=C(OEt)(Th)]$, **C6**, complexes onto the amino-functionalized Si-wafers formed **C7** and **C8** modified Si-wafers respectively.
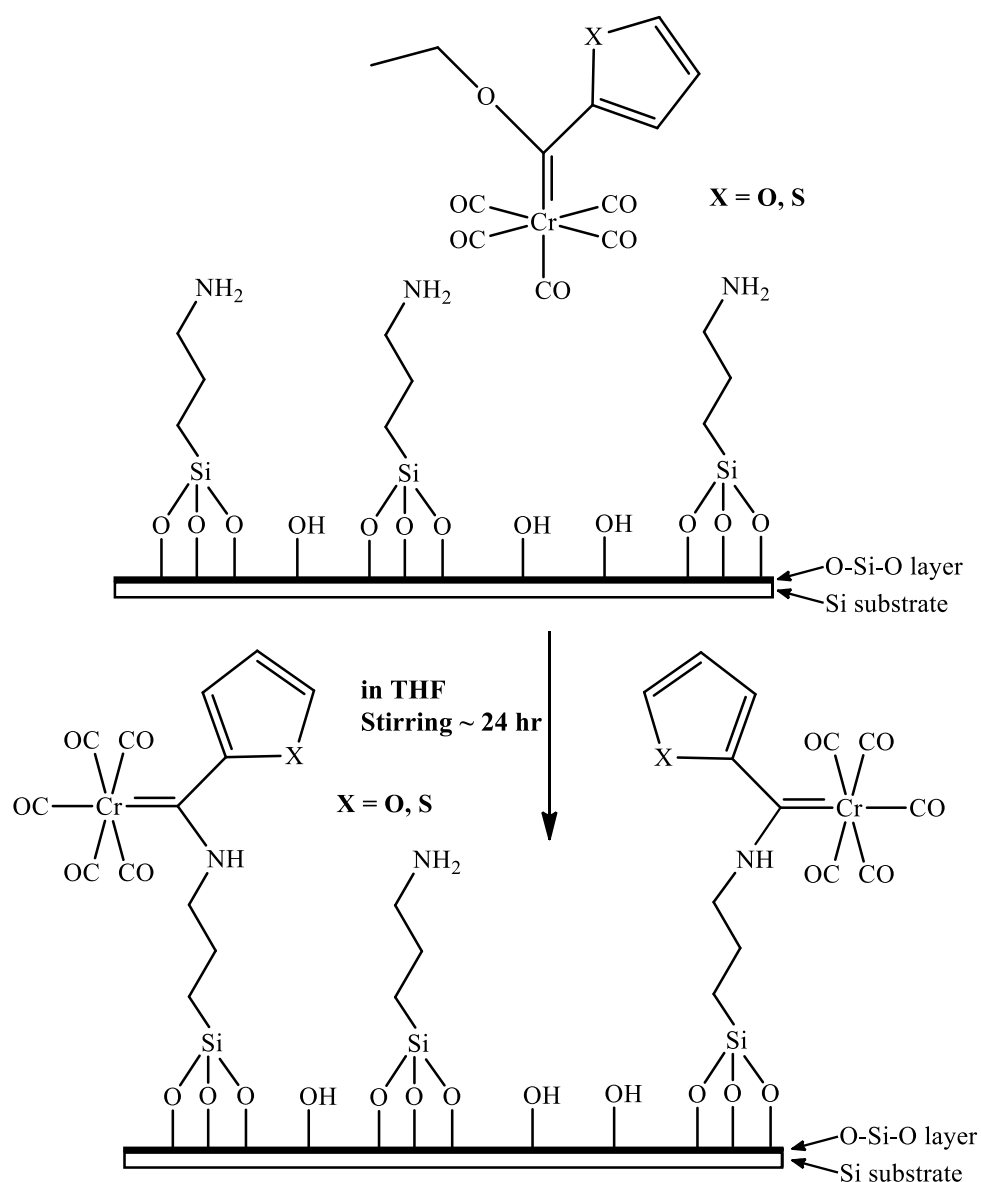
Scheme 3.14: The chemical grafting of [Cr(CO)$_5$=C(OEt)(Fu)], **C5**, and [Cr(CO)$_5$=C(OEt)(Th)], **C6**, Fischer carbene complexes onto an amino-functionalized Si-wafer to form Cr-grafted Si-wafers **C7** and **C8**.

The XPS data obtained from these two Cr-Fischer carbene complexes chemically grafted onto amino-functionalized Si-wafer and the free complexes from **Section 3.1.5.1** are summarized in **Table 3.50**.

Table 3.50: The binding energies in eV of N, S, and Cr obtained for the Fischer carbene complexes grafted onto amino-functionalized Si-wafers from XPS measurements.

Complex	N 1s	Cr 2p$_{3/2}$	Cr 2p$_{1/2}$	Cr 2p$_{1/2}$ − Cr 2p$_{3/2}$	S 2p$_{3/2}$	S 2p$_{1/2}$
[Cr(CO)$_5$=C(OEt)(Fu)] + amino-functionalized wafer **C7**	395.26 (26.62%) [a] 400.35 (73.38%) [b]	577.14	586.89	9.75	-	-
[Cr(CO)$_5$=C(OEt)(Th)] + amino-functionalized wafer **C8**	396.34 (29.06%) [a] 399.49 (70.94%) [b]	576.57	586.36	9.79	165.07	166.25
[Cr(CO)$_5$=C(OEt)(Fu)] **C5**	-	574.68	583.25	8.57	-	-
[Cr(CO)$_5$=C(OEt)(Th)] **C6**	-	574.41	583.14	8.73	163.30	164.84
[Cr(CO0$_5$)(NHCy)(Fu)] **C2**	399.80	576.64	586.38	9.74	-	-
[Cr(CO)$_5$=C(NHCy)(Th)] **C3**	399.34	576.52	586.12	9.71	163.52	166.20

[a] Amine bound Fischer carbene

[b] Unreacted amine group

(i)   *Cr2p peaks*

The Cr 2p$_{3/2}$ and Cr 2p$_{1/2}$ peaks of the bound [Cr(CO)$_5$=C(OEt)(Fu)], **C7**, carbene complex (577.14 eV and 586.89 respectively) is higher in binding energy than that of the bound [Cr(CO)$_5$=C(OEt)(Th)], **C8**, carbene complex (576.57 eV and 586.36 eV respectively), see **Table 3.50**, **Figure 3.60**.   This difference is seen due to the higher Pauling electronegativity of the oxygen substituent in the Fischer carbene complex.   This is the same pattern that was observed between the unbound furyl (Fu, **C5** and **C2**) and thiophene (Th, **C6** and **C3**) containing Cr-Fischer carbene complexes, see **Table 3.50**.
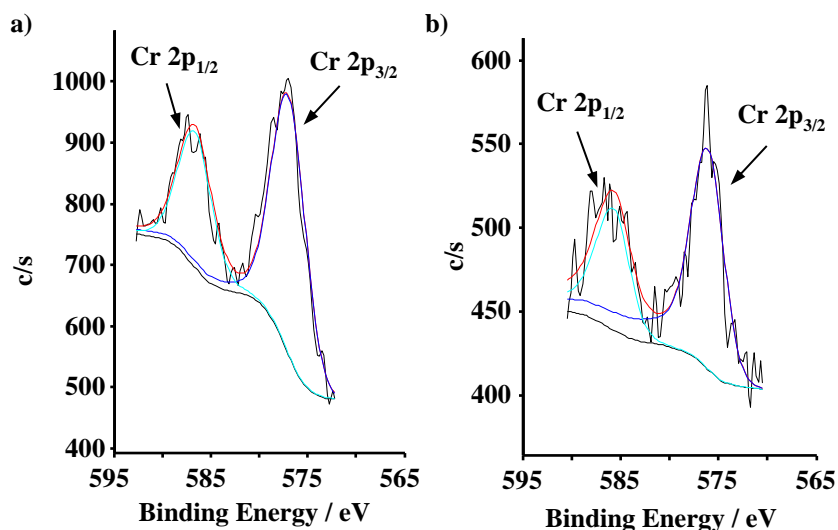
Figure 3.60: The fitting (deconvolution) of the **a)** bound [Cr(CO)$_5$=C(OEt)(Fu)] complex, **C7**, and **b)** bound [Cr(CO)$_5$=C(OEt)(Th)] complex, **C8**, Cr 2p XPS peaks.

Comparing the Cr 2p$_{3/2}$ binding energies of **C5** and **C6** (574.64 and 574.38 eV respectively) with the Cr 2p$_{3/2}$ binding energies of the grafted complexes **C7** and **C8** (577.14 and 576.57 eV respectively), clearly shows how complexation onto the amino-functionalized Si-wafer decreases the electron density on the chromium (thus an increased binding energy). This increase in binding energies was also observed when the ethoxy group was replaced by the aminocyclohexane (**Table 3.50**), giving further confirmation that the complexes did bind to the amino-functionalized Si-wafer. The Cr 2p$_{3/2}$ binding energy of the anchored Fischer carbene complexes **C7** (577.14 eV) and **C8** (576.57 eV) is *ca.* 0.18 eV higher than the free Fischer carbene complexes **C2** (576.95 eV) and **C3** (576.41 eV). This shows the small (*ca.* 0.18 eV) but still noteworthy influence of how the large surface of the Si-wafer decreases the electron density of the chromium metal centre.

The spin orbit splitting (*ca.* 9.77 eV) between the Cr 2p$_{3/2}$ and Cr 2p$_{1/2}$ peaks of the **C7** and **C8** wafers corresponds very well to the spin orbit splitting (9.74 eV) of the free amino-containing complexes **C2** and **C3**. It is known that an increase in spin orbit splitting is caused by a decrease in electron density on the atom,[102] in this case Cr. This difference further confirms that the [Cr(CO)$_5$=C(OEt)(Fu)], **C5**, and [Cr(CO)$_5$=C(OEt)(Th)], **C6**, complexes were indeed anchored onto the amino-functionalized Si-wafers.

---

[102] S.P. Kowalczyk, L. Ley, F.R. Mcfeely, D.A. Shirley, *Physical Review B* **1975** (11) 1721-1727, "Multiplet splitting of the manganese 2p and 3p levels in MnF$_2$ single crystals" DOI: 10.1103/PhysRevB.11.1721.

(ii) *S 2p peaks*

The sulphur (S 2p) peak of [Cr(CO)$_5$=C(OEt)(Th)] grafted on to the amino-functionalized Si-wafer, **C8**, was fitted the two 2p peaks (S 2p$_{3/2}$ and S 2p$_{1/2}$), see **Table 3.50**. The S 2p peaks of the immobilized carbene complex (**C8**) are at higher binding energies than that of the free [Cr(CO)$_5$=C(OEt)(Th)], **C6** . This trend was also observed for the Cr 2p peaks, see **Section 3.2.4.3 (i)**, where the lower electron density (due to the influence of the large surface area of the Si-wafer) results in the increase of the binding energies.

(iii) *N 1s peak*

The nitrogen (N 1s) peak has been fitted with two different peaks (see **Figure 3.61**), the peak at higher binding energy (400-402 eV) are assigned to the unreacted amine groups on the surface, this is in agreement with literature.[103]   The N 1s peaks at lower binding energy (398-400 eV) are assigned to the covalently bound amine groups to the Fischer carbene complexes. The ratio between the bound an unbound nitrogen of the chemically grafted [Cr(CO)$_5$=C(OEt)(Fu)], **C5**, carbene complex onto amino-functionalized Si-wafer is 1:2.75 respectively, therefore for every one amine group bound to a [Cr(CO)$_5$=C(OEt)(Fu)], **C5**, carbene complex there are ~3 amine groups not bound. Thus we obtained a ~33% anchoring of the Cr-complexes. In the case of the chemically grafted [Cr(CO)$_5$=C(OEt)(Th)], **C6**, carbene complex on to amino-functionalized Si-wafer the ratio 1: 2.44 was found of the bound against the unbound amine groups respectively. This implies that for every one amine group bound to a [Cr(CO)$_5$=C(OEt)(Th)], **C6**, carbene complex there are ~2 unbound amine groups. Thus we obtained a ~50 % anchoring of the Cr-complexes.

It is known that during the preparation method used 4 - 6 –OH functional groups per nm^2 are obtained,[104, 105] From the XPS results of the Si peaks a 1 : 1.85 : 0.35 (31 % : 58 % : 11 %), silane to –O-Si-OH to –O-Si-O- ratio was obtained, which implies that there are one -O–Si-CH$_2$- group for every two -Si-OH groups, thus there are *ca.* 2 – 3 silane molecules per nm^2. By implication also 2 – 3 nitrogen atoms per nm^2. As mentioned previously a 33% and a 50%

[103] A. Adenier, M.M. Chehimi, I. Gallardo, J. Pinson, N. Vila, *Langmuir* **2004** (20) 8243-8253, "Electrochemical Oxidation of Aliphatic Amines and Their Attachment to Carbon and Metal Surfaces" DOI: 10.1021/la049194c.

[104] J.W. Niemantsverdriet, A.F.P. Engelen, A.M. de Jong, W. Wieldraaijer, G.J. Kramer, *Appl. Surf. Sci.* **1999** (144-145) 366-374, "Realistic surface science models of industrial catalysts" DOI: 10.1016/S0169-4332(98)00749-1.

[105] L.T. Zhuravlev, *Langmuir* **1987** (316) 316-318, "Concentration of hydroxyl groups on the surface of amorphous silicas" DOI: 10.1021/la00075a004.

anchoring was obtained for **C5** and **C6** respectively, therefore a coverage of 0.66 -1 and 1 – 1.5 Cr Fisher-carbene complexes per nm^2, was calculated for **C5** and **C6** respectively.
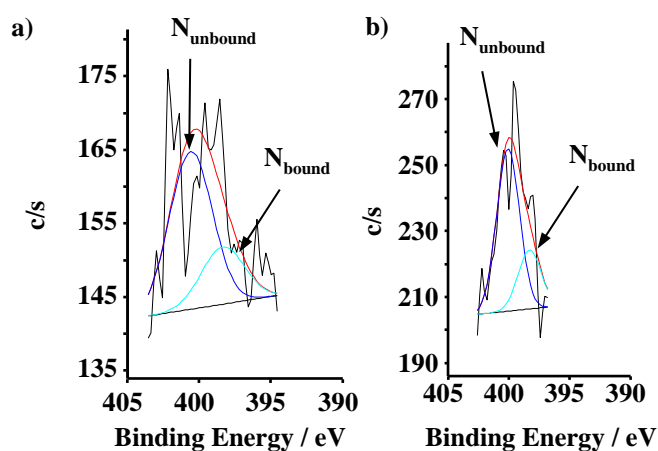
Figure 3.61: The fitting (deconvolution) of the **a)** [Cr(CO)$_5$=C(OEt)(Fu)] + amino-functionalized wafer, **C7**, and **b)** [Cr(CO)$_5$=C(OEt)(Th)] + amino-functionalized wafer, **C8**, N 1s XPS peaks.

This concludes the section discussing the results obtained from the study as outlined in chapter 1. All aims have been met and final conclusions, summations and future perspectives may be found in the final section (Chapter 5).

4 Experimental.

4.1 Materials

The solid and liquid chemicals from Merck and Sigma Aldrich were used in the synthesis without further purification unless otherwise specified in the procedure. Solvents were used as is and dried when stated in the procedure. The solvents were dried according to published methods with an appropriate drying agent such as sodium wire. The n-type, single crystalline (100) Si-wafers were obtained from Topsil. Tosoh Corp (Japan) supplied the KL-zeolite (HSZ-500KOA) and HY-zeolite (HSZ-350HUA), these zeolites were used without modification except calcination.

4.2 Characterization techniques and instrumentation

4.2.1 Spectroscopic measurements

Due to the paramagnetic properties of the $[Mn^{III}(\beta\text{-diketonato})_3]$ complexes, ^1H NMR could not be used as a characterization technique.

Bruker Tensor 27 infrared spectrophotometer fitted with Pike MIRacle single bounce diamond Attenuated Total Reflectance (ATR) was used to do Fourier transform infrared (FTIR) analysis.

X-ray photoelectron spectroscopy (XPS) analysis were recorded on a PHI 5000 Versaprobe system with monochromatic Al Kα X-ray source. The instrument was calibrated to give an instrument work function binding energy of 284.5 eV for lowest binding energy peak of the carbon 1s, attributed to the adventitious carbon peak that is not affected by neighbouring atoms. A constant pass energy of 187.85 eV was used during survey scans. The detailed scans' pass energy was varied from 23.4 to 187.85 eV depending on the pass energy needed to obtain spectra with good resolution. The background pressure was set as 2 x 10^{-8} mbar. Fitting of the XPS data was done using MultiPak V 8.2C computer software.[1]

---

[1] F. Moulder, W.F. Stickle, P.E. Sobol, K.D. Bomben, In *Handbook of X-ray Photo- 367 electron Spectroscopy,* ULVAC-PHI, Inc., 370 Enzo, Chigasaki 253-8522, Japan, 368 **1995**, pp. 45, 57, 143.

4.2.2 Melting point (m.p.) determination

The melting points were determined on an Olympus BX51 microscope that is fitted with a Linkam THMS600 hot stage that is connected to a Linkam TMS94 temperature programmer. The melting points given were the onset temperature of melting.

4.2.3 Thermal analysis

The Mettler/Toledo TGA/SDTA857 instrument was used to perform thermal stability of [M(β-diketonato)$_3$] impregnated on different 3D-support systems. Samples between 5-10 mg was heated to 700 ºC at the rate of 10 ºC/min. The mass loss of the samples during the temperature program was determined with the use of STAR^e Evaluation software.

4.2.4 Electrochemistry

Cyclic voltammetry (CV), linear sweep voltammetry (LSV) was done by the use of a BAS100B Electrochemical Analyzer where data was recorded using BAS100W (Version 2.3). The three electrodes used during measurements are a Pt auxiliary electrode, Ag/Ag$^+$ (0.01 mM AgNO$_3$ in CH$_3$CN) reference electrode mounted on a Luggin capillary and a glassy carbon (surface area 0.1257 cm^2) working electrode. The working electrode was polished on a Bühler polishing mat first with 1 micron and then with ¼ micron diamond paste.

4.2.4.1 Acetonitrile (CH$_3$CN) solvent system

The electrochemistry measurements were performed in CH$_3$CN containing 0.1 M tetrabutylammonium hexafluorophosphate (TBAHFP, [NBu$_4$][PF$_6$]) as supporting electrolyte. The voltammogram was obtained at room temperature under a blanket of argon. The concentration of the chromium Fischer carbene complexes were 1.0 mM. Ferrocene (FcH/FcH$^+$) was used as an internal standard.

4.2.4.2 Dichloromethane (DCM) solvent system

Voltammograms were performed in spectrochemical grade DCM (Sigma-Aldrich) containing 0.1 M tetrabutylammonium hexafluorophosphate (TBAHFP, [NBu$_4$][PF$_6$]) as supporting electrolyte. The measurements were obtained at room temperature under a blanket of argon. The [Mn(dpm)$_3$] complex with a concentration of 0.5 mM was used. Ferrocene (FcH/FcH$^+$) was used as an internal standard.

4.3 Synthesis

4.3.1 [Mn(β-diketonato)₃] complexes 1, 2, 5, 6, 7, 8

The [Mn(β-diketonato)₃] complexes (**1**, **2**, **5**, **6**, **7**, **8**) were prepared by adapting a direct synthesis method as follows. [2]

The β-diketone (11 mmol) was added to the filtrate of a potassium permanganate (0.25 g, 1.59 mmol) solution (in a minimum amount of water), while stirring the filtrate vigorously over a steam bath for five minutes. After 10 minutes of cooling the mixture, it was filtered and the resulting precipitate was washed with water to obtain the desired [Mn(β-diketonato)₃] complex.

4.3.1.1 Tris(dipivaloylmethanato)manganese(III) [Mn(dpm)₃], 1
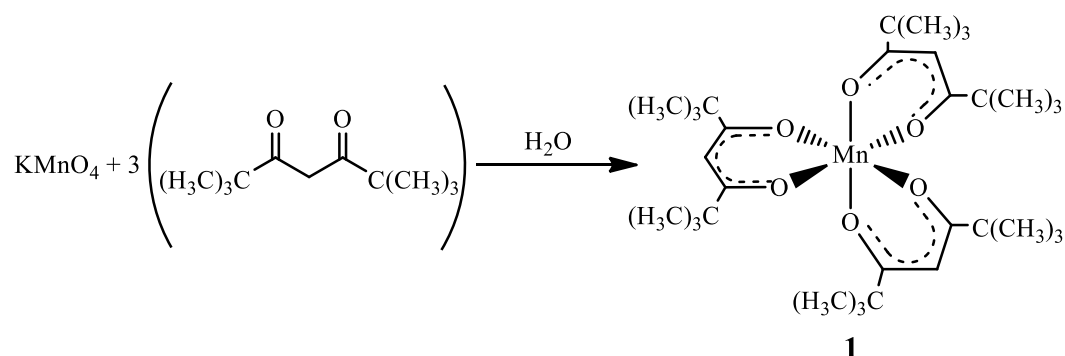
Yield 24 %. Colour: dark brown-black. Melting point 173.4 ℃.

4.3.1.2 Tris(acetylacetonato)manganese(III) [Mn(acac)₃], 2
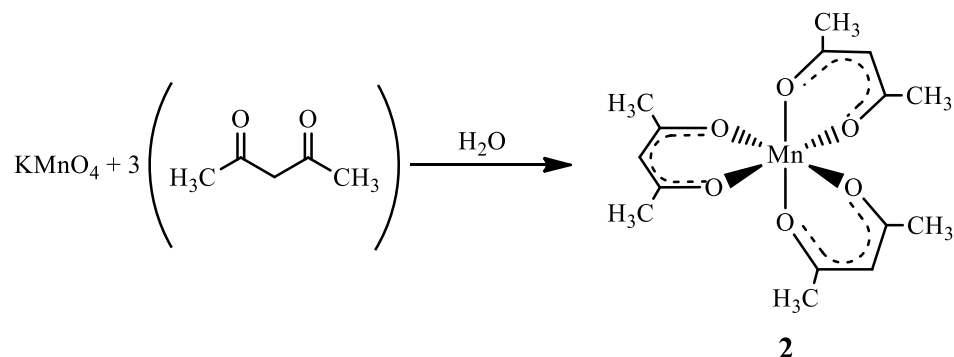
Yield 21 %. Colour: Black. Melting point 156.5 ℃.

---

[2] M.N. Bhattacharjee, M.K. Chaudhuri, D.T Khathing, *Dalton Trans*. **1982** (3) 669-670, "Direct synthesis of tris(acetylacetonato)manganese(III)". DOI: 10.1039/DT9820000669.

4.3.1.3 Tris(trifluoroacetylacetonato)manganese(III) [Mn(tfaa)₃], 5
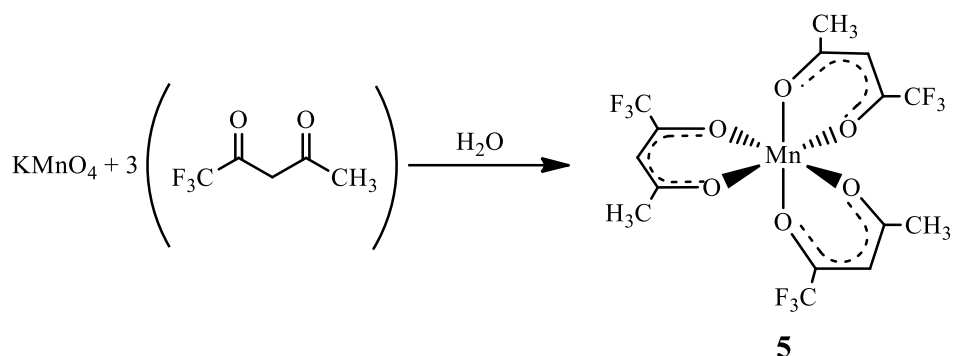
Yield 66 %. Colour: Dark brown-black. Melting point 117.3 °C. MS Calculated: Mr = 514.18 g/mol, Found: 515.1 g/mol. Elemental analysis; Calculated for $MnC_{15}H_{12}O_6F_9$: C, 35.0; H, 2.4 Found: C, 33.6; H, 2.3.

4.3.1.4 Tris(thenoyltrifluoroacetonato)manganese(III) [Mn(tfth)₃], 6
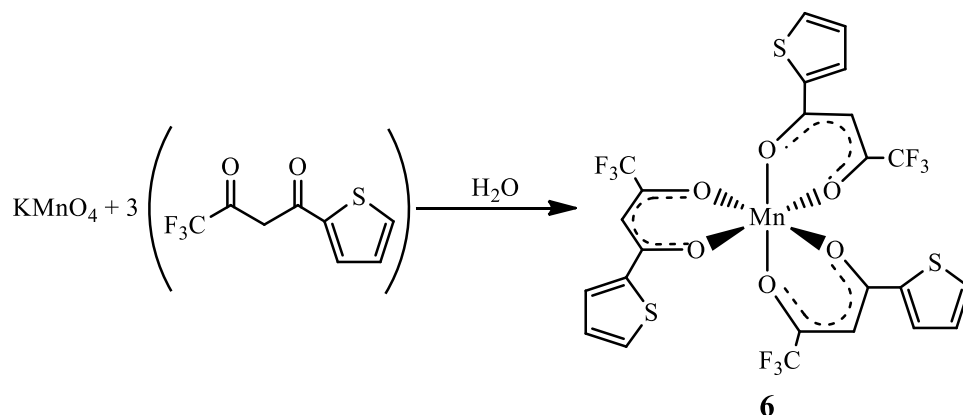
Yield 94 %. Colour: Brown. Melting point 157.2 °C. MS Calculated: Mr = 718.45 g/mol, Found: 722.1 g/mol. Elemental analysis; Calculated for $MnC_{24}H_{12}O_6F_6S_3$: C, 40.1; H, 1.7 Found: C, 40.7; H, 1.99.

4.3.1.5 Tris(trifluorofuroylacetonato)manganese(III) [Mn(tffu)₃], 7
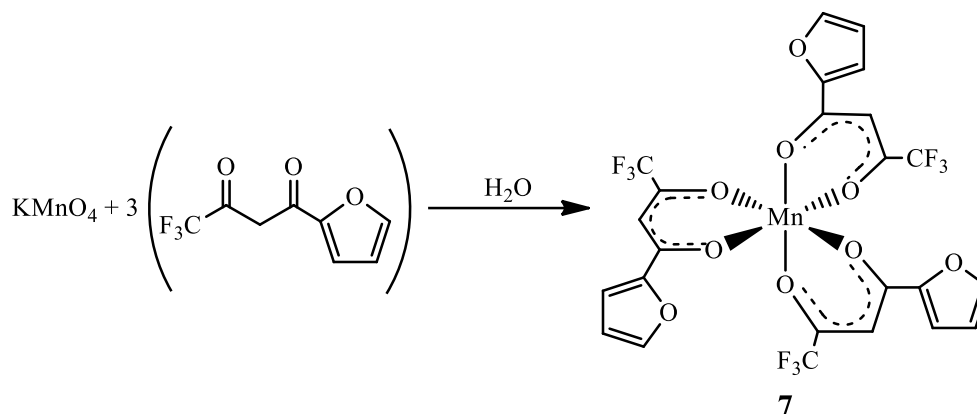
Yield 70 %. Colour: Black. Melting point 171.4 ℃. MS Calculated: Mr = 670.27 g/mol, Found: 681.2 g/mol. Elemental analysis; Calculated for $MnC_{24}H_{12}O_9F_9$: C, 43.0; H, 1.8 Found: C, 42.25; H, 1.78.

4.3.1.6 Tris(trifluorobenzoylacetonato)manganese(III) [Mn(tfba)₃], 8
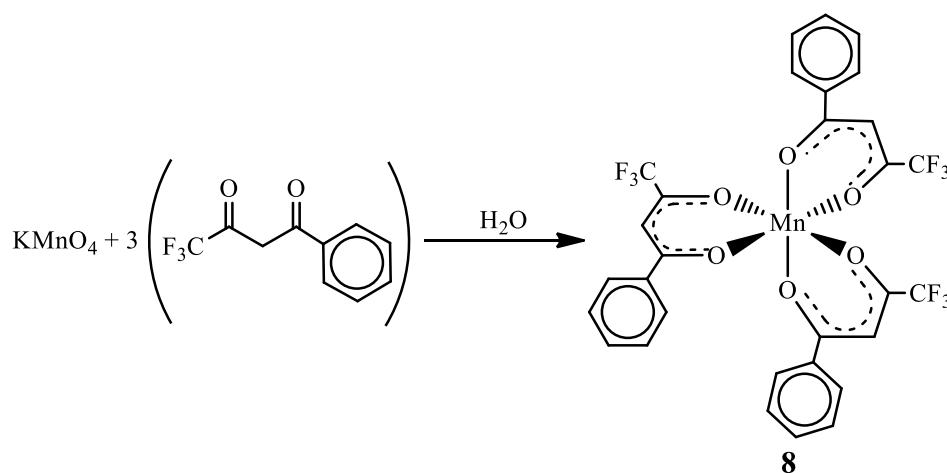
Yield 95 %. Colour: Black. Melting point 88.9 ℃. MS Calculated: Mr = 700.39 g/mol, Found: 703.25 g/mol. Elemental analysis; Calculated for $MnC_{30}H_{18}O_6F_9$: C, 51.4; H, 2.6 Found: C, 54.6; H, 3.0.

4.3.2 [Mn(β-diketonato)$_3$] complexes 3, 4

The [Mn(β-diketonato)$_3$] complexes (**3** and **4**) were prepared by adapting a direct synthesis method as follows.[3]

The β-diketone (11 mmol, dissolved in ethanol) was added to the filtrate of a potassium permanganate (0.25 g, 1.59 mmol) solution (in a minimum amount of water), while stirring the filtrate vigorously over a steam bath for five minutes. After 10 minutes of cooling the mixture, it was filtered and the resulting precipitate was washed with water to obtain the desired [Mn(β-diketonato)$_3$] complex.

4.3.2.1 Tris(benzoylacetonato)manganese(III) [Mn(ba)$_3$], 2

3
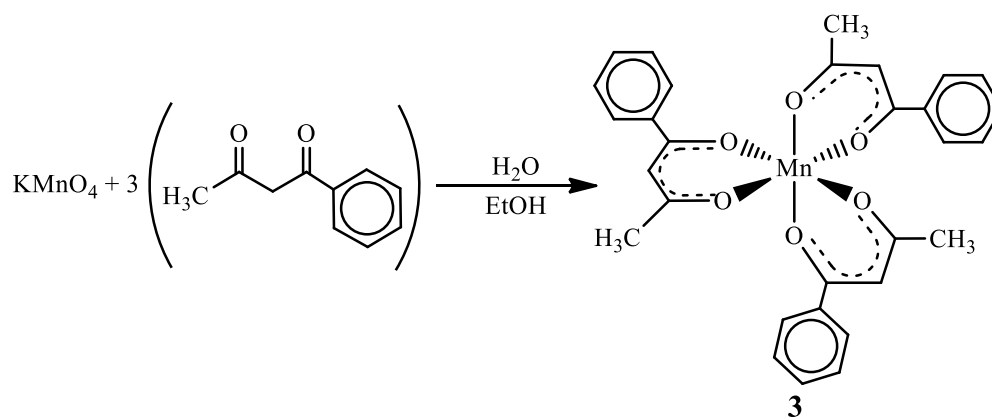
Yield 72 %. Colour: Green. Melting point 186.2 °C. MS Calculated: Mr = 538.48 g/mol, Found: 540.3 g/mol. Elemental analysis; Calculated for MnC$_{30}$H$_{27}$O$_6$: C, 66.9; H, 5.1 Found: C, 72.3; H, 5.8.

---

[3] M.N. Bhattacharjee, M.K. Chaudhuri, D.T Khathing, *Dalton Trans.* **1982** (3) 669-670, "Direct synthesis of tris(acetylacetonato)manganese(III)". DOI: 10.1039/DT9820000669

4.3.2.2 Tris(dibenzoylmethanato)manganese(III) [Mn(dbm)₃], 3
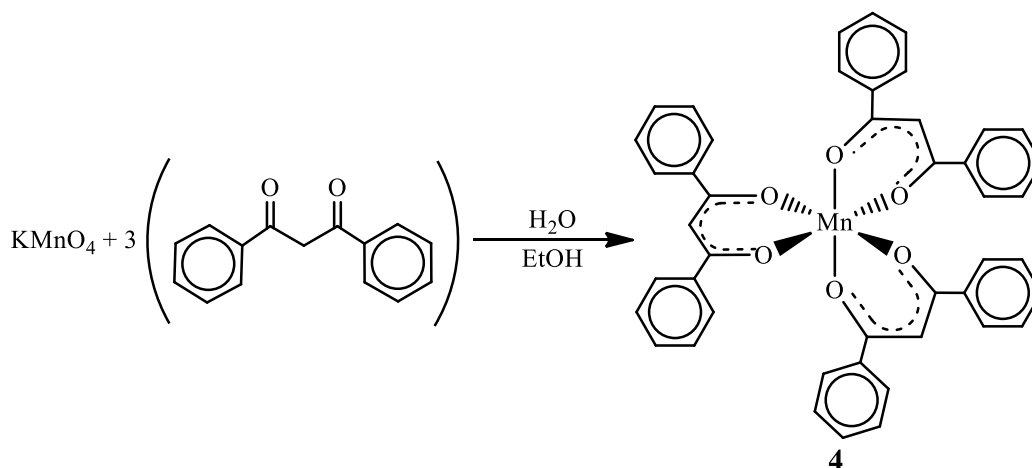
Yield 83 %. Colour: Black. Melting point 234.8 ℃. Elemental analysis; Calculated for MnC$_{45}$H$_{33}$O$_6$: C, 74.6; H, 4.6 Found: C, 76.5; H, 4.72.

4.3.3 Tris(hexafluoroacetylacetonato)manganese(III) [Mn(hfaa)₃], 9

The [Mn(hfaa)₃] complex **9** was prepared by the following adapted procedure.[4,5]

4.3.3.1 Tris(hexafluoroacetylacetonato)manganese(III) [Mn(hfac)₃], 8
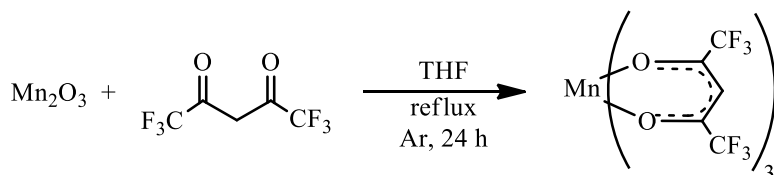
The excess solvent and Hhfaa of a Mn$_2$O$_3$ (0.418 g, 2.65 mmol), Hhfaa (3 mL, 21.19 mmol) and dry THF (20 mL) reaction mixture that was refluxing under Ar for 24 hours, were removed under vacuum. Sublimation (under vacuum at 60 ℃) of the resulting dark green residue was commenced to form the yellow [Mn(hfaa)₃] solid on the cold finger. This yellow solid was collected as the product. The hygroscopic nature of the [Mn(hfaa)₃] prevented the determination of the yield of the reaction and melting point of the product.

---

[4] H. Zhang, B. Li, E.V. Dikarev, *Journal of Cluser Scencei* **2008** (19) 311-321, "Mn(III) Hexafluoroacetylacetonate as an Oxidative Agent in the Synthesis of Heterobimetallic β-Diketonates". DOI: 10.1007/s10876-007-0174-1

[5] J.R. Bryant, J.E. Taves, J.M. Mayer, *Inorganic Chemistry* **2002** (41) 2769-2776, "Oxidations of Hydrocarbons by Manganese(III) Tris(hexafluoroacetylacetonate)". DOI: 10.1021/ic025541z.

4.4 Preparation of heterogeneous catalyst

4.4.1 2-D model catalyst on Amino-functionalized Si-wafer

4.4.1.1 Preparation of amino-functionalized Si-wafer (Si-wafer) as catalyst support

The amino-functionalized Si-wafer was prepared through a 3 step process as illustrated in **Scheme 4.1** and discussed below.
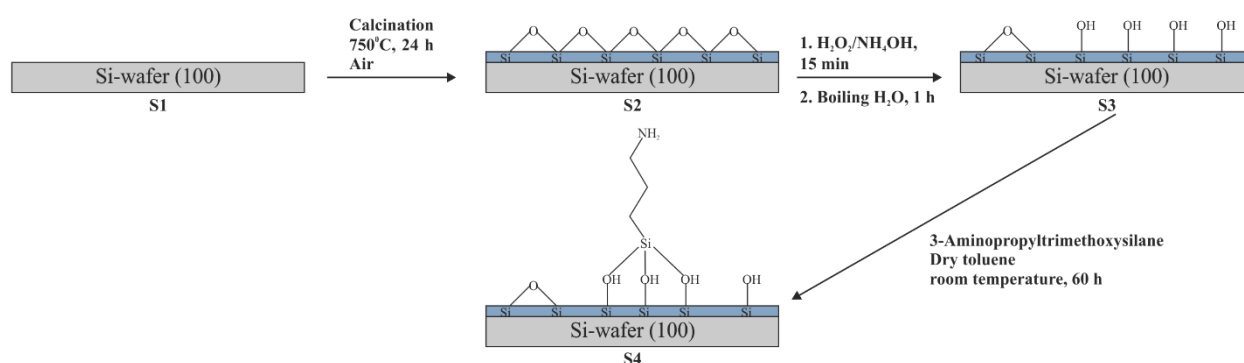
Scheme 4.1: Amino-functionalization of Si-wafers.

(i)   *Formation of silicon oxide layer on Si-wafer by calcination*

The Si-wafer (100) was placed in a quartz chamber in a calcination oven which was heated to 750 ℃. After temperature of 750 ℃ was reached the Si-wafer was kept at this temperature for 24 hours under ambient air. The calcination oven was switched off after the 24 hours and left closed to cool down to a temperature of about 25 ℃ which took approximately 12 hours. The calcined Si-wafer **S2** was used with no further analysis.

(ii)   *Formation of silanol groups on the calcined Si-wafer, S2*

The calcined Si-wafer, **S2**, was etched by submerging it into 1:1 (v:v) H_2O_2 (25% solution) and NH_4OH (35% solution) at room temperature for 15 minutes. The surface silanol (Si-OH) groups were formed by placing the cleaned calcined Si-wafers into boiling doubly distilled H_2O for 1 hour, there after the wafers were dried under a stream of nitrogen, forming a hydroxylated Si-wafer, **S3**. The hydroxylated Si-wafer samples was analysed with XPS.

(iii)   *Grafting of 3-aminopropyltrimethoxysilane onto the hydroxylated Si-wafer, S3*

The hydroxylated Si-wafer, **S3**, was immersed (with the activated side facing up) in a solution of 3-aminopropyltrimethoxysilane (500 mg, 2.79 mmol) in dry toluene (20 cm^{-3}) with gentle stirring under nitrogen atmosphere for ~60 hours. Care was taken to prevent magnetic stirrer bar from touching the Si-wafer during the grafting process. After *ca.* 60 hours the amino-functionalized Si-wafers, **S4**, were removed and washed 3 times with isopropanol in a sonic bath, followed by drying under a stream of nitrogen.

XPS of amino-functionalized Si-wafer (S4): Binding energy: 399.18 eV (N 1s of free amine), 400.27 eV (N 1s of hydrogen bonded amine) and 401.12 eV (N 1s of protonated amine).

4.4.1.2 Grafting of [Mn(β-diketonato)₃] complexes onto amino-functionalized Si-wafers
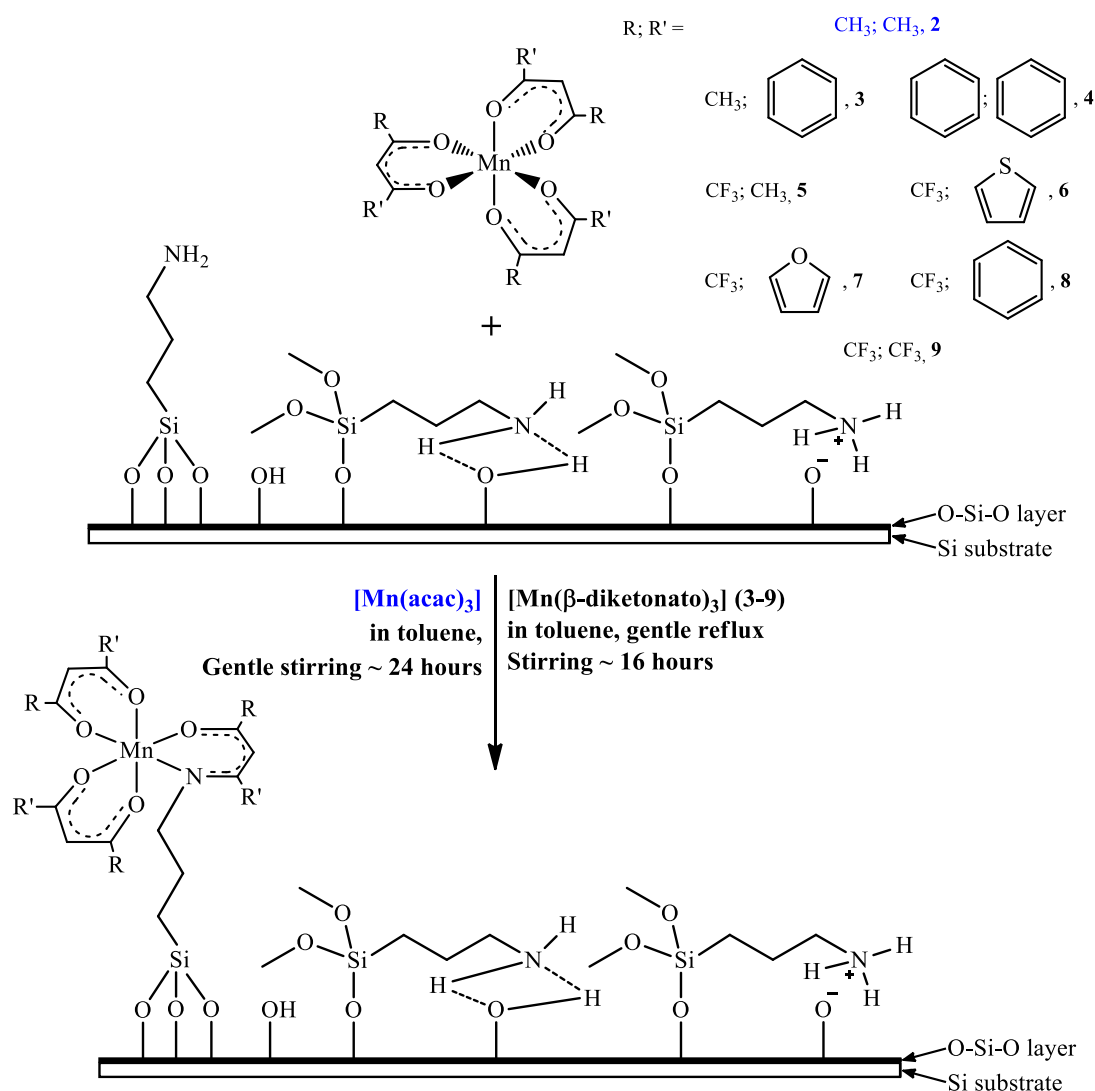
Scheme 4.2: The heterogenization of [Mn(β-diketonato)₃] onto amino-functionalized Si-wafers.

(i)   *Heterogenization of Tris(acetylacetonato)manganese(III) [Mn(acac)₃], **S5***

[Mn(acac)$_3$] was grated onto amino-functionalized Si-wafers by submerging the wafer in a solution of [Mn(acac)$_3$] (0.25 M) in 2 cm^3 of toluene, with gentle stirring for ~24 hours. The resulting [Mn(acac)$_3$] 2-D model catalyst, **S5**, was washed three times with isopropanol followed by drying under a stream of nitrogen.

XPS of [Mn(acac)$_3$] *grafted on to amino-functionalized Si-wafer (**S5**):* Binding energy: 641.55 eV and 653.37 eV (Mn 2p$_{3/2main}$ and Mn 2p$_{1/2main}$) and 645.95 eV and 657.37 eV (Mn 2p$_{3/2satel}$ and Mn 2p$_{1/2satel}$)

(ii)   *Heterogenization of Tris(β-diketonato)manganese(III) [Mn(β-diketonato)₃], **S6**-**S12***

Amino-functionalized Si-wafers were placed in a solution of [Mn(β-diketonato)$_3$] (**3-9**, 0.25 M) in toluene (2 cm^3). This suspension was refluxed gently for ~16 hours. The resulting [Mn(β-diketonato)$_3$] 2-D model catalysts (**S6-S12**) were washed three times with isopropanol and finally dried under a nitrogen stream. XPS analysis was done on these 2-D model catalysts.

*XPS of [Mn(ba)₃] grafted on to amino-functionalized Si-wafer (**S6**):* Binding energy: 641.90 eV and 653.62 eV (Mn 2p$_{3/2main}$ and Mn 2p$_{1/2main}$) and, 645.75 eV and 657.48 eV (Mn 2p$_{3/2satel}$ and Mn 2p$_{1/2satel}$)

*XPS of [Mn(dbm)₃] grafted on to amino-functionalized Si-wafer (**S7**):* Binding energy: 641.71 eV and 653.79 eV (Mn 2p$_{3/2main}$ and Mn 2p$_{1/2main}$) and, 645.79 eV and 657.48 eV (Mn 2p$_{3/2satel}$ and Mn 2p$_{1/2satel}$)

*XPS of [Mn(tfaa)₃] grafted on to amino-functionalized Si-wafer (**S8**):* Binding energy: 641.77 eV and 653.55 eV (Mn 2p$_{3/2main}$ and Mn 2p$_{1/2main}$) and, 645.63 eV and 657.32 eV (Mn 2p$_{3/2satel}$ and Mn 2p$_{1/2satel}$); 684.85 eV and 687.92 eV (F 1s$_{main}$ and F 1s$_{satel}$ respectively)

*XPS of [Mn(tfth)₃] grafted on to amino-functionalized Si-wafer (**S9**):* Binding energy: 641.58 eV and 653.14 eV (Mn 2p$_{3/2main}$ and Mn 2p$_{1/2main}$) and, 645.86 eV and 657.41 eV (Mn 2p$_{3/2satel}$ and Mn 2p$_{1/2satel}$); 685.07 eV and 688.17 eV (F 1s$_{main}$ and F 1s$_{satel}$ respectively); 164.20 eV and 165.25 eV (S 2p$_{3/2main}$ and S 2p$_{1/2main}$) and, 168.04 eV and 169.84 eV (S 2p$_{3/2satel}$ and S 2p$_{1/2satel}$)

*XPS of [Mn(tffu)₃] grafted on to amino-functionalized Si-wafer (**S10**):* Binding energy: 642.01 eV and 653.90 eV (Mn 2p$_{3/2main}$ and Mn 2p$_{1/2main}$) and, 645.79 eV and 657.48 eV (Mn 2p$_{3/2satel}$ and Mn 2p$_{1/2satel}$); 688.13 eV (F 1s)

*XPS of [Mn(tfba)$_3$] grafted on to amino-functionalized Si-wafer (**S11**):* Binding energy: 641.59 eV and 653.37 eV (Mn 2p$_{3/2main}$ and Mn 2p$_{1/2main}$) and, 645.79 eV and 657.48 eV (Mn 2p$_{3/2satel}$ and Mn 2p$_{1/2satel}$); 685.60 eV and 688.19 eV (F 1s$_{main}$ and F 1s$_{satel}$ respectively)

*XPS of [Mn(hfaa)$_3$] grafted on to amino-functionalized Si-wafer (**S12**):* Binding energy: 642.29 eV and 654.07 eV (Mn 2p$_{3/2main}$ and Mn 2p$_{1/2main}$) and, 646.19 eV and 657.88eV (Mn 2p$_{3/2satel}$ and Mn 2p$_{1/2satel}$); 685.21 eV and 688.36 eV (F 1s$_{main}$ and F 1s$_{satel}$ respectively)

4.4.1.3 Grafting of [M(acac)$_3$] complexes onto amino-functionalized Si-wafers (M = Co, Rh and Ir), S29-S31

Amino-functionalized Si-wafers were placed in a solution of [M(acac)$_3$] (M = Co, Rh and Ir, 0.1 M) in toluene (3, 1 and 1 cm^3 respectively). The solution of [M(acac)$_3$] complex with the amino-functionalized Si-wafer was stirred gently for ~163 hours. The resulting [M(acac)$_3$] 2-D model catalysts (**S29-S31**) were washed three times with isopropanol and finally dried under a nitrogen stream. XPS analysis was done on these 2-D model catalysts.

*XPS of [Co(acac)$_3$] grafted on to amino-functionalized Si-wafer (**S29**):* Binding energy: 781.53 eV and 796.60 eV (Co 2p$_{3/2main}$ and Co 2p$_{1/2main}$ of [Co(acac)$_3$]), 786.76 eV and 803.12 eV (Co 2p$_{3/2sat}$ and Co 2p$_{1/2sat}$ of [Co(acac)$_3$])

*XPS of [Rh(acac)$_3$] grafted on to amino-functionalized Si-wafer (**S30**):* Binding energy: 309.13 eV and 313.93 eV (Rh 3d$_{5/2}$ and Rh 3d$_{3/2}$ of Rh$_2$O$_3$), 310.59 eV and 315.34 eV (Rh 3d$_{5/2}$ and Rh 3d$_{3/2}$ of [Rh(acac)$_3$])

*XPS of [Ir(acac)$_3$] grafted on to amino-functionalized Si-wafer (**S31**):* Binding energy: 63.21 eV and 66.11 eV (Ir 4f$_{7/2}$ and Ir 4f$_{5/2}$ of [Ir(acac)$_3$])

4.4.1.4 Grafting of [Cr(CO)$_5$=C(OEt)(Fu)], C5, and [Cr(CO)$_5$=C(OEt)(Th)], C6 complexes onto amino-functionalized Si-wafers, C7 and C8

Amino-functionalized Si-wafers were placed in a solution of chromium Fischer carbene complex (Cr-FCC) [Cr(CO)$_5$=C(OEt)(Fu)], **C5**, or [Cr(CO)$_5$=C(OEt)(Th)] [M(acac)$_3$] (1.2 x 10^{-8} M) in toluene (2 cm^3 respectively). The solution of Cr-FCC with the amino-functionalized Si-wafer was stirred gently for ~24 hours. The resulting Cr-FCC 2-D model catalysts (**C7** and **C8**) were washed three times with isopropanol and finally dried under a nitrogen stream. XPS analysis was done on these 2-D model catalysts.

*XPS of [*Cr(CO)$_5$=C(OEt)(Fu)*] grafted on to amino-functionalized Si-wafer (**C7**):* Binding energy: 577.14 eV and 586.89 eV (Cr 2p$_{3/2}$ and Cr 2p$_{1/2}$)

*XPS of [*Cr(CO)$_5$=C(OEt)(Th)*] grafted on to amino-functionalized Si-wafer (**C8**):* Binding energy: 576.57 eV and 586.36 eV (Cr 2p$_{3/2}$ and Cr 2p$_{1/2}$); 165.07 eV and 166.25 eV (S 2p$_{3/2}$ and S 2p$_{1/2}$)

4.4.2 Immobilization of complexes onto 3-D supports

The 3-D supports that was used in this study (SiO$_2$, TiO$_2$, MgO, acidic zeolite and basic zeolite) was first calcined by placing it in a calcination oven at 400 ºC for ~ 16 hours. The preparations of the 3-D heterogeneous catalyst will be discussed in the following sections.

4.4.2.1 Immobilization of [Mn(acac)$_3$] complex onto various 3-D supports

[Mn(acac)$_3$] (0.0834g) was dissolved in acetone. The 0.1 g 3-D supports (SiO$_2$, TiO$_2$, MgO, acidic zeolite and basic zeolite forming **S14**, **S21**, **S22**, **S23** and **S24** respectively) were added to the [Mn(acac)$_3$] solution targeting 13 wt% metal immobilization on the support. The mixture was left open at room temperature till all the solvent evaporated.

*XPS of [Mn(acac)$_3$] immobilized on SiO$_2$ (**S14**):* Binding energy: 641.68 eV and 653.32 eV (Mn 2p$_{3/2main}$ and Mn 2p$_{1/2main}$ of [Mn(acac)$_3$]) and, 645.48 eV and 657.08 eV (Mn 2p$_{3/2satel}$ and Mn 2p$_{1/2satel}$ of [Mn(acac)$_3$])

*XPS of [Mn(acac)$_3$] immobilized on TiO$_2$ (**S21**):* Binding energy: 642.05 eV and 653.64 eV (Mn 2p$_{3/2main}$ and Mn 2p$_{1/2main}$ of [Mn(acac)$_3$]) and, 645.73 eV and 657.33 eV (Mn 2p$_{3/2satel}$ and Mn 2p$_{1/2satel}$ of [Mn(acac)$_3$])

*XPS of [Mn(acac)$_3$] immobilized on MgO (**S22**):* Binding energy: 641.41 eV and 653.13 eV (Mn 2p$_{3/2main}$ and Mn 2p$_{1/2main}$ of [Mn(acac)$_3$]) and, 645.16 eV and 656.87 eV (Mn 2p$_{3/2satel}$ and Mn 2p$_{1/2satel}$ of [Mn(acac)$_3$])

*XPS of [Mn(acac)$_3$] immobilized on acidic zeolite (**S23**):* Binding energy: 642.07 eV and 653.71 eV (Mn 2p$_{3/2main}$ and Mn 2p$_{1/2main}$ of [Mn(acac)$_3$]) and, 645.77 eV and 657.41 eV (Mn 2p$_{3/2satel}$ and Mn 2p$_{1/2satel}$ of [Mn(acac)$_3$])

*XPS of [Mn(acac)$_3$] immobilized on basic zeolite (**S24**):* Binding energy: 641.09 eV and 652.95 eV (Mn 2p$_{3/2main}$ and Mn 2p$_{1/2main}$ of [Mn(acac)$_3$]) and, 644.89 eV and 656.72 eV (Mn 2p$_{3/2satel}$ and Mn 2p$_{1/2satel}$ of [Mn(acac)$_3$])

4.4.2.2 Immobilization of [Mn(tfaa)₃] complex onto various 3-D supports

[Mn(tfaa)$_3$] (0.0501g) was dissolved in acetone. The 0.0416 g 3-D supports (SiO$_2$, TiO$_2$, MgO, acidic zeolite and basic zeolite forming **S14**, **S21**, **S22**, **S23** and **S24** respectively) were added to the [Mn(tfaa)$_3$] solution targeting 13 wt% metal immobilization on the support. The mixture was left open at room temperature till all the solvent evaporated.

XPS of [Mn(tfaa)₃] immobilized on SiO₂ (S17): Binding energy: Binding energy: 642.14 eV and 653.85 eV (Mn 2p$_{3/2main}$ and Mn 2p$_{1/2main}$ of [Mn(tfaa)$_3$]) and, 645.99 eV and 657.58 eV (Mn 2p$_{3/2satel}$ and Mn 2p$_{1/2satel}$ of [Mn(tfaa)$_3$]); 684.48 eV and 688.19 eV (F 1s$_{main}$ and F 1s$_{satel}$ respectively)

XPS of [Mn(tfaa)₃] immobilized on TiO₂ (S25): Binding energy: 642.71 eV and 654.11 eV (Mn 2p$_{3/2main}$ and Mn 2p$_{1/2main}$ of [Mn(tfaa)$_3$]) and, 646.45 eV and 657.80 eV (Mn 2p$_{3/2satel}$ and Mn 2p$_{1/2satel}$ of [Mn(tfaa)$_3$]); 685.73 eV and 688.99 eV (F 1s$_{main}$ and F 1s$_{satel}$ respectively)

XPS of [Mn(tfaa)₃] immobilized on MgO (S26): Binding energy: 641.82 eV and 653.54 eV (Mn 2p$_{3/2main}$ and Mn 2p$_{1/2main}$ of [Mn(tfaa)$_3$]) and, 645.56 eV and 657.23 eV (Mn 2p$_{3/2satel}$ and Mn 2p$_{1/2satel}$ of [Mn(tfaa)$_3$]); 684.98 eV and 688.64 eV (F 1s$_{main}$ and F 1s$_{satel}$ respectively)

XPS of [Mn(tfaa)₃] immobilized on acidic zeolite (S27): Binding energy: 642.77 eV and 654.54 eV (Mn 2p$_{3/2main}$ and Mn 2p$_{1/2main}$ of [Mn(tfaa)$_3$]) and, 646.47 eV and 658.24 eV (Mn 2p$_{3/2satel}$ and Mn 2p$_{1/2satel}$ of [Mn(tfaa)$_3$]); 684.40 eV and 688.46 eV (F 1s$_{main}$ and F 1s$_{satel}$ respectively)

XPS of [Mn(tfaa)₃] immobilized on basic zeolite (S28): Binding energy: 641.67 eV and 653.59 eV (Mn 2p$_{3/2main}$ and Mn 2p$_{1/2main}$ of [Mn(tfaa)$_3$]) and, 645.41 eV and 657.31 eV (Mn 2p$_{3/2satel}$ and Mn 2p$_{1/2satel}$ of [Mn(tfaa)$_3$]); 683.37 eV and 687.37 eV (F 1s$_{main}$ and F 1s$_{satel}$ respectively)

4.4.2.3 Immobilization of [Mn(β-diketonato)₃] onto SiO₂ 3-D support

[Mn(β-diketonato)$_3$] complexes ([Mn(dpm)$_3$], **1**; [Mn(ba)$_3$], **3**; [Mn(dbm)$_3$], **4**; [Mn(tfth)$_3$], **6**; [Mn(tffu)$_3$], **7** and [Mn(tfba)$_3$], **8**) were dissolved in acetone. The 0.0416 g SiO$_2$ 3-D supports were added to the [Mn(β-diketonato)$_3$] solution forming **S13**, **S15**, **S16**, **S18**, **S19** and **S20** respectively, with a targeted 13 wt% metal immobilization on the support. The mixture was left open at room temperature till all the solvent evaporated.

XPS of [Mn(dpm)₃] immobilized on SiO₂ (S13): Binding energy: 641.46 eV and 652.86 eV (Mn 2p$_{3/2main}$ and Mn 2p$_{1/2main}$ of [Mn(dpm)$_3$]) and, 645.16 eV and 656.58 eV (Mn 2p$_{3/2satel}$ and Mn 2p$_{1/2satel}$ of [Mn(dpm)$_3$])

XPS of [Mn(ba)₃] immobilized on SiO₂ (S15): 641.68 eV and 652.36 eV (Mn $2p_{3/2main}$ and Mn $2p_{1/2main}$ of [Mn(ba)₃]) and, 645.43 eV and 657.04 eV (Mn $2p_{3/2satel}$ and Mn $2p_{1/2satel}$ of [Mn(ba)₃])

XPS of [Mn(dbm)₃] immobilized on SiO₂ (S16): Binding energy: 641.32 eV and 653.03 eV (Mn $2p_{3/2main}$ and Mn $2p_{1/2main}$ of [Mn(dbm)₃]) and, 645.04 eV and 656.72 eV (Mn $2p_{3/2satel}$ and Mn $2p_{1/2satel}$ of [Mn(dbm)₃])

XPS of [Mn(tfth)₃] immobilized on SiO₂ (S18): Binding energy: 641.86 eV and 653.50 eV (Mn $2p_{3/2main}$ and Mn $2p_{1/2main}$ of [Mn(tfth)₃]) and, 645.55 eV and 657.25 eV (Mn $2p_{3/2satel}$ and Mn $2p_{1/2satel}$ of [Mn(tfth)₃]); 684.35 eV and 688.25 eV (F $1s_{main}$ and F $1s_{satel}$ respectively); 163.58 eV and 165.34 eV (S $2p_{3/2}$ and S $2p_{1/2}$ of [Mn(tfth)₃])

XPS of [Mn(tffu)₃] immobilized on SiO₂ (S19): 641.95 eV and 653.23 eV (Mn $2p_{3/2main}$ and Mn $2p_{1/2main}$ of [Mn(tffu)₃]) and, 645.68 eV and 656.90 eV (Mn $2p_{3/2satel}$ and Mn $2p_{1/2satel}$ of [Mn(tffu)₃]); 684.92 eV and 688.66 eV (F $1s_{main}$ and F $1s_{satel}$ respectively)

XPS of [Mn(tfba)₃] immobilized on SiO₂ (S20): Binding energy: 641.98 eV and 653.77 eV (Mn $2p_{3/2main}$ and Mn $2p_{1/2main}$ of [Mn(tfba)₃]) and, 645.68 eV and 657.50 eV (Mn $2p_{3/2satel}$ and Mn $2p_{1/2satel}$ of [Mn(tfba)₃]); 684.48 eV and 688.25 eV (F $1s_{main}$ and F $1s_{satel}$ respectively)

4.4.2.4 Immobilization of [M(acac)₃] onto SiO₂ 3-D support (M = Cr, Fe, Co, Rh and Ir)

[M(acac)₃] complexes (M = Cr, Fe, Co, Rh and Ir) were dissolved in acetone. The SiO₂ 3-D support was added to the [M(acac)₃] solutions forming **S13**, **S15**, **S16**, **S18**, **S19** and **S20** respectively, with a targeted 13 wt% metal immobilization on the support. The mixture was left open at room temperature till all the solvent evaporated.

XPS of [Cr(acac)₃] immobilized on SiO₂ (S32): Binding energy: 577.59 eV and 586.97 eV (Cr $2p_{3/2}$ and Cr $2p_{1/2}$ of [Cr(acac)₃])

XPS of [Fe(acac)₃] immobilized on SiO₂ (S33): Binding energy: 710.24 eV and 723.86 eV (Fe $2p_{3/2}$ and Fe $2p_{1/2}$ of [Fe(acac)₃])

XPS of [Co(acac)₃] immobilized on SiO₂ (S34): Binding energy: 780.17 eV and 795.97 eV (Co $2p_{3/2}$ and Co $2p_{1/2}$ of [Co(acac)₃])

XPS of [Rh(acac)₃] immobilized on SiO₂ (S35): Binding energy: 310.27 eV and 314.04 eV (Rh $3d_{5/2}$ and Rh $3d_{3/2}$ of [Rh(acac)₃])

XPS of [Ir(acac)₃] immobilized on SiO₂ (S36): Binding energy: 63.81 eV and 67.02 eV (Ir $4f_{7/2}$ and Ir $4f_{5/2}$ of [Ir(acac)₃])

4.5 Computational calculations

4.5.1 Tris(β-diketonato)manganese(III), [Mn(β-diketonato)₃]

Density Functional Theory (DFT) calculations were executed by the use of Amsterdam Density Functional (ADF) program with three Generalized Gradient Approximation functionals (GGA), namely PW91 (Perdew-Wang 1991),[6] BP86 (Becke-Perdew),[7,8] and OLYP (Handy-Cohen and Lee-Yang-Parr),[9] and one hybrid functional B3LYP (Becke 1993 and Lee-Yang-Parr)[10,11]. Triple zeta polarized (TZP) basis set was used during the calculations and a spin

---

[6] J.P. Perdew, J.A. Chevary, S.H. Vosko, K.A. Jackson, M.R. Pederson, D.J. Singh and C. Fiolhais, *Phys. Rev. B* 1992 (46) 6671-6687, "Atoms, molecules, solids, and surfaces: Applications of the generalized gradient approximation for exchange and correlation" DOI: 10.1103/PhysRevB.46.6671; Erratum: J.P. Perdew, J.A. Chevary, S.H. Vosko, K.A. Jackson, M.R. Perderson, D.J. Singh and C. Fiolhais, *Phys. Rev. B* **1993** (48) 4978, "Erratum: Atoms, molecules, solids, and surfaces: Applications of the generalized gradient approximation for exchange and correlation". DOI: 10.1103/PhysRevB.48.4978.2

[7] A.D. Becke, *Phys. Rev. A* **1988** (38) 3098-3100, "Density-functional exchange-energy approximation with correct asymptotic behavior". DOI: 10.1103/PhysRevA.38.3098

[8] J.P. Perdew, *Phys. Rev. B* **1986** (33) 8822-8824, "Density-functional approximation for the correlation energy of the inhomogeneous electron gas". DOI: 10.1103/PhysRevB.33.8822; Erratum: J.P. Perdew, *Phys. Rev. B* **1986** (34) 7406, "Erratum: Density-functional approximation for the correlation energy of the inhomogeneous electron gas". DOI: 10.1103/PhysRevB.34.7406

[9] N.C. Handy, A.J. Cohen, *Mol. Phys.* **2001** (99) 403-412, "Left-right correlation energy". DOI: 10.1080/00268970010018431; C. Lee, W. Yang, R.G. Parr, *Phys. Rev. B: Condens. Matter* **1988** (37) 785-789, "Development of the Colle-Salvetti correlation-energy formula into a functional of the electron density". DOI: 10.1103/PhysRevB.37.785; B.G. Johnson, P.M.W. Gill, J.A. Pople, *J. Chem. Phys.* **1993** (98) 5612-5626, "The performance of a family of density functional methods". DOI: 10.1063/1.464906; T.V. Russo, R.L. Martin, P.J. Hay, *J. Chem. Phys.* **1994** (101) 7729-7737, "Density Functional Calculations on First Row Transition Metals". DOI: 10.1063/1.468265

[10] A.D. Becke, *J. Chem. Phys.* **1993** (98) 5648-5652, "Density-functional thermochemistry. III. The role of exact exchange". DOI: 10.1063/1.464913

[11] P.J. Stephens, F.J. Devlin, C.F. Chabalowski and M.J. Frisch, *J. Phys. Chem.* **1994** (98) 11623-11627, "Ab Initio Calculation of Vibrational Absorption and Circular Dichroism Spectra Using Density Functional Force Fields". DOI: 10.1021/j100096a001

state of S = 4/2 = 2 was used for all the [Mn(β-diketonato)$_3$] complexes, which is in agreement with previous DFT studies.[12]

4.5.2 Chromium(0) Fischer Carbene Complexes

Density functional theory (DFT) calculations on the carbene complexes were performed with the hybrid functional B3LYP [13,14], (20% Hartree-Fock exchange) [11] as implemented in the Gaussian 09 program package [15]. Geometries of the neutral complexes were optimized in gas phase with the triple-ζ basis set 6-311G(d,p)[16] on all atoms except Cr, where def2-TZVPP [17] was used. Energies reported are gas phase electronic energies.

[12] R. Freitag, MSc study, "COMPUTATIONAL, STRUCTURAL AND ELECTROCHEMICAL PROPERTIES OF METAL(III) TRIS-BETADIKETONATO COMPLEXES", 2012, University of the Free State, Bloemfontein, South Africa.

[13] A.D. Becke, *Phys. Rev. A* **1988** (38) 3098-3100, "Density-functional exchange-energy approximation with correct asymptotic behavior". DOI: 10.1103/PhysRevA.38.3098

[14] C.T. Lee, W.T. Yang, R.G. Parr, *Phys. Rev. B* **1988** (37) 785-789, "Development of the Colle-Salvetti correlation-energy formula into a functional of the electron density". DOI: 10.1103/PhysRevB.37.785

[15] M.J. Frisch, G.W. Trucks, H.B. Schlegel, G.E. Scuseria, M.A. Robb, J.R. Cheeseman, G. Scalmani, V. Barone, B. Mennucci, G.A. Petersson, H. Nakatsuji, M. Caricato, X. Li, H.P. Hratchian, A.F. Izmaylov, J. Bloino, G. Zheng, J.L. Sonnenberg, M. Hada, M. Ehara, K. Toyota, R. Fukuda, J. Hasegawa, M. Ishida, T. Nakajima, Y. Honda, O. Kitao, H. Nakai, T. Vreven, J.A. Montgomery (Jr), J.E. Peralta, F. Ogliaro, M. Bearpark, J.J. Heyd, E. Brothers, K.N. Kudin, V.N. Staroverov, T. Keith, R. Kobayashi, J. Normand, K. Raghavachari, A. Rendell, J.C. Burant, S.S. Iyengar, J. Tomasi, M. Cossi, N. Rega, J.M. Millam, M. Klene, J.E. Knox, J.B. Cross, V. Bakken, C. Adamo, J. Jaramillo, R. Gomperts, R.E. Stratmann, O. Yazyev, A.J. Austin, R. Cammi, C. Pomelli, J.W. Ochterski, R.L. Martin, K. Morokuma, V.G. Zakrzewski, G.A. Voth, P. Salvador, J.J. Dannenberg, S. Dapprich, A.D. Daniels, O. Farkas, J.B. Foresman, J.V. Ortiz, J. Cioslowski, D.J. Fox, Gaussian 09, Revision B.01, Gaussian, Inc., Wallingford, CT, **2013**.

[16] C.J. Cramer, *Essentials of Computational Chemistry – Theories and Models*, 2nd edition, John Wiley & Sons Ltd, Chichester, **2004**, p271, 252-256.

[17] F. Weigend, R. Ahlrichs, Phys. Chem. Chem. Phys. **2005** (7) 3297-3305, "Balanced basis sets of split valence, triple zeta valence and quadruple zeta valence quality for H to Rn: Design and assessment of accuracy". DOI: 10.1039/B508541A

4.6 2-D model heterogeneous catalytic study [Mn(β-diketonato)₃, S5-S12; [M(acac)₃], S29-S31]

Four [Mn(β-diketonato)₃] 2-D model catalysts ([Mn(acac)₃], **S5**; [Mn(dbm)₃], **S7**; [Mn(tfaa)₃], **S8**; and [Mn(hfaa)₃] **S12** respectively) and three [M(acac)₃] 2-D model catalysts ([Co(acac)₃], **S29**; [Rh(acac)₃], **S30**; and [Ir(acac)₃], **S31**, respectively) were tested by the synthesis of hexamethylenediurethane through a catalytic conversion of hexamethylenediisocyanate (HDI) and ethanol. A 1.27 cm^3 solution of HDI and ethanol (1:10, C_{HDI} = [1.33 mol.dm^{-3}]) and 2-D model catalyst (ca. 4.5 mm^2) was placed into an enclosed 10 ml reaction vessel at 30 °C, under argon atmosphere. No stirring of the solution was done as the convection currents within the reaction mixture was sufficient. Pasteur pipettes were used to remove a small amount of the reaction mixture at pre-determined times. These samples were analysed by ATR FTIR. Turnover frequency was used to evaluate the catalytic behaviour of the different 2-D model catalysts.

5 Summary and future perspectives

5.1 Summary

This chapter describes the outputs achieved to fulfil the objectives set as goals in Chapter 1.

5.1.1 Tris(β-diketonato)manganese(III) / [Mn(β-diketonato)₃]

Goals i-ii) [Mn(dpm)₃] was successfully synthesized with melting point of 173.4 ºC and yield of 24% (Published melting point 160-170 ºC). Experimental and computational methods were used to compare the results of the [Mn(dpm)₃], **1**, complex to a series of [Mn(β-diketonato)₃] complexes (β-diketonato = acetylacetonate (acac), **2**; benzoylacetonato (ba), **3**; dibenzoylmethanato (dbm), **4**; trifluoroacetylacetonato (tfaa), **5**; thenoyltrifluoroacetonato (tfth), **6**; trifluorofuroylacetonato (tffu), **7**; trifluorobenzoylacetonato (tfba), **8**; hexafluoroacetylacetonato (hfac), **9**) which formed part of a previous study. The trend found in the previous study concluded that the more electron donating the R-groups (lower sum of the Gordy scale electronegativities $3(\chi_R + \chi_{R'})$ value) are on the β-diketonato ligand backbone (RCOCHCOR')⁻, the more the reduction potential will shift to more negative potentials. As expected for [Mn(dpm)₃] with six electron donating *t*Bu groups, the reduction potential of [Mn(dpm)₃] was observed at a greater negative potential than complexes **1** - **9**. Results of a computational chemistry study on the OLYP/TZP level, concluded that the [Mn(dpm)₃] complex preferred the elongation Jahn-Teller distortion (80%) over the compression distortion (20%).

Goals iii-iv) 2-D amino-functionalized Si-wafers were successfully prepared through a three step process. First the Si-wafer was oxidized forming an -O-Si-O- layer on top of the wafer (**S2**), secondly this silicon oxide layer was hydroxylated forming silanol (-Si-OH) groups on the surface (**S3**) and finally 3-aminopropyltrimethoxysilane was covalently bound to the hydroxylated Si-wafer surface forming the amino-functionalized Si-wafer (**S4**). XPS analysis confirmed that the amino-functionalized Si-wafer was prepared by comparing the C 1s XPS spectra of the hydroxylated Si-wafer, **S3**, with that of the amino-functionalized Si-wafer, **S4**. An increase in the C 1s peak intensity of **S4** relative to **S3**'s C 1s peak intensity was observed. This peak intensity

change indicates that for the amino-functionalized surface more C is present in **S4** than in **S3**. The C 1s spectra of the **S4** surface also showed an extra peak at higher binding energy that was attributed to -C-N-. The peak deconvolution of the Si 2p spectra of **S4** showed the presence of three silicon environments (-O-Si-O-, -O-Si-OH and -O-Si-CH$_2$-). The -O-Si-CH$_2$- is assigned to the silane bound to the surface. The ratios of the silicon peaks (0.35:1.85:1; -O-Si-O- : -O-Si-OH : -O-Si-CH$_2$-) indicates that for every Si bound to a silane there are ~2 unbound Si-OH groups. The **S4** surface also has an N 1s XPS spectra which is another indication that the hydroxylated Si-wafer was successfully functionalized with a silane linker.

The preparation of eight covalently bound [Mn(β-diketonato)$_3$] complexes (**2-9**) on amino-functionalized Si-wafers forming **S5**-**S12** respectively, gave small amounts of the aimed binding mode, while the rest decomposed to oxides. XPS studies showed that the Mn:F ratios expected for fluorine containing [Mn(β-diketonato)$_3$] complexes were not achieved. It was confirmed that the Mn 2p photoelectron line consists mostly of Mn$_2$O$_3$ by grafting Mn$_2$O$_3$ onto a hydroxylated Si-wafer (**S3**, forming **S13**) and amino-functionalized surface (**S4**, forming **S14**). It was found that the binding energies of the Mn 2p photoelectron lines correlates with Mn$_2$O$_3$ on the Si-OH surface and not that of the Mn$_2$O$_3$ that has interactions with the amino-functional group. Furthermore the XPS results of a neat [Mn(tfaa)$_3$] complex that was exposed to the grafting process conditions showed that *ca.* 80 % of the complex decomposed to Mn$_2$O$_3$.

Computational chemistry was used to optimize the ideal geometry of [Mn(β-diketonato)$_3$] complexes grafted onto amino-functionalized Si-wafers if no decomposition took place. The [Mn(β-diketonato)$_3$] complexes was modified by substituting one of the oxygen atoms with an amine (NH). This modification was done to mimic the environment that will be found on the amino-functionalized Si-wafers. Eight possible isomers were identified when the [Mn(β-diketonato)$_3$] complexes contains unsymmetrical β-diketonato ligands. All the isomers optimized to an elongation (in the *z*-direction) Jahn-Teller geometry with the amine in the *xy*-plane.

Goal v) The catalytic testing of four [Mn(β-diketonato)$_3$] 2-D model catalysts ([Mn(acac)$_3$], **S5**; [Mn(dbm)$_3$], **S7**; [Mn(tfaa)$_3$], **S8**; and [Mn(hfaa)$_3$] **S12**) by monitoring the catalytic reaction of hexamethylenediisocyante (HDI) and ethanol (formation of hexamethylenediurethane (HDU)) using ATR FTIR was successful. The TOF of the 2-D model catalysts are an estimate of all the Mn species present on the support surface (both [Mn(β-diketonato)$_3$] and Mn$_2$O$_3$) The turnover frequency (TOF) of each of the 2-D model catalysts during the catalytic reaction indicated that the electron withdrawing or donating properties of the R-groups on the β-diketonato ligands play an

overall role in the catalytic activity of the 2-D model catalyst. As the total Gordy group electronegativity ($\chi_R + \chi_{R'}$) increased a general decrease in TOF was observed.

Goals vi-vii) In addition to the preparation of 2-D model [Mn(β-diketonato)$_3$] catalyst on amino-functionalized Si-wafers, [Mn(β-diketonato)$_3$] complexes **1-8** were impregnated onto 3-D supports through the wetness impregnation method. The binding mode is through hydrogen bonding. [Mn(β-diketonato)$_3$] complexes **1-8** were impregnated onto SiO_2, where [Mn(acac)$_3$], **2**, and [Mn(tfaa)$_3$], **5**, was also impregnated onto MgO, TiO_2, alkaline KL-zeolites and acidic HY-zeolites. The success of the impregnation of the catalyst on the 3-D supports was confirmed by XPS and the thermal stability of [Mn(acac)$_3$], **2**, and [Mn(tfaa)$_3$], **5**, impregnated onto SiO_2, MgO, TiO_2, alkaline KL-zeolites and acidic HY-zeolites was tested by TGA. The binding energies of Mn 2p peaks of the different [Mn(β-diketonato)$_3$] complexes on the 3-D supports are shifted ~3 eV to higher binding energies relative to the Mn 2p peak of Mn^0, indicating that Mn^{3+} species are present on the supports. The spin orbit splitting of the two Mn 2p peaks of the [Mn(β-diketonato)$_3$] complexes impregnated onto the 3-D supports (average 11.61 eV) are comparable with the spin orbit splitting observed for the [Mn(β-diketonato)$_3$] complexes that is grafted onto amino-functionalized Si-wafers. The full width half maximum (FWHM) values of the Mn 2p peaks of the [Mn(β-diketonato)$_3$] - 3D complexes with unsymmetrical β-diketonato ligands (R $\neq$ R') are larger than the FWHM of [Mn(β-diketonato)$_3$]-3D complexes with symmetrical β-diketonato ligands (R = R'), which is an indication of the presence of more than one [Mn(β-diketonato)$_3$] isomer present on the surface, attributed to the possible *fac* and *mer* isomers of the complexes.

The TGA of the neat [Mn(acac)$_3$] complex with a total % mass loss of 62.39 % indicated that the possible decomposition product is MnO_2 with trapped CO_2 with a theoretical % mass loss of 62.83 %. All the [Mn(acac)$_3$], **2**, impregnated onto SiO_2, **S14**; MgO, **S21**; TiO_2, **S22**; acidic HY-zeolites, **S23**; and alkaline KL-zeolites, **S24**, showed 5, 3, 4, 2 and 2 mass loss steps during the thermogravimetric analyses (TGA) respectively. Taking into consideration, the decomposition product of the neat [Mn(acac)$_3$] complex, the % Mn loaded onto the 3-D supports was calculated. The % Mn loaded onto the 3-D support was the highest for MgO (% Mn_{loaded} = 7.39 %), followed by SiO_2 (2.96 %), basic zeolite (2.20 %), acidic zeolite (1.41 %) and TiO_2 (0.44 %). TGA of the [Mn(acac)$_3$] complex impregnated onto SiO_2, **S14**, heat treated at 100, 130, 250 and 350 °C showed the [Mn(acac)$_3$] complex losing β-diketonato ligands as temperature is increased with a final Mn-oxide species as a result at 350 °C.

The TGA of the neat [Mn(tfaa)$_3$] complex with a total % mass loss of 50.56 % indicated that the possible decomposition product is Mn_2O_3 with a theoretical % mass loss of 69.30 % (closest

calculated to actual % mass loss). All the [Mn(tfaa)$_3$], **5**, impregnated onto SiO$_2$, **S17**; MgO, **S25**; TiO$_2$, **S26**; acidic HY-zeolites, **S27**; and alkaline KL-zeolites, **S28**, showed 4, 4, 7, 3 and 3 mass loss steps during the thermogravimetric analyses (TGA) respectively. Taking consideration, the decomposition product of the neat [Mn(tfaa)$_3$] complex the % Mn loaded onto the 3-D supports was calculated. The % Mn loaded onto the 3-D is the highest for MgO (% Mn$_{loaded}$ = 7.47 %), followed by basic zeolite (4.87 %), acidic zeolite (4.36 %), SiO$_2$ (3.57 %) and TiO$_2$ (2.56 %).

Goal viii) The catalytic testing of the [Mn(acac)$_3$] complex impregnated onto SiO$_2$, **S14**, as is as well as the heat treated at 100, 130, 250 and 350 °C samples by monitoring the catalytic reaction of hexamethylenediisocyante (HDI) and ethanol (formation of hexamethylenediurethane (HDU)) using ATR FTIR was successful. The TOF of the [Mn(acac)$_3$] complex impregnated onto SiO$_2$ heat treated at 100 °C before the catalytic testing has the highest TOF (10.3 s^{-1}), which is most probably due to the loss of one β-diketonato ligand.

5.1.2 Tris(acetylacetonate)metal(III), [M(acac)$_3$] (M = Cr, Fe, Co, Rh and Ir)

Goals iii - v) The preparation of three covalently bound [M(acac)$_3$] complexes (M = Cr, **10**; Rh, **13**; and Ir, **14**) on 2-D amino-functionalized Si-wafers, forming **S29**-**S31** respectively, was successful. XPS studies of the 2-D model catalysts **S29**-**S31**, showed that the M^{+3} is present on the surfaces. The [Rh(acac)$_3$] grafted on amino-functionalized Si-wafer, **S30**, is the only one of the three that showed the presence of another Rh-metal specie on the surface. It was concluded that the second Rh specie on the surface was Rh$_2$O$_3$.

The catalytic testing of three [M(acac)$_3$] 2-D model catalysts ([Cr(acac)$_3$], **S29**; [Rh(acac)$_3$], **S30**, and [Ir(acac)$_3$], **S31**), by monitoring the catalytic reaction of hexamethylenediisocyante (HDI) and ethanol (formation of hexamethylenediurethane (HDU)) using ATR FTIR was successful. The turnover frequency (TOF) of each of the 2-D model catalyst during the catalytic reaction indicated that the Pauling electronegativity of the metal centre plays a role in the catalytic activity of the 2-D model catalyst. As the Pauling electronegativity of the metal increased a general increase in TOF was observed. The greater electronegativity of the metal centre indicates that the metal centre attracts electron density from the ligands stronger and in turn makes the metal centre of the [M(acac)$_3$] complex immobilized onto the amino-functionalized Si-wafer surface more electron rich.

194

Goals vi-viii) The impregnation of [M(acac)$_3$] (M = Cr, Fe, Co, Rh and Ir) onto 3-D SiO$_2$ support was successful through the wetness impregnation method and was attached to the surface through hydrogen bonding. This was confirmed by XPS analysis of the resulting 3-D [M(acac)$_3$] catalyst. The respective metal peak of all the [M(acac)$_3$] complexes were observed at ~3 eV higher in binding energy when compared to the known M^0 species, confirming that the metal species on the support is that of M^{3+} which is expected of [M(acac)$_3$] complexes.

The TGA of the neat [M(acac)$_3$] complexes (M = Cr, **10**; Fe, **11**, and Co, **12)** with a total % mass loss of 94.84 %, 89.04 % and 83.11 %, indicated that the possible decomposition product of all the [M(acac)$_3$] complexes, are their respective metal centres with a theoretical % mass loss of 85.12 %, 84.19 % and 83.46 % (closest calculated to actual % mass loss). The [M(acac)$_3$], immobilized onto SiO$_2$ (M = Cr, **S32**; Fe, **S33**, and Co, **S34**), showed 2, 3, and 3 mass loss steps during the thermogravimetric analyses (TGA) respectively. Taking consideration, the decomposition product of the neat [M(acac)$_3$] complexes the % M loaded onto the 3-D supports was calculated. The % M loaded as [M(acac)$_3$], immobilized onto SiO$_2$ 3-D catalysts, are Cr (1.03 %), Mn (2.98 %), Fe (0.90 %) and Co (0.75 %). The Pauling electronegativity of the metal centre plays a role in the %M loaded onto the SiO$_2$ 3-D support. As the Pauling electronegativity increased a general decrease in %M loaded onto the SiO$_2$ 3-D support was observed. The linear equation describing the correlation between the [M(acac)$_3$] metal centre Pauling electronegativity and the % metal loaded onto the SiO$_2$ is given by:

$$M_{Electronegativity} = (-5.82)(\%M_{loaded}) + 11.48 \qquad R^2 = 0.71$$

5.1.3 Chromium(0) Fischer Carbene Complexes

Goal i) Four Cr(0) Fischer carbene complexes were studied in this thesis namely, [Cr(CO)$_4$(PPh$_3$)=C(OEt)(Fu)], **C1**; [Cr(CO)$_5$=C(NHCy)(Fu)], **C2**; [Cr(CO)$_5$=C(NHCy)(Th)], **C3** and [Cr(CO)$_5$=C(OEt)(ThTh)], **C4**. The possible isomers/conformations are as follows; [Cr(CO)$_4$(PPh$_3$)=C(OEt)(Fu)], **C1**, has six possible isomer-conformation mixtures (*cis(1)-syn*, *cis(1)-anti*, *cis(2)-syn*, *cys(2)-anti*, *trans-syn* and *trans-anti*), [Cr(CO)$_5$=C(NHCy)(Fu)], **C2**, and [Cr(CO)$_5$=C(NHCy)(Th)], **C3**, both has four possible conformations (*Z-syn*, *Z-anti*, *E-syn* and *E-anti*) and [Cr(CO)$_5$=C(OEt)(ThTh)], **C4**, can obtain the following four conformations *syn-syn*, *syn-anti*, *anti-syn* and *anti-anti*. By the use of computational chemistry on the B3LYP/6-311G(d,p) (all atoms except Cr), def2-TZVPP (Cr) level and the Boltzmann equation, the %population possibility of each isomer/conformation of these four Fischer carbene complexes (FCCs) were calculated.

Goals ii-iv) The oxidation of the metal centres and the reduction of the carbene ligands of the four chromium FCCs were studied by cyclic voltammetry. The chromium centre is oxidized from Cr^0 to a Cr^{1+} specie. The oxidation process of **C1** is electrochemically reversible (ΔE = 57 mV at scan rate 0.10 $mV.s^{-1}$) and chemically quasi-reversible, **C2-C4** are all electrochemically and chemically quasi-reversible. The oxidation process of **C1** shows the oxidation of both the *trans-* and the *cis* isomer. Through computational chemistry it is found that the highest occupied molecular orbital (HOMO) of the *cis* isomer is lower in energy (more stable) than that of the *trans* isomer. Therefore greater amount of energy is needed for the removal of an electron (oxidation) of the *cis* isomer. This concludes that the oxidations peak at higher potential is that of the *cis* isomer. The **C3** complex also showed the splitting of the chromium oxidation process. This splitting is attributed to the *Z* and the *E* isomers. Computational chemistry results concluded that the HOMO energy of the different *E* isomers of **C3** are all higher than that of the possible *Z* isomers. Therefore it will be easier for the *E* isomers to be oxidized and will be found at lower potentials in the oxidation process of cyclic voltammetry analysis. The FCC **C2** which is similar to **C3** does not show the splitting of the oxidation peaks in the cyclic voltammetry analysis. Computational chemistry shows that the HOMO energy of the *Z* isomers are not consistently higher than those of its *E* isomers. This is consistent with the oxidation potential of the *Z* and *E* isomers of **C2** to be closely overlapping. It is the first time that the splitting of the oxidation peaks of the *E-* and *Z* isomers of **C3** is observed and was not seen in similar tungsten carbene complexes ($[W(CO)_5=C(NHCy)(Fu)]$ and $[W(CO)_5=C(NHCy)(Th)]$).

The electrochemical results of the **C1-C4** as well as previously published electrochemical results of related Cr(0) Fischer carbene complexes, were compared to computational chemistry results. The relationship between the redox potentials of the oxidation process (E_{pa}) and that of the reduction process (E_{pc}) with the computationally calculated energies of the HOMO and lowest unoccupied molecular orbital (LUMO) respectively, are represented by the following linear equations:

$$E_{pa} = (-0.752)(E_{HOMO}) - 3.91 \qquad\qquad R^2 = 0.97$$

$$E_{pc} = (-0.687)(E_{LUMO}) - 3.50 \qquad\qquad R^2 = 0.94$$

Goals v-vi) The $[Cr(CO)_5=C(OEt)(Fu)]$, **C5**, and $[Cr(CO)_5=C(OEt)(Th)]$, **C6**, complexes were successfully grafted onto the amino-functionalized Si-wafers forming **C7** and **C8** respectively. The covalent anchoring of **C5** and **C6** onto the amino-functionalized Si-wafers was confirmed by XPS. When comparing the Cr $2p_{3/2}$ binding energies of **C5** and **C6** (574.64 and 574.38 eV respectively) with the Cr $2p_{3/2}$ binding energies of the grafted complexes **C7** and **C8** (577.14 and 576.57 eV respectively), it clearly shows how complexation onto the

amino-functionalized Si-wafer decreases the electron density on the chromium (thus an increased binding energy). This increase in binding energies was also observed [**C5** and **C6** (574.64 and 574.38 eV respectively)] when the ethoxy group was replaced by the aminocyclohexane [**C2** and **C3** (576.95 and 576.41 eV respectively)], giving further confirmation that the complexes did bind to the amino-functionalized Si-wafer.

5.2 Future perspectives.

The [Mn(β-diketonato)$_3$] complex series study can be expanded as follows:

   i.   Optimizing the grafting of the [Mn(β-diketonato)$_3$] complexes onto amino-functionalized Si-wafers.

   ii.   Do an in-depth study of the binding and activation as well as a catalytic study on the [Mn(β-diketonato)$_3$] complexes immobilized onto 3-D supports, to evaluate the catalytic activity of these complexes. Determine the effect of the different β-diketonato ligands on the catalytic activities.

The [M(acac)$_3$] complex series study can be expanded as follows:

   i.   Do a catalytic study on the [M(acac)$_3$] complexes (M=Co, Cr, Fe, Rh and Ir) immobilized onto 3-D supports, to evaluate the catalytic activity of these complexes. Determine the effect of the metal centre on the catalytic activities. Link this to possible industrial processes.

The Cr(0) Fischer carbenes (FCCs) series study can be expanded as follows:

   i.   The grafting of various Cr(0) Fischer carbenes onto 2-D and 3-D supports.

   ii.   Evaluating the catalytic activity of these 2-D model and 3-D catalysts, in order to determine the effect the metal centre and different ligands have on the catalytic activity.

   iii. Linking these catalysts to possible industrial processes.

A Appendix

A. Cyclic Voltammetry data.

Table A.1: The electrochemical data of the [Mn(dpm)$_3$]. Measurements were performed on 0.5 mM analyte in 0.1 M [^{n}(Bu$_4$)N][PF$_6$]/DCM on a glassy carbon working electrode; the CV initiated in the direction of the arrow. The CV is referenced against ferrocene as an internal standard.

Scan Rate (V.s^{-1})	Mn^{III} / Mn^{II}							Mn^{III} / Mn^{IV}						
	E_{pa} (V)	E_{pc} (V)	ΔE (V)	$\frac{E_{pc} - E_{pa}}{2}$ (V)	i_{pa} (μA)	i_{pc} (μA)	i_{pa}/i_{pc}	E_{pa} (V)	E_{pc} (V)	ΔE (V)	$\frac{E_{pc} - E_{pa}}{2}$ (V)	i_{pa} (μA)	i_{pc} (μA)	i_{pc}/i_{pa}
0.05	-0.510	-1.422	0.913	-0.966	0.33	3.21	0.10	0.478	0.089	0.389	0.283	1.04	0.69	0.67
0.10	-0.500	-1.427	0.926	-0.964	0.40	3.60	0.11	0.502	0.080	0.422	0.291	1.04	0.69	0.67
0.15	-0.501	-1.432	0.931	-0.966	0.52	4.25	0.12	0.502	0.078	0.424	0.290	1.05	0.73	0.70
0.20	-0.481	-1.435	0.954	-0.958	0.52	4.41	0.12	0.523	0.076	0.447	0.299	1.20	0.83	0.69
0.25	-0.461	-1.499	1.039	-0.980	0.60	5.29	0.11	0.547	0.108	0.439	0.327	1.67	1.19	0.71
0.30	-0.452	-1.507	1.055	-0.980	0.60	5.33	0.11	0.560	0.105	0.455	0.332	1.69	1.19	0.70
0.50	-0.447	-1.525	1.078	-0.986	0.71	6.64	0.11	0.579	0.097	0.482	0.338	2.14	1.43	0.67
1.0								0.533	0.039	0.494	0.286	9.27	5.37	0.58
5.0								0.668	-0.030	0.698	0.319	14.63	7.80	0.53
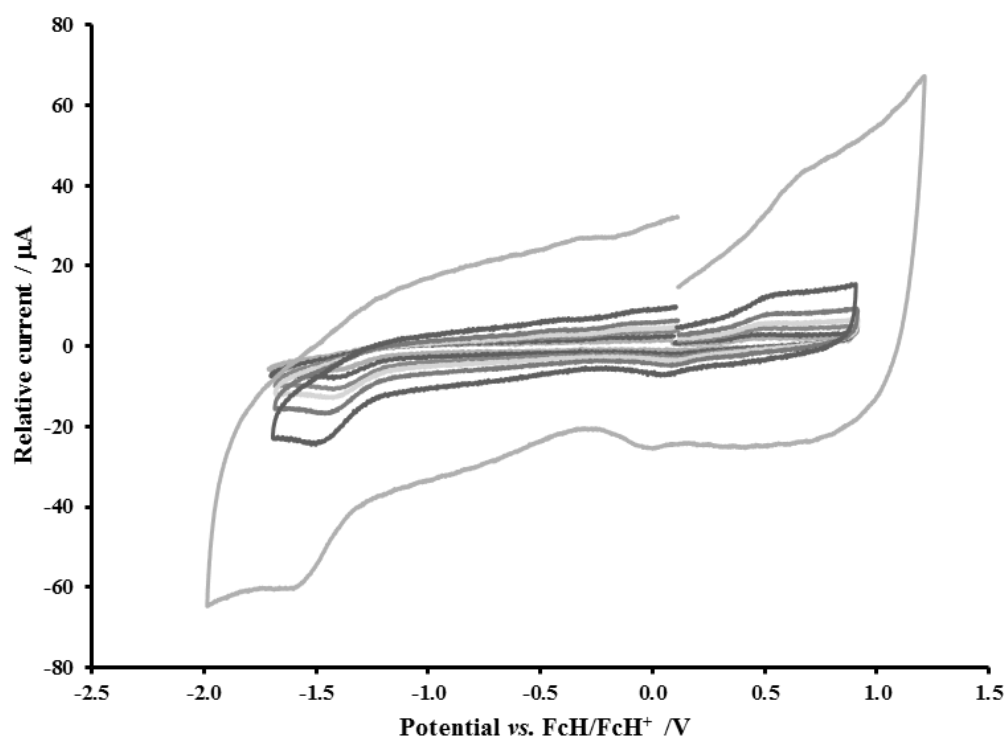
Figure A.1: Cyclic voltammogram of Mn(dpm)$_3$, **1**, at a scan rate of 0.05 – 5.0 V.s^{-1}. Measurements were performed on 0.5 mM analyte in 0.1 M [^{n}(Bu$_4$)N][PF$_6$]/DCM on a glassy carbon working electrode; the CV initiated in the direction of the arrow. The CV is referenced against ferrocene as an internal standard.

Table A.2: The first reduction electrochemical data of the Fischer carbene complex [Cr(CO)$_4$(PPh$_3$)=C(OEt)(Fu)], **C1**. Measurements were performed in on 1.0 mM analyte in 0.1 M [^{n}(Bu$_4$)N][PF$_6$]/CH$_3$CN on a glassy carbon working electrode with ferrocene as an internal standard.

Scan Rate (V.s^{-1})	First Reduction	
	E_{pc} (V)	i_{pc} (μA)
0.050	-1.899	2.55
0.100	-1.900	4.09
0.150	-1.909	5.57
0.200	-1.918	7.07
0.250	-1.921	8.26
0.300	-1.924	9.02
0.500	-1.929	10.92
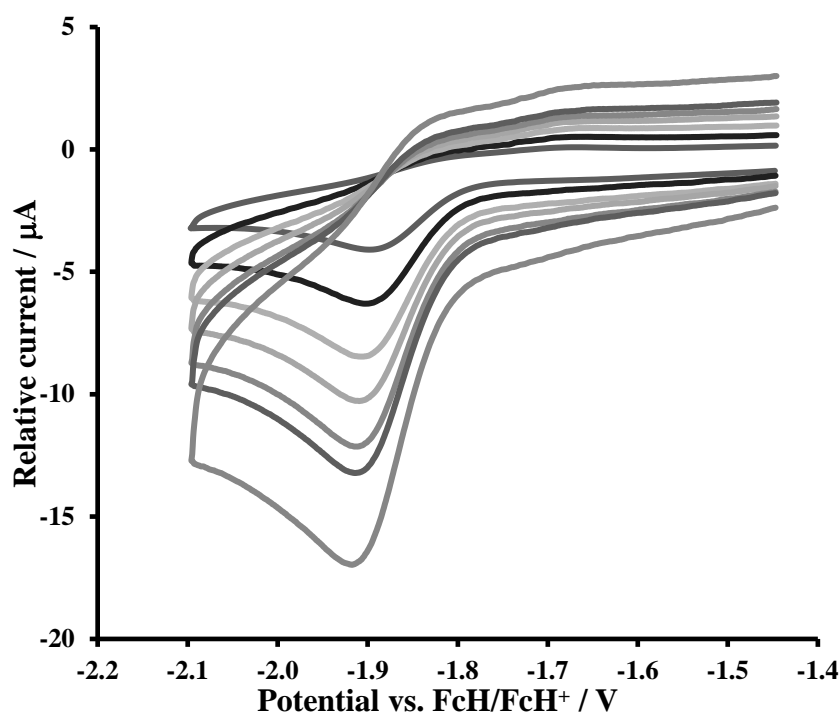
Figure A.2: First reduction peak of cyclic voltammorgram of $[Cr(CO)_4(PPh_3)=C(OEt)(Fu)]$, **C1**. Measurements were performed in on 1.0 mM analyte in 0.1 M $[^n(Bu_4)N][PF_6]/CH_3CN$ on a glassy carbon working electrode with ferrocene as an internal standard.
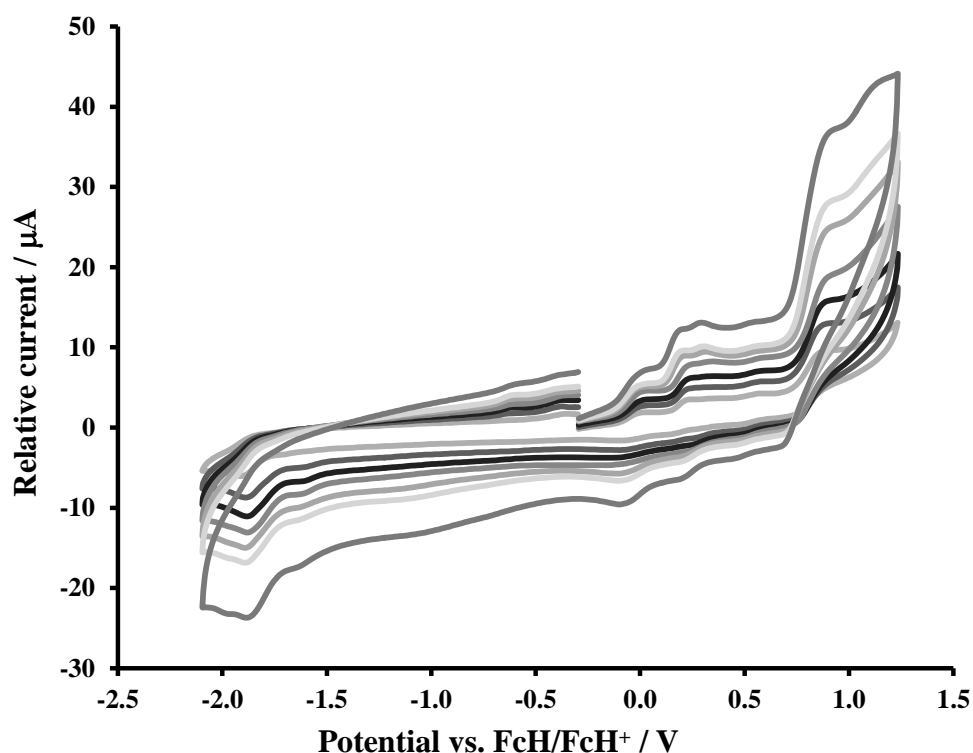
Figure A.3: Full cyclic voltammorgram of $[Cr(CO)_4(PPh_3)=C(OEt)(Fu)]$, **C1**, with unwanted side products. Measurements were performed in on 1.0 mM analyte in 0.1 M $[^n(Bu_4)N][PF_6]/CH_3CN$ on a glassy carbon working electrode with ferrocene as an internal standard.

Table A.3: Electrochemical data obtained of the Fischer carbene complex [Cr(CO)$_5$=C(NHCy)(Fu)], **C2**. Measurements were performed in on 1.0 mM analyte in 0.1 M [^{n}(Bu$_4$)N][PF$_6$]/CH$_3$CN on a glassy carbon working electrode with ferrocene as an internal standard.

Scan Rate (V.s^{-1})	First oxidation					First Reduction				
	E_{pa} (V)	E_{pc} (V)	ΔE (V)	$E^{0'}$ (V)	i_{pa}/i_{pc}	E_{pc} (V)	E_{pa} (V)	ΔE (V)	$E^{0'}$ (V)	i_{pc}/i_{pa}
0.050	0.430	0.297	0.133	0.363	-	-	-2.268	-	-1.179	-
0.100	0.432	0.287	0.145	0.359	-	-	-2.278	-	-1.184	-
0.150	0.434	0.282	0.152	0.358	-	-	-2.279	-	-1.184	-
0.200	0.439	0.264	0.175	0.351	-	-	-2.284	-	-1.187	-
0.250	0.445	0.273	0.172	0.359	0.23	-2.186	-2.284	0.098	-2.235	0.23
0.300	0.446	0.268	0.177	0.357	0.27	-2.186	-2.286	0.099	-2.236	0.27
0.500	0.456	0.254	0.202	0.355	0.31	-2.188	-2.288	0.101	-2.238	0.31
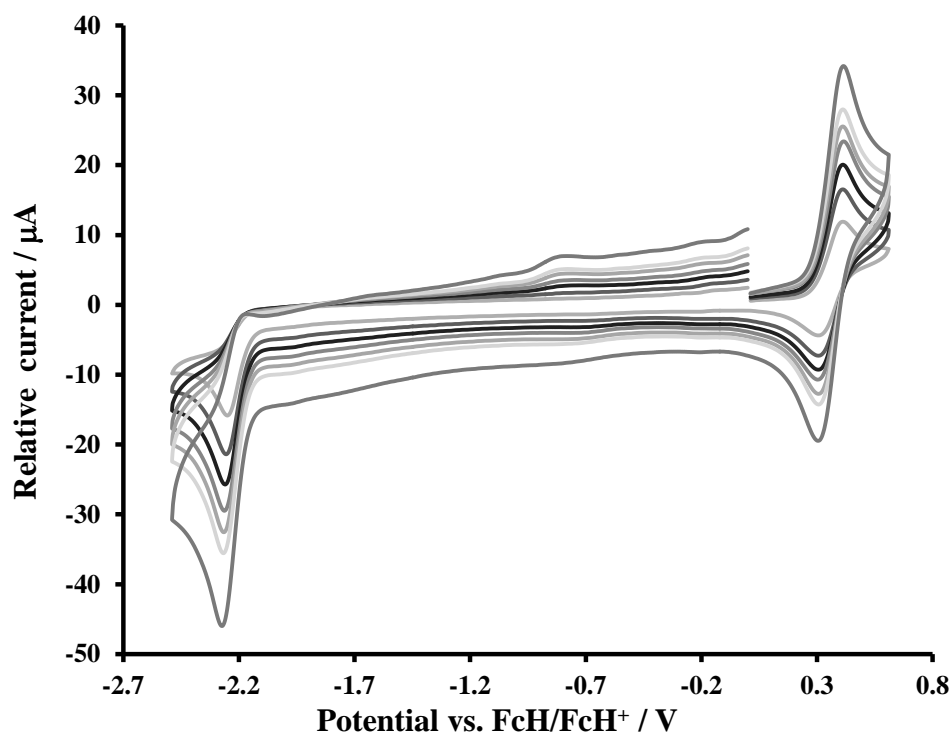
Figure A.4: First oxidation and reduction peaks of cyclic voltammorgram of [Cr(CO)$_5$=C(NHCy)(Fu)], **C2**. Measurements were performed in on 1.0 mM analyte in 0.1 M [^{n}(Bu$_4$)N][PF$_6$]/CH$_3$CN on a glassy carbon working electrode with ferrocene as an internal standard.
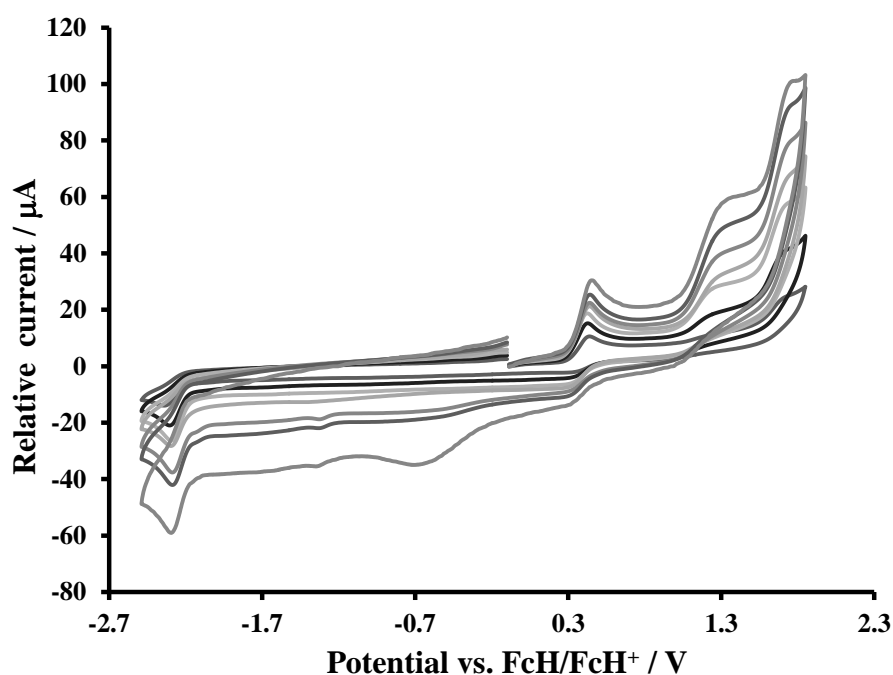
Figure A.5: Full cyclic voltammorgram of [Cr(CO)$_5$=C(NHCy)(Fu)], **C2**, with unwanted side products. Measurements were performed in on 1.0 mM analyte in 0.1 M [^{n}(Bu$_4$)N][PF$_6$]/CH$_3$CN on a glassy carbon working electrode with ferrocene as an internal standard.

Table A.4: Electrochemical data obtained of the Fischer carbene complex [Cr(CO)$_5$=C(NHCy)(Th)], **C3**. Measurements were performed in on 1.0 mM analyte in 0.1 M [^{n}(Bu$_4$)N][PF$_6$]/CH$_3$CN on a glassy carbon working electrode with ferrocene as an internal standard.

Scan Rate (V.s^{-1})	Oxidation						First Reduction				
	1st					2nd					
	E$_{pa}$ (V)	E$_{pc}$ (V)	ΔE (V)	E$^{0'}$ (V)	i_{pa}/i_{pc}	E$_{pa}$ (V)	E$_{pc}$ (V)	E$_{pa}$ (V)	ΔE (V)	E$^{0'}$ (V)	i_{pc}/i_{pa}
0.050	0.455	0.323	0.131	0.389	0.41	0.563	-2.147	-	-	-	-
0.100	0.456	0.323	0.133	0.389	0.50	0.569	-2.148	-	-	-	-
0.150	0.458	0.320	0.138	0.389	0.61	0.578	-2.149	-	-	-	-
0.200	0.458	0.318	0.140	0.388	0.61	0.581	-2.154	-	-	-	-
0.250	0.459	0.317	0.142	0.388	0.40	0.582	-2.153	-2.058	0.095	-2.106	0.363
0.300	0.460	0.316	0.144	0.388	0.40	0.582	-2.158	-2.058	0.100	-2.108	0.410
0.500	0.469	0.312	0.157	0.391	0.43	0.591	-2.160	-2.060	0.100	-2.110	0.472
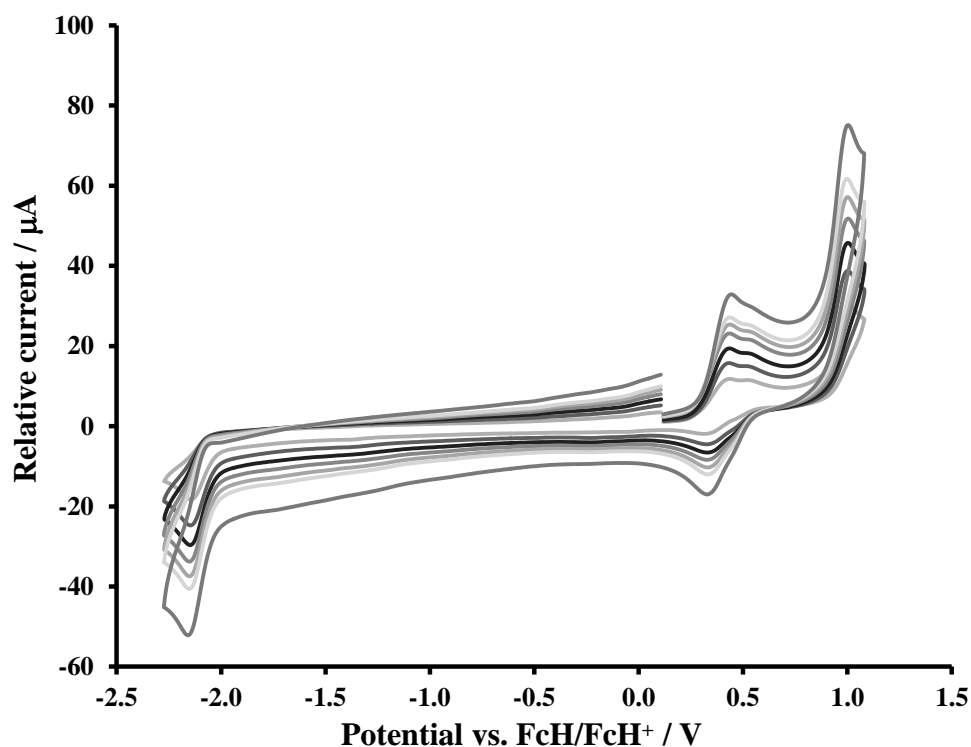
Figure A.6: Full cyclic voltammorgram of [Cr(CO)$_5$=C(NHCy)(Th)], **C3**, with unwanted side products. Measurements were performed in on 1.0 mM analyte in 0.1 M [^{n}(Bu$_4$)N][PF$_6$]/CH$_3$CN on a glassy carbon working electrode with ferrocene as an internal standard.

Table A.5: Electrochemical data obtained of the Fischer carbene complex $[Cr(CO)_5=C(OEt)(ThTh)]$, **C4**. Measurements were performed in on 1.0 mM analyte in 0.1 M $[^n(Bu_4)N][PF_6]/CH_3CN$ on a glassy carbon working electrode with ferrocene as an internal standard.

Scan Rate (V.s^{-1})	First oxidation					First Reduction				
	E_{pa} (V)	E_{pc} (V)	ΔE (V)	$E^{0'}$ (V)	i_{pa}/i_{pc}	E_{pc} (V)	E_{pa} (V)	ΔE (V)	$E^{0'}$ (V)	i_{pc}/i_{pa}
0.050	0.531	0.429	0.102	0.480	0.56	-1.423	-1.491	0.067	-1.457	0.72
0.100	0.531	0.429	0.102	0.480	0.65	-1.489	-1.423	0.066	-1.456	0.8
0.150	0.532	0.428	0.104	0.480	0.70	-1.423	-1.489	0.066	-1.456	0.83
0.200	0.532	0.428	0.104	0.480	0.73	-1.423	-1.488	0.066	-1.455	0.83
0.250	0.534	0.429	0.105	0.481	0.62	-1.422	-1.488	0.066	-1.455	0.74
0.300	0.535	0.427	0.108	0.481	0.65	-1.423	-1.489	0.066	-1.456	0.79
0.500	0.538	0.424	0.114	0.481	0.67	-1.420	-1.491	0.070	-1.455	0.86
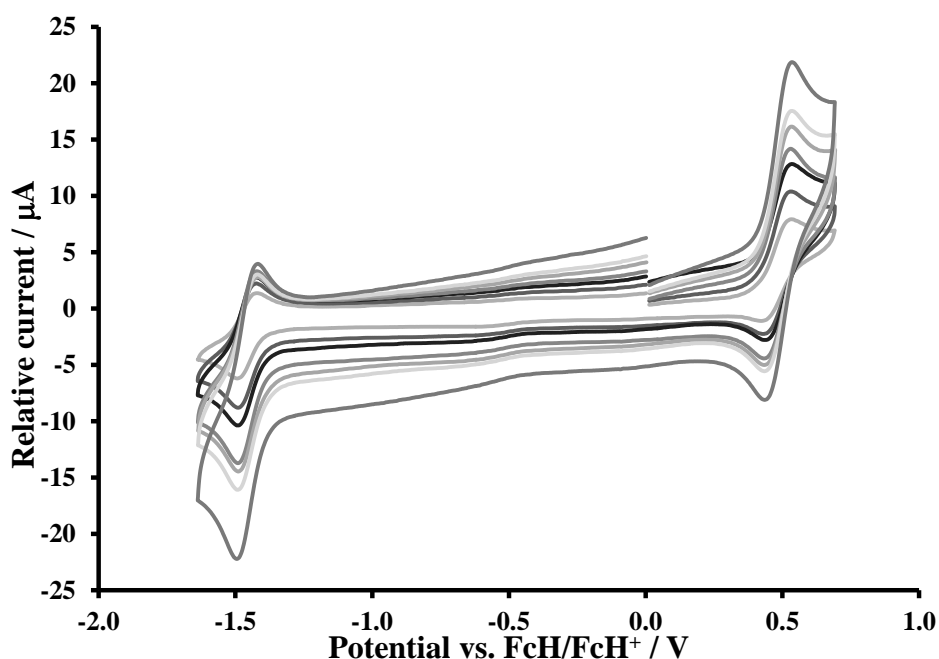
Figure A.7: First oxidation and reduction peaks of cyclic voltammorgram of $[Cr(CO)_5=C(OEt)(ThTh)]$, **C4**. Measurements were performed in on 1.0 mM analyte in 0.1 M $[^n(Bu_4)N][PF_6]/CH_3CN$ on a glassy carbon working electrode with ferrocene as an internal standard.
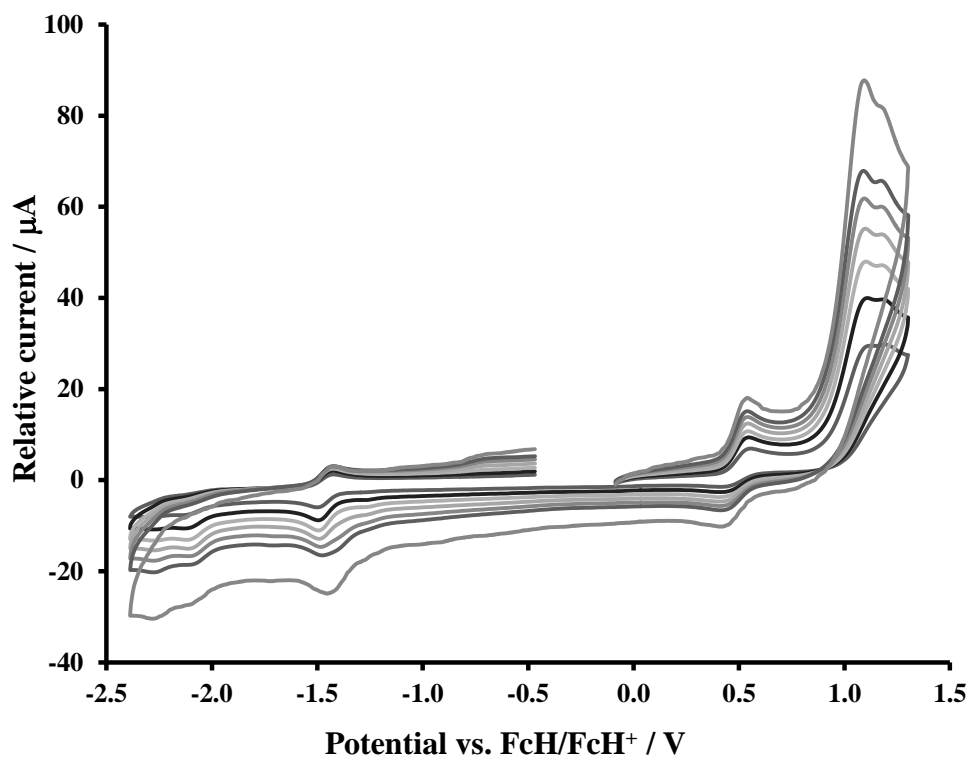
Figure A.8: Full cyclic voltammorgram of [Cr(CO)$_5$=C(OEt)(ThTh)], **C4**, with unwanted side products. Measurements were performed in on 1.0 mM analyte in 0.1 M [^{n}(Bu$_4$)N][PF$_6$]/CH$_3$CN on a glassy carbon working electrode with ferrocene as an internal standard.

B. X-ray photoelectron spectroscopy (XPS) data
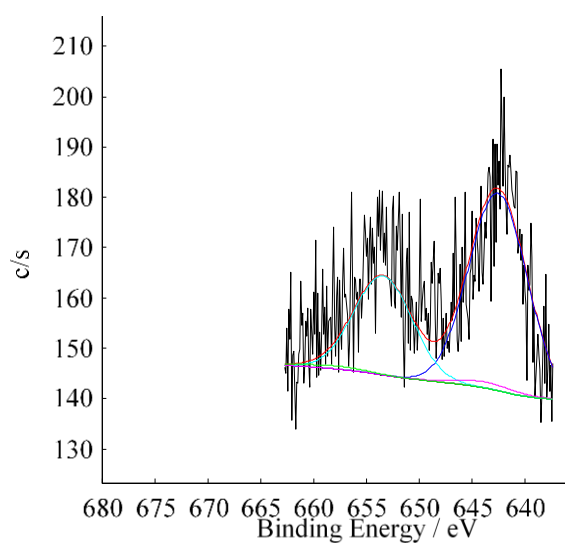
Figure B.1: The deconvolution of the Mn 2p photoelectron XPS lines of [Mn(tffu)$_3$], **7**.
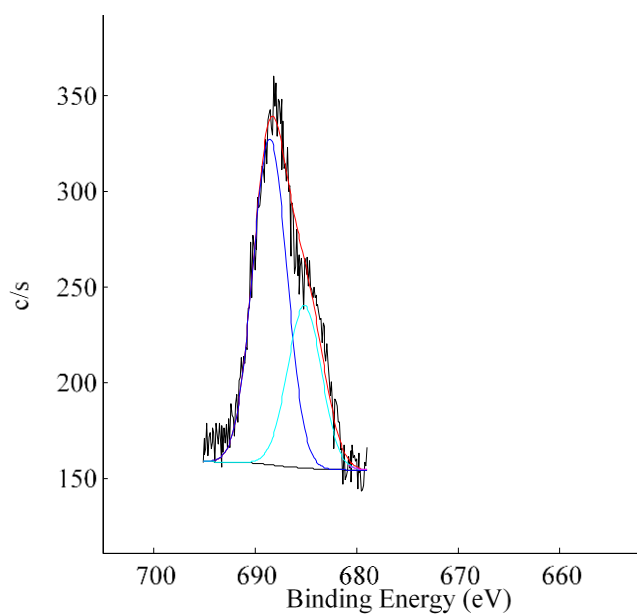
Figure B.2: The deconvolution of the F 1s photoelectron XPS line of [Mn(tffu)$_3$], **7**.
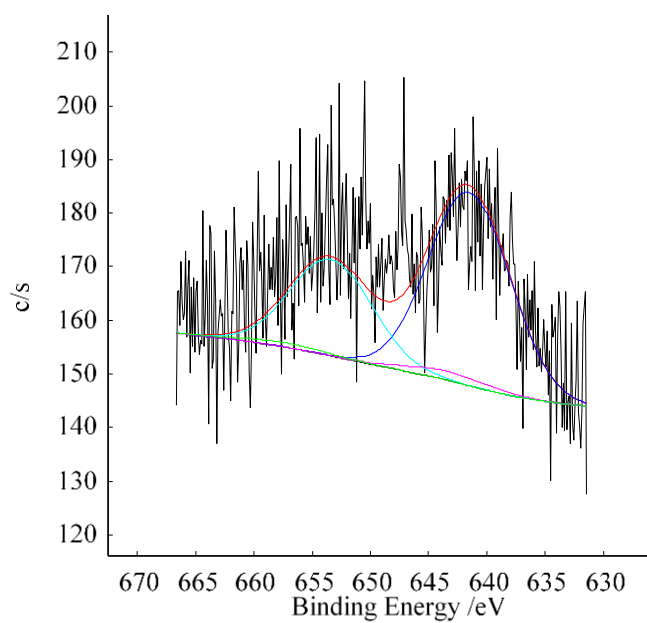
Figure B.3: The deconvolution of the Mn 2p photoelectron XPS lines of [Mn(tfba)$_3$], **8**.
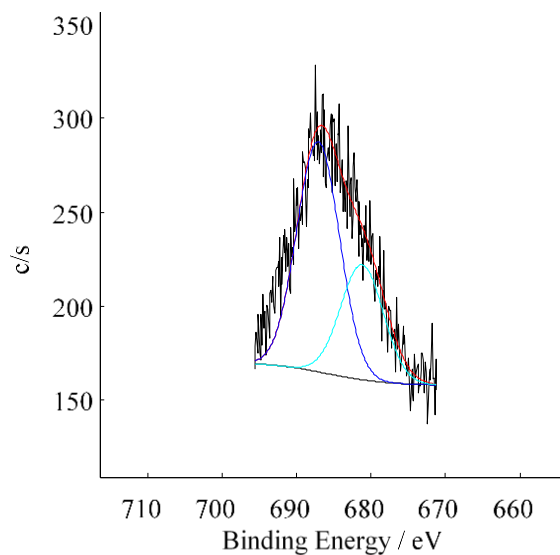
Figure B.4: The deconvolution of the F 1s photoelectron XPS line of [Mn(tfba)$_3$], **8**.
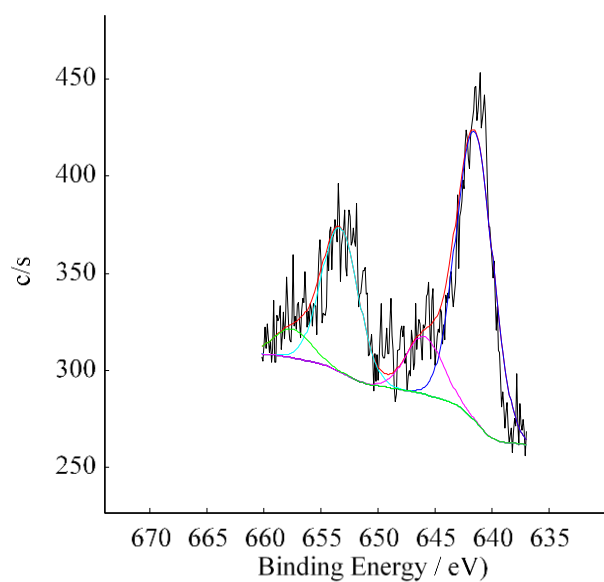
Figure B.5: The fitting (deconvolution) of the [Mn(acac)₃] complex grafted onto the amino-functionalized Si-wafer, **S5**, Mn 2p XPS peak.
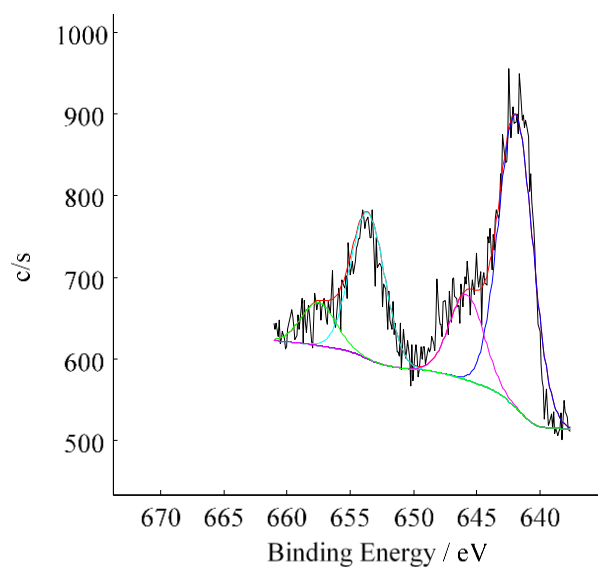
Figure B.6: The fitting (deconvolution) of the [Mn(ba)₃] complex grafted onto the amino-functionalized Si-wafer, **S6**, Mn 2p XPS peak.
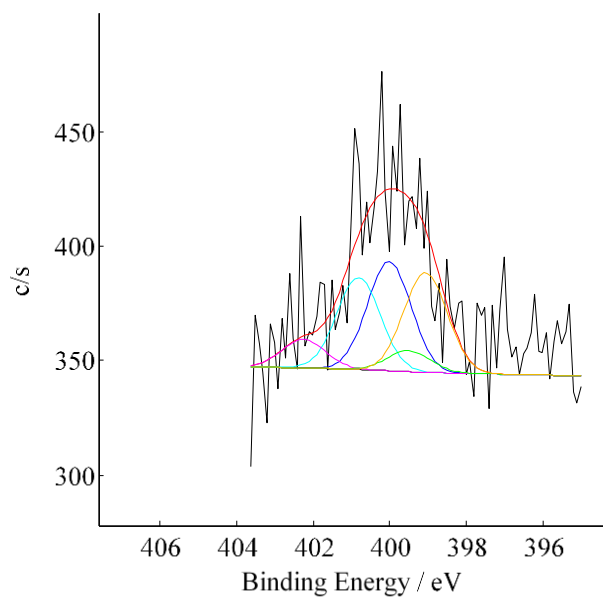
Figure B.7: The fitting (deconvolution) of the N 1s peak of [Mn(ba)$_3$] grafted onto the amino-functionalized Si-wafer, **S6.**
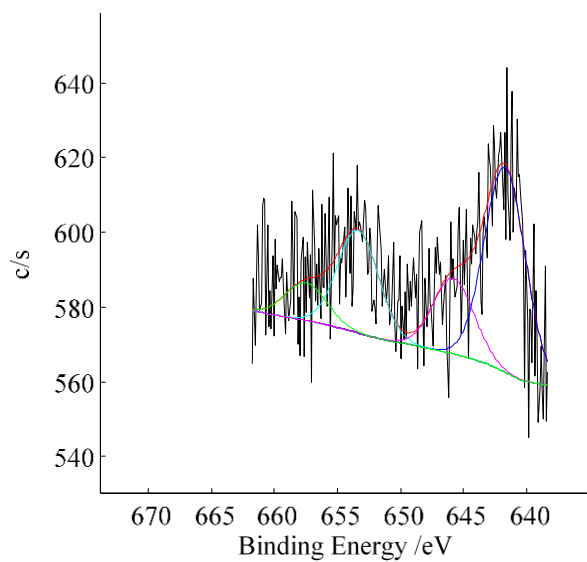
Figure B.8: The fitting (deconvolution) of the [Mn(dbm)$_3$] complex grafted onto the amino-functionalized Si-wafer, **S7**, Mn 2p XPS peak.
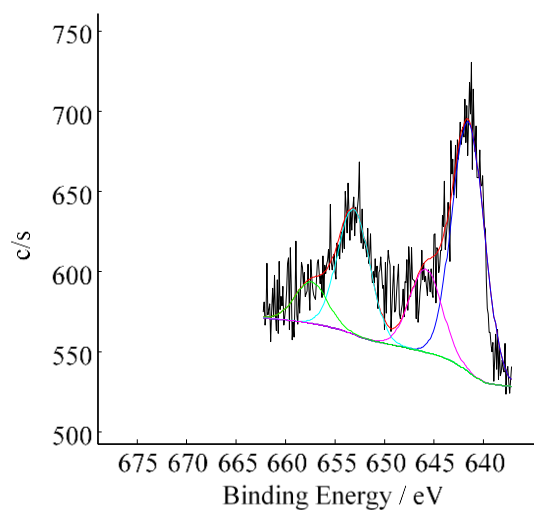
Figure B.9: The fitting (deconvolution) of the [Mn(tfth)$_3$] complex grafted onto the amino-functionalized Si-wafer, **S9**, Mn 2p XPS peak.
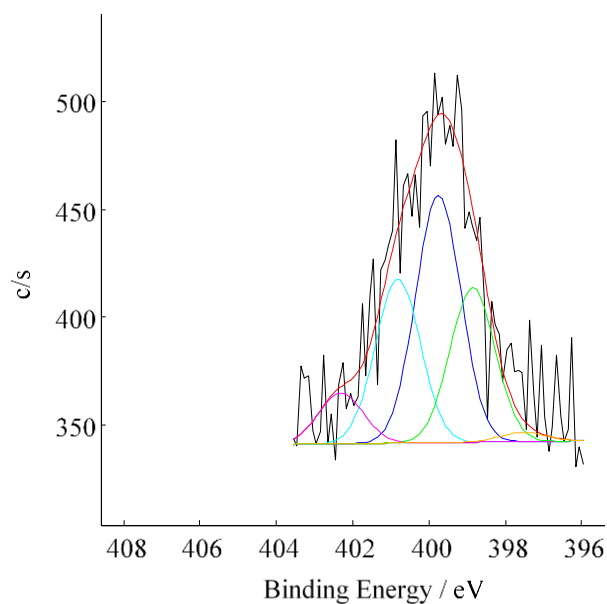
Figure B.10: The fitting (deconvolution) of the N 1s peak of [Mn(tfth)$_3$] grafted onto the amino-functionalized Si-wafer, **S9.**
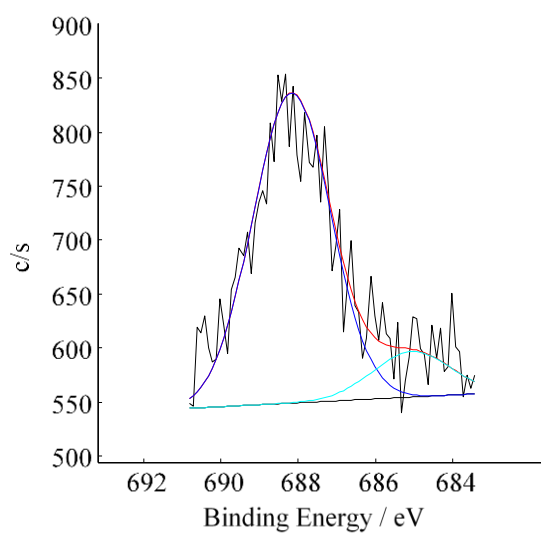
Figure B.11: The F 1s peak deconvolution of the [Mn(tfth)₃] grafted onto the amino-functionalized Si-wafer, **S9**.
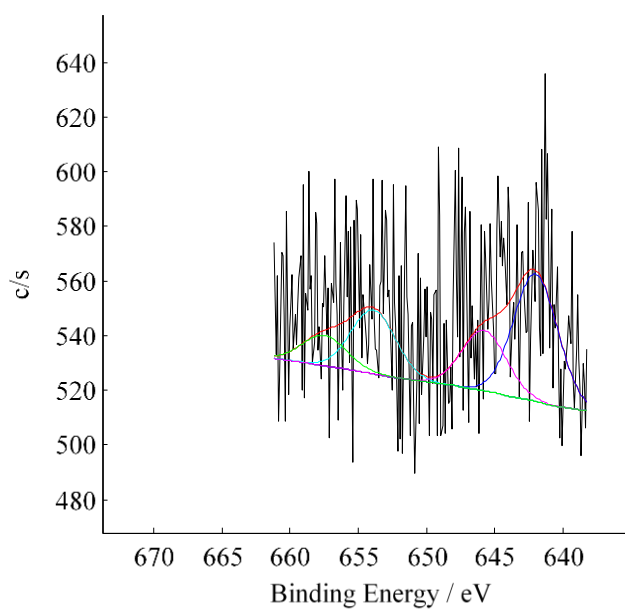
Figure B.12: The fitting (deconvolution) of the [Mn(tffu)₃] complex grafted onto the amino-functionalized Si-wafer, **S10**, Mn 2p XPS peak.
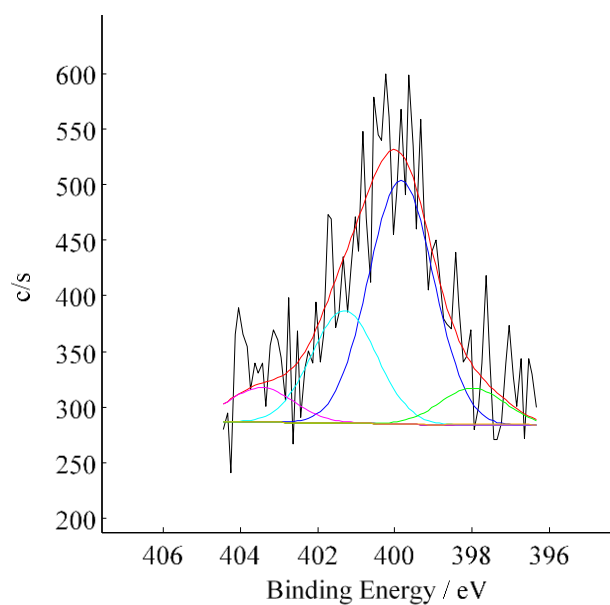
Figure B.13: The fitting (deconvolution) of the N 1s peak of [Mn(tffu)$_3$] grafted onto the amino-functionalized Si-wafer, **S10.**
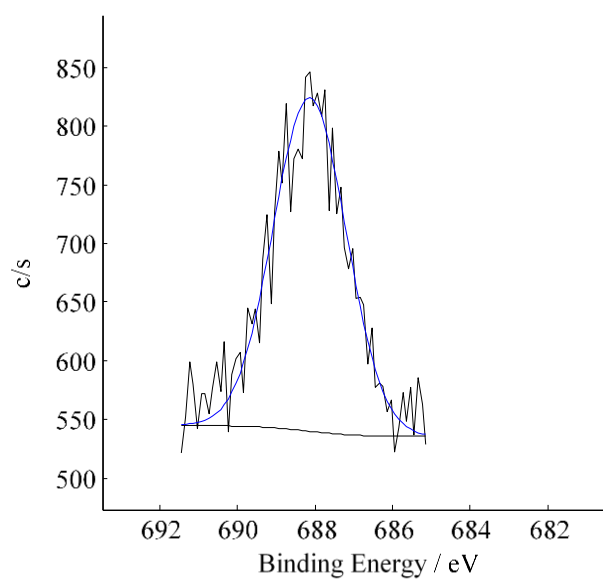
Figure B.14: The F 1s peak deconvolution of the [Mn(tffu)$_3$] grafted onto the amino-functionalized Si-wafer, **S10**.
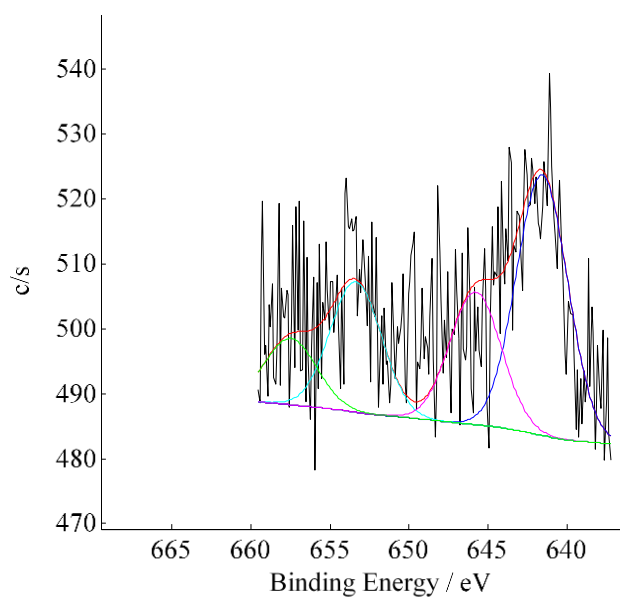
Figure B.15: The fitting (deconvolution) of the [Mn(tfba)$_3$] complex grafted onto the amino-functionalized Si-wafer, **S11**, Mn 2p XPS peak.
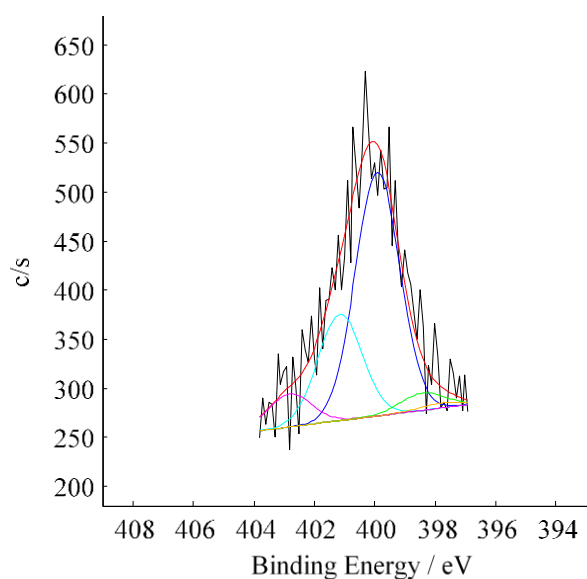
Figure B.16: The fitting (deconvolution) of the N 1s peak of [Mn(tfba)$_3$] grafted onto the amino-functionalized Si-wafer, **S11.**

A-16
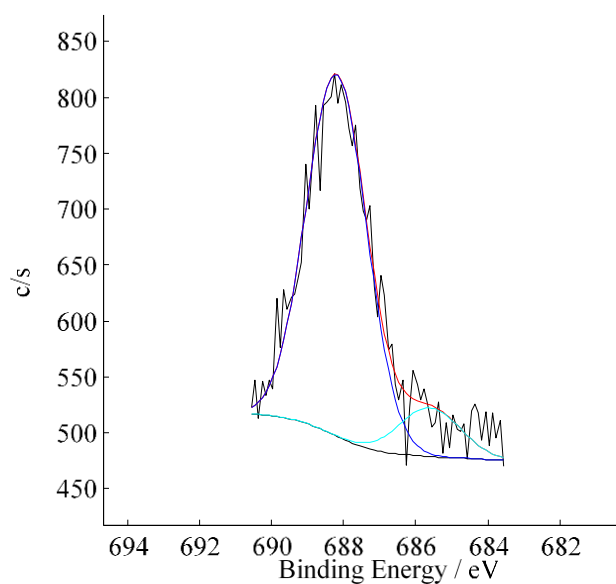
Figure B.17: The F 1s peak deconvolution of the [Mn(tfba)$_3$] grafted onto the amino-functionalized Si-wafer, **S11**.
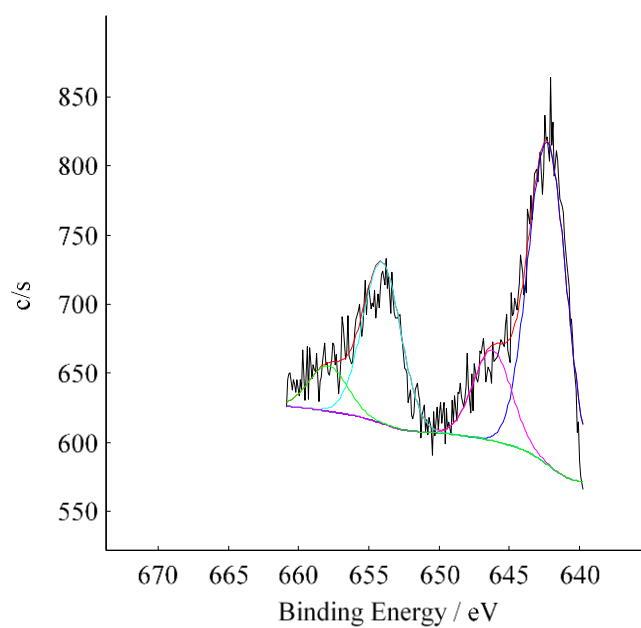
Figure B.18: The fitting (deconvolution) of the [Mn(hfaa)$_3$] complex grafted onto the amino-functionalized Si-wafer, **S12**, Mn 2p XPS peak.
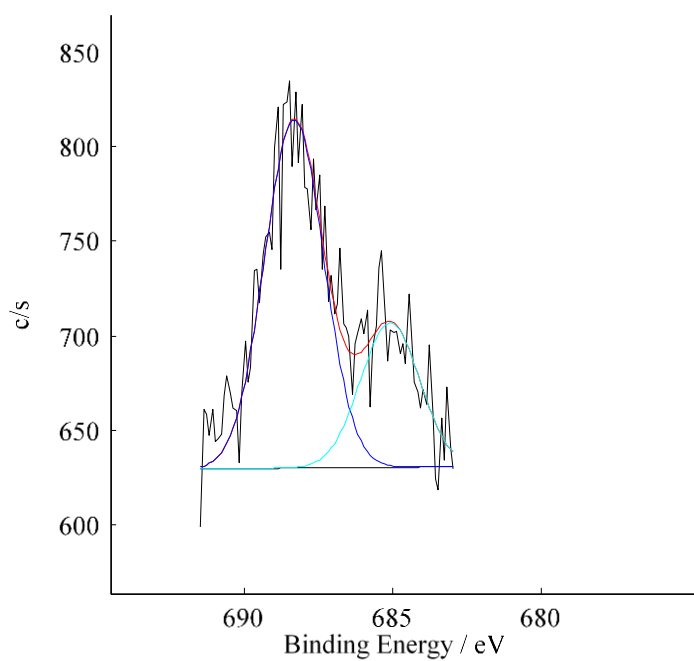
Figure B.19: The F 1s peak deconvolution of the [Mn(hfaa)$_3$] grafted onto the amino-functionalized Si-wafer, **S12**.
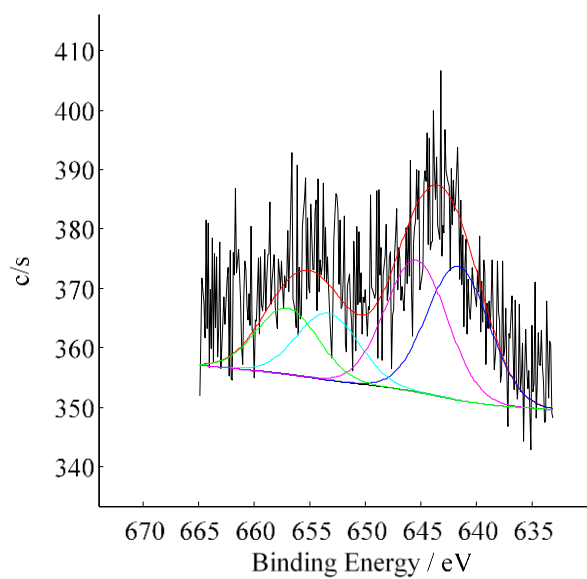
Figure B.20: The fitting (deconvolution) of the [Mn(ba)$_3$] immobiulized onto SiO$_2$, **S15**, Mn 2p photoelectron peaks.
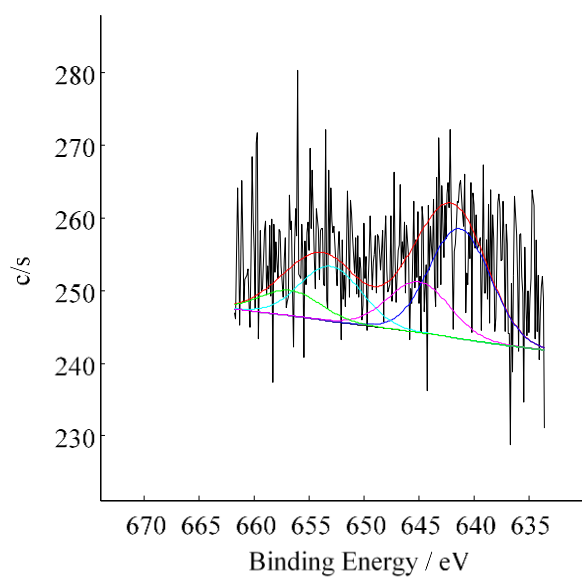
Figure B.21: The fitting (deconvolution) of the [Mn(dbm)$_3$] immobiulized onto SiO$_2$, **S16**, Mn 2p photoelectron peaks.
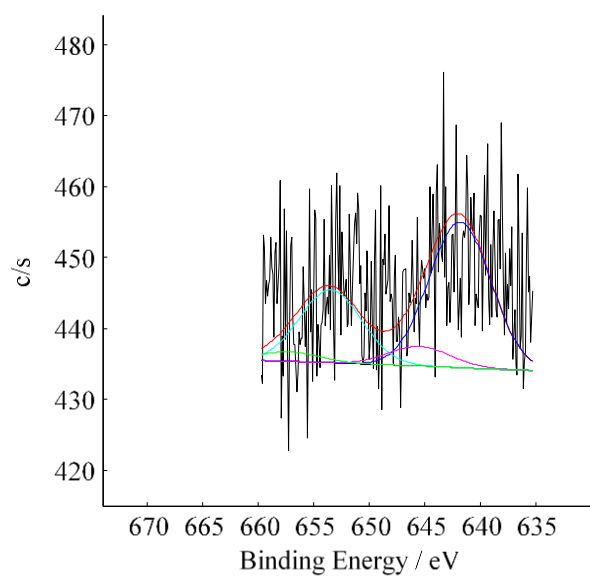
Figure B.22: The fitting (deconvolution) of the [Mn(tfth)$_3$] immobiulized onto SiO$_2$, **S18**, Mn 2p photoelectron peaks.
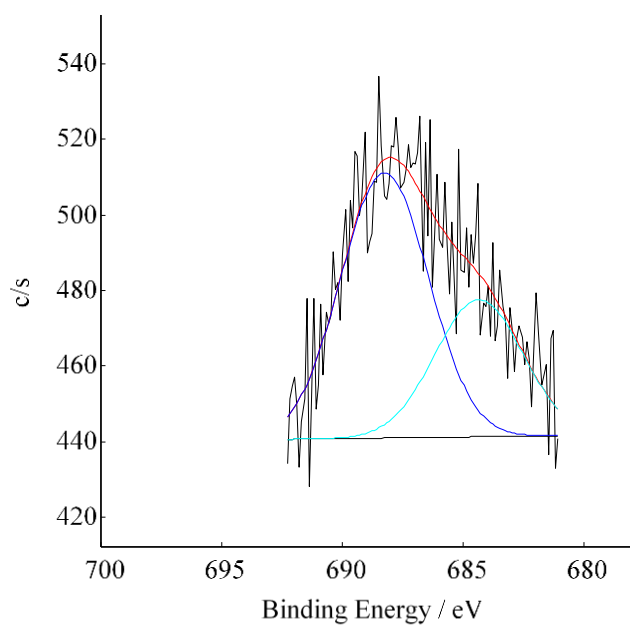
Figure B.23: The fitting (deconvolution) of the [Mn(tfth)$_3$] wet impregnated onto SiO$_2$, **S18**, F 1s XPS peak.
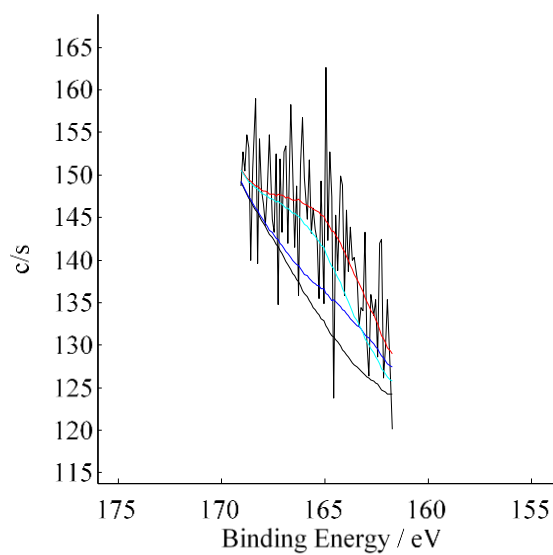
Figure B.24: The fitting (deconvolution) of the [Mn(tfth)$_3$] immobiulized onto SiO$_2$, **S18**, S 2p photoelectron peaks.
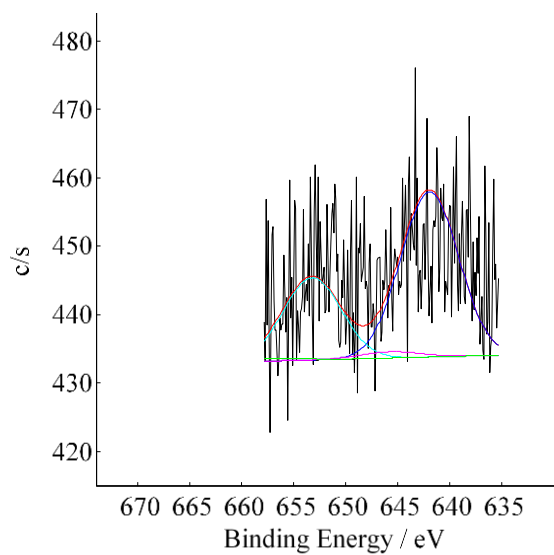
Figure B.25: The fitting (deconvolution) of the [Mn(tffu)$_3$] immobiulized onto SiO$_2$, **S19**, Mn 2p photoelectron peaks.
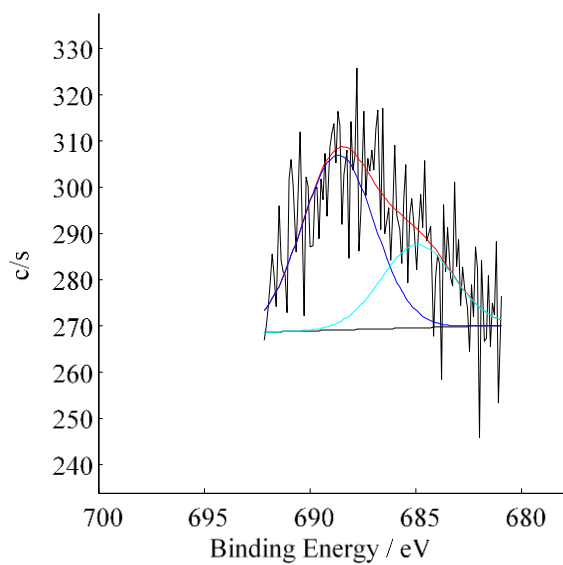
Figure B.26: The fitting (deconvolution) of the [Mn(tffu)$_3$] wet impregnated onto SiO$_2$, **S19**, F 1s XPS peak.
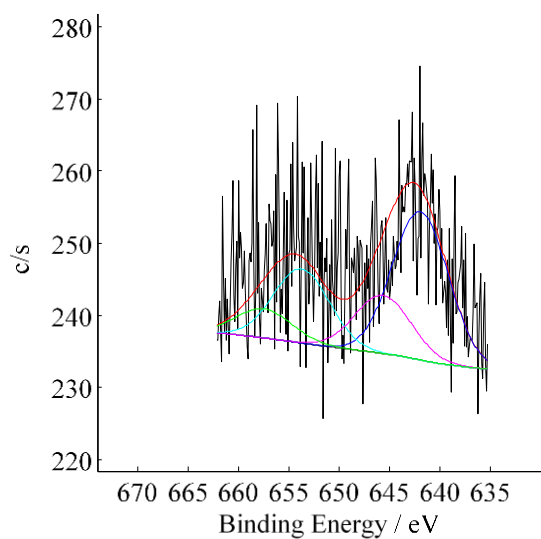
Figure B.27: The fitting (deconvolution) of the [Mn(tfba)$_3$] immobiulized onto SiO$_2$, **S20**, Mn 2p photoelectron peaks.
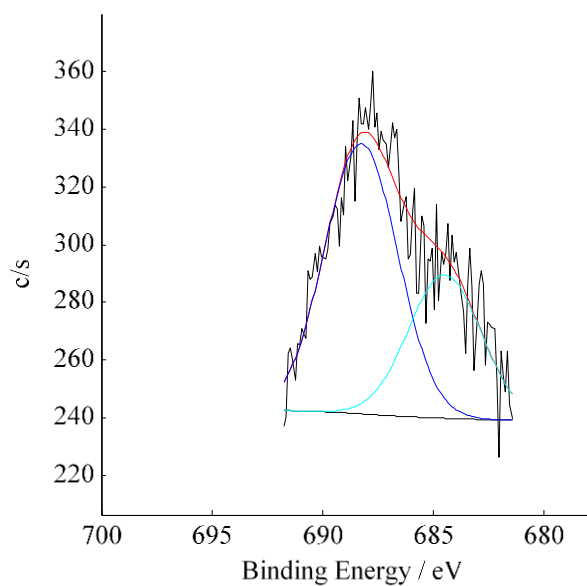
Figure B.28: The fitting (deconvolution) of the [Mn(tfba)$_3$] wet impregnated onto SiO$_2$, **S20**, F 1s XPS peak.
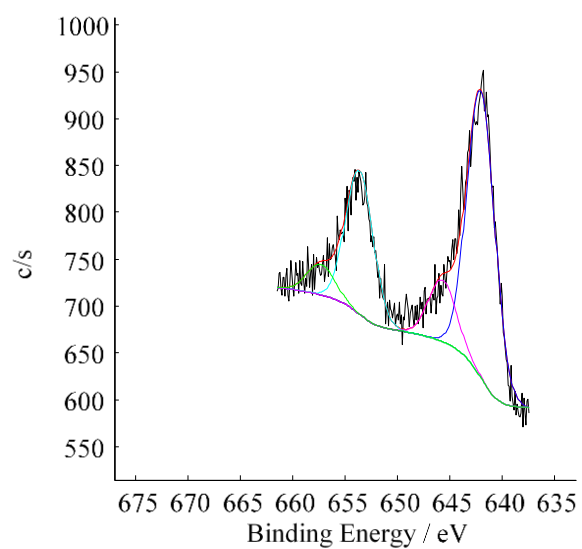
Figure B.29: Mn 2p peak fitting (deconvolution) of [Mn(acac)₃] impregnated onto TiO₂ 3-D surface, **S21**.
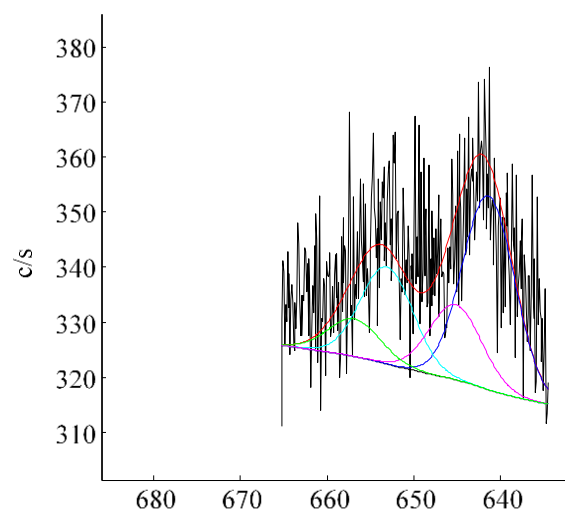
Figure B.30: Mn 2p peak fitting (deconvolution) of [Mn(acac)₃] impregnated onto MgO 3-D surface, **S22**.
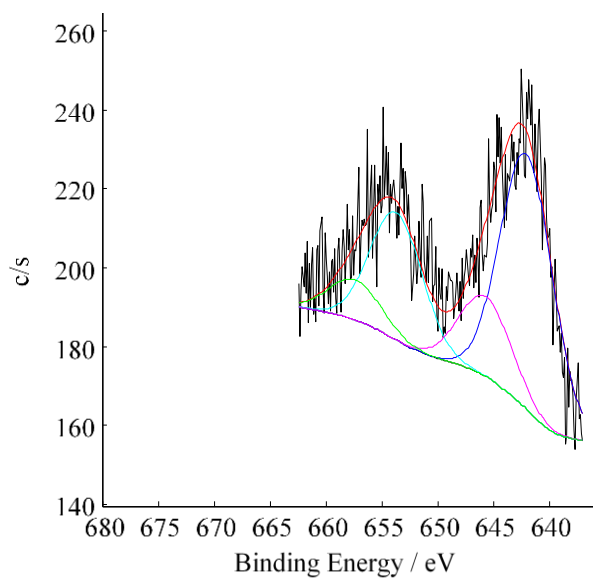
Figure B.31: Mn 2p peak fitting (deconvolution) of [Mn(acac)$_3$] impregnated onto acidic zeolite 3-D surface, **S23**.
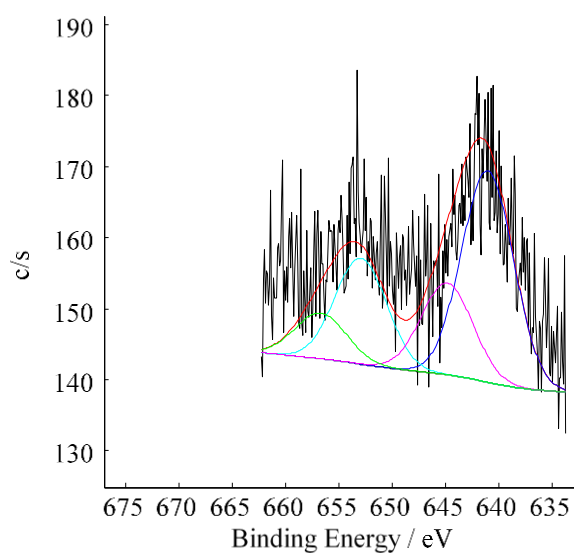
Figure B.32: Mn 2p peak fitting (deconvolution) of [Mn(acac)$_3$] impregnated onto basic zeolite 3-D surface, **S24**.
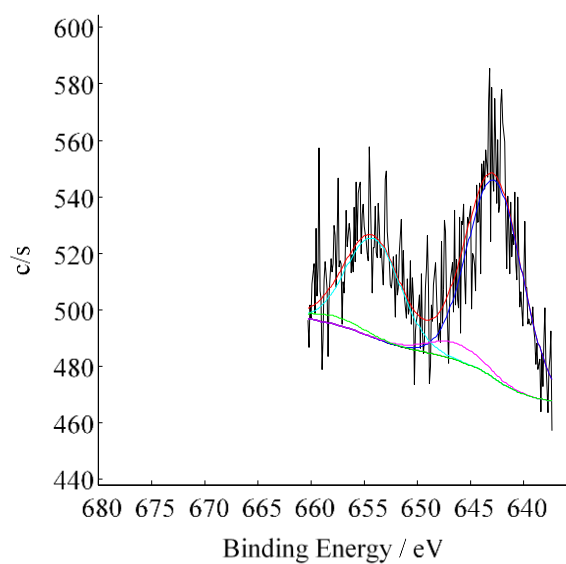
Figure B.33: Mn 2p peak fitting (deconvolution) of [Mn(tfaa)$_3$] on TiO$_2$ 3-D surface, **S25**.
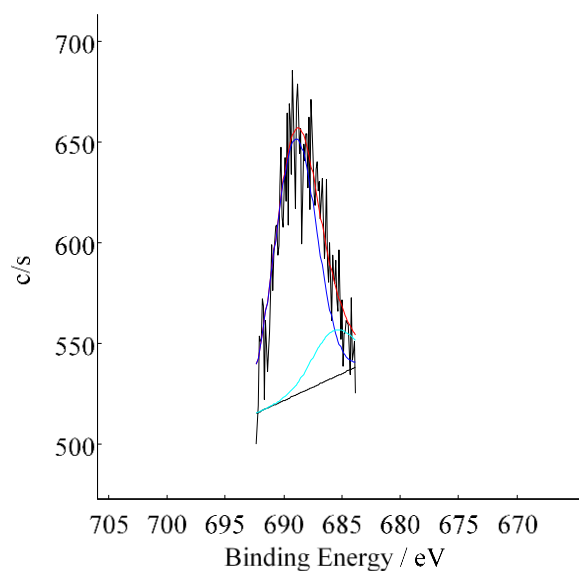
Figure B.34: The fitting (deconvolution) of the [Mn(tfaa)$_3$] wet impregnated onto TiO$_2$, **S25**, F 1s XPS peak
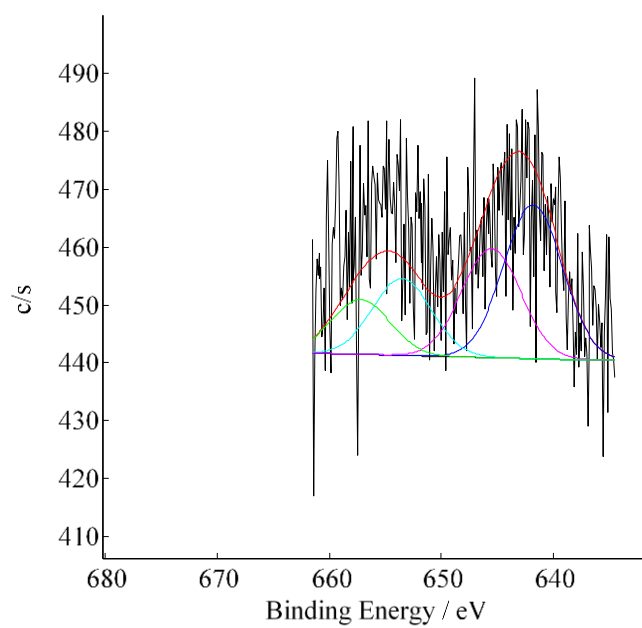
Figure B.35: Mn 2p peak fitting (deconvolution) of [Mn(tfaa)$_3$] on MgO 3-D surface, **S26**.
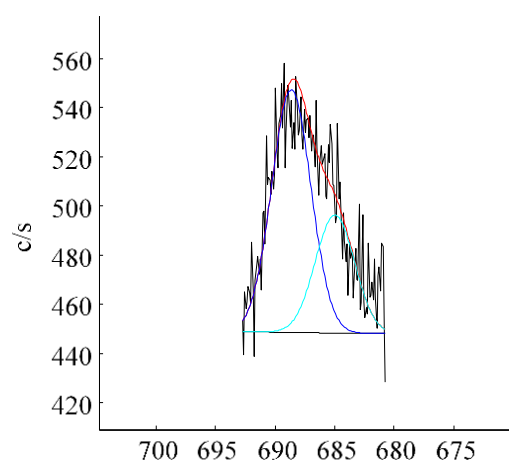
Figure B.36: The fitting (deconvolution) of the [Mn(tfaa)$_3$] wet impregnated onto MgO, **S26**, F 1s XPS peak
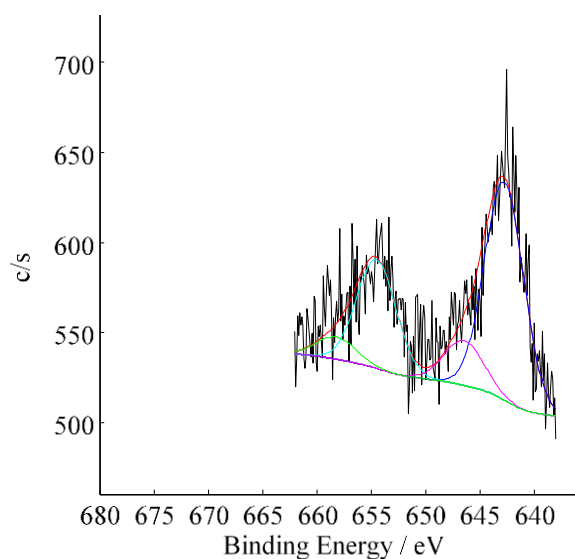
Figure B.37: Mn 2p peak fitting (deconvolution) of [Mn(tfaa)$_3$] on acidic zeolite 3-D surface, **S27**.
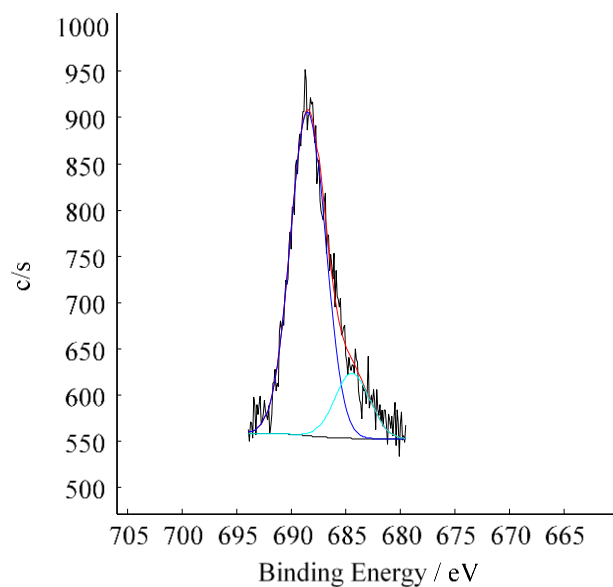
Figure B.38: The fitting (deconvolution) of the [Mn(tfaa)$_3$] wet impregnated onto acidic zeolite, **S27**, F 1s XPS peak
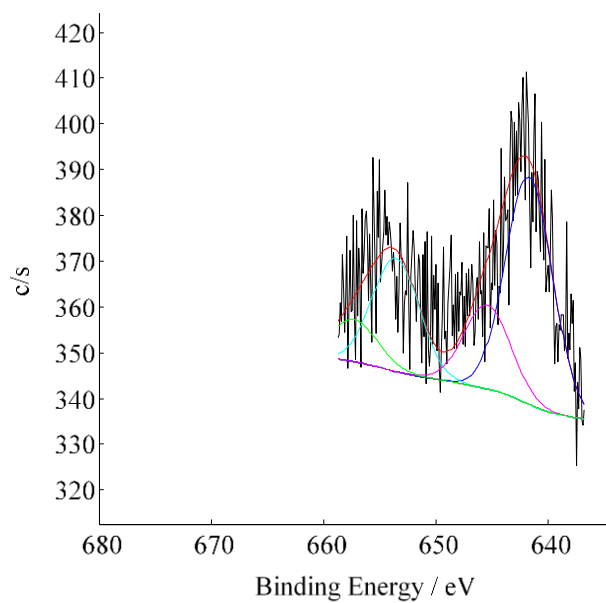
Figure B.39: Mn 2p peak fitting (deconvolution) of [Mn(tfaa)$_3$] on basic zeolite 3-D surface, **S28**.
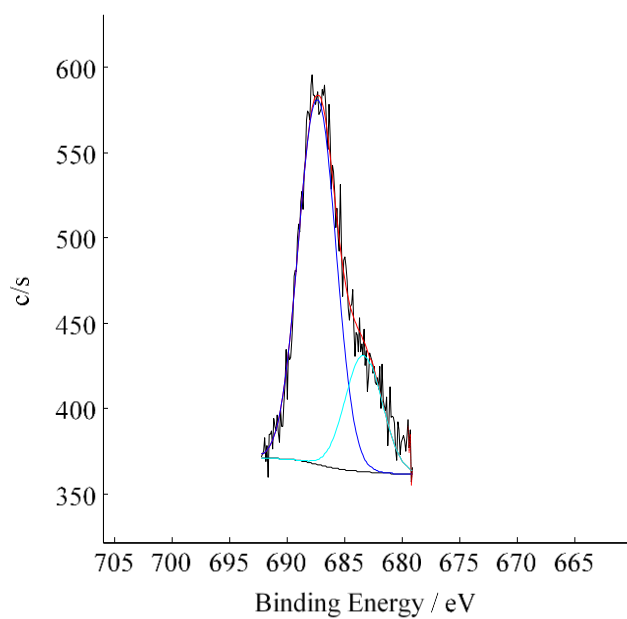
Figure B.40: The fitting (deconvolution) of the [Mn(tfaa)$_3$] wet impregnated onto basic zeolite, **S28**, F 1s XPS peak
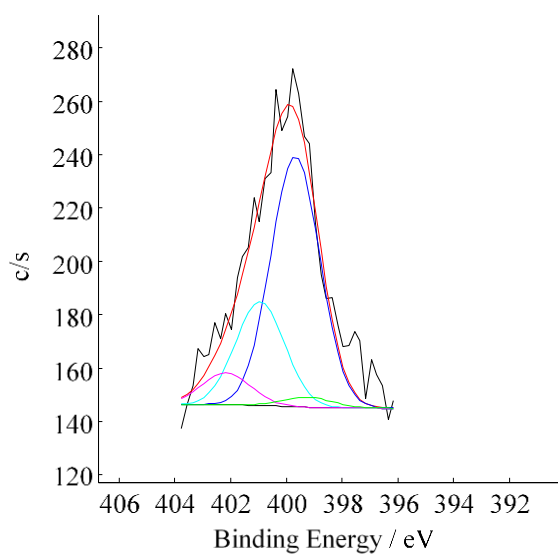
Figure B.41: The fitting (deconvolution) of the [Rh(acac)₃] complex grafted onto the amino-functionalized Si-wafer, **S30**, N 1s XPS peak.
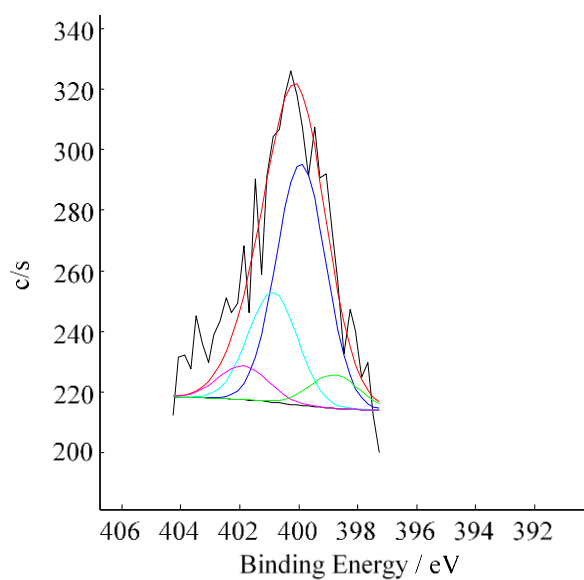
Figure B.42: The fitting (deconvolution) of the [Ir(acac)₃] complex grafted onto the amino-functionalized Si-wafer, **S31**, N 1s XPS peak.
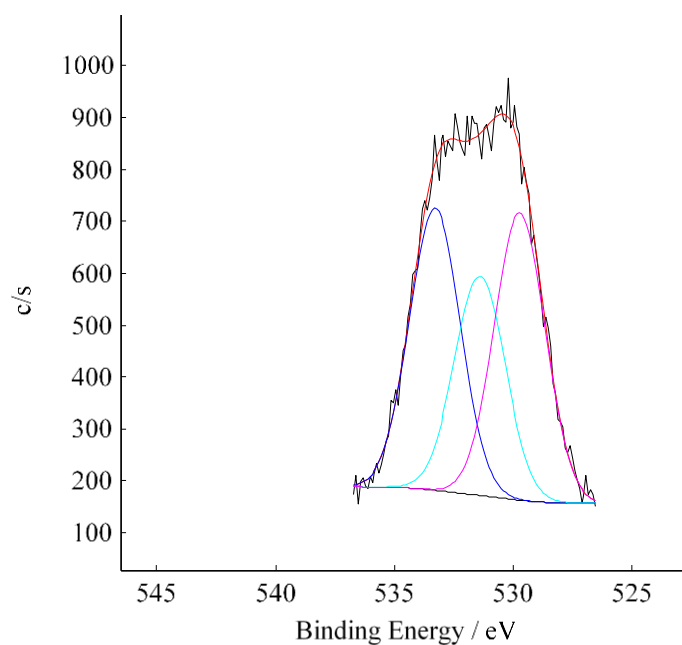
Figure B.43: The O 1s fitting (deconvolution) of the SiO_2 surface containing [Fe(acac)$_3$], **S33.**
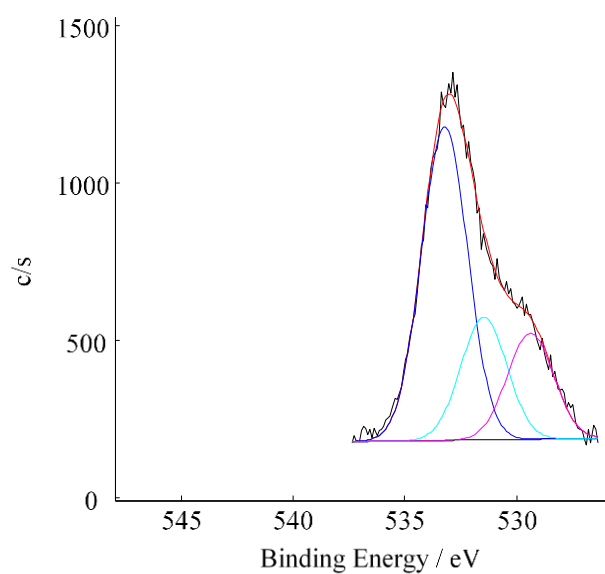
Figure B.44: The O 1s fitting (deconvolution) of the SiO_2 surface containing [Co(acac)$_3$], **S34.**
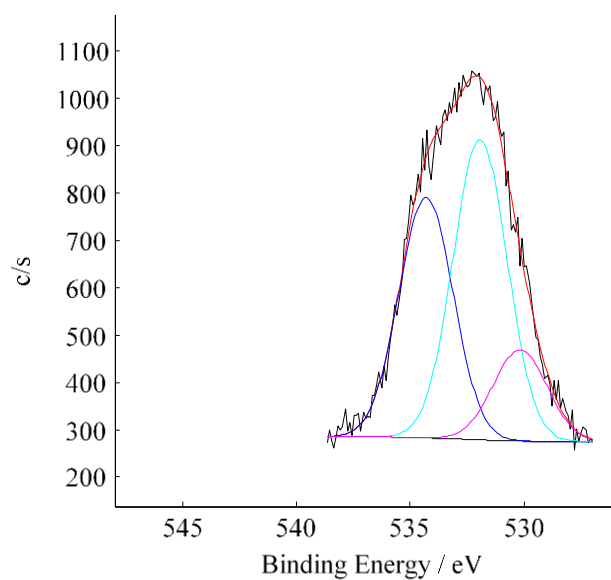
Figure B.45: The O 1s fitting (deconvolution) of the SiO$_2$ surface containing [Rh(acac)$_3$], **S35.**
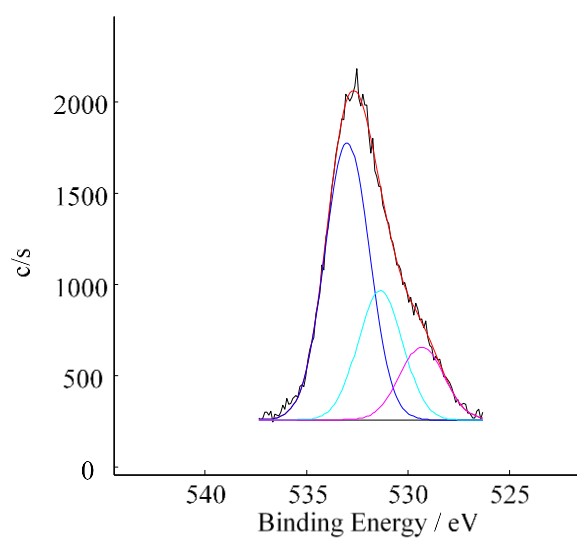
Figure B. 46: The O 1s fitting (deconvolution) of the SiO$_2$ surface containing [Ir(acac)$_3$], **S36.**
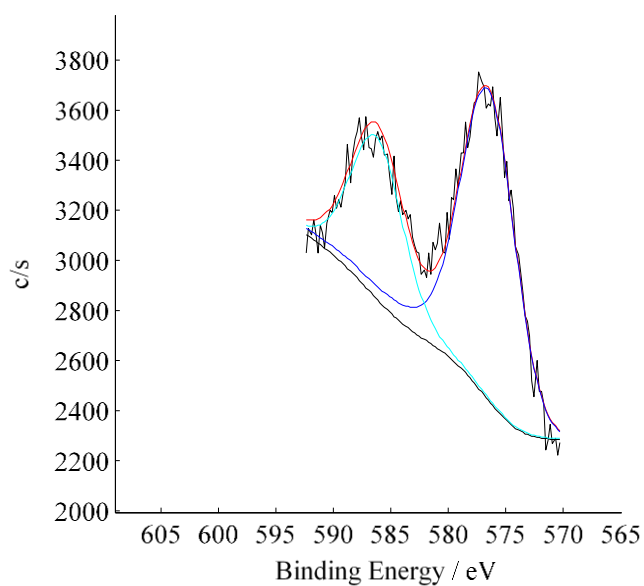
Figure B.47: The deconvolution of the [Cr(CO)$_5$=C(NHCy)(Fu)], **C2**, Cr 2p XPS peaks.
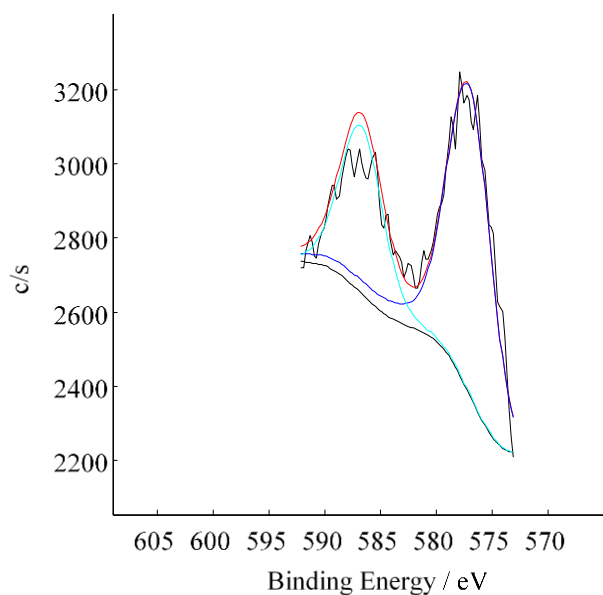
Figure B.48: The deconvolution of the [Cr(CO)$_5$=C(OEt)(Fu)], **C5**, Cr 2p XPS peaks.

A-32

C. Computational data

Optimized Cartesian coordinates (Å), calculations were with Amsterdam Density Fucntional (ADF).

Coordinate C.1: Optimized Cartesian coordinates of Mn(dpm)$_3$, **1**; S=4/2 with no symmetry (BP86/TZP).

Mn	0.008796000	-0.001523000	-0.026528000
O	0.338658000	-1.358816000	1.328423000
O	2.146545000	0.420363000	0.036452000
O	0.269445000	-1.357532000	-1.411412000
O	-0.254074000	1.361087000	-1.404787000
O	-2.129801000	-0.426904000	0.026288000
O	-0.327375000	1.348315000	1.334406000
C	-2.997434000	0.163243000	0.739649000
C	-2.698351000	1.210553000	1.651274000
C	-1.428737000	1.736044000	1.895686000
C	1.434702000	-1.738741000	1.905202000
C	2.704706000	-1.208211000	1.673880000
C	3.009532000	-0.164896000	0.759593000
C	0.217659000	-1.216674000	-2.689479000
C	-0.021945000	0.001024000	-3.344379000
C	-0.237869000	1.219958000	-2.683830000
C	4.469900000	0.326927000	0.583851000
C	1.211738000	-2.882657000	2.922968000
C	-1.213314000	2.882561000	2.911964000
C	-4.456733000	-0.328879000	0.556910000
C	-0.473292000	2.532675000	-3.459760000
C	0.446574000	-2.527150000	-3.470862000
H	3.524763000	-1.633392000	2.239730000
H	-0.037314000	0.000583000	-4.427288000
H	-3.522731000	1.641329000	2.206464000
C	5.484312000	-0.380475000	1.494640000
H	6.488365000	0.027821000	1.309226000
H	5.258175000	-0.226593000	2.559094000
H	5.529307000	-1.461340000	1.300597000

C	4.490009000	1.841824000	0.880356000
H	4.241728000	2.043031000	1.932406000
H	5.492127000	2.249651000	0.683179000
H	3.763818000	2.367755000	0.249498000
C	4.859459000	0.088716000	-0.891271000
H	5.863765000	0.492855000	-1.084979000
H	4.873505000	-0.984837000	-1.128609000
H	4.145660000	0.581448000	-1.562148000
C	0.229150000	-2.370598000	3.999024000
H	-0.000667000	-3.178501000	4.708722000
H	0.663961000	-1.533952000	4.564098000
H	-0.706028000	-2.028442000	3.540654000
C	2.503167000	-3.355176000	3.606654000
H	2.981184000	-2.551987000	4.184231000
H	2.263578000	-4.167500000	4.307589000
H	3.231881000	-3.747481000	2.883820000
C	0.574786000	-4.070784000	2.169403000
H	1.260123000	-4.468117000	1.407180000
H	0.345641000	-4.881041000	2.876589000
H	-0.352971000	-3.764335000	1.672685000
C	-4.480273000	-1.840050000	0.871963000
H	-3.750009000	-2.374322000	0.252902000
H	-4.239677000	-2.028383000	1.928196000
H	-5.481325000	-2.249524000	0.672743000
C	-5.477819000	0.390475000	1.450552000
H	-6.481076000	-0.017292000	1.259950000
H	-5.262098000	0.247244000	2.518632000
H	-5.517863000	1.469346000	1.244675000
C	-4.834311000	-0.108506000	-0.923940000
H	-4.847967000	0.962242000	-1.173628000
H	-4.114273000	-0.607871000	-1.583132000
H	-5.836422000	-0.516295000	-1.121264000
C	-2.511794000	3.366051000	3.574358000
H	-3.002665000	2.568989000	4.149675000
H	-2.277780000	4.181152000	4.273940000

H	−3.227741000	3.758083000	2.838740000
C	−0.558309000	4.063664000	2.162876000
H	−0.333748000	4.875102000	2.870156000
H	0.374084000	3.749482000	1.679919000
H	−1.230598000	4.462513000	1.389899000
C	−0.249768000	2.369245000	4.004504000
H	−0.025288000	3.178834000	4.713979000
H	−0.698017000	1.537867000	4.566816000
H	0.689967000	2.019388000	3.561379000
C	0.662678000	3.508789000	−3.078821000
H	0.694838000	3.665907000	−1.994552000
H	1.640588000	3.123591000	−3.400360000
H	0.498421000	4.477644000	−3.571716000
C	−0.489543000	2.343977000	−4.983808000
H	−0.669852000	3.315373000	−5.465236000
H	0.468869000	1.962723000	−5.362608000
H	−1.289843000	1.663278000	−5.305708000
C	−1.829371000	3.116154000	−3.005345000
H	−2.658670000	2.447174000	−3.274755000
H	−1.845628000	3.265105000	−1.919653000
H	−1.998547000	4.084487000	−3.497423000
C	0.388871000	−2.345305000	−4.994763000
H	1.163503000	−1.655450000	−5.357459000
H	0.559776000	−3.316349000	−5.480276000
H	−0.591627000	−1.978784000	−5.328917000
C	1.836060000	−3.074921000	−3.075642000
H	2.635535000	−2.386501000	−3.383620000
H	1.904260000	−3.219316000	−1.991259000
H	2.007602000	−4.040729000	−3.571893000
C	−0.646620000	−3.528632000	−3.035416000
H	−0.480539000	−4.495758000	−3.530993000
H	−0.626618000	−3.680288000	−1.950162000
H	−1.647147000	−3.169331000	−3.314564000

Appendix

Coordinate C.2: Optimized Cartesian coordinates of Mn(acac)$_3$, **2**; S=4/2 with no symmetry (PW91/TZP).

Mn	0.001624000	0.004075000	0.033694000
O	2.052141000	0.749215000	0.065136000
O	0.511191000	-1.290961000	1.386698000
O	-2.046590000	-0.746829000	0.059199000
O	-0.513737000	1.301064000	1.383513000
O	-0.469821000	1.317228000	-1.339440000
O	0.475228000	-1.311687000	-1.336741000
C	4.366915000	0.855981000	0.554439000
C	3.003750000	0.218562000	0.710041000
C	2.874623000	-0.909559000	1.561456000
C	1.685499000	-1.578335000	1.846277000
C	1.697206000	-2.759918000	2.783039000
C	-4.358745000	-0.869602000	0.555389000
C	-2.999169000	-0.224151000	0.709154000
C	-2.874292000	0.901817000	1.564005000
C	-1.688829000	1.578503000	1.847159000
C	-1.706769000	2.757458000	2.787073000
C	-0.824708000	2.374977000	-3.409917000
C	-0.411530000	1.166910000	-2.613085000
C	-0.006388000	-0.002601000	-3.270176000
C	0.407099000	-1.167574000	-2.610592000
C	0.819477000	-2.377826000	-3.404644000
H	4.317221000	1.891886000	0.915569000
H	4.623883000	0.901211000	-0.511708000
H	5.151960000	0.321682000	1.098770000
H	3.775001000	-1.277766000	2.047654000
H	1.016937000	-2.566505000	3.622667000
H	2.699319000	-2.971622000	3.166849000
H	1.313500000	-3.642761000	2.255346000
H	-4.616391000	-0.917162000	-0.510467000
H	-5.146468000	-0.339931000	1.100342000
H	-4.302261000	-1.904973000	0.917080000
H	-3.775626000	1.262586000	2.054058000
H	-1.327337000	3.643687000	2.261976000

H	−1.025800000	2.565095000	3.626418000
H	−2.710034000	2.962841000	3.171171000
H	−1.862083000	2.634403000	−3.161276000
H	−0.737940000	2.209932000	−4.487511000
H	−0.200589000	3.228857000	−3.116807000
H	−0.010020000	−0.005061000	−4.356798000
H	0.191528000	−3.229510000	−3.113081000
H	1.854974000	−2.640179000	−3.151582000
H	0.737092000	−2.213986000	−4.482793000

Coordinate C.3: Optimized Cartesian coordinates of Mn(acac)$_3$, **2**; S=4/2 with no symmetry (BP86/TZP).

Mn	0.000862000	0.002829000	0.010149000
O	2.059580000	0.736709000	0.056087000
O	0.501182000	−1.299125000	1.365273000
O	−2.057827000	−0.731841000	0.050026000
O	−0.504041000	1.305491000	1.362749000
O	−0.464048000	1.318411000	−1.366821000
O	0.469471000	−1.314542000	−1.363675000
C	4.363021000	0.877036000	0.605708000
C	2.999706000	0.227227000	0.737936000
C	2.857459000	−0.888312000	1.606808000
C	1.665988000	−1.567257000	1.865493000
C	1.660266000	−2.738846000	2.820086000
C	−4.358771000	−0.884629000	0.606532000
C	−2.997832000	−0.229646000	0.737436000
C	−2.857561000	0.882600000	1.610819000
C	−1.668486000	1.566518000	1.867551000
C	−1.665215000	2.735519000	2.825307000
C	−0.824746000	2.379707000	−3.439652000
C	−0.408766000	1.168399000	−2.642970000
C	−0.003651000	−0.002586000	−3.301472000
C	0.407027000	−1.169995000	−2.640169000
C	0.822967000	−2.383250000	−3.433892000
H	4.293557000	1.921004000	0.943290000
H	4.650120000	0.901617000	−0.454643000

H	5.139091000	0.361888000	1.183724000
H	3.748153000	−1.239623000	2.125472000
H	0.957400000	−2.538253000	3.640901000
H	2.655054000	−2.939185000	3.232975000
H	1.295474000	−3.632680000	2.294848000
H	−4.648606000	−0.906715000	−0.453122000
H	−5.135414000	−0.374797000	1.188474000
H	−4.283961000	−1.929467000	0.940305000
H	−3.748158000	1.228065000	2.133522000
H	−1.305400000	3.632265000	2.301606000
H	−0.959464000	2.535590000	3.643808000
H	−2.659784000	2.930633000	3.241210000
H	−1.861872000	2.641190000	−3.186639000
H	−0.743372000	2.213505000	−4.519205000
H	−0.196979000	3.233978000	−3.150637000
H	−0.006374000	−0.004851000	−4.389536000
H	0.198406000	−3.238028000	−3.139471000
H	1.861650000	−2.641197000	−3.183663000
H	0.737327000	−2.221203000	−4.513738000

Coordinate C.4: Optimized Cartesian coordinates of Mn(acac)₃, **2**; S=4/2 with no symmetry (OLYP/TZP).

Mn	0.000000000	0.000000000	−0.043405000
O	2.114668000	0.715460000	0.038977000
O	0.509010000	−1.325189000	1.323648000
O	−2.114668000	−0.715460000	0.038977000
O	−0.509010000	1.325189000	1.323648000
O	−0.424585000	1.337662000	−1.454721000
O	0.424585000	−1.337662000	−1.454721000
C	4.374408000	0.921991000	0.725728000
C	3.006066000	0.261640000	0.808410000
C	2.822329000	−0.806960000	1.729714000
C	1.635900000	−1.516073000	1.922884000
C	1.595804000	−2.649603000	2.929930000
C	−4.374408000	−0.921991000	0.725728000
C	−3.006066000	−0.261640000	0.808410000
C	−2.822329000	0.806960000	1.729714000

C	−1.635900000	1.516073000	1.922884000
C	−1.595804000	2.649603000	2.929930000
C	−0.748651000	2.408938000	−3.525729000
C	−0.370571000	1.181699000	−2.723983000
C	0.000000000	0.000000000	−3.385310000
C	0.370571000	−1.181699000	−2.723983000
C	0.748651000	−2.408938000	−3.525729000
H	4.270856000	1.984823000	0.969923000
H	4.738124000	0.863341000	−0.305582000
H	5.111569000	0.471326000	1.393987000
H	3.675529000	−1.105417000	2.330383000
H	0.831463000	−2.437500000	3.685261000
H	2.557932000	−2.800542000	3.422880000
H	1.300468000	−3.574337000	2.422592000
H	−4.738124000	−0.863341000	−0.305582000
H	−5.111569000	−0.471326000	1.393987000
H	−4.270856000	−1.984823000	0.969923000
H	−3.675529000	1.105417000	2.330383000
H	−1.300468000	3.574337000	2.422592000
H	−0.831463000	2.437500000	3.685261000
H	−2.557932000	2.800542000	3.422880000
H	−1.764475000	2.716614000	−3.256252000
H	−0.695734000	2.236227000	−4.602048000
H	−0.078907000	3.232709000	−3.256987000
H	0.000000000	0.000000000	−4.469653000
H	0.078907000	−3.232709000	−3.256987000
H	1.764475000	−2.716614000	−3.256252000
H	0.695734000	−2.236227000	−4.602048000

Coordinate C.5: Optimized Cartesian coordinates of Mn(acac)₃, **2**; S=4/2 with no symmetry (B3LYP/TZP).

Mn	−0.000503000	0.000219000	−0.080888000
O	2.068397000	0.661832000	−0.024878000
O	0.448794000	−1.312934000	1.277319000
O	−2.069485000	−0.661657000	−0.024458000
O	−0.450169000	1.313942000	1.276579000

O	-0.406339000	1.328544000	-1.458363000
O	0.407374000	-1.327731000	-1.457916000
C	4.266792000	0.976635000	0.778858000
C	2.923409000	0.283042000	0.816801000
C	2.712828000	-0.733228000	1.781967000
C	1.540925000	-1.460449000	1.942559000
C	1.476146000	-2.552000000	2.980977000
C	-4.266502000	-0.979326000	0.782235000
C	-2.923731000	-0.284435000	0.818712000
C	-2.712926000	0.731705000	1.783954000
C	-1.541660000	1.460324000	1.942967000
C	-1.477233000	2.552839000	2.980419000
C	-0.695878000	2.412710000	-3.519978000
C	-0.349603000	1.182287000	-2.725076000
C	0.001456000	0.000410000	-3.383579000
C	0.351754000	-1.181454000	-2.724712000
C	0.697951000	-2.412210000	-3.519110000
H	4.126200000	2.025714000	1.047448000
H	4.652639000	0.954457000	-0.240967000
H	4.992507000	0.529641000	1.455652000
H	3.537042000	-0.978883000	2.434992000
H	0.672147000	-2.332208000	3.685553000
H	2.413198000	-2.661734000	3.522544000
H	1.226181000	-3.495268000	2.492342000
H	-4.654125000	-0.956287000	-0.236905000
H	-4.991513000	-0.533808000	1.460752000
H	-4.124473000	-2.028580000	1.049346000
H	-3.536560000	0.976497000	2.438029000
H	-1.230750000	3.496312000	2.490375000
H	-0.671112000	2.335724000	3.683382000
H	-2.413354000	2.660802000	3.523912000
H	-1.687998000	2.760208000	-3.228189000
H	-0.672009000	2.232112000	-4.592216000
H	0.010581000	3.205818000	-3.268814000
H	0.002016000	0.000389000	-4.462703000

H	-0.010283000	-3.204253000	-3.269527000
H	1.688901000	-2.761295000	-3.225309000
H	0.676443000	-2.231462000	-4.591363000

Coordinate C.6: Optimized Cartesian coordinates of Mn(ba)₃, **3**; *fac*, S=4/2 with no symmetry (OLYP/TZP).

Mn	-0.282760000	0.063084000	0.320352000
O	1.839279000	0.561884000	-0.098445000
O	0.413864000	-1.334331000	1.520120000
O	-2.358463000	-0.439826000	0.957545000
O	-0.312445000	1.408893000	1.755505000
O	-0.908981000	1.436820000	-0.959821000
O	-0.368619000	-1.289306000	-1.129017000
C	2.830341000	0.106679000	0.540112000
C	2.772186000	-0.918561000	1.521035000
C	1.613809000	-1.588740000	1.927855000
C	-3.011520000	0.092022000	1.900802000
C	-2.511322000	1.156574000	2.704177000
C	-1.249671000	1.736384000	2.582182000
C	-1.552049000	2.568409000	-2.919634000
C	-1.153412000	1.291374000	-2.211054000
C	-1.080379000	0.090470000	-2.927488000
C	-0.709635000	-1.142321000	-2.356839000
H	3.702786000	-1.195129000	1.998866000
H	-3.163967000	1.589744000	3.450178000
H	-2.438374000	2.989339000	-2.433373000
H	-1.761435000	2.409599000	-3.978943000
H	-0.746318000	3.302899000	-2.816225000
H	-1.295972000	0.131116000	-3.985987000
C	-0.675973000	-2.390313000	-3.180890000
C	0.068656000	-3.490057000	-2.720015000
C	-1.381406000	-2.517593000	-4.390664000
H	0.603937000	-3.404918000	-1.780146000
H	-1.995707000	-1.701539000	-4.758029000
C	0.121857000	-4.671370000	-3.455833000
C	-1.334970000	-3.703977000	-5.120314000

H	0.709480000	-5.509273000	-3.086453000
H	-1.896738000	-3.787496000	-6.048240000
C	-0.578946000	-4.783873000	-4.658813000
H	-0.541891000	-5.709133000	-5.230566000
C	4.183987000	0.716854000	0.209123000
H	5.009692000	0.259661000	0.758984000
H	4.367309000	0.619166000	-0.866024000
H	4.154479000	1.788615000	0.434003000
C	1.697456000	-2.704328000	2.927411000
C	0.562019000	-3.028226000	3.689532000
C	2.866571000	-3.461941000	3.115994000
C	0.602694000	-4.058262000	4.627212000
C	2.903360000	-4.497945000	4.047950000
C	1.773202000	-4.797289000	4.812243000
H	-0.351159000	-2.462287000	3.538485000
H	3.748455000	-3.264414000	2.514151000
H	-0.285347000	-4.287156000	5.213048000
H	3.815259000	-5.078873000	4.170869000
H	1.802945000	-5.605821000	5.540280000
C	-4.398882000	-0.438096000	2.150104000
C	-5.088658000	-0.257634000	3.361203000
H	-4.623978000	0.277329000	4.183822000
H	-6.877551000	-0.647491000	4.493053000
C	-6.365458000	-0.788557000	3.543280000
C	-6.982460000	-1.503474000	2.514692000
H	-7.980591000	-1.913976000	2.655835000
C	-6.306266000	-1.693728000	1.306880000
H	-6.777385000	-2.253348000	0.501022000
C	-5.026046000	-1.173799000	1.130685000
H	-4.489774000	-1.330747000	0.200083000
C	-0.866107000	2.887932000	3.491911000
H	-1.665610000	3.153106000	4.186245000
H	0.031066000	2.619014000	4.059655000
H	-0.613079000	3.762251000	2.882564000

Coordinate C.7: Optimized Cartesian coordinates of Mn(ba)₃, **3**; *mer2* Ph-Ph, S=4/2 with no symmetry (OLYP/TZP).

```
Mn      0.237859000      0.005769000      0.092780000
O       2.138349000      0.583012000      0.180101000
O       0.605472000     -1.349318000      1.492234000
O      -1.650500000     -0.536868000      0.098995000
O      -0.335064000      1.531355000      1.598065000
O      -0.066950000      1.312125000     -1.351392000
O       0.687671000     -1.455805000     -1.524917000
C       3.073606000      0.150626000      0.944882000
C       2.918073000     -0.890805000      1.878562000
C       1.715528000     -1.576607000      2.092618000
C       1.658152000     -2.698771000      3.107101000
C      -2.650985000     -0.074141000      0.773211000
C      -2.633924000      0.955189000      1.712756000
C      -1.485088000      1.705546000      2.094636000
C      -0.405004000      2.429937000     -3.388178000
C      -0.076725000      1.155707000     -2.633287000
C       0.181431000     -0.015996000     -3.343240000
C       0.550838000     -1.265592000     -2.767904000
H       3.783921000     -1.216697000      2.438491000
H       0.926034000     -2.444834000      3.881186000
H       2.625942000     -2.887760000      3.574842000
H       1.306365000     -3.612089000      2.616185000
H      -3.587332000      1.215785000      2.152774000
H      -1.394891000      2.786911000     -3.084085000
H      -0.390060000      2.287921000     -4.470442000
H       0.314787000      3.209394000     -3.116197000
H       0.147767000      0.061313000     -4.421970000
H       5.133691000      0.446580000      2.774059000
C       6.580441000      1.505933000      1.600904000
C       4.402134000      0.814636000      0.768427000
C       5.355628000      0.871094000      1.799611000
C       4.706139000      1.419287000     -0.463079000
H       3.970370000      1.387389000     -1.260190000
```

C	5.936640000	2.040462000	-0.664165000
H	7.301169000	1.552224000	2.414527000
H	6.161153000	2.491489000	-1.628562000
C	6.878543000	2.087079000	0.366426000
H	7.837353000	2.577860000	0.210860000
C	0.837570000	-2.434869000	-3.671548000
C	1.660046000	-3.467444000	-3.191781000
C	0.303092000	-2.554450000	-4.965353000
H	2.062991000	-3.385229000	-2.187007000
H	-0.363814000	-1.791059000	-5.354972000
C	1.957945000	-4.572088000	-3.986588000
C	0.587949000	-3.667619000	-5.756045000
H	2.608117000	-5.355451000	-3.601398000
H	0.153129000	-3.748456000	-6.750314000
C	1.422443000	-4.677550000	-5.272904000
H	1.649412000	-5.543002000	-5.892723000
C	-3.957809000	-0.775675000	0.456080000
H	-3.851892000	-1.847369000	0.655622000
H	-4.178534000	-0.667458000	-0.611286000
H	-4.792869000	-0.381073000	1.037963000
C	-1.618640000	2.788781000	3.131381000
C	-2.653869000	2.822730000	4.080790000
C	-0.644642000	3.800427000	3.170388000
H	-3.405305000	2.039043000	4.101085000
H	0.165006000	3.768741000	2.447736000
C	-2.716137000	3.838890000	5.034220000
C	-0.714041000	4.823574000	4.113226000
H	-3.518443000	3.840112000	5.769471000
H	0.044437000	5.604187000	4.119692000
C	-1.750260000	4.847176000	5.050379000
H	-1.802233000	5.642675000	5.791481000

Coordinate C.8: Optimized Cartesian coordinates of Mn(ba)$_3$, **3**; *mer3* CH$_3$-Ph, S=4/2 with no symmetry (OLYP/TZP).

Mn	0.115032000	-0.087947000	-0.070805000

O	2.235757000	0.599224000	0.034536000
O	0.626096000	−1.450589000	1.253448000
O	−1.996464000	−0.759495000	0.018067000
O	−0.357412000	1.200471000	1.335796000
O	−0.296734000	1.287425000	−1.435884000
O	0.532240000	−1.377306000	−1.523781000
C	3.096883000	0.220076000	0.880477000
C	2.884551000	−0.834564000	1.812975000
C	1.718547000	−1.589758000	1.928555000
C	1.659104000	−2.723209000	2.934633000
C	−2.894254000	−0.252244000	0.748111000
C	−2.696314000	0.806251000	1.674454000
C	−1.482369000	1.455163000	1.919504000
C	−0.579199000	2.434562000	−3.470663000
C	−0.234854000	1.170652000	−2.711837000
C	0.118854000	0.010646000	−3.411938000
C	0.479378000	−1.201880000	−2.793313000
H	3.706481000	−1.122110000	2.455341000
H	0.869594000	−2.515984000	3.665283000
H	2.605948000	−2.862642000	3.459640000
H	1.388600000	−3.652282000	2.421912000
H	−3.568249000	1.163655000	2.206435000
H	−1.590781000	2.754009000	−3.198942000
H	−0.519698000	2.301167000	−4.552265000
H	0.103903000	3.234615000	−3.166184000
H	0.157281000	0.072520000	−4.490833000
H	4.973551000	0.554659000	2.918364000
C	6.493846000	1.671700000	1.902226000
C	4.430814000	0.916861000	0.853519000
C	5.275736000	0.995818000	1.973116000
C	4.839580000	1.540712000	−0.336566000
H	4.182327000	1.493951000	−1.199524000
C	6.063619000	2.201635000	−0.413101000
H	7.127825000	1.734342000	2.784484000
H	6.369271000	2.666690000	−1.348553000

C	6.896361000	2.270906000	0.706927000
H	7.850016000	2.792521000	0.650355000
C	0.864942000	−2.386994000	−3.620062000
C	1.704934000	−3.365589000	−3.061700000
C	0.404631000	−2.566899000	−4.935994000
H	2.055905000	−3.237972000	−2.042746000
H	−0.276250000	−1.847810000	−5.381322000
C	2.092062000	−4.477454000	−3.806083000
C	0.781788000	−3.687384000	−5.674071000
H	2.754084000	−5.218394000	−3.362691000
H	0.405225000	−3.817025000	−6.686504000
C	1.632402000	−4.643529000	−5.114719000
H	1.930321000	−5.515426000	−5.693836000
C	−4.291489000	−0.836376000	0.602715000
H	−4.253368000	−1.908548000	0.823101000
H	−4.614622000	−0.735038000	−0.438894000
H	−5.027988000	−0.361288000	1.254670000
C	−1.411586000	2.570783000	2.919776000
C	−2.297561000	2.666266000	4.006565000
C	−0.411439000	3.548586000	2.784639000
H	−3.055399000	1.904045000	4.161311000
H	0.288555000	3.473289000	1.958496000
C	−2.195679000	3.714627000	4.919840000
C	−0.317717000	4.602223000	3.691830000
H	−2.884070000	3.764084000	5.761172000
H	0.457765000	5.354913000	3.563666000
C	−1.209257000	4.690989000	4.763322000
H	−1.131934000	5.510165000	5.475784000

Coordinate C.9: Optimized Cartesian coordinates of Mn(dbm)$_3$, **4**; S=4/2 with no symmetry (PW91/TZP).

Mn	11.973657000	0.412528000	13.402320000
O	10.865475000	0.999037000	11.928234000
O	12.013626000	−1.513155000	12.454422000
O	13.524590000	1.083870000	12.441599000
O	13.114636000	−0.188760000	14.846072000

O	11.635857000	2.340272000	14.345155000
O	10.448105000	-0.215793000	14.419371000
C	10.100426000	0.286027000	11.159062000
C	10.153225000	-1.103638000	11.034843000
C	11.103637000	-1.939833000	11.672075000
C	14.757625000	1.102891000	12.818165000
C	15.216361000	0.586366000	14.039983000
C	14.389971000	-0.036527000	14.984846000
C	11.048648000	2.494343000	15.462873000
C	10.283761000	1.481307000	16.099866000
C	10.008685000	0.224852000	15.558926000
H	9.390409000	-1.572768000	10.425222000
H	16.262066000	0.714375000	14.287807000
H	9.893521000	1.687035000	17.089624000
C	9.106960000	1.079517000	10.378673000
C	8.792720000	2.379148000	10.807905000
H	9.283800000	2.764451000	11.699255000
C	7.868193000	3.151300000	10.108598000
H	7.627338000	4.154852000	10.458814000
C	7.250936000	2.643570000	8.963357000
H	6.530215000	3.249304000	8.414196000
C	7.566267000	1.356800000	8.519946000
H	7.099488000	0.959837000	7.619122000
C	8.486423000	0.581239000	9.221019000
H	8.743113000	-0.408869000	8.847981000
C	11.060908000	-3.419523000	11.441185000
C	10.361854000	-4.013539000	10.378067000
H	9.826734000	-3.395024000	9.659523000
C	10.365757000	-5.397008000	10.210108000
H	9.826088000	-5.842228000	9.374762000
C	11.063306000	-6.210448000	11.105336000
H	11.062827000	-7.292430000	10.974523000
C	11.766504000	-5.630142000	12.164067000
H	12.316053000	-6.259637000	12.863661000
C	11.771020000	-4.247309000	12.325783000

H	12.323527000	−3.775840000	13.136660000
C	15.698797000	1.744745000	11.858158000
C	15.166966000	2.485338000	10.789230000
H	14.085447000	2.562012000	10.698654000
C	16.008792000	3.105319000	9.870264000
H	15.582342000	3.680566000	9.049275000
C	17.394864000	2.988539000	9.996884000
H	18.053814000	3.470555000	9.275047000
C	17.934574000	2.244914000	11.048595000
H	19.014437000	2.139564000	11.145437000
C	17.094579000	1.628827000	11.972699000
H	17.534423000	1.037075000	12.773269000
C	14.948634000	−0.568083000	16.258313000
C	16.323128000	−0.794390000	16.442445000
H	17.024575000	−0.602519000	15.632470000
C	16.802125000	−1.296944000	17.649488000
H	17.869286000	−1.475559000	17.775295000
C	15.917011000	−1.579306000	18.692237000
H	16.293855000	−1.970732000	19.636921000
C	14.548496000	−1.363091000	18.517709000
H	13.852856000	−1.582091000	19.326937000
C	14.066396000	−0.866459000	17.310199000
H	13.002174000	−0.695199000	17.163085000
C	11.190251000	3.834302000	16.118222000
C	12.177639000	4.707244000	15.635276000
H	12.803341000	4.368135000	14.811765000
C	12.347111000	5.969669000	16.196794000
H	13.123253000	6.632615000	15.815592000
C	11.523604000	6.387647000	17.245094000
H	11.652200000	7.377644000	17.682511000
C	10.530193000	5.533082000	17.727219000
H	9.876705000	5.857279000	18.536510000
C	10.366252000	4.266320000	17.170147000
H	9.573132000	3.622345000	17.545876000
C	9.154819000	−0.747865000	16.302220000

C	8.255371000	-0.352292000	17.306128000
H	8.137532000	0.702792000	17.548067000
C	7.479474000	-1.296234000	17.975069000
H	6.778253000	-0.973024000	18.743622000
C	7.588511000	-2.650849000	17.651964000
H	6.979414000	-3.387937000	18.174861000
C	8.472043000	-3.053456000	16.648122000
H	8.557151000	-4.107338000	16.385398000
C	9.243828000	-2.110589000	15.974584000
H	9.929278000	-2.411039000	15.184639000

Coordinate C.10: Optimized Cartesian coordinates of Mn(dbm)₃, **4**; S=4/2 with no symmetry (BP86/TZP).

Mn	11.973393000	0.360720000	13.454320000
O	10.828719000	0.949557000	12.002706000
O	11.999807000	-1.569599000	12.500447000
O	13.495854000	1.044326000	12.452994000
O	13.159841000	-0.237944000	14.868315000
O	11.679007000	2.293170000	14.409813000
O	10.462975000	-0.261276000	14.503691000
C	10.106864000	0.240164000	11.187065000
C	10.176626000	-1.147900000	11.036592000
C	11.113968000	-1.992610000	11.686746000
C	14.731942000	1.119411000	12.819873000
C	15.223620000	0.624429000	14.039987000
C	14.432998000	-0.039440000	14.990699000
C	11.074649000	2.473803000	15.515983000
C	10.240710000	1.496220000	16.124421000
C	9.956705000	0.235161000	15.593442000
H	9.443215000	-1.603792000	10.381009000
H	16.266449000	0.796996000	14.278654000
H	9.767151000	1.743444000	17.067712000
C	9.137642000	1.038452000	10.375242000
C	8.759089000	2.314084000	10.830404000
H	9.182560000	2.679195000	11.765128000
C	7.856680000	3.088465000	10.101263000
H	7.564440000	4.071884000	10.472718000

C	7.327548000	2.608214000	8.898752000
H	6.624815000	3.215911000	8.326218000
C	7.709850000	1.347310000	8.428386000
H	7.314798000	0.973200000	7.482778000
C	8.606811000	0.568481000	9.160051000
H	8.919118000	−0.399030000	8.766758000
C	11.095985000	−3.471893000	11.423994000
C	10.303990000	−4.074851000	10.429567000
H	9.662483000	−3.468889000	9.790711000
C	10.335780000	−5.456116000	10.232958000
H	9.718538000	−5.906255000	9.454105000
C	11.158518000	−6.260669000	11.027702000
H	11.181767000	−7.340753000	10.872950000
C	11.953021000	−5.672704000	12.017965000
H	12.599143000	−6.294139000	12.640140000
C	11.924050000	−4.292042000	12.211150000
H	12.540385000	−3.815726000	12.972797000
C	15.636601000	1.797868000	11.845806000
C	15.061561000	2.518987000	10.782976000
H	13.975747000	2.555299000	10.706987000
C	15.867541000	3.171534000	9.851234000
H	15.407189000	3.730648000	9.035451000
C	17.260765000	3.108328000	9.959167000
H	17.891619000	3.616102000	9.227778000
C	17.843732000	2.385335000	11.005244000
H	18.929471000	2.321635000	11.087823000
C	17.039487000	1.735783000	11.941358000
H	17.512964000	1.160291000	12.736171000
C	15.032397000	−0.566812000	16.250878000
C	16.419065000	−0.748201000	16.410210000
H	17.100588000	−0.523983000	15.590022000
C	16.936075000	−1.248069000	17.605208000
H	18.012172000	−1.391406000	17.711155000
C	16.077705000	−1.573044000	18.660986000
H	16.484226000	−1.962218000	19.595915000

C	14.697523000	-1.402511000	18.510793000
H	14.022453000	-1.655553000	19.329487000
C	14.178052000	-0.908766000	17.315062000
H	13.105342000	-0.773368000	17.185939000
C	11.252819000	3.815015000	16.170529000
C	11.954905000	4.805705000	15.461169000
H	12.341039000	4.551300000	14.474856000
C	12.149794000	6.073169000	16.008116000
H	12.694689000	6.830347000	15.441966000
C	11.651275000	6.373548000	17.280369000
H	11.804667000	7.364313000	17.711478000
C	10.958201000	5.395373000	18.000406000
H	10.573798000	5.619617000	18.996454000
C	10.759007000	4.128318000	17.450236000
H	10.225228000	3.380731000	18.036122000
C	9.005075000	-0.679822000	16.296900000
C	8.033626000	-0.210532000	17.200081000
H	7.933250000	0.858731000	17.387310000
C	7.163353000	-1.099518000	17.831687000
H	6.407037000	-0.718998000	18.519720000
C	7.249299000	-2.471820000	17.572709000
H	6.567160000	-3.165777000	18.066701000
C	8.204829000	-2.947317000	16.668745000
H	8.272930000	-4.015175000	16.455486000
C	9.070531000	-2.059066000	16.030719000
H	9.811182000	-2.416154000	15.316664000

Coordinate C.11: Optimized Cartesian coordinates of Mn(dbm)$_3$, **4**; S=4/2 with no symmetry (OLYP/TZP).

Mn	0.000000000	0.000000000	0.022873000
O	-0.721381000	1.350803000	1.463584000
O	-1.731439000	-0.856259000	0.057645000
O	0.563718000	-1.317963000	-1.519757000
O	-0.563718000	1.317963000	-1.519757000
O	1.731439000	0.856259000	0.057645000
O	0.721381000	-1.350803000	1.463584000
C	-1.871462000	1.356153000	2.010519000

C	−2.888891000	0.415407000	1.721494000
C	−2.772618000	−0.617547000	0.787111000
C	0.455982000	−1.168169000	−2.785282000
C	0.000000000	0.000000000	−3.427624000
C	−0.455982000	1.168169000	−2.785282000
C	2.772618000	0.617547000	0.787111000
C	2.888891000	−0.415407000	1.721494000
C	1.871462000	−1.356153000	2.010519000
H	−3.791516000	0.449411000	2.310954000
H	0.000000000	0.000000000	−4.506569000
H	3.791516000	−0.449411000	2.310954000
H	−4.277327000	2.425174000	2.922613000
C	−3.575182000	3.870651000	4.336537000
C	−2.112473000	2.426008000	3.033458000
C	−3.400451000	2.857378000	3.395247000
C	−1.005333000	3.045806000	3.637286000
H	−0.007844000	2.725801000	3.353775000
C	−1.180634000	4.049589000	4.586805000
H	−4.579717000	4.199556000	4.594405000
H	−0.310886000	4.510057000	5.051021000
C	−2.466126000	4.466940000	4.940392000
H	−2.603389000	5.255343000	5.677921000
C	2.112473000	−2.426008000	3.033458000
C	1.005333000	−3.045806000	3.637286000
C	3.400451000	−2.857378000	3.395247000
H	0.007844000	−2.725801000	3.353775000
H	4.277327000	−2.425174000	2.922613000
C	1.180634000	−4.049589000	4.586805000
C	3.575182000	−3.870651000	4.336537000
H	0.310886000	−4.510057000	5.051021000
H	4.579717000	−4.199556000	4.594405000
C	2.466126000	−4.466940000	4.940392000
H	2.603389000	−5.255343000	5.677921000
C	−0.884498000	2.344880000	−3.617786000
C	−0.380130000	2.589542000	−4.906404000

C	−1.809035000	3.255311000	−3.079768000
H	0.366423000	1.927586000	−5.335513000
H	−2.188596000	3.081845000	−2.077643000
C	−0.796868000	3.701629000	−5.637460000
C	−2.235949000	4.359092000	−3.815374000
H	−0.383953000	3.880292000	−6.628366000
H	−2.962527000	5.045831000	−3.385073000
C	−1.732286000	4.587461000	−5.098336000
H	−2.060718000	5.452599000	−5.671435000
C	5.958120000	3.452089000	0.152900000
C	6.253752000	2.181393000	0.651813000
C	4.634771000	3.785128000	−0.144054000
H	7.283743000	1.905943000	0.868447000
H	4.395181000	4.770283000	−0.538733000
C	5.233560000	1.256062000	0.863335000
C	3.614387000	2.858168000	0.057118000
H	5.490157000	0.265071000	1.225432000
H	2.587490000	3.114372000	−0.183005000
C	3.896585000	1.582805000	0.576595000
H	6.755672000	4.174226000	−0.010751000
C	2.235949000	−4.359092000	−3.815374000
C	1.732286000	−4.587461000	−5.098336000
C	1.809035000	−3.255311000	−3.079768000
H	2.060718000	−5.452599000	−5.671435000
H	2.188596000	−3.081845000	−2.077643000
C	0.796868000	−3.701629000	−5.637460000
C	0.884498000	−2.344880000	−3.617786000
H	0.383953000	−3.880292000	−6.628366000
C	0.380130000	−2.589542000	−4.906404000
H	−0.366423000	−1.927586000	−5.335513000
H	2.962527000	−5.045831000	−3.385073000
C	−3.614387000	−2.858168000	0.057118000
C	−4.634771000	−3.785128000	−0.144054000
C	−3.896585000	−1.582805000	0.576595000
H	−4.395181000	−4.770283000	−0.538733000

C	-5.958120000	-3.452089000	0.152900000
C	-5.233560000	-1.256062000	0.863335000
H	-6.755672000	-4.174226000	-0.010751000
H	-5.490157000	-0.265071000	1.225432000
C	-6.253752000	-2.181393000	0.651813000
H	-7.283743000	-1.905943000	0.868447000
H	-2.587490000	-3.114372000	-0.183005000

Coordinate C.12: Optimized Cartesian coordinates of Mn(dbm)₃, **4**; S=4/2 with no symmetry (B3LYP/TZP).

Mn	11.500601000	0.372862000	13.693165000
O	10.244126000	0.803744000	12.291488000
O	11.638693000	-1.622561000	12.853979000
O	12.946123000	0.927444000	12.505788000
O	12.776374000	-0.133228000	15.076314000
O	11.389557000	2.365373000	14.546933000
O	10.062285000	-0.131706000	14.889516000
C	10.108543000	0.222402000	11.144026000
C	10.646211000	-1.013405000	10.781213000
C	11.388212000	-1.873379000	11.640221000
C	14.208028000	0.799034000	12.698974000
C	14.787720000	0.269615000	13.864274000
C	14.056753000	-0.160843000	14.983781000
C	10.991868000	2.572403000	15.729037000
C	10.161491000	1.674782000	16.459361000
C	9.717046000	0.432651000	15.999327000
H	10.391020000	-1.387390000	9.801253000
H	15.863231000	0.287200000	13.943885000
H	9.824373000	1.983785000	17.437194000
C	9.261050000	0.981239000	10.168474000
C	8.237891000	1.810594000	10.656423000
H	8.085932000	1.876826000	11.727196000
C	7.430460000	2.530715000	9.777326000
H	6.634926000	3.156792000	10.168017000
C	7.647003000	2.451845000	8.398656000
H	7.023399000	3.018688000	7.715027000

A-54

C	8.676240000	1.646223000	7.904605000
H	8.861897000	1.593798000	6.836783000
C	9.474619000	0.912484000	8.782386000
H	10.286006000	0.309729000	8.390386000
C	11.893285000	−3.183554000	11.102184000
C	12.185162000	−3.377831000	9.742764000
H	12.047662000	−2.565912000	9.037998000
C	12.692771000	−4.597099000	9.292152000
H	12.927949000	−4.727279000	8.240884000
C	12.904527000	−5.643908000	10.192630000
H	13.294740000	−6.593579000	9.841094000
C	12.619606000	−5.459901000	11.549192000
H	12.786027000	−6.268389000	12.253710000
C	12.128566000	−4.236409000	12.001177000
H	11.922585000	−4.074542000	13.052559000
C	15.077794000	1.299947000	11.590797000
C	14.581753000	2.300875000	10.738598000
H	13.579986000	2.678575000	10.904433000
C	15.370083000	2.802937000	9.704659000
H	14.980559000	3.586059000	9.062641000
C	16.656408000	2.298525000	9.493098000
H	17.267900000	2.686302000	8.684869000
C	17.150424000	1.287433000	10.321682000
H	18.141340000	0.879576000	10.151802000
C	16.369021000	0.794518000	11.366003000
H	16.754407000	−0.005632000	11.987169000
C	14.772937000	−0.662995000	16.196207000
C	16.039111000	−1.266392000	16.117040000
H	16.516248000	−1.400901000	15.153176000
C	16.674461000	−1.732913000	17.267163000
H	17.646636000	−2.208425000	17.190043000
C	16.057418000	−1.595096000	18.513352000
H	16.554642000	−1.953809000	19.408701000
C	14.794988000	−1.001473000	18.601316000
H	14.310530000	−0.895782000	19.566344000

C	14.151762000	−0.547481000	17.451137000
H	13.168679000	−0.094867000	17.508044000
C	11.424014000	3.859461000	16.375279000
C	11.775384000	4.941832000	15.552473000
H	11.701470000	4.820152000	14.478342000
C	12.214327000	6.142419000	16.107467000
H	12.474132000	6.973439000	15.459830000
C	12.330039000	6.273568000	17.494710000
H	12.683240000	7.204407000	17.926697000
C	11.999752000	5.197851000	18.322309000
H	12.104185000	5.286746000	19.398732000
C	11.543271000	4.001745000	17.767158000
H	11.312590000	3.167511000	18.419966000
C	8.779303000	−0.378726000	16.840311000
C	7.837358000	0.214246000	17.696497000
H	7.750584000	1.294367000	17.737885000
C	6.985443000	−0.576292000	18.467988000
H	6.253621000	−0.105096000	19.115842000
C	7.067438000	−1.969867000	18.400105000
H	6.407083000	−2.583958000	19.003746000
C	7.996230000	−2.568682000	17.544407000
H	8.061804000	−3.650156000	17.483793000
C	8.838587000	−1.779965000	16.762174000
H	9.554194000	−2.234557000	16.087501000

Coordinate C.13: Optimized Cartesian coordinates of Mn(tfaa)₃, **5**; *fac*, S=4/2 with no symmetry (PW91/TZP).

Mn	0.093026000	−0.299892000	0.105084000
O	1.925678000	0.376896000	−0.015443000
O	0.643346000	−1.624209000	1.431711000
O	−1.746620000	−0.880901000	0.279003000
O	−0.291741000	1.120246000	1.706933000
O	−0.443548000	1.058578000	−1.166097000
O	0.514982000	−1.591516000	−1.586140000
C	2.853601000	0.119352000	0.823761000
C	2.828349000	−0.784924000	1.873759000
C	1.730015000	−1.637429000	2.109141000

C	-2.751703000	-0.203138000	0.724224000
C	-2.669406000	0.969318000	1.485155000
C	-1.462842000	1.530872000	1.927557000
C	-0.107997000	1.117204000	-2.409361000
C	0.448620000	0.143175000	-3.208270000
C	0.732873000	-1.184177000	-2.761192000
H	3.708340000	-0.879481000	2.501277000
H	-3.596986000	1.447586000	1.781242000
H	0.658576000	0.395850000	-4.242705000
C	-1.522944000	2.795056000	2.818444000
F	-0.809205000	3.801469000	2.259887000
F	-2.790523000	3.249969000	3.019495000
F	-0.986890000	2.531424000	4.040798000
C	4.144014000	0.910610000	0.535984000
F	3.884745000	2.229626000	0.409453000
F	5.072887000	0.758272000	1.515274000
F	4.697823000	0.476290000	-0.629184000
C	1.790433000	-2.648503000	3.216059000
H	1.146609000	-2.305304000	4.038026000
H	1.386369000	-3.604518000	2.864784000
H	2.806538000	-2.782871000	3.596041000
C	-4.096759000	-0.769844000	0.363324000
H	-4.252312000	-0.655227000	-0.718248000
H	-4.112202000	-1.844798000	0.579995000
H	-4.909015000	-0.269442000	0.896825000
C	-0.426836000	2.497187000	-3.012188000
F	0.231248000	3.474335000	-2.343316000
F	-0.081666000	2.590061000	-4.323541000
F	-1.759487000	2.753891000	-2.920507000
C	1.344576000	-2.150649000	-3.741698000
H	2.439077000	-2.061814000	-3.679180000
H	1.074248000	-3.176131000	-3.472667000
H	1.050848000	-1.933452000	-4.774175000

Coordinate C.14: Optimized Cartesian coordinates of Mn(tfaa)$_3$, **5**; *mer1* CF$_3$-CF$_3$, S=4/2 with no symmetry (PW91/TZP).

Mn	-0.014283000	-0.238689000	0.306032000
O	1.809325000	0.428249000	0.113760000
O	0.589593000	-1.607376000	1.567510000
O	-1.831031000	-0.876796000	0.516698000
O	-0.431927000	1.207930000	1.849968000
O	-0.585060000	1.090445000	-0.989804000
O	0.380280000	-1.556808000	-1.374550000
C	2.856756000	-0.116963000	0.604683000
C	2.935333000	-1.213394000	1.446566000
C	1.789181000	-1.896490000	1.906401000
C	-2.854783000	-0.234328000	0.967379000
C	-2.806799000	0.980054000	1.663616000
C	-1.611825000	1.605293000	2.049830000
C	-0.196288000	1.219576000	-2.214783000
C	0.434364000	0.225461000	-2.972094000
C	0.669979000	-1.075105000	-2.503723000
H	3.912558000	-1.545907000	1.779768000
H	-3.745890000	1.436085000	1.959196000
H	0.730813000	0.469417000	-3.986848000
C	-1.697160000	2.942642000	2.822369000
F	-1.135255000	3.938430000	2.088142000
F	-2.975293000	3.316851000	3.107071000
F	-1.023603000	2.860364000	3.995962000
C	1.373482000	-2.079767000	-3.446136000
F	1.654209000	-1.561788000	-4.672592000
F	2.549037000	-2.484981000	-2.895603000
F	0.602462000	-3.179748000	-3.632207000
C	4.147196000	0.597934000	0.160524000
F	4.132833000	1.890875000	0.565177000
F	5.264438000	0.015467000	0.666419000
F	4.248195000	0.582813000	-1.191740000
C	1.932529000	-3.034331000	2.873863000
H	1.491745000	-2.739900000	3.836014000

H	1.362438000	-3.896629000	2.507710000
H	2.978015000	-3.314302000	3.028597000
C	-4.175708000	-0.898490000	0.699544000
H	-4.350277000	-0.931428000	-0.384288000
H	-4.135585000	-1.937945000	1.048559000
H	-5.004451000	-0.376998000	1.186240000
C	-0.471809000	2.568066000	-2.816168000
H	0.147895000	3.317591000	-2.304991000
H	-0.258564000	2.592690000	-3.888208000
H	-1.518744000	2.842452000	-2.637118000

Coordinate C.15: Optimized Cartesian coordinates of Mn(tfaa)$_3$, **5**; *mer2* CH$_3$-CH$_3$, S=4/2 with no symmetry (PW91/TZP).

Mn	0.341811000	-0.141707000	0.194355000
O	2.178754000	0.535486000	0.235880000
O	0.801571000	-1.543642000	1.465540000
O	-1.492811000	-0.784022000	0.184549000
O	-0.252726000	1.224818000	1.779207000
O	-0.119368000	1.228469000	-1.086848000
O	0.792962000	-1.451751000	-1.490139000
C	3.134867000	0.051361000	0.929204000
C	3.103952000	-1.034077000	1.791615000
C	1.931209000	-1.781150000	2.019911000
C	-2.523836000	-0.113778000	0.576054000
C	-2.581679000	1.017067000	1.360035000
C	-1.432641000	1.643472000	1.938540000
C	-0.407397000	1.053161000	-2.333609000
C	-0.229338000	-0.058981000	-3.123030000
C	0.386814000	-1.269301000	-2.669464000
H	4.014850000	-1.316263000	2.308207000
H	-3.559784000	1.438128000	1.570873000
H	-0.543783000	0.000304000	-4.160679000
C	4.456706000	0.818788000	0.728150000
F	4.299266000	2.123415000	1.052947000
F	5.465702000	0.320862000	1.490867000

F	4.847963000	0.750413000	-0.568434000
C	1.946453000	-2.934454000	2.979624000
H	1.350152000	-2.668267000	3.863252000
H	1.462763000	-3.801623000	2.514760000
H	2.960076000	-3.192984000	3.296177000
C	-1.639406000	2.878439000	2.775604000
H	-2.589816000	2.852428000	3.319747000
H	-0.802129000	3.003514000	3.468327000
H	-1.661569000	3.751400000	2.106571000
C	-3.831631000	-0.738553000	0.059450000
F	-3.830416000	-0.785860000	-1.299153000
F	-3.965091000	-2.010643000	0.516527000
F	-4.936456000	-0.047333000	0.443317000
C	0.564513000	-2.381542000	-3.669918000
H	1.084723000	-2.018064000	-4.565426000
H	1.124763000	-3.204341000	-3.219309000
H	-0.420233000	-2.744473000	-3.994544000
C	-1.013907000	2.325071000	-2.952201000
F	-0.118836000	3.345403000	-2.912768000
F	-1.386862000	2.153794000	-4.247170000
F	-2.115533000	2.714437000	-2.258271000

Coordinate C.16: Optimized Cartesian coordinates of Mn(tfaa)$_3$, **5**; *mer2* CF$_3$-CH$_3$, S=4/2 with no symmetry (PW91/TZP).

Mn	0.087816000	-0.139452000	0.342097000
O	1.906179000	0.575685000	0.209819000
O	0.683511000	-1.505749000	1.598614000
O	-1.725781000	-0.838070000	0.443234000
O	-0.449472000	1.211093000	1.943897000
O	-0.495764000	1.143850000	-0.979627000
O	0.612550000	-1.503704000	-1.275421000
C	2.954971000	-0.033045000	0.614135000
C	3.033485000	-1.189165000	1.374761000
C	1.887558000	-1.854840000	1.857920000
C	-2.748870000	-0.188286000	0.875998000

C	-2.793001000	0.930195000	1.682907000
C	-1.630626000	1.567453000	2.215574000
C	-0.405070000	1.107090000	-2.267878000
C	0.131138000	0.060048000	-3.024340000
C	0.610231000	-1.141293000	-2.481186000
H	4.012305000	-1.572078000	1.642031000
H	-3.768349000	1.324536000	1.949742000
H	0.174324000	0.187035000	-4.100923000
C	1.234282000	-2.182843000	-3.441192000
F	1.203797000	-1.800269000	-4.746580000
F	2.536131000	-2.393097000	-3.109314000
F	0.584563000	-3.368154000	-3.344451000
C	4.248916000	0.677590000	0.173584000
F	4.297975000	1.930287000	0.691166000
F	5.366526000	0.018734000	0.573842000
F	4.290894000	0.780562000	-1.177431000
C	2.030825000	-3.054475000	2.747217000
H	1.448988000	-2.897711000	3.664150000
H	1.597185000	-3.925211000	2.237616000
H	3.074065000	-3.261030000	2.998916000
C	-0.941522000	2.329366000	-2.957884000
H	-0.441661000	3.221757000	-2.560592000
H	-0.804660000	2.280452000	-4.041208000
H	-2.011280000	2.428975000	-2.730802000
C	-1.807826000	2.710148000	3.181743000
H	-2.817148000	3.132217000	3.152325000
H	-1.613645000	2.343820000	4.199444000
H	-1.064514000	3.485959000	2.968729000
C	-4.066549000	-0.809378000	0.377283000
F	-4.112127000	-0.783252000	-0.982044000
F	-4.168932000	-2.103010000	0.769297000
F	-5.165338000	-0.151458000	0.833342000

Coordinate C.17: : Optimized Cartesian coordinates of Mn(tfaa)₃, **5**; *fac*, S=4/2 with no symmetry (BP86/TZP).

Mn	0.130296000	-0.261934000	0.107427000

O	1.973541000	0.399382000	0.023894000
O	0.650226000	−1.598461000	1.437425000
O	−1.715199000	−0.848468000	0.246579000
O	−0.295010000	1.162292000	1.701796000
O	−0.385254000	1.097382000	−1.172056000
O	0.563552000	−1.566360000	−1.585398000
C	2.900475000	0.103403000	0.854470000
C	2.860247000	−0.823109000	1.887063000
C	1.739008000	−1.650644000	2.113807000
C	−2.733591000	−0.195497000	0.704259000
C	−2.672881000	0.970018000	1.481232000
C	−1.474269000	1.549556000	1.928808000
C	−0.122255000	1.125296000	−2.436302000
C	0.394191000	0.134174000	−3.242800000
C	0.706162000	−1.186137000	−2.781832000
H	3.740636000	−0.949754000	2.510136000
H	−3.610105000	1.426721000	1.786138000
H	0.543952000	0.362405000	−4.294995000
C	−1.555335000	2.803596000	2.838046000
F	−0.870354000	3.835268000	2.284654000
F	−2.833423000	3.226883000	3.056898000
F	−1.000666000	2.537718000	4.053800000
C	4.209350000	0.874816000	0.577952000
F	3.973043000	2.199582000	0.449577000
F	5.128449000	0.706151000	1.567098000
F	4.767495000	0.429957000	−0.583091000
C	1.773776000	−2.677466000	3.212153000
H	1.205730000	−2.289134000	4.071488000
H	1.276628000	−3.595751000	2.877971000
H	2.796212000	−2.894075000	3.538991000
C	−4.069905000	−0.789797000	0.343946000
H	−4.228466000	−0.683793000	−0.739228000
H	−4.066198000	−1.864844000	0.567279000
H	−4.892726000	−0.301586000	0.876463000
C	−0.493520000	2.489404000	−3.053629000

F	0.158740000	3.495778000	-2.421079000
F	-0.190994000	2.568352000	-4.378812000
F	-1.831612000	2.715378000	-2.926300000
C	1.239397000	-2.177455000	-3.788347000
H	2.273972000	-1.906920000	-4.050595000
H	1.232484000	-3.185005000	-3.360955000
H	0.653310000	-2.153952000	-4.716875000

Coordinate C.18: Optimized Cartesian coordinates of Mn(tfaa)$_3$, **5**; *mer1* CF$_3$-CF$_3$, S=4/2 with no symmetry (BP86/TZP).

Mn	0.048731000	-0.230976000	0.248749000
O	1.883053000	0.434304000	0.098075000
O	0.620933000	-1.590567000	1.533781000
O	-1.781710000	-0.858192000	0.427852000
O	-0.386316000	1.208939000	1.810400000
O	-0.494149000	1.105065000	-1.048774000
O	0.435785000	-1.569173000	-1.423859000
C	2.903359000	-0.033417000	0.714236000
C	2.950513000	-1.086199000	1.616085000
C	1.799331000	-1.816502000	1.986073000
C	-2.807717000	-0.236009000	0.906222000
C	-2.763442000	0.953155000	1.649525000
C	-1.570170000	1.578695000	2.045823000
C	-0.189293000	1.192561000	-2.303026000
C	0.365827000	0.165500000	-3.077831000
C	0.623505000	-1.126878000	-2.590898000
H	3.907056000	-1.358682000	2.051550000
H	-3.705338000	1.387013000	1.973122000
H	0.582899000	0.375923000	-4.121066000
C	-1.664690000	2.887728000	2.872310000
F	-1.215080000	3.937328000	2.130137000
F	-2.936525000	3.183751000	3.266539000
F	-0.898304000	2.809046000	3.989232000
C	1.185254000	-2.183732000	-3.577367000
F	1.503321000	-1.663615000	-4.796659000

F	2.308449000	-2.756173000	-3.072558000
F	0.269948000	-3.170652000	-3.779316000
C	4.201197000	0.720283000	0.351090000
F	4.083762000	2.037049000	0.654377000
F	5.285478000	0.235264000	1.013178000
F	4.448955000	0.616276000	-0.980185000
C	1.906273000	-2.938228000	2.981774000
H	1.367136000	-2.654264000	3.897474000
H	1.411298000	-3.831394000	2.578599000
H	2.946570000	-3.167892000	3.233390000
C	-4.129638000	-0.897443000	0.617140000
H	-4.305440000	-0.896017000	-0.468234000
H	-4.086667000	-1.948613000	0.933141000
H	-4.960897000	-0.393637000	1.121229000
C	-0.485126000	2.533155000	-2.920838000
H	0.154835000	3.292638000	-2.448708000
H	-0.313698000	2.535163000	-4.002246000
H	-1.525653000	2.813599000	-2.708514000

Coordinate C.19: Optimized Cartesian coordinates of Mn(tfaa)$_3$, **5**; *mer2* CH$_3$-CH$_3$, S=4/2 with no symmetry (BP86/TZP).

Mn	0.332099000	-0.126140000	0.182937000
O	2.176892000	0.533509000	0.232698000
O	0.780025000	-1.530330000	1.463207000
O	-1.502010000	-0.768028000	0.166846000
O	-0.268858000	1.244996000	1.774836000
O	-0.124731000	1.250094000	-1.099926000
O	0.790510000	-1.430681000	-1.506650000
C	3.127138000	0.048850000	0.937919000
C	3.083100000	-1.027772000	1.813821000
C	1.903120000	-1.769564000	2.034422000
C	-2.539467000	-0.124292000	0.591459000
C	-2.604577000	0.992491000	1.396140000
C	-1.455678000	1.630199000	1.970404000
C	-0.382332000	1.088540000	-2.356633000

```
C      -0.177116000     -0.013987000     -3.156125000
C       0.423462000     -1.232274000     -2.698372000
H       3.988882000     -1.310122000      2.341830000
H      -3.587610000      1.392087000      1.632457000
H      -0.464086000      0.057264000     -4.202154000
C       4.465499000      0.786827000      0.715292000
F       4.307280000      2.122853000      0.858368000
F       5.429049000      0.385951000      1.589820000
F       4.925197000      0.546411000     -0.542470000
C       1.902616000     -2.921137000      3.001559000
H       1.289190000     -2.652969000      3.874344000
H       1.429928000     -3.792780000      2.530843000
H       2.912662000     -3.176362000      3.337795000
C      -1.686527000      2.814345000      2.878270000
H      -2.283669000      3.579139000      2.361187000
H      -2.259099000      2.504547000      3.765071000
H      -0.728091000      3.240125000      3.190775000
C      -3.844546000     -0.774552000      0.091234000
F      -3.869406000     -0.812230000     -1.269024000
F      -3.941340000     -2.055289000      0.541056000
F      -4.958995000     -0.110289000      0.501616000
C       0.622547000     -2.341401000     -3.703095000
H       1.055413000     -1.957531000     -4.636798000
H       1.264453000     -3.119972000     -3.279375000
H      -0.355083000     -2.781043000     -3.954293000
C      -0.986854000      2.366424000     -2.974860000
F      -0.095231000      3.391867000     -2.921723000
F      -1.346593000      2.201885000     -4.277149000
F      -2.097156000      2.748799000     -2.288586000
```

Coordinate C.20: Optimized Cartesian coordinates of Mn(tfaa)$_3$, **5**; *mer3* CF$_3$-CH$_3$, S=4/2 with no symmetry (BP86/TZP).

```
Mn      0.112533000     -0.088768000      0.258858000
O       1.949046000      0.592199000      0.186843000
O       0.648196000     -1.459967000      1.543270000
```

O	−1.712329000	−0.765400000	0.329798000
O	−0.438797000	1.304696000	1.829899000
O	−0.399802000	1.205263000	−1.087132000
O	0.615159000	−1.479065000	−1.350666000
C	2.973818000	−0.002979000	0.671231000
C	3.010090000	−1.150696000	1.450435000
C	1.836420000	−1.815748000	1.868388000
C	−2.731657000	−0.197674000	0.877306000
C	−2.779147000	0.896734000	1.718967000
C	−1.619077000	1.596914000	2.177259000
C	−0.305583000	1.155872000	−2.376716000
C	0.166724000	0.069870000	−3.125577000
C	0.590395000	−1.147523000	−2.567082000
H	3.973334000	−1.529731000	1.778407000
H	−3.753947000	1.222610000	2.071617000
H	0.202887000	0.178211000	−4.205695000
C	1.107961000	−2.254439000	−3.524011000
F	1.089789000	−1.883734000	−4.835634000
F	2.391109000	−2.581758000	−3.210926000
F	0.352775000	−3.376323000	−3.404132000
C	4.292082000	0.719267000	0.319255000
F	4.317782000	1.952863000	0.889399000
F	5.388167000	0.039530000	0.750801000
F	4.405332000	0.875043000	−1.023041000
C	1.926753000	−3.022333000	2.760563000
H	1.294368000	−2.870014000	3.645623000
H	1.521883000	−3.891112000	2.221887000
H	2.955749000	−3.231977000	3.069311000
C	−0.762372000	2.408724000	−3.076733000
H	−0.197244000	3.268041000	−2.690348000
H	−0.634559000	2.341202000	−4.161949000
H	−1.822034000	2.586898000	−2.844964000
C	−1.798782000	2.728075000	3.162534000
H	−2.807425000	3.156007000	3.126800000
H	−1.626236000	2.341652000	4.178954000

H	−1.047573000	3.503483000	2.972514000
C	−4.046393000	−0.906762000	0.489033000
F	−4.223177000	−0.873717000	−0.859707000
F	−4.018663000	−2.209751000	0.872048000
F	−5.143146000	−0.334524000	1.058086000

Coordinate C.21: Optimized Cartesian coordinates of Mn(tfaa)₃, **5**; *fac*, S=4/2 with no symmetry (OLYP/TZP).

Mn	0.224390000	0.106716000	0.084353000
O	2.146456000	0.673172000	0.169674000
O	0.585678000	−1.252872000	1.487447000
O	−1.641418000	−0.512534000	0.045212000
O	−0.454147000	1.570181000	1.661204000
O	−0.095005000	1.362111000	−1.410599000
O	0.687452000	−1.426710000	−1.452724000
C	3.058478000	0.122953000	0.870133000
C	2.933825000	−0.930627000	1.769337000
C	1.696226000	−1.560691000	2.036222000
C	−2.677430000	−0.164203000	0.725632000
C	−2.732667000	0.836120000	1.707806000
C	−1.628863000	1.616692000	2.101966000
C	−0.094854000	1.112703000	−2.673004000
C	0.186320000	−0.064858000	−3.341015000
C	0.569980000	−1.288723000	−2.697613000
H	3.813270000	−1.279909000	2.293501000
H	−3.686697000	1.009177000	2.188531000
H	0.123076000	−0.058886000	−4.421459000
C	−1.841539000	2.658905000	3.258372000
F	−1.313198000	3.864003000	2.933866000
F	−3.155186000	2.864432000	3.577278000
F	−1.220027000	2.225813000	4.395374000
C	4.469040000	0.745728000	0.618692000
F	4.441533000	2.090083000	0.778989000
F	5.423054000	0.251878000	1.459879000
F	4.876927000	0.481339000	−0.652741000
C	1.618111000	−2.693390000	3.033181000

H	0.905106000	-2.428228000	3.821395000
H	1.223482000	-3.583150000	2.530017000
H	2.585224000	-2.926980000	3.480263000
C	-3.919520000	-0.959861000	0.384467000
H	-4.145000000	-0.837988000	-0.680613000
H	-3.721693000	-2.024683000	0.550741000
H	-4.784866000	-0.655511000	0.975002000
C	-0.489927000	2.373787000	-3.502870000
F	0.337485000	3.414608000	-3.227180000
F	-0.443190000	2.166816000	-4.851285000
F	-1.760495000	2.763755000	-3.202966000
C	0.867517000	-2.505850000	-3.553269000
H	1.919378000	-2.783161000	-3.418577000
H	0.268041000	-3.348510000	-3.192763000
H	0.673522000	-2.348214000	-4.615733000

Coordinate C.22: Optimized Cartesian coordinates of Mn(tfaa)$_3$, **5**; *mer1* CF$_3$-CF$_3$, S=4/2 with no symmetry (OLYP/TZP).

Mn	0.199843000	0.047158000	-0.020995000
O	2.088760000	0.694351000	0.091656000
O	0.585516000	-1.316074000	1.349163000
O	-1.703341000	-0.452059000	-0.017772000
O	-0.372921000	1.525301000	1.633169000
O	-0.081471000	1.244927000	-1.529587000
O	0.630841000	-1.580182000	-1.566862000
C	2.988491000	0.234097000	0.869286000
C	2.890676000	-0.835334000	1.751958000
C	1.694489000	-1.569796000	1.930036000
C	-2.708598000	-0.041116000	0.674900000
C	-2.685260000	0.916115000	1.701823000
C	-1.529492000	1.608430000	2.112311000
C	-0.059580000	1.037913000	-2.803008000
C	0.205936000	-0.176047000	-3.456007000
C	0.527784000	-1.380837000	-2.800620000
H	3.761280000	-1.122911000	2.325789000

H	−3.620131000	1.128088000	2.204349000
H	0.173476000	−0.172221000	−4.537774000
C	−1.653877000	2.601712000	3.325208000
F	−1.194660000	3.836044000	2.991751000
F	−2.933342000	2.758719000	3.782991000
F	−0.909264000	2.153841000	4.376347000
C	0.796001000	−2.657556000	−3.678819000
F	0.747628000	−2.424700000	−5.024839000
F	2.022410000	−3.178703000	−3.407086000
F	−0.129601000	−3.620655000	−3.407917000
C	4.332469000	1.020839000	0.756659000
F	4.146932000	2.322445000	1.096890000
F	5.309007000	0.522738000	1.567642000
F	4.804559000	0.984491000	−0.516483000
C	1.657519000	−2.754611000	2.864038000
H	0.903629000	−2.577588000	3.638878000
H	1.335934000	−3.636276000	2.298612000
H	2.623182000	−2.952091000	3.330602000
C	−4.017979000	−0.697831000	0.292440000
H	−4.239343000	−0.469542000	−0.756365000
H	−3.916406000	−1.785583000	0.368102000
H	−4.848846000	−0.363897000	0.915852000
C	−0.353988000	2.278160000	−3.616661000
H	0.391965000	3.045070000	−3.380762000
H	−0.345921000	2.082465000	−4.689740000
H	−1.330297000	2.679735000	−3.324372000

Coordinate C.23: Optimized Cartesian coordinates of Mn(tfaa)$_3$, **5**; *mer2* CH$_3$-CH$_3$, S=4/2 with no symmetry (OLYP/TZP).

Mn	0.342640000	−0.333386000	0.081533000
O	2.202147000	0.354171000	0.085486000
O	0.893021000	−1.770116000	1.328400000
O	−1.531690000	−0.849265000	0.279374000
O	−0.085066000	1.107681000	1.775119000
O	−0.153418000	1.070463000	−1.177559000

O	0.669767000	−1.617891000	−1.708957000
C	3.074848000	0.076569000	0.968930000
C	3.043956000	−0.936633000	1.919018000
C	1.971655000	−1.850205000	2.008057000
C	−2.488347000	−0.078804000	0.671284000
C	−2.435604000	1.058046000	1.447393000
C	−1.221239000	1.596186000	1.994044000
C	−0.405364000	0.976058000	−2.435898000
C	−0.222197000	−0.086122000	−3.292322000
C	0.340731000	−1.342749000	−2.891211000
H	3.891973000	−1.061286000	2.577736000
H	−3.366967000	1.561677000	1.671404000
H	−0.491469000	0.047031000	−4.332279000
C	4.307999000	1.009156000	0.883636000
F	3.921518000	2.303172000	0.897174000
F	5.171290000	0.827082000	1.912740000
F	4.984382000	0.782047000	−0.269477000
C	2.062288000	−3.033292000	2.937783000
H	1.162896000	−3.076878000	3.560037000
H	2.085066000	−3.950789000	2.337738000
H	2.951414000	−2.996603000	3.568631000
C	−1.317024000	2.830900000	2.864154000
H	−2.219601000	2.832077000	3.482153000
H	−0.426406000	2.914722000	3.489828000
H	−1.361730000	3.713452000	2.211855000
C	−3.853780000	−0.584928000	0.156463000
F	−3.837774000	−0.694982000	−1.196099000
F	−4.128368000	−1.812799000	0.664696000
F	−4.882841000	0.233662000	0.484501000
C	0.546710000	−2.391201000	−3.963283000
H	1.087986000	−1.972996000	−4.819151000
H	1.093616000	−3.242337000	−3.556143000
H	−0.427640000	−2.732984000	−4.334646000
C	−0.978698000	2.306216000	−2.978423000
F	−0.079256000	3.308091000	−2.814071000

| F | −1.295643000 | 2.250726000 | −4.294136000 |
| F | −2.105907000 | 2.648439000 | −2.304404000 |

Coordinate C.24: Optimized Cartesian coordinates of Mn(tfaa)$_3$, **5**; *mer3* CF$_3$-CH$_3$, S=4/2 with no symmetry (OLYP/TZP).

Mn	0.213801000	−0.088751000	0.111300000
O	2.118646000	0.591448000	0.155358000
O	0.707014000	−1.464118000	1.434309000
O	−1.695052000	−0.709905000	0.162325000
O	−0.375801000	1.318275000	1.723785000
O	−0.181110000	1.240739000	−1.252311000
O	0.609822000	−1.515080000	−1.553715000
C	3.059354000	0.133592000	0.877701000
C	3.012715000	−0.934065000	1.769352000
C	1.836502000	−1.682090000	1.992314000
C	−2.674539000	−0.250486000	0.849421000
C	−2.688282000	0.755316000	1.800772000
C	−1.527844000	1.489253000	2.204145000
C	−0.188473000	1.162545000	−2.539161000
C	0.088490000	0.024612000	−3.308478000
C	0.460267000	−1.219009000	−2.764286000
H	3.910252000	−1.209072000	2.306792000
H	−3.632783000	0.992984000	2.273208000
H	0.021739000	0.119450000	−4.384249000
C	0.733415000	−2.407850000	−3.743710000
F	0.613187000	−2.069188000	−5.060685000
F	1.990559000	−2.891471000	−3.566220000
F	−0.138722000	−3.422067000	−3.507723000
C	4.394271000	0.915254000	0.691720000
F	4.235132000	2.212687000	1.058497000
F	5.415125000	0.404712000	1.435869000
F	4.785123000	0.891595000	−0.605836000
C	1.850970000	−2.844684000	2.955628000
H	1.111832000	−2.666773000	3.743963000
H	1.542718000	−3.751021000	2.423960000

H	2.832917000	-3.000357000	3.404130000
C	-0.531945000	2.469263000	-3.218132000
H	0.209666000	3.224038000	-2.934458000
H	-0.555776000	2.376009000	-4.304536000
H	-1.504858000	2.820087000	-2.858639000
C	-1.671220000	2.528629000	3.300220000
H	-2.711069000	2.784793000	3.513085000
H	-1.213949000	2.136459000	4.216779000
H	-1.115147000	3.428253000	3.022168000
C	-4.008409000	-0.976041000	0.504562000
F	-4.337960000	-0.774063000	-0.799352000
F	-3.894951000	-2.315001000	0.699383000
F	-5.063651000	-0.547638000	1.255766000

Coordinate C.25: Optimized Cartesian coordinates of Mn(tfaa)$_3$, **5**; *fac*, S=4/2 with no symmetry (B3LYP/TZP).

Mn	0.229461000	0.072494000	0.122328000
O	2.095088000	0.658820000	0.206451000
O	0.578303000	-1.254272000	1.519990000
O	-1.603842000	-0.546259000	0.032880000
O	-0.405901000	1.502499000	1.626362000
O	-0.104644000	1.338871000	-1.306925000
O	0.779606000	-1.383857000	-1.398334000
C	3.024278000	0.091511000	0.861850000
C	2.922963000	-0.969182000	1.741205000
C	1.690353000	-1.578826000	2.044459000
C	-2.657875000	-0.133892000	0.638445000
C	-2.710833000	0.893031000	1.582497000
C	-1.591503000	1.617814000	2.009743000
C	-0.101963000	1.118400000	-2.569616000
C	0.233755000	-0.021049000	-3.258290000
C	0.676813000	-1.229508000	-2.638022000
H	3.813141000	-1.326101000	2.231210000
H	-3.669031000	1.132076000	2.012773000
H	0.172456000	0.005065000	-4.333642000
C	-1.794207000	2.685863000	3.116233000

F	−1.262434000	3.864747000	2.747549000
F	−3.097445000	2.899396000	3.415433000
F	−1.179880000	2.288600000	4.255187000
C	4.410362000	0.715753000	0.588717000
F	4.404574000	2.029405000	0.874453000
F	5.389045000	0.137335000	1.319851000
F	4.734374000	0.569299000	−0.713570000
C	1.628522000	−2.690157000	3.052113000
H	0.943669000	−2.405601000	3.852515000
H	1.213402000	−3.578946000	2.573872000
H	2.604087000	−2.922045000	3.471402000
C	−3.914418000	−0.867726000	0.257250000
H	−4.076557000	−0.762843000	−0.816903000
H	−3.782498000	−1.931832000	0.460679000
H	−4.785134000	−0.498927000	0.793631000
C	−0.561337000	2.361226000	−3.360880000
F	0.231049000	3.417111000	−3.093500000
F	−0.545560000	2.166862000	−4.698888000
F	−1.825996000	2.693465000	−3.016500000
C	1.061975000	−2.393414000	−3.515813000
H	2.136772000	−2.562255000	−3.419973000
H	0.561148000	−3.292929000	−3.156777000
H	0.821354000	−2.228784000	−4.563696000

Coordinate C.26: Optimized Cartesian coordinates of Mn(tfaa)$_3$, **5**; *mer1* CF$_3$-CF$_3$, S=4/2 with no symmetry (B3LYP/TZP).

Mn	0.148215000	0.062931000	0.038988000
O	2.016620000	0.654527000	0.075911000
O	0.517044000	−1.235227000	1.450655000
O	−1.709347000	−0.508406000	0.003357000
O	−0.424651000	1.515833000	1.556235000
O	−0.172184000	1.295637000	−1.409617000
O	0.637680000	−1.457625000	−1.443744000
C	2.945443000	0.142968000	0.776318000
C	2.854094000	−0.890119000	1.688553000

C	1.633852000	-1.527700000	1.985915000
C	-2.710350000	-0.158131000	0.723343000
C	-2.698501000	0.818328000	1.723319000
C	-1.567332000	1.567925000	2.065225000
C	-0.073435000	1.134721000	-2.679057000
C	0.280827000	-0.048163000	-3.333118000
C	0.601208000	-1.241197000	-2.675922000
H	3.744869000	-1.211159000	2.201540000
H	-3.615474000	1.002471000	2.258071000
H	0.314790000	-0.034411000	-4.409783000
C	-1.693247000	2.595900000	3.220199000
F	-1.348377000	3.828957000	2.799922000
F	-2.945577000	2.674355000	3.728729000
F	-0.867135000	2.256608000	4.234892000
C	0.956046000	-2.479700000	-3.539476000
F	1.026614000	-2.204695000	-4.862681000
F	2.147173000	-2.990787000	-3.167550000
F	0.022741000	-3.442966000	-3.375366000
C	4.314473000	0.811432000	0.523465000
F	4.262353000	2.119566000	0.839227000
F	5.304387000	0.250594000	1.251857000
F	4.653695000	0.707818000	-0.776967000
C	1.591101000	-2.632893000	2.999997000
H	0.870188000	-2.376046000	3.777506000
H	1.231136000	-3.541188000	2.513455000
H	2.563684000	-2.819779000	3.447636000
C	-3.983420000	-0.899484000	0.418103000
H	-4.247131000	-0.740385000	-0.629020000
H	-3.812877000	-1.969703000	0.546073000
H	-4.807242000	-0.581626000	1.052436000
C	-0.374663000	2.369689000	-3.481746000
H	0.338430000	3.150261000	-3.210347000
H	-0.322888000	2.186615000	-4.552104000
H	-1.367833000	2.736433000	-3.218257000

Coordinate C.27: Optimized Cartesian coordinates of Mn(tfaa)₃, **5**; *mer2* CH₃-CH₃, S=4/2 with no symmetry (B3LYP/TZP).

Mn	0.245810000	-0.058005000	0.167995000
O	2.105520000	0.587200000	0.204825000
O	0.692338000	-1.419884000	1.490263000
O	-1.591912000	-0.711796000	0.142518000
O	-0.354556000	1.304948000	1.731786000
O	-0.177715000	1.279644000	-1.158053000
O	0.719637000	-1.418904000	-1.442854000
C	3.060865000	0.071530000	0.862188000
C	3.015888000	-1.001987000	1.732247000
C	1.820606000	-1.691131000	2.011409000
C	-2.615225000	-0.184837000	0.706538000
C	-2.678813000	0.862611000	1.591025000
C	-1.531237000	1.560276000	2.080579000
C	-0.258099000	1.123441000	-2.429841000
C	0.014782000	0.016627000	-3.191907000
C	0.505024000	-1.217120000	-2.660971000
H	3.922616000	-1.315618000	2.221612000
H	-3.649357000	1.163020000	1.950296000
H	-0.128808000	0.090880000	-4.257163000
C	4.410748000	0.777001000	0.602953000
F	4.323577000	2.087895000	0.893018000
F	5.415548000	0.257254000	1.343027000
F	4.756249000	0.655869000	-0.695599000
C	1.819663000	-2.831808000	2.987533000
H	1.123220000	-2.605694000	3.796726000
H	1.447958000	-3.726783000	2.486075000
H	2.807371000	-3.024202000	3.398284000
C	-1.731405000	2.647554000	3.105585000
H	-2.755395000	3.014338000	3.129212000
H	-1.484626000	2.245320000	4.091637000
H	-1.041558000	3.465404000	2.903178000
C	-3.919420000	-0.892988000	0.285465000
F	-4.082479000	-0.828393000	-1.053193000

F	−3.881294000	−2.197982000	0.632604000
F	−5.020349000	−0.354126000	0.854899000
C	0.813905000	−2.342302000	−3.613830000
H	1.898878000	−2.452430000	−3.681378000
H	0.417049000	−3.273020000	−3.209159000
H	0.415774000	−2.168688000	−4.610798000
C	−0.732577000	2.415863000	−3.125303000
F	0.129843000	3.425016000	−2.884012000
F	−0.837893000	2.281816000	−4.465762000
F	−1.943683000	2.787641000	−2.657962000

Coordinate C.28: Optimized Cartesian coordinates of Mn(tfaa)$_3$, **5**; *mer3* CF$_3$-CH$_3$, S=4/2 with no symmetry (B3LYP/TZP).

Mn	0.248920000	−0.199001000	0.131703000
O	2.086996000	0.516273000	0.115130000
O	0.787022000	−1.570134000	1.401817000
O	−1.609297000	−0.812823000	0.209786000
O	−0.239424000	1.126368000	1.786193000
O	−0.238892000	1.151864000	−1.145039000
O	0.635520000	−1.544253000	−1.514562000
C	3.029993000	0.148062000	0.881125000
C	3.027573000	−0.887781000	1.795941000
C	1.905882000	−1.716393000	1.990505000
C	−2.592413000	−0.239085000	0.796878000
C	−2.583633000	0.789511000	1.707189000
C	−1.390657000	1.412014000	2.190563000
C	−0.322772000	1.094203000	−2.426099000
C	−0.047125000	−0.021912000	−3.216686000
C	0.405612000	−1.245062000	−2.707960000
H	3.922803000	−1.086212000	2.360937000
H	−3.528980000	1.127171000	2.099247000
H	−0.178087000	0.071928000	−4.281768000
C	0.674990000	−2.400821000	−3.706537000
F	0.445590000	−2.054048000	−4.994604000
F	1.959440000	−2.806295000	−3.619663000

F	-0.114266000	-3.456778000	-3.423321000
C	4.304967000	1.002928000	0.709506000
F	4.042090000	2.294667000	0.992373000
F	5.308857000	0.602308000	1.520596000
F	4.751495000	0.935450000	-0.559823000
C	1.983436000	-2.872041000	2.944720000
H	1.209996000	-2.758469000	3.706040000
H	1.765293000	-3.792727000	2.401104000
H	2.958142000	-2.949037000	3.419579000
C	-0.756749000	2.381565000	-3.068604000
H	-0.041849000	3.164598000	-2.809692000
H	-0.827452000	2.296765000	-4.150002000
H	-1.723853000	2.678707000	-2.659909000
C	-1.512209000	2.450370000	3.277564000
H	-2.498926000	2.908850000	3.304167000
H	-1.335604000	1.966332000	4.242015000
H	-0.744000000	3.209871000	3.143816000
C	-3.946307000	-0.842978000	0.367195000
F	-4.140185000	-0.658573000	-0.958407000
F	-3.979031000	-2.168835000	0.607839000
F	-4.999075000	-0.286720000	1.009309000

Coordinate C.29: Optimized Cartesian coordinates of Mn(tfth)$_3$, **6**; *fac* CF$_3$-C$_4$H$_3$S, S=4/2 with no symmetry (PW91/TZP).

Mn	-0.761325000	4.004286000	-7.585427000
O	0.054255000	2.809478000	-5.962555000
O	0.965152000	4.874572000	-7.680750000
O	-1.391642000	5.209690000	-9.266259000
O	-0.214514000	2.662647000	-8.870676000
O	-2.518240000	3.162014000	-7.479191000
O	-1.315911000	5.381525000	-6.330509000
C	1.004706000	3.190811000	-5.212604000
C	1.862894000	4.293798000	-5.521714000
C	1.787683000	5.008727000	-6.694769000
C	-0.815667000	5.088016000	-10.384360000

C	-0.038932000	4.017487000	-10.839244000
C	0.193485000	2.853278000	-10.087045000
C	-3.594239000	3.636467000	-6.957137000
C	-3.644476000	4.830699000	-6.196830000
C	-2.516819000	5.580681000	-5.927744000
H	2.644567000	4.569220000	-4.819726000
H	0.381481000	4.082962000	-11.838081000
H	-4.591721000	5.159127000	-5.780627000
C	1.994624000	-0.341349000	-10.811108000
C	2.152526000	0.119589000	-12.099992000
S	1.448126000	1.668774000	-12.322007000
C	0.924770000	1.726828000	-10.660535000
C	1.295809000	0.571407000	-9.993436000
H	2.374878000	-1.301807000	-10.471664000
H	2.649309000	-0.367836000	-12.932665000
H	1.062871000	0.419307000	-8.943390000
C	0.510196000	1.321536000	-3.568417000
C	1.232354000	2.428161000	-3.981392000
S	2.487710000	2.799663000	-2.830785000
C	2.032303000	1.486261000	-1.827495000
C	0.964281000	0.785632000	-2.345760000
H	-0.318176000	0.933411000	-4.154686000
H	2.574339000	1.300533000	-0.905610000
H	0.526914000	-0.080815000	-1.854977000
C	2.805198000	6.132094000	-6.956834000
F	2.172083000	7.314786000	-7.146724000
F	3.683776000	6.295123000	-5.930520000
F	3.529548000	5.864213000	-8.075446000
C	-1.045679000	6.281129000	-11.340690000
F	-0.678072000	7.443012000	-10.751036000
F	-0.348755000	6.173084000	-12.507157000
F	-2.364277000	6.376853000	-11.664161000
C	-2.629102000	6.821849000	-5.023967000
F	-2.248143000	7.934803000	-5.692565000
F	-3.896923000	7.021437000	-4.572990000

A-78

F	−1.823723000	6.687192000	−3.939596000
C	−4.797179000	2.847913000	−7.178774000
C	−4.882830000	1.679806000	−7.919365000
H	−4.014025000	1.248809000	−8.409014000
H	−6.461255000	0.240416000	−8.493402000
C	−6.186287000	1.148028000	−7.962025000
H	−8.153388000	1.739011000	−7.119111000
C	−7.090129000	1.910619000	−7.253645000
S	−6.356318000	3.281005000	−6.532761000

Coordinate C.30: Optimized Cartesian coordinates of Mn(tfth)$_3$, **6**; *mer1* CF$_3$- CF$_3$, S=4/2 with no symmetry (PW91/TZP).

Mn	−0.923593000	4.683111000	−7.577814000
O	−0.127039000	3.407318000	−6.012877000
O	0.749512000	5.684941000	−7.468056000
O	−1.529592000	5.954787000	−9.211615000
O	−0.165007000	3.461597000	−8.870115000
O	−2.567428000	3.637366000	−7.607404000
O	−1.695378000	5.917570000	−6.299398000
C	1.121132000	3.246965000	−5.898889000
C	2.144370000	4.070689000	−6.377726000
C	1.914185000	5.258379000	−7.097707000
C	−1.121024000	5.778293000	−10.393950000
C	−0.396600000	4.701258000	−10.910554000
C	0.016711000	3.595621000	−10.145779000
C	−3.560650000	3.796630000	−6.813114000
C	−3.756479000	4.792965000	−5.876391000
C	−2.822539000	5.838210000	−5.681625000
H	3.169764000	3.786904000	−6.159882000
H	−0.158558000	4.713698000	−11.969802000
H	−4.672802000	4.780412000	−5.294708000
C	1.798187000	0.427789000	−11.020437000
C	1.815792000	0.880985000	−12.321094000
S	1.063921000	2.414361000	−12.481308000
C	0.709399000	2.476070000	−10.775506000

C	1.169155000	1.333528000	-10.141362000
H	2.222677000	-0.525725000	-10.716510000
H	2.230253000	0.393246000	-13.197801000
H	1.038595000	1.176843000	-9.073853000
C	-2.810514000	8.893750000	-3.542452000
C	-4.056589000	8.501685000	-3.100900000
S	-4.571141000	7.037688000	-3.828315000
C	-3.097711000	6.921808000	-4.752366000
C	-2.264463000	7.995707000	-4.480766000
H	-2.313905000	9.797011000	-3.197070000
H	-4.701583000	8.998794000	-2.383254000
H	-1.296966000	8.104577000	-4.962470000
C	-4.640503000	2.715348000	-6.999657000
F	-5.184748000	2.800185000	-8.240337000
F	-4.106696000	1.479519000	-6.860324000
F	-5.651067000	2.833792000	-6.096701000
C	-1.493778000	6.930431000	-11.355409000
F	-0.948176000	8.098645000	-10.921040000
F	-1.058018000	6.730611000	-12.631256000
F	-2.838438000	7.096225000	-11.403948000
C	3.026688000	6.126052000	-7.480070000
C	2.939719000	7.280038000	-8.241217000
H	1.990542000	7.639549000	-8.629395000
C	4.188335000	7.903638000	-8.448150000
H	4.329407000	8.816129000	-9.022653000
C	5.223186000	7.224859000	-7.843337000
H	6.279856000	7.472562000	-7.840629000
S	4.679264000	5.823638000	-7.015761000
C	1.515409000	1.964358000	-5.130676000
F	0.961458000	1.954906000	-3.893139000
F	1.064181000	0.865019000	-5.794351000
F	2.862259000	1.818884000	-4.977674000

Coordinate C.31: Optimized Cartesian coordinates of Mn(tfth)₃, **6**; *mer2* C₄H₃S -C₄H₃S, S=4/2 with no symmetry (PW91/TZP).

Mn	-0.168940000	2.882399000	-11.008286000
O	0.337167000	0.836840000	-10.515371000
O	-2.012127000	2.287874000	-11.158541000
O	-0.760796000	4.949005000	-11.335060000
O	-0.410784000	3.187305000	-9.113592000
O	1.704185000	3.426403000	-10.864841000
O	0.033240000	2.597071000	-12.920634000
C	-0.458467000	0.060140000	-9.902890000
C	-1.880877000	0.236047000	-9.898159000
C	-2.518159000	1.281920000	-10.523500000
C	-1.311549000	5.703715000	-10.477678000
C	-1.491940000	5.344804000	-9.103192000
C	-1.035689000	4.169043000	-8.554328000
C	2.522699000	3.540902000	-11.842326000
C	2.303752000	3.279067000	-13.182669000
C	1.060923000	2.807600000	-13.666452000
H	-2.502123000	-0.493862000	-9.386770000
H	-1.993146000	6.042032000	-8.438058000
H	3.121862000	3.437567000	-13.878460000
C	1.483024000	-1.331418000	-9.053578000
C	0.129315000	-1.071998000	-9.185901000
S	-0.807552000	-2.279973000	-8.348121000
C	0.608239000	-3.103499000	-7.840945000
C	1.755879000	-2.484092000	-8.288419000
H	2.231963000	-0.682779000	-9.499583000
H	0.521102000	-4.000378000	-7.236373000
H	2.755040000	-2.850164000	-8.065654000
C	-0.179165000	1.886811000	-17.064791000
C	1.082432000	2.189124000	-17.529799000
S	2.129384000	2.706014000	-16.273929000
C	0.870480000	2.522897000	-15.082289000
C	-0.300780000	2.076559000	-15.673832000
H	-0.983599000	1.541042000	-17.708852000

H	1.454002000	2.133397000	-18.548133000
H	-1.203334000	1.900944000	-15.094026000
C	3.912500000	4.026134000	-11.390880000
F	3.812956000	5.187076000	-10.701738000
F	4.493043000	3.105694000	-10.579294000
F	4.753706000	4.239072000	-12.438866000
C	-4.054111000	1.337033000	-10.513921000
F	-4.539366000	1.299887000	-11.784142000
F	-4.617185000	0.304025000	-9.832302000
F	-4.489506000	2.489414000	-9.941486000
C	-1.764308000	7.020521000	-10.934797000
C	-1.665418000	7.512276000	-12.225321000
H	-1.231646000	6.921024000	-13.027212000
C	-2.176084000	8.819896000	-12.362996000
H	-2.189961000	9.378354000	-13.295659000
C	-2.663684000	9.323137000	-11.175944000
H	-3.110516000	10.294978000	-10.991364000
S	-2.501402000	8.203610000	-9.887077000
C	-1.246615000	3.915650000	-7.051150000
F	-1.947513000	4.909640000	-6.442673000
F	-1.927019000	2.756799000	-6.852793000
F	-0.053028000	3.806660000	-6.413249000

Coordinate C.32: Optimized Cartesian coordinates of Mn(tfth)$_3$, **6**; *mer3* CF$_3$ -C$_4$H$_3$S, S=4/2 with no symmetry (PW91/TZP).

Mn	-0.802442000	4.256335000	-7.888999000
O	0.225363000	2.883436000	-6.548093000
O	0.883779000	5.228192000	-7.997340000
O	-1.620006000	5.672127000	-9.287370000
O	-0.346937000	3.130138000	-9.386280000
O	-2.490611000	3.286249000	-7.721715000
O	-1.287473000	5.416179000	-6.411267000
C	1.205284000	3.213772000	-5.813420000
C	1.977068000	4.403457000	-6.014693000
C	1.761727000	5.280372000	-7.053837000

C	−1.255481000	5.680249000	−10.498151000
C	−0.588995000	4.675606000	−11.203333000
C	−0.213134000	3.445215000	−10.636039000
C	−3.461988000	3.622801000	−6.957974000
C	−3.522888000	4.665337000	−6.052182000
C	−2.423626000	5.523335000	−5.812754000
H	2.790349000	4.627778000	−5.330355000
H	−0.382321000	4.845096000	−12.255658000
H	−4.446130000	4.815497000	−5.501514000
C	1.302059000	0.340445000	−12.063087000
C	1.244036000	0.961584000	−13.291059000
S	0.576839000	2.538809000	−13.186727000
C	0.364789000	2.390989000	−11.463538000
C	0.802640000	1.152532000	−11.023425000
H	1.693363000	−0.664059000	−11.921963000
H	1.560042000	0.576439000	−14.255247000
H	0.750968000	0.867121000	−9.976495000
C	0.899821000	1.129454000	−4.398877000
C	1.551001000	2.310353000	−4.712141000
S	2.868433000	2.591946000	−3.604851000
C	2.529250000	1.144728000	−2.748840000
C	1.454677000	0.467573000	−3.283296000
H	0.048420000	0.779539000	−4.976618000
H	3.139914000	0.869028000	−1.895203000
H	1.083755000	−0.471818000	−2.880487000
C	−1.934752000	8.484485000	−3.594961000
C	−3.194489000	8.228284000	−3.097783000
S	−3.916548000	6.858440000	−3.834105000
C	−2.515131000	6.600523000	−4.839237000
C	−1.546879000	7.560095000	−4.584618000
H	−1.319935000	9.314997000	−3.257498000
H	−3.739359000	8.775347000	−2.335000000
H	−0.601153000	7.578804000	−5.119968000
C	−4.679471000	2.695160000	−7.118711000
F	−5.119216000	2.702880000	−8.399389000

F	−4.343762000	1.419204000	−6.798659000
F	−5.719470000	3.059148000	−6.321677000
C	2.638541000	6.538610000	−7.161229000
F	1.883687000	7.653515000	−6.945309000
F	3.652243000	6.557327000	−6.253423000
F	3.188421000	6.648443000	−8.393623000
C	−1.624421000	6.979045000	−11.250787000
F	−1.023422000	8.047384000	−10.667819000
F	−1.250274000	6.964570000	−12.561273000
F	−2.966021000	7.185527000	−11.213184000

Coordinate C.33: Optimized Cartesian coordinates of Mn(tfth)$_3$, **6**; *fac* CF$_3$ -C$_4$H$_3$S, S=4/2 with no symmetry (BP86/TZP).

Mn	−0.735849000	3.991577000	−7.545392000
O	0.073650000	2.808640000	−5.906614000
O	0.987378000	4.874636000	−7.629823000
O	−1.391262000	5.213746000	−9.210401000
O	−0.178186000	2.668667000	−8.853804000
O	−2.489023000	3.133328000	−7.446154000
O	−1.317285000	5.372650000	−6.302394000
C	1.040458000	3.173966000	−5.166415000
C	1.916163000	4.263001000	−5.487907000
C	1.831092000	4.987725000	−6.656415000
C	−0.843928000	5.100030000	−10.345184000
C	−0.073138000	4.034502000	−10.825940000
C	0.189587000	2.866854000	−10.084111000
C	−3.583782000	3.625138000	−6.975336000
C	−3.659835000	4.853214000	−6.268363000
C	−2.536836000	5.604051000	−5.973241000
H	2.713820000	4.523177000	−4.796365000
H	0.317463000	4.105891000	−11.837920000
H	−4.623766000	5.206171000	−5.911808000
C	1.972264000	−0.325916000	−10.897448000
C	2.097677000	0.152658000	−12.184765000
S	1.390416000	1.708899000	−12.367939000

C	0.908412000	1.745047000	-10.689282000
C	1.295437000	0.578351000	-10.047682000
H	2.358924000	-1.292967000	-10.580784000
H	2.572004000	-0.324511000	-13.038148000
H	1.088641000	0.410285000	-8.993105000
C	0.515334000	1.326636000	-3.500482000
C	1.264577000	2.410240000	-3.932593000
S	2.548233000	2.754353000	-2.797549000
C	2.066218000	1.459032000	-1.777183000
C	0.969590000	0.786281000	-2.276748000
H	-0.332534000	0.957000000	-4.073167000
H	2.615476000	1.263840000	-0.859999000
H	0.512714000	-0.064042000	-1.773423000
C	2.864353000	6.098883000	-6.930554000
F	2.247252000	7.291891000	-7.119497000
F	3.754657000	6.252139000	-5.910175000
F	3.578293000	5.817295000	-8.055181000
C	-1.113546000	6.296158000	-11.292107000
F	-0.769442000	7.464498000	-10.697893000
F	-0.426568000	6.214316000	-12.469018000
F	-2.440031000	6.360359000	-11.601026000
C	-2.677999000	6.889428000	-5.132475000
F	-2.223827000	7.961958000	-5.823669000
F	-3.969473000	7.139278000	-4.778369000
F	-1.950279000	6.787869000	-3.988748000
C	-4.778898000	2.819691000	-7.197940000
C	-4.844498000	1.631101000	-7.911907000
H	-3.964161000	1.194497000	-8.378489000
H	-6.405438000	0.163702000	-8.477644000
C	-6.145770000	1.086847000	-7.962868000
H	-8.133680000	1.682990000	-7.164671000
C	-7.068356000	1.859878000	-7.286620000
S	-6.355674000	3.255689000	-6.585068000

Appendix

Coordinate C.34: Optimized Cartesian coordinates of Mn(tfth)₃, **6**; *mer1* CF₃ –CF₃, S=4/2 with no symmetry (BP86/TZP).

Mn	-0.670276000	4.805414000	-7.666756000
O	0.003055000	3.450432000	-6.109687000
O	0.991433000	5.786512000	-7.414000000
O	-1.196034000	6.125884000	-9.302434000
O	0.152712000	3.634797000	-8.979425000
O	-2.325496000	3.809888000	-7.892667000
O	-1.509974000	5.953708000	-6.325372000
C	1.226335000	3.349395000	-5.804426000
C	2.279775000	4.203292000	-6.151470000
C	2.111063000	5.388302000	-6.895856000
C	-1.252800000	5.709822000	-10.496572000
C	-0.776171000	4.500586000	-11.016749000
C	-0.094988000	3.534508000	-10.250906000
C	-3.379662000	3.936740000	-7.167369000
C	-3.612512000	4.833025000	-6.142246000
C	-2.661669000	5.816636000	-5.763828000
H	3.275006000	3.954924000	-5.791130000
H	-0.933858000	4.305548000	-12.074475000
H	-4.568312000	4.788025000	-5.627418000
C	1.368444000	0.187900000	-11.080886000
C	1.091388000	0.471689000	-12.401866000
S	0.358138000	2.015136000	-12.592605000
C	0.412177000	2.310834000	-10.871112000
C	0.984688000	1.233505000	-10.211063000
H	1.828047000	-0.743391000	-10.754760000
H	1.277760000	-0.144906000	-13.277076000
H	1.101878000	1.219389000	-9.130152000
C	-2.660769000	8.489583000	-3.150906000
C	-3.933307000	8.067137000	-2.820899000
S	-4.459367000	6.760830000	-3.802865000
C	-2.953154000	6.756860000	-4.689365000
C	-2.103543000	7.746228000	-4.212816000
H	-2.153404000	9.306026000	-2.640495000

H	−4.592017000	8.456941000	−2.049415000
H	−1.114276000	7.904421000	−4.636251000
C	−4.482739000	2.933595000	−7.561301000
F	−4.892964000	3.159126000	−8.837284000
F	−4.019883000	1.661254000	−7.488517000
F	−5.576549000	3.022958000	−6.755006000
C	−1.937517000	6.704323000	−11.467704000
F	−1.255185000	7.882086000	−11.496857000
F	−2.009155000	6.244379000	−12.750327000
F	−3.206543000	6.971359000	−11.059882000
C	3.239212000	6.294422000	−7.120378000
C	3.215693000	7.459057000	−7.872496000
H	2.314016000	7.794365000	−8.380525000
C	4.460609000	8.128549000	−7.900843000
H	4.645408000	9.056362000	−8.439383000
C	5.429085000	7.474073000	−7.169115000
H	6.467443000	7.757342000	−7.018668000
S	4.827868000	6.037357000	−6.439916000
C	1.546352000	2.141587000	−4.888132000
F	1.077636000	2.373969000	−3.628984000
F	0.954264000	1.011550000	−5.346839000
F	2.883790000	1.888862000	−4.782324000

Coordinate C.35: Optimized Cartesian coordinates of Mn(tfth)$_3$, **6**; *mer2* C$_4$H$_3$S -C$_4$H$_3$S, S=4/2 with no symmetry (BP86/TZP).

Mn	−0.257124000	2.959866000	−10.994214000
O	0.363869000	0.932681000	−10.499934000
O	−2.069919000	2.272003000	−11.132276000
O	−0.902237000	5.008543000	−11.347975000
O	−0.508013000	3.279374000	−9.101742000
O	1.609616000	3.528964000	−10.849861000
O	−0.045320000	2.667251000	−12.907292000
C	−0.395195000	0.084022000	−9.936100000
C	−1.827013000	0.180331000	−9.944576000
C	−2.518835000	1.211898000	−10.539375000

A-87

C	−1.375557000	5.806345000	−10.480424000
C	−1.512938000	5.477820000	−9.091186000
C	−1.082419000	4.292579000	−8.539292000
C	2.472221000	3.501234000	−11.797962000
C	2.281767000	3.159905000	−13.126594000
C	1.016709000	2.767173000	−13.631236000
H	−2.411939000	−0.604420000	−9.471159000
H	−1.964613000	6.203711000	−8.419578000
H	3.134880000	3.204968000	−13.798137000
C	1.615813000	−1.237287000	−9.121868000
C	0.249304000	−1.048617000	−9.262489000
S	−0.628459000	−2.350289000	−8.494184000
C	0.830068000	−3.115417000	−8.004128000
C	1.946149000	−2.409548000	−8.405808000
H	2.333024000	−0.526282000	−9.525882000
H	0.787560000	−4.044778000	−7.442410000
H	2.963573000	−2.728359000	−8.185795000
C	−0.212594000	1.792466000	−17.024520000
C	1.068112000	2.031215000	−17.480902000
S	2.120094000	2.546741000	−16.224522000
C	0.836954000	2.446279000	−15.042707000
C	−0.344970000	2.028682000	−15.639246000
H	−1.022809000	1.458456000	−17.670057000
H	1.450822000	1.931448000	−18.493161000
H	−1.262387000	1.905621000	−15.067801000
C	3.883288000	3.896319000	−11.314993000
F	3.860350000	5.097572000	−10.688278000
F	4.351203000	2.971530000	−10.433995000
F	4.780428000	3.980206000	−12.336939000
C	−4.058521000	1.170093000	−10.550170000
F	−4.525025000	1.130767000	−11.829899000
F	−4.564205000	0.085436000	−9.900022000
F	−4.575123000	2.278786000	−9.957799000
C	−1.785450000	7.137566000	−10.945816000
C	−1.727566000	7.597460000	−12.252668000

H	-1.368871000	6.966344000	-13.062770000
C	-2.173574000	8.930561000	-12.395454000
H	-2.205153000	9.470194000	-13.340411000
C	-2.570880000	9.485856000	-11.195773000
H	-2.954267000	10.485933000	-11.011099000
S	-2.400401000	8.385707000	-9.887794000
C	-1.259758000	4.064439000	-7.024400000
F	-1.918382000	5.086907000	-6.410828000
F	-1.966744000	2.926576000	-6.792528000
F	-0.052058000	3.931223000	-6.414081000

Coordinate C.36: Optimized Cartesian coordinates of Mn(tfth)$_3$, **6**; *mer3* CF$_3$ -C$_4$H$_3$S, S=4/2 with no symmetry (BP86/TZP).

Mn	-0.808912000	4.527603000	-7.549468000
O	0.070151000	3.189996000	-6.075609000
O	0.851345000	5.537042000	-7.507773000
O	-1.672043000	5.822777000	-9.068863000
O	-0.101895000	3.414043000	-8.977923000
O	-2.451923000	3.479500000	-7.526545000
O	-1.527650000	5.738465000	-6.200641000
C	1.308637000	3.096910000	-5.811301000
C	2.289636000	4.034548000	-6.273938000
C	1.988478000	5.140648000	-7.040119000
C	-1.449255000	5.674138000	-10.304295000
C	-0.690256000	4.682281000	-10.935340000
C	-0.063745000	3.617777000	-10.260025000
C	-3.540587000	3.824060000	-6.938221000
C	-3.772458000	4.923923000	-6.132309000
C	-2.746499000	5.843725000	-5.793719000
H	3.331293000	3.888128000	-5.998868000
H	-0.594289000	4.733141000	-12.016970000
H	-4.773945000	5.071366000	-5.737449000
C	2.034826000	0.752355000	-11.455307000
C	1.856555000	1.246190000	-12.730644000
S	0.887029000	2.665224000	-12.745567000

C	0.700975000	2.619381000	-11.008635000
C	1.378095000	1.532553000	-10.476765000
H	2.619105000	-0.140061000	-11.238174000
H	2.244482000	0.852444000	-13.666316000
H	1.383546000	1.327353000	-9.408889000
C	0.901785000	0.951360000	-4.512624000
C	1.728842000	1.961511000	-4.979271000
S	3.371427000	1.702305000	-4.440489000
C	2.928929000	0.262954000	-3.611674000
C	1.582982000	-0.014577000	-3.737959000
H	-0.161147000	0.934337000	-4.743827000
H	3.685367000	-0.301837000	-3.073093000
H	1.109136000	-0.884481000	-3.286293000
C	-2.689328000	8.982185000	-3.764334000
C	-4.012666000	8.727965000	-3.464528000
S	-4.578797000	7.281874000	-4.197554000
C	-3.020930000	6.986972000	-4.932788000
C	-2.124478000	7.992845000	-4.597357000
H	-2.152608000	9.854952000	-3.396855000
H	-4.688322000	9.317085000	-2.850065000
H	-1.101152000	7.994988000	-4.965820000
C	-4.686039000	2.828417000	-7.209279000
F	-4.923514000	2.725055000	-8.540582000
F	-4.358072000	1.592782000	-6.745461000
F	-5.851075000	3.197038000	-6.608810000
C	3.121712000	6.113758000	-7.422443000
F	2.909255000	7.335034000	-6.858901000
F	4.348431000	5.684215000	-7.013111000
F	3.177559000	6.284051000	-8.768774000
C	-2.149303000	6.731376000	-11.196897000
F	-1.877695000	7.987615000	-10.764054000
F	-1.776301000	6.659826000	-12.507864000
F	-3.500867000	6.559066000	-11.149781000